University of Southampton

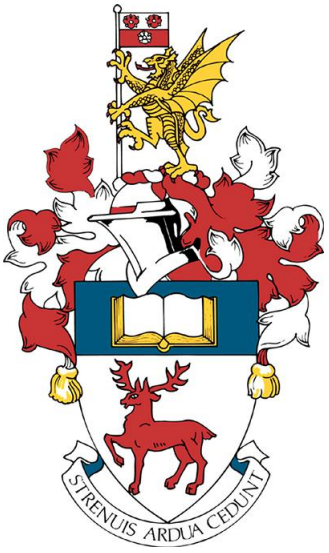

FACULTY OF MEDICINE

School of Cancer Sciences

Volume 1 of 1

The contribution of the FcγRIIB immunoreceptor tyrosine-based inhibitory motif (ITIM) to the modulation of antibody immunotherapy

---

Alexander Patrick Simpson, MBiochem

ORCiD: 0000-0003-3439-2236

A thesis for the degree of Doctor of Philosophy

January 2022

University of Southampton

Abstract

Faculty of Medicine

School of Cancer Sciences

Doctor of Philosophy

The contribution of the FcγRIIB immunoreceptor tyrosine-based inhibitory motif (ITIM) to the modulation of antibody immunotherapy

Alexander Patrick Simpson

Monoclonal antibodies (mAb) are an important therapeutic tool in the treatment of cancers and autoimmunity. Direct targeting mAbs tend to elicit their efficacy through engagement of activatory Fc gamma receptors (FcγR), resulting in target cell depletion by immune effector cells. These activatory FcγRs are negatively influenced by the single inhibitory FcγR, FcγRIIB. FcγRIIB has been shown to reduce the efficacy of mAbs through impairment of activatory FcγR function and upregulation of FcγRIIB has been identified as a resistance mechanism of mAb therapeutics in cancer.

FcγRIIB contains an intracellular immunoreceptor-tyrosine-based inhibition motif (ITIM), which delivers inhibitory signalling. Whether the ITIM is required for all FcγRIIB-mediated inhibitory activities of therapeutic mAbs is not yet clear. To address this issue, we developed and characterised a novel transgenic mouse model (NoTIM), in which the endogenous inhibitory mouse (m)FcγRII is replaced with a non-signalling ITIM mutant of human (h)FcγRIIB. Cells from mice expressing the NoTIM receptor were no longer able to elicit phosphorylation of the FcγRIIB ITIM, mediate efficient internalisation of immune complexes or prevent B cell receptor mediated calcium flux, confirming the expected phenotype.

To understand how FcγRIIB inhibitory signalling impacts mAb-mediated depletion of target cells, different mouse models were treated with anti-mouse CD20 mAbs. The extent of depletion was compared to mice either expressing mFcγRII (wild-type), lacking mFcγRII or where mFcγRII was replaced with a signalling competent or non-competent hFcγRIIB (hFcγRIIB Tg and NoTIM mice respectively). B cell depletion was reduced in wild-type, hFcγRIIB Tg and NoTIM mice compared to those lacking mFcγRII. Subsequent experiments revealed that differences in depletion this was not due to accelerated mAb internalisation nor enhanced clearance from the serum. Using a series of adoptive transfer experiments we determined that the NoTIM hFcγRIIB was mediating inhibition of direct targeting CD20 mAbs, by competing with activatory FcγRs on the surface of myeloid cells.

These findings were then assessed with respect to the depletion of both T regulatory cell and malignant murine B cell in murine tumour models. It was found that in both cases, depletion was negatively impacted by the expression of FcγRIIB at the myeloid surface rather than by its ability to signal. These data indicate that signalling through the ITIM is not critical for the ability of hFcγRIIB to prevent mAb-mediated depletion of target cells, questioning current paradigms for its mechanism of action.

Contents

List of Figures

List of Tables

Deceleration of Authorship

I, Alexander Patrick Simpson, declare that this thesis titled, The contribution of the FcγRIIB immunoreceptor tyrosine-based inhibitory motif (ITIM) to the modulation of antibody immunotherapy, and the work presented in it is my own and has been generated by me as the result of my own original research.

I confirm that:

- This work was done wholly or mainly while in candidature for a research degree at this University;
- Where any part of this thesis has previously been submitted for a degree or any other qualification at this University or any other institution, this has been clearly stated;
- Where I have consulted the published work of others, this is always clearly attributed;
- Where I have quoted from the work of others, the source is always given. With the exception of such quotations, this thesis is entirely my own work;
- I have acknowledged all main sources of help;
- Where the thesis is based on work done by myself jointly with others, I have made clear exactly what was done by others and what I have contributed myself;
- None of this work has been published before submission.

Signed:

_____

Date:

_____

Acknowledgements

I would like to start by thanking my supervisors Professor Mark Cragg and Dr Ali Roghanian for their constant guidance and support throughout my PhD, without their stewardship the work within this thesis would have not been possible. I am particularly thankful for Robert Oldham's patience, wisdom and FcγR knowledge for which without him I would not have the high(ish) calibre of scientific skills today. Kerry Cox, Vikki English, Lisa Dunning, Kirstie Cleary, Jane Willoughby, Josh Sopp, Tom Murray and Matthew Carter were also instrumental in helping deliver the work presented in this thesis. I am indebted to all members of the Antibody & Vaccine Group, the antibody production team and BRF technicians for providing excellent training, assistance and for fostering an inclusive and wonderful working environment, I fear I will never have it as good as it has been again!

I would also like to thank Peter Morley and Daniel Rycroft at GSK for providing their valuable insight into antibody pharmacology and supporting this project throughout. Also, to GSK BioPharm Discovery for making me feel welcome during the rare occasion I was on placement! A special mention for Rena Liu, she was a good friend during the PhD years at Southampton and made a substantial effort in helping me find my feet at GSK. Finally, I would like to thank both GSK and BBSRC for funding this project.

Personally I have many people to thank for providing emotional support, endless laughter, and an escape from the PhD itself. Firstly, to all residents of Ranelagh Gardens - you shattered the PhD stereotype, given me life long friends and memories I shall hold dear for many years to come. To all those who attended Tenovus and CCI coffee breaks, I have never been so embarrassed but equally entertained by the events and conversations. They made those horribly long stressed days within the lab that little bit easier. To my old friends and new, you have all constantly reminded me that I was more than the PhD and helped maintain my sanity more than you would ever appreciate. Finally, I would like to thank my family. Although you have never understood what I do, your support has been unwavering and I would have never been able to reach this milestone without any of you.

Abbreviations and definitions

2-ME	β-mercaptoethanol
6G	6G11 hIgG1
6Q	6G11 hIgG1 N297Q mutation
ACK	Ammonium-Chloride-Potassium
ADA	Anti-drug antibody
ADC	Antibody-drug conjugate
ADE	Antibody-dependent enhancement
ADCC	Antibody-dependent cellular cytotoxicity
ADCP	Antibody-dependent cellular phagocytosis
Ag	Antigen
ahIgG	Heat-aggregated IgG
AID	Cytidine deaminase
ALL	Acute lymphocytic leukaemia
AO	Acridine orange
APC	Antigen presenting cell
Asn	Asparagine
AUC_{0-t}	Area under the curve
BCR	B cell receptor
BRCA	Breast cancer associated gene
BSA	Bovine serum albumin
BMDM	Bone marrow derived macrophage
Btk	Bruton's tyrosine kinase
C	Constant region
C1q	Complement component 1q
CDC	Complement-dependent cytotoxicity
cDNA	Complimentary DNA
CDR	Complementary determining region

CFSE	Carboxyflourescin succinimidyl ester
C_H	Constant heavy chain domain
CHO	Chinese hamster ovary
CL	Clearance
C_L	Constant light chain domain
CLL	Chronic lymphocytic leukaemia
CNV	Copy number variation
CO_2	Carbon dioxide
CTL	Cytotoxic T lymphocyte
CTLA4	Cytotoxic T-lymphocyte-associated protein 4
DC	Dendritic cell
DCD	Direct cell death
DC-SIGN	Dendritic Cell-Specific Intercellular adhesion molecule-3-Grabbing Non-integrin
DEREG	diphtheria toxin receptor-FOXP3
DMEM	Dulbecco's Modified Eagle Medium
DLBCL	Diffuse large B cell lymphoma
DR5	Death receptor 5
E.coli	Escherichia coli
ECP	Eosinophil cationic protein
EDTA	Ethylenediaminetetraacetic acid
EGFR	Epidermal growth factor receptor
EGTA	Ethylene glycol tetraacetic acid
ES cells	Embryonic stem cells
ELISA	Enzyme-linked immunosorbent assay
EU	European Union
F(ab)	Fragment antigen binding
FACS	Fluorescence-activated cell sorting
Fc	Fragment crystallisable
FcαR	Fc alpha receptor
FcδR	Fc delta receptor
FcϵR	Fc epsilon receptor
FcγR	Fc gamma receptor
FcRn	Neonatal Fc receptor
FCS	Foetal calves serum
FDC	Follicular dendritic cell
Fgl2	Fibrinogen-like 2

FL	Follicular lymphoma
FSC	Forward scatter
GC	Germinal centre
GlcNAc	N-acetylglucosamine
GPI	Glycolphosphatidylinositol
GvHD	Graft versus host disease
h	Human
HAT	Hypoxanthine-aminopterin-thymidine
HC	Heavy Ig chain
HER2	Human epidermal growth factor-2
hFcγRIIB Tg	Human FcγRIIB ITIM wild-type mouse
HGPRT	Hypoxanthine-guanine phosphoribosyltransferase
HPLC	High performance liquid chromatography
HPV	Human papilloma virus
HIV	Human immunodeficiency virus
HRP	Horse radish peroxidase
HSC	Haematopoietic stem cell
I.P	Intraperitoneal
I.V	Intravenous
ICOS	Inducible T-cell Co-Stimulator
IFN	Interferon
Ig	Immunoglobulin
IL	Interlukin
iLN	Inguinal lymph node
ITAM	Immunoreceptor tyrosine-based activatory motif
ITIM	Immunoreceptor tyrosine-based inhibitory motif
ITSM	Immunoreceptor tyrosine-based switch motif
ITAMi	ITAM mediated inhibitory signalling
ITP	Immune thrombocytopenic purpura
IVIG	Intravenous immunoglobulin
J	Joining region
K_A	Affinity constant
KIR	Killer Ig-like receptor
KO	Knockout
LC	Light Ig chain
LPS	Lipopolysaccharide

LSE	Liver sinusoidal endothelium
LSEC	Liver sinusoidal endothelial cell
LTC	Leukotriene
m	Mouse
mAb	Monoclonal antibody
MAC	Membrane attack complex
MCL	Mantle cell lymphoma
m-CSF	Macrophage colony-stimulating factor
mFcγRII KO	Mouse FcγRII knockout mouse
MFI	Mean fluorescence intensity
MHC	Major histocompatability complex
MO	Monocyte
MS	Multiple Sclerosis
Mw	Molecular weight
Mϕ	Macrophage
NfκB	Nuclear factor kappa-B
NHL	Non-Hodgkin's lymphoma
NK cell	Natural killer cell
NMR	Nuclear magnetic resonance
NOD	Non-obese diabetic
NoTIM	Human FcγRIIB ITIM mutant mouse
NSCLC	Non-small cell lung carcinoma
NSG	NOD-SCID-IL2R gamma null
OVA	Ovalbumin
PBS	Phosphate buffered saline
PCD	Programmed cell death
PCR	Polymerase chain reaction
PD-1	Programmed cell death protein 1
PD-L1	Programmed cell death protein ligand 1
Phe	Phenylalanine
PI	Propidium iodide
PI3K	PI-3-Kinase
PIP_2	Phosphatidylinositol 4,5-bisphosphate
PIP_3	Phosphatidylinositol 3,4,5-trisphosphate
PLCγ	Phospholipase C gamma
Prkdc	Protein kinase DNA activated catalytic polypeptide

PRR	Pattern recognition receptors
r	Rat
RAG	Recombination activating gene
RBC	Red blood cell
ROS	Reactive oxygen species
RPMI	Roswell Park Memorial Institute medium
RTX	Rituximab
S.C	Subcutaneous
ScFv	Small chain variable fragment
SCID	Severe combined immunodeficiency
SD	Standard deviation
SDS-PAGE	Sodium dodecyl sulfate polyacrylamide gel electrophoresis
SHIP	SH2 domain-containing inositol 5'-phosphatase
SHP-1	Src homology region 2 domain-containing phosphatase-1
SIC	Small immune complex
SLE	Systemic lupus erythematosus
SPA	Single peanut allergen
SSC	Side scatter
T:NT	Target:Non-target ratio
$t_{1/2}$	Half-life
TAM	Tumour associated macrophages
TBS	Tris-buffered saline
TCL1	Eμ- T cell leukemia-1 oncogene
TCR	T cell receptor
TD	T cell dependent antigen
Tem	T effector memory cells
Tg	Transgenic
TGF	Transforming growth factor
T_h cell	T helper cell
TI	T cell independent antigen
TIGIT	T cell immunoreceptor with Ig and ITIM domains
TIL	Tumour infiltrating lymphocyte
TIM-3	T cell immunoglobulin and mucin-domain containing-3
TLR	Toll-like receptor
TNF	Tumour necrosis factor
TNFR	Tumour necrosis factor receptor

TPA	2-O-tetradecanoylphorbol-13-acetate
TRAIL	TNF-related apoptosis-inducing ligand
TRIM21	Tripartite motif-containing protein 21
T_{reg} cell	T regulatory cell
Tyr	Tyrosine
UV	Ultraviolet
VDJ	Variable-Diversity-Joining
V_H	Variable heavy chain domain
V_L	Variable light chain domain
VEGF	Vascular endothelial growth factor
V_z	Volume of distribution
WT	Wild type
β-sheet	Beta sheet
γ-chain	IgG heavy chain
κ-chain	Kappa light chain
λ-chain	Lambda light chain

Chapter 1

Literature review

The study of immunology has led to an understanding of how the immune system functions and what leads to dysfunction and disease. Immunological responses are complex and coordinated across multiple cell types mediated through interactions of numerous molecules with their cognate receptors in order to protect the host from pathogens and malignant cells. The work in this thesis aims to dissect how one such receptor, the human inhibitory Fc gamma Receptor (FcγR) IIB, modulates Immunoglobulin G (IgG) antibody effector functions. Specifically, it concerns whether inhibitory signalling is important for the function of FcγRIIB and how this knowledge can be harnessed to improve monoclonal antibody (mAb), immunotherapy of cancer. This literature review will concern the generation of the immune response, the critical role antibodies play in immunity, the importance of FcγRs and how FcγRIIB modulates antibody immunotherapy in the context of cancer.

1.1 Cancer and the immune system

The lifetime risk of getting cancer in the UK has increased dramatically within the past 50 years; those born in in the 1930s were predicted to have a 1 in 3 chance of being diagnosed with some form of cancer in their lifetime. It is now predicted that those born since 1960 will have a 1 in 2 chance [1]. A unifying characteristic between all cancers is the presentation of an uncontrolled, malignant proliferation of cells. Nevertheless, cancer is a collection of over 200 different diseases that has historically been classified by cell type and tissue of origin. Advances in genomic sequencing, transcriptomics and epigenetics

has led to the recognition of still greater tumour heterogeneity, diversity and complexity which makes treating cancer a formidable challenge [2].

Despite this heterogeneity, at the turn of the century, Hanahan and Weinberg described six fundamental properties of all cancerous cells that must typically be acquired in order to become malignant [3]. These hallmarks include: Self-sufficiency in growth signals, insensitivity to anti-growth signals, evading apoptosis, limitless replicative potential, sustained angiogenesis, tissue invasion and metastasis. Ten years later, a further two hallmarks were identified: reprogramming of energy metabolism and evasion of immune destruction [4]. These eight hallmarks unify all cancers and underline the complexities of tumour development.

Genomic instability is the foundation of tumourigenesis and is considered to underpin the hallmarks of cancer. A diverse number of factors drive genomic instability which include lifestyle choices (such as diet, smoking and alcohol [5]), to inherited genetic mutations (such as those found in the breast cancer associated BRCA1 and BRCA2 tumour suppressor genes [6]) and exposure to viral infections (most commonly associated with cervical cancer and infections with human papilloma virus [HPV] 16 & 18) [7]. These cells then harness alterations and mutations that give them a selective advantage over their healthy counterparts and allow them to selectively detect and expand. However, these mutations also provide an opportunity to selectively detect and target cancerous cells.

As described above, immune evasion was recently highlighted as one of the eight steps required for cancer development and understanding the biological processes that drive evasion have in some instances led to successful therapeutic intervention. The field of cancer immunology has become of paramount interest to academia and industry in the development of next generation immune-oncology therapeutics. This is because a substantial body of evidence points to an interplay between both the innate and adaptive immune system and cancer that results in the detection and destruction of tumours. Nevertheless, strong experimental evidence also now indicates that tumours can evade the immune system and even co-opt it into promoting a tumourigenic environment (Figure 1.1) [8]. Such mechanisms include the recruitment of innate immune cells (e.g. tumour associated macrophages [TAMs]) to create a proliferative tumour microenvironment that is suppressive to adaptive immune cells (e.g. T cells) to enhance tumour survival [9]. If the immune system could be re-activated to target cancerous cells this may lead to effective and highly specific treatments which are likely to be less toxic than current chemother-

apeutic approaches. Such approaches have been used clinically for the past decade, but the field is still very much in it's infancy. Whilst some patients who have responded to immunotherapy show robust tumour regression and even remission, there are still a significant number who do not respond to treatment, and those who do respond can also have (sometimes fatal) immune toxicities [10] [11]. Therefore, a greater understanding of the immune system in general and the perturbations made by cancer and immunotherapy is required to allow the development of further safe and effective immune-based treatments.

Evidence for the interplay between the immune system and cancer was generated from a number of key experiments over the past 40 years. One pivotal study involved knocking out recombination activating gene-1 (RAG1) and recombination activating gene-2 (RAG2) in mice. RAG1 and RAG2 are critical for allowing the adaptive immune system to able to respond to a wide repertoire of antigens [12], with the loss of RAG1 and RAG2 evoking a loss of mature T and B cells within these mice [13]. Results showed that these mice were significantly more likely to develop chemically induced and spontaneous tumours than their wild type (WT) counterparts [13]. These studies were further extrapolated to humans when epidemiological studies found those who were immunologically compromised due to human immunodeficiency virus (HIV) or acquired immunodeficiency syndrome (AIDS) had higher incidences of cancer than the general population [14] [15]. Further research indicated that this immune surveillance is a key process in preventing carcinogenesis and that it in immune-competent individuals cancers develop through evading this process. The co-evolution of the immune system and the tumour also provides the possibility for "immune-editing" whereby the immune system deletes the most immunogenic cells, leaving behind those with lower immunogenicity, which paradoxically therefore are more likely to escape ongoing immune surveillance [8]. This lowered immunogenicity can be achieved through a number of tumour-mediated processes such as increased shedding of major histocompatibility complex (MHC) receptors or the decreased expression of β2-microglobulin to downregulate presentation of tumour antigens (Ag). Critically, complete loss of MHC expression would drive Natural Killer (NK) cell mediated depletion, so there would be a selection pressure to maintain a certain level of MHC expression [16]. Other mechanisms of lowering immunogenicity include up regulation of inhibitory receptors such as programmed cell death protein 1 [PD-1]) and the down-regulation of inflammatory molecules that alert and stimulate the immune cells (e.g. interferon-γ [IFN-γ]) [8]. This overall evolution between cancer and the immune system has been described as cancer immuno-editing and progresses through three stages – elimination, equilibrium and escape (Figure 1.1).

To fully appreciate how cancer co-opts and evades immune destruction, it is critical to understand the immune system and how it safely disposes of threats to the host.

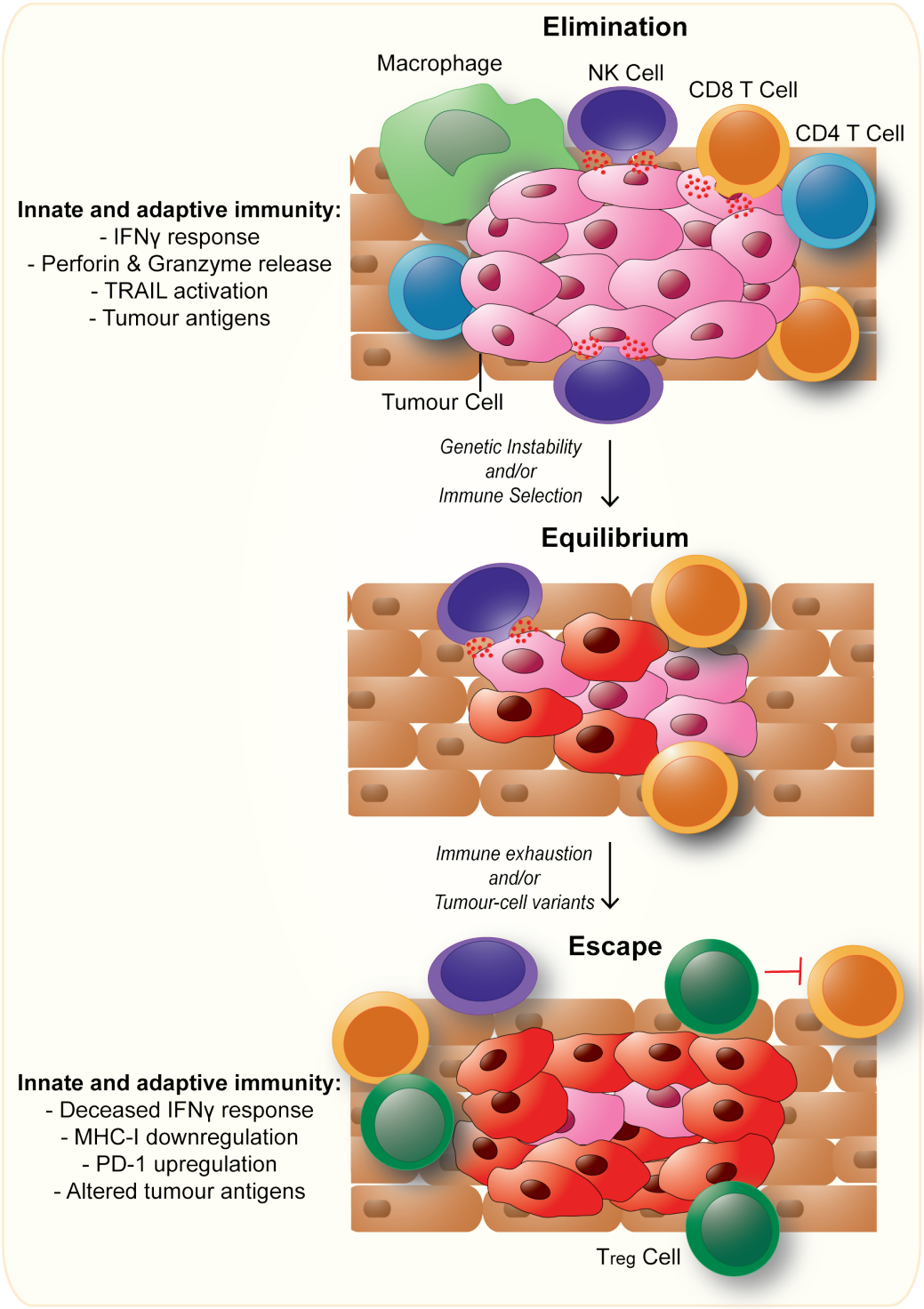

Figure 1.1: The process of cancer immuno-editing
The heterogeneous cancer population present immunogenic markers which indicate to the immune cells (Effector $CD4^+/CD8^+$, NK [natural killer] cells, macrophages etc.) that these cells are mutated self, resulting in destruction of these cells – Elimination. When this immunogenic population is removed it puts a selection pressure on the less-immunogenic population that allows these cells to grow alongside the immune system by suppression, in a state of equilibrium. These less immunogenic cells may then create a further immunosuppressive environment that inhibits the actions of the immune system and allows them to finally grow unchecked – this is known as escape. Adapted from Dunn et al [17].

1.2 The immune system

The fundamental purpose of the immune system is to defend the host or 'self', against a pathogen or 'non-self' which includes damaged and malignant cells [18]. This function is achieved through a myriad of differentiated cell types, chemical mediators and immune molecules that enable the host to maintain homeostasis. The immune system is a complex and dynamic cellular network that achieves its function through the innate and adaptive immune system which in turn can provide both short and long term protection. A fine balance is achieved through the elimination of pathogens and dysregulated host cells, whilst limiting excessive or unwanted damage and maintaining tolerance to self. Perturbations to this balance can result in an array of disorders such as allergies, autoimmune diseases, immunodeficiency and cancer [18]. The host is constantly challenged by environmental insults that work through a broad range of pathogenic mechanisms and the immune system utilises a range of protective mechanisms to control or remove the insult. The first line of defence relies on the innate immune system.

1.2.1 Innate immunity

On the front line of defence are the physical barriers provided by skin and the mucosal layers which help keep a broad range of pathogens from entering the body. Within these mucosal surfaces and within the circulation are secreted bioactive molecules such as defensins and complement proteins which have a broad spectrum of activity against pathogens and can provide a response [19]. These molecules can interact with the cellular aspect of the innate immune system to launch a coordinated attack with the aim of neutralising or controlling an infection until an adaptive immune response can be mounted. The innate immune system is genetically hard-wired to recognise conserved molecular patterns that are shared by many pathogens but are not present within the host. These molecular patterns are recognized by a series of secreted molecules and receptors expressed on various immune cells. For example, pattern recognition receptors (PRR) are found mainly on innate immune cells and can detect common pathogenic molecules such as lipopolysaccharide (LPS) through toll-like receptor 4 (TLR-4) and single-stranded RNA by TLR-7 [20]. PRR-ligand binding results in the activation of cells such as neutrophils and macrophages, triggering a potent cellular response that can result in the immediate release of molecules toxic to the pathogen and recruitment of further immune cells to

the site of infection. For example, the release of interleukin 8 (IL-8) can recruit neutrophils whilst IFN-γ can inhibit viral replication [21] [22]. Innate immunity provides an antimicrobial and tissue-protective function, however it lacks the ability to recognise diverse antigens outside those hard-wired in the genome and it does not elicit immunological memory [23]. Innate immune cells can trace their lineage from haematopoietic stem cells (HSCs) which differentiate into cells such as monocytes, macrophages, dendritic cells (DCs), neutrophils and NK cells [19]. Further detail on key innate immune cells and their development can be found in Table 1.1 and Figure 1.2.

1.2.1.1 Monocytes

Monocytes are a heterogeneous population of cells which can initiate inflammation, phagocytose particles, act as antigen-presenting cells (APCs) and infiltrate tissues to terminally differentiate into DCs and macrophages [24] [25]. Human monocytes can be characterised into three main populations: classical (cluster of differentiation 14 $(CD14)^{++}$, $CD16^{-}$), non-classical ($CD14^{+}$, $CD16^{++}$) and intermediate ($CD14^{++}$, $CD16^{+}$), each subset has differing gene expression and functions [26]. Murine monocytes are defined by their expression of the cell surface marker Ly6C; human classical monocytes are analogous to Ly6C high populations and human non-classical monocytes are analogous to Ly6C low populations [26]. Classical monocytes are considered to be migratory; they rapidly enter tissues under inflammatory conditions and differentiate into macrophages or DCs. Non-classical monocytes are thought to be accessory cells of the vascular endothelium and arise from classical monocytes. They are considered to have a more suppressive role, such as participating in the clearance of dying/infected cells during wound healing [27]. Monocytes are recognised as a functionally diverse population, able to differentiate into populations of tissue macrophages, DCs and osteoclasts based on the needs of the local immune environment [28].

1.2.1.2 Macrophages

Macrophages are the main phagocytic cell of the immune system. They can also release cytokines, take part in tissue immunosurveillance and maintain tissue homeostasis through the clearance of damaged cells and tissue remodelling [23]. Macrophages express a wide variety of cellular receptors that allow them to sense and respond to

their environment, resulting in diverse and seemingly opposing functions. For example, macrophages can create an inflammatory environment in response to a pathogen. Once the pathogen is cleared, these same macrophages can dampen the immune response to limit tissue damage and promote a wound healing environment [23]. The differential activation of macrophages is driven by their transcriptional and epigenetic plasticity. This plasticity gives rise to many macrophage subtypes such as microglia, Kupffer cells and alveolar macrophages, each occupying a different physiological niche [29]. Due to their diverse nature and involvement in homeostasis, macrophages have also been implicated in several diseases including neurodegeneration, liver fibrosis and cancer [30].

An extensive body of research has conducted in murine models to understand the origins of tissue resident macrophages. Broadly, development begins within the extra-embryonic yolk sac, where both progenitor cells and resident macrophages develop and migrate to colonise their respective tissues which happens prior to the development of monocytes [31]. Macrophages that occupy niches such as the kidneys and liver have a high proliferative capacity, enabling self-renewal. Microglia are the only tissue resident population that are maintained from primitive haematopoiesis throughout adulthood [31].

As previously mentioned, tissue-resident macrophages support a diverse number of functions and therefore each population have a unique set of receptors tailored to the tissue of origin. For example one family of receptors, FcγRs, show differential receptor expression dependent on the tissue-resident macrophage. Human Kupffer cells were found to express moderate levels of FcγRIIA and FcγRIIB, high levels of FcγIII and little to no FcγRI whilst alveolar macrophages express moderate levels of FcγRIIA, high levels of FcγRI and FcγRIII with no expression of FcγRIIB [32]. In contrast mouse tissue was found to have a different expression compared to humans, with murine Kupffer cells expressing relative low levels of FcγRI, FcγII, FcγRIII with moderate expression of FcγRIV whilst murine alveolar macrophages were found to express moderate levels of FcγRI, FcγRII, FcγRIII and FcγIV [33].

in vitro, macrophages can be differentiated and generally characterised as either M0, M1 or M2. Macrophages in the quiescent state (i.e. not further activated) are described as M0. Exposure to IFN-γ and LPS polarises macrophages into an M1 phenotype, whilst exposure to IL-4 and IL-13 polarises them into an M2 phenotype - two extreme poles of a broad spectrum of phenotypes and activity [34]. M1 macrophages are typically pro-inflammatory whilst M2 macrophages are linked to tissue repair and immunosuppression.

The activation state of a macrophage is ultimately driven by the stimuli they are exposed to which can be complex and diverse. In addition, macrophages do not terminally differentiate, they can switch between states based on their microenvironment [34].

Component	Characteristics	Location
Mast cell	Dilates blood vessels, induces inflammation via histamine + heparin. Involved in wound healing, pathogen defence and allergic reactions	Connective tissues, mucosal membranes and peripheral blood
Macrophages	Phagocytic cell, consuming pathogens, apoptotic cells and cancerous cells. Involved in antigen presentation cytokines release as well as tissue remodelling and homeostasis	Tissues contain resident macrophages. Monocytes can be recruited and differentiate at the tissue
NK cell	Surveys all cells, eliminates those identified as non-self - typically through the loss of major histocompatibility (MHC)-I-inhibitory killer Ig-like (KIR) receptor interaction. Efficient at targeting virally infected and cancerous cells, these are destroyed through the release of cytolytic enzymes	Circulating in blood and lymphatic system. Also present in bone marrow, liver, uterus, spleen and lungs
Dendritic cell	Professional antigen-presenting cells. DCs are efficient at sensing their environment and capturing antigens. These antigens are then processed and presented to cells of the adaptive immune system to drive a potent immune response	Heterogeneous population found mainly in epithelial tissues. they migrate to lymph nodes upon activation
Monocyte	Differentiate into macrophages and DCs in response to inflammation. Involved in phagocytosis, antigen presentation and cytokine production	Migrates through blood vessels to infected tissues
Neutrophil	Phagocytic cells. First responders to infection/trauma. Releases toxins to kill/inhibit bacteria and fungi and recruits other immune cells to the site of infection	Circulates in blood vessels, migrates to tissues when infected
Basophil	Share many similarities with mast cells and are key to providing defenses against parasites. Releases histamine, leukotriene $(LTC)_4$ and IL-4	Circulates in blood vessels, migrates to tissues during infection
Eosinophil	Releases toxins that kill bacteria, nematodes and parasites. Unique in their ability to produce cytotoxic proteins such as eosinophil cationic protein (ECP). Implicated in allergic reactions such as allergic asthma	Circulates in blood vessels, migrates to tissues when infected
$\gamma\delta$ T cells	Activated in an MHC-independent manner. Recognise microbial, cellular stress markers and lipid antigens. Recognition results in lysis of target cells, release of cytokines and chemokines	Produced in the thymus, found enriched in epithelial and mucosal tissues
Complement	A protein system that enhances the ability of antibodies and phagocytic cells to clear microbes and damaged cells and promotes inflammation. The complement cascade results in the production of the membrane attack complex (MAC)	Produced in the liver, circulates in the blood as inactive precursors

Table 1.1: Key immune components of the innate immune system.
Adapted from Murphy et al [19].

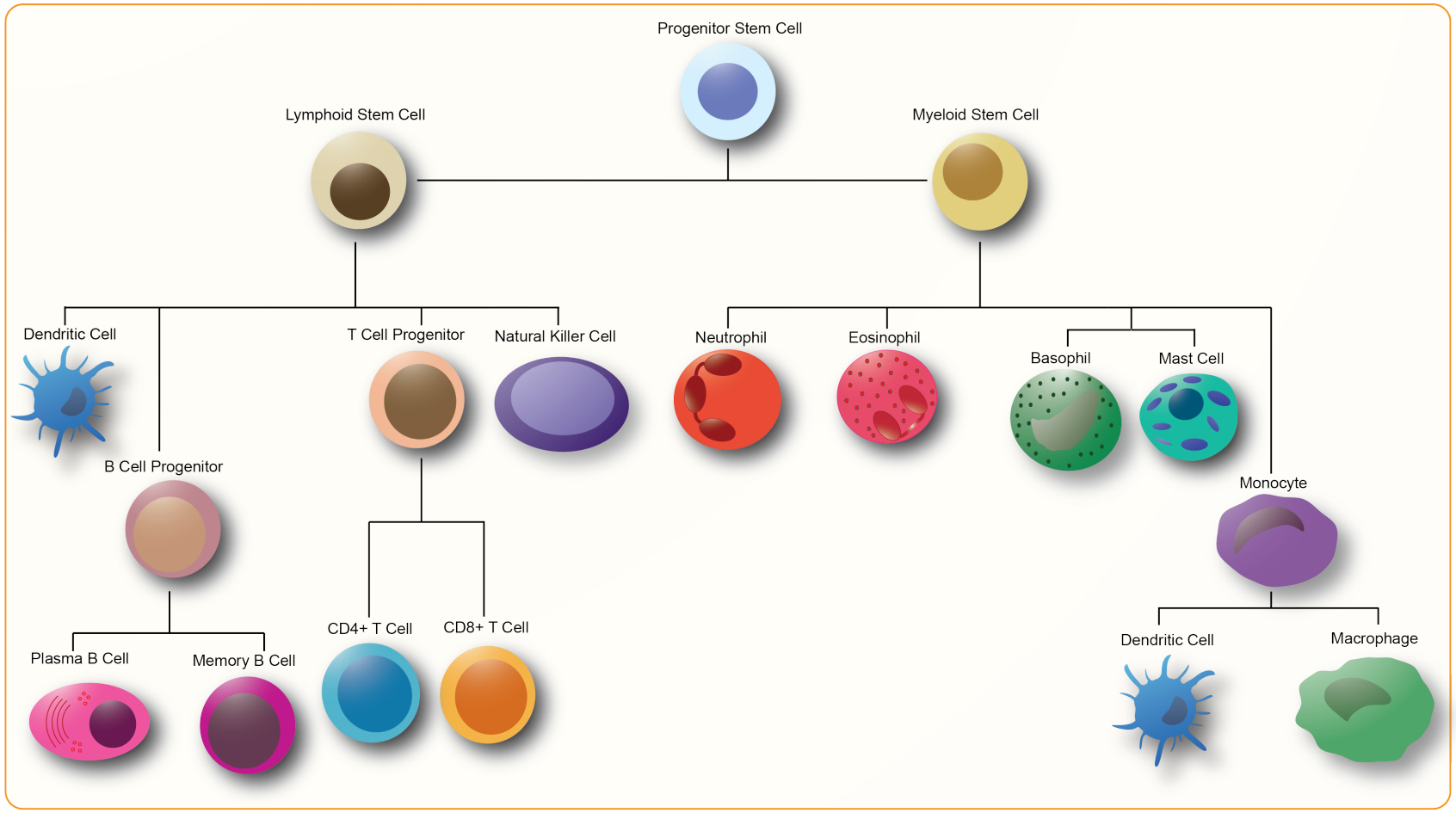

Figure 1.2: The Development of the innate and adaptive immune system
All immune cells are generated from haematopoietic stem cells (also known as progenitor stem cells) which can differentiate into a lymphoid stem cell or a myeloid stem cell. The lymphoid population terminally differentiates into B cells, T cells natural killer cells and DCs. The myeloid population differentiates into neutrophils, eosinophils, basophils, mast cells, monocytes, DCs and macrophages. Adapted from Murphy et al [19].

1.2.2 Adaptive immunity

The innate immune system operates as the first line of defence against pathogens to either prevent their entry or to destroy them. If this fails, it works to contain and/or control the spread of the pathogen. This enables the adaptive immune system to spend time generating a highly specific response towards pathogen-specific antigens and produce long term immunological memory. This immunological memory ensures that subsequent encounters with the same antigen activate a rapid and robust protective response [35]. T and B cells form the adaptive immune system, they comprise a highly specific and potent set of cells that can detect a wide repertoire of different antigens. In mammals, T and B cells are generated from HSCs and mature within either the thymus (T cells) or bone marrow (B cells) (Figure 1.2). Each cell expresses a specific antigen recognition receptor that is capable of recognising virtually any potential target [35].

1.2.2.1 T cells

A naïve T cell migrates from the bone marrow and matures in the thymus, where it generates a T cell receptor (TCR) specific for a MHC-peptide complex. The TCR is generated through variable-diversity-joining (VDJ) gene rearrangement creating a repertoire of receptors that can recognise a diverse range of MHC-peptide complexes [35]. The TCR consists of an α and β chain. The TCRα chain genetic locus contains multiple V and J gene segments, whilst the TCRβ chain genetic locus contains multiple V, D and J segments. These segments undergo gene rearrangement within the thymus to generate a unique TCR expressing particular VD and VDJ combinations. The TCR associates with CD3 and a homodimeric ζ chain to mediate intracellular signalling. Once generated, the TCR can either interact with loaded MHC-I, which binds cytosolic peptides or MHC-II, which loads peptides presented from the endosome or lysosome [36]. When the TCR engages its cognate MHC/peptide complex it initiates a signalling cascade that results in the activation of transcription factors (such as NfκB [37]) and changes in gene expression.

For full T cell activation, co-stimulatory signalling is also required. The classical T cell two signal hypothesis involves TCR-MHC interactions (signal one) as well as the engagement of molecules such as CD28 on T cells with its ligand B7-1 (signal two) on APCs [38]. T cell activation can create a highly inflammatory environment, hence regulation is required to ensure a controlled and directed T cell response. CTLA-4, a co-inhibitory receptor

expressed on T cells, also interacts with B7-1 [39]. CTLA-4 has a higher affinity for B7 and thus if expressed it can outcompete CD28 and will inhibit signal two. Discovery of the CD28:CTLA-4/B7 axis shed light on the highly complex regulation of T cell activation [40]. A diverse family of activatory (ICOS, OX40, CD27, 4-1BB and CD40) and inhibitory (PD-1, TIM-3, TIGIT and LAG3) receptors have since been identified. The balance of expression and engagement of co-stimulatory and co-inhibitory molecules on the surface of a T cell fine-tunes their response and in doing so sculpts the immune response to eliminate the pathogen whilst protecting the host. Many of these inhibitory and co-stimulatory molecules are currently under investigation as potential targets for immunotherapy to either enhance or suppress immune activation [40] [41].

Through signalling from these and other receptors, T cells can differentiate into a number of diverse subsets, such as effector $CD4^+$, effector $CD8^+$ and regulatory T cells (T_{reg} cell). Terminal differentiation into CD4 or $CD8^+$ cells is determined during T cell development and is based on the ability of the TCR to bind efficiently to either peptide loaded MHC-I (CD8) or MHC-II (CD4). T_{reg} cells can be induced by exposure to cytokines such as transforming growth factor-beta (TGF-β) or develop in the thymus in response to self-peptide and activation of co-stimulatory molecules [42].

Effector $CD4^+$ T cells (T helper cells [T_h cells]) engage with and are activated by MHC-II complexes in the presence of 11-30 amino acid peptides presented by APCs [43]. T_h cell activation can in turn can activate effector $CD8^+$ cells and provide signal two to B cells, driving the adaptive immune response [44]. T_h cells can differentiate into several lineages dependent on the cytokine profile they are exposed to - some are inflammatory such as T_h1 which release cytokines such as IFN-γ, IL-2 and tumour necrosis factor-alpha (TNF-α). Others can be considered immuno-suppressive such as T_h2 cells which release IL-10 and TGF-β [45].

$CD8^+$ T cells, also known as cytotoxic T lymphocytes (CTL), can elicit target cell death after recognising MHC-I loaded with peptides of 8-15 amino acids presented by nucleated cells [46]. Cell death is achieved through the release of granzymes and perforins into the target cell. Additionally, CTLs can trigger receptor-mediated apoptosis (e.g. via the Fas receptor) and release several cytokines (e.g. TNF-α, IFN-γ) to recruit innate and adaptive immune cells to create an inflammatory environment [47].

Both T_h cells and CTLs can form memory T cells that are long-lived and have immunological memory for the specific antigen that they developed as a naïve T cell. If this antigen is

re-introduced to the T cell, it can proliferate rapidly and mount a strong immune response [48]. Due to the magnitude of cell death and inflammation that can be induced by T cells, they can have detrimental effects on surrounding healthy tissues and therefore both effector cell types require tight regulation. When this system becomes dysregulated and over activated it can initiate autoimmunity (destruction of self-tissue) or even cytokine release syndrome which is characterised by systemic inflammation, and multi-organ failure [49]. T_{reg} cells are a subset of T cells that can help prevent this dysregulation.

T_{reg} cells are crucial to the regulation of the immune system, they are typically identified as CD4+CD25+FOXP3+ in mice and humans, although multiple types and subsets exist [50]. Physiologically T_{reg} cells serve to downregulate immune responses to non-pathogenic entities like gut flora and are found in chronically inflamed environments [51]. T_{reg} cells can release many immunosuppressive cytokines such as TGF-β and express ligands such as CTLA-4 to maintain an immunosuppressive environment [51]. Manipulation of T_{reg} cells for the treatment of autoimmunity and cancer is an ongoing area of intensive research [52].

1.2.2.2 B cells

B cells are a critical component of humoral immunity. They generate antibodies, secreted Y shaped proteins that are specific to the tertiary and/or quaternary structure of an antigen. Antibodies typically bind with high affinity and specificity, effectively labelling their targets for destruction by the innate immune system. Most B cells initially develop within the bone marrow, specifically from haematopoietic precursor cells [53]. However, B cells come in two broad forms - B1 and B2 lymphocytes. B1 lymphocytes arise from B1 progenitors in the foetal liver whilst B2 lymphocytes develop from B2 progenitors in the bone marrow (Figure 1.3). Like T cells, B cells have an antigen receptor – the B cell receptor (BCR). The BCR, like the TCR, undergoes genetic rearrangement during development to produce a unique receptor on each B cell, able to bind to a diverse range of antigens (approximately $5x10^{13}$ combinations [54]).

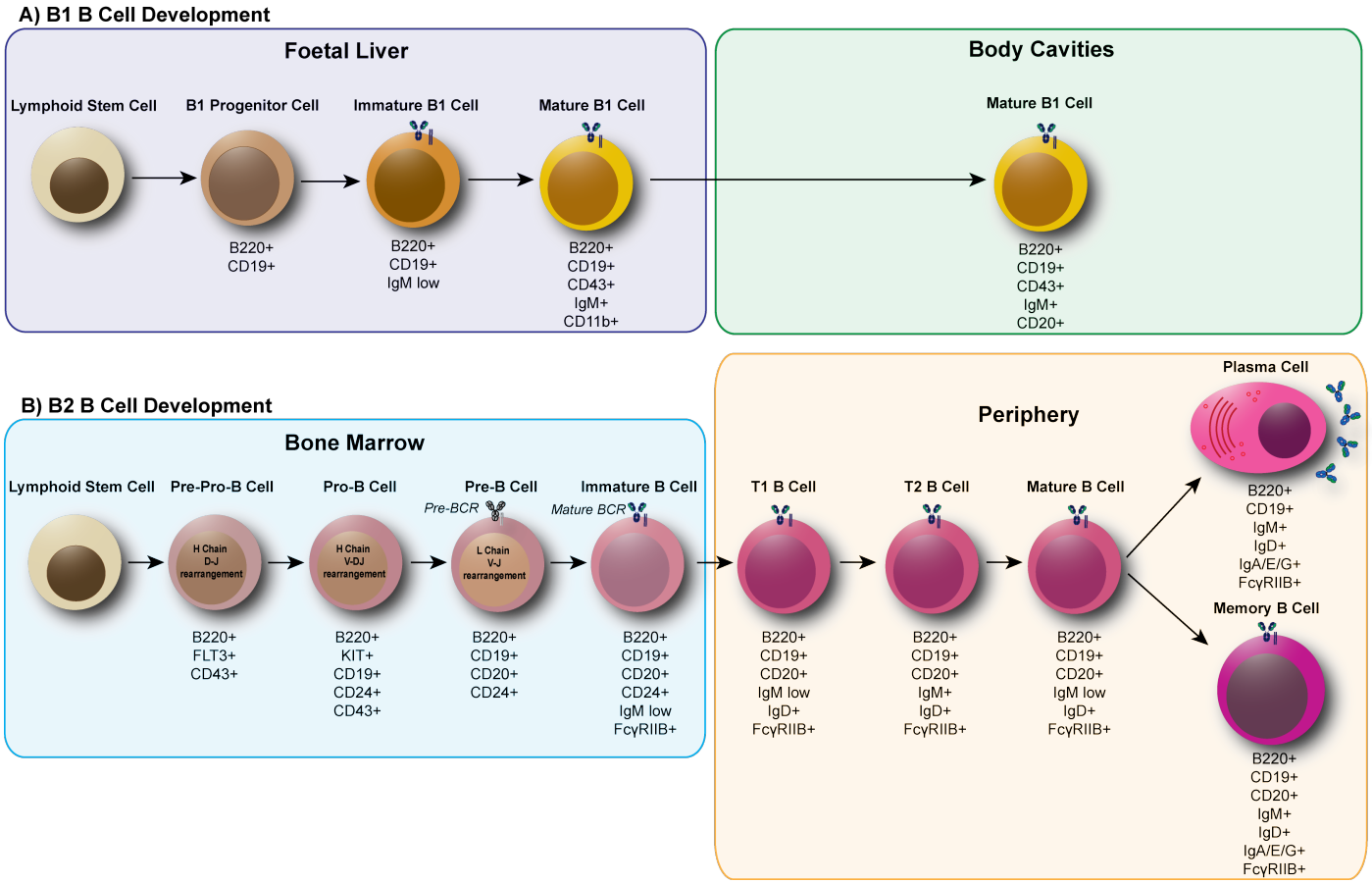

Figure 1.3: The development of B1 and B2 B cells
A) The development of B1 B cells which undergo less developmental stages and have a BCR that can recognise pathogen molecular patterns. B1 B cells provide a quick response but it are less potent, specific and do not evoke memory. B) The development of B2 B cells, which undergo a number of development stages including clonal selection and affinity maturation to produce highly specific non-self BCRs that can produce a potent, memory response. Figure adapted from Nagasawa et al [55], FcγRIIB expression data adapted from Tutt et al [56].

The BCR initially consists of an immunoglobulin (Ig) molecule (initially IgM and/or IgD) composed of two identical heavy and two identical light chains, joined by disulphide bonds. The IgM or IgD is complexed non-covalently with a CD79A (Igα) and CD79B (Igβ) heterodimer which facilitates surface expression and propagates intracellular signalling in the B cells [19]. However, prior to this, multiple stages of gene rearrangement are required. During B cell development the Ig heavy chain undergoes gene rearrangement starting with D-J gene rearrangement, in which random D and J sections are joined together within pre-pro-B cells. This is then followed by V recombination, joined with D-J (V-DJ) which produces a functional Ig heavy chain in pro-B cells [19]. Further sequence variability can be introduced at the joining sites between each segment by the introduction or removal of nucleotide bases by error prone DNA repair mechanisms [57]. A surrogate light chain associates with the heavy chain to produce the pre-BCR, this is then expressed in large pre-B cells. If correctly folded, the pre-BCR traffics to the cell surface and starts signalling, which drives proliferation and differentiation into small-pre-B cells. The light chain gene locus then undergoes V-J recombination, producing a light chain to replace the surrogate light chain. A functioning BCR is then produced, forming an immature B cell (Figure 1.3). Until this stage, development is entirely agnostic of the specificity of the BCR. From this point however, the interaction with antigen is central. For example, if the BCR through its random generation binds to a self-antigen present in the bone marrow, it will signal for the deletion of the B cell (negative selection) [19]. If immature B cells cognate BCR does not bind to self-antigen, it will migrate to the spleen where they differentiate into T1 and T2 B cells. These B cells will then fully mature into follicular or marginal B cells (Figure 1.3). Antigen-BCR binding is required for B cell survival (positive selection), with strong BCR signals supporting maturation to follicular lineages whilst weaker BCR signalling favours differentiation into marginal zone B cells [58]. Follicular B cells will then circulate between secondary lymphoid organs. If they encounter the antigen specific for their BCR, they will become activated and differentiate into plasma cells and/or memory B cells [54].

BCR signalling is propagated through the CD79A and CD79B heterodimer via their intracellular immunoreceptor tyrosine-based activation motifs (ITAMs). Upon ligation of antigen, the ITAM tyrosine residues becomes phosphorylated and recruit Syk kinase which initiates downstream signalling pathways (For further detail on ITAM signalling please see Section 1.4.3) [59]. The antigen is also internalised and degraded in lysosomes to be presented as peptides on MHC-II to $CD4^+$ T cells. For full B cell activation, a co-stimulatory signal (signal two) is required. This is provided through either T_h cells (via CD40-CD40L interactions) or in the absence of T cells, can be provided by PRRs such as TLR-9 in re-

sponse to unmethylated CpG oligonucleotides [60]. Antigens that elicit a B cell response can be categorised as T dependent (TD) or T independent (TI). TD antigens requires presentation of the antigen along with activation signals from cognate T_h cells which in turn regulate B cell proliferation, antibody production, antibody class switching and generation of B cell memory. In contrast, TI antigens tend to be repetitive glycoproteins, which do not need T lymphocyte interactions and instead only require very strong BCR cross-linking to produce an antibody response [61]. B1 B cells are associated with TI antigen responses whilst B2 B cells are associated with TD antigen responses [58]. TD antigens can initiate the production of antibodies from any class, with high affinity and a memory response. TI antigens generate responses that are typically of one antibody class (IgM), demonstrate modest affinity and have no memory [58]. TI antigens allow B cells to mount a quick response whilst specific TD antigens generate a higher affinity, typically more potent (through higher antibody titres and eliciting stronger effector mechanisms) and longer lasting response [62].

When the BCR of a follicular B cell is activated by a respective antigen within the secondary lymphoid organ, downstream BCR signalling results in an upregulation of activatory receptors and the internalisation of the BCR-antigen complex. The antigen is then internalised, degraded and presented on MHC-II molecules to T follicular helper cells. If the TCR strongly engages the MHC-II-peptide complex, additional activation via CD40-CD40L and CD80-CD28 interactions form an immunological synapse driving strong activatory signals in both T and B cells [63]. This interaction induces the formation of the germinal centre, where B cells undergo proliferation, class switch recombination and somatic hypermutation to produce B cells with the highest affinity BCR (and therefore antibodies) for the respective antigen [63].

The germinal centre is split into the dark zone and the light zone [64]. B cells initially enter the dark zone, where they rapidly proliferate and undergo somatic hypermutation. Here, the enzyme cytidine deaminase (AID) is activated, introducing C:T to A:T or T:A DNA base pair mutations in order to increase the diversity of the variable domain of the BCR, which can increase or decrease the affinity for the cognate antigen [63]. These B cells then enter the light zone of the germinal centre where they are positively selected for high affinity clones. At least in mice, it has been shown that follicular DCs within the light zone trap and retain the unprocessed cognate antigen through receptors such as FcγRIIB, acting as long-term antigen deposits. These are presented to the B cell clones; if there is high affinity binding these clones receive pro-survival signals and continue proliferating. If there

is poor affinity for the antigen, they die due to neglect, typically undergoing apoptosis [65]. Within the light zone, B cells may also undergo class switch recombination, determining the isotype of antibody produced. Class switching also depends on the activation of AID which can be induced by IL-4 and CD40 signalling on the B cell. The final isotype class of the B cell is determined by cytokines produced by T helper cells and DCs [66]. The constant (C) region of the immunoglobulin heavy chain locus is recombined so that the $C\mu$ encoding IgM, is replaced with $C\gamma$, $C\alpha$ or $C\epsilon$ giving rise to IgG, IgA and IgE, respectively [67] (Figure 1.5). Clones may then leave the germinal centre as either a plasma cell or a memory B cell or re-enter the dark zone to undergo further somatic hypermutation (Figure 1.4). It is the plasma cells that then go on to secrete antibodies.

Plasma cells function to provide a high titre of antibody. These terminally differentiated plasma cells produce a highly specific antibody that correlates to the antigen that stimulated the BCR, with production occurring at a rate of approximately 2000 antibody molecules per second [45]. These plasma cells can either be short-lived with a life span of 3-5 days or long-lived, secreting antibody from bone marrow niches with a life span of several months to a lifetime [68] [69]. To ensure a rapid response following re-exposure to a given pathogen or antigen, memory B cells are also produced during the humoral immune response. Memory B cells have several unique properties that include stemness, longevity, robust responsiveness and re-diversification through the germinal centre [70]. The generation of robust memory B cells is critical to the success of vaccination and the production of highly effective antibodies.

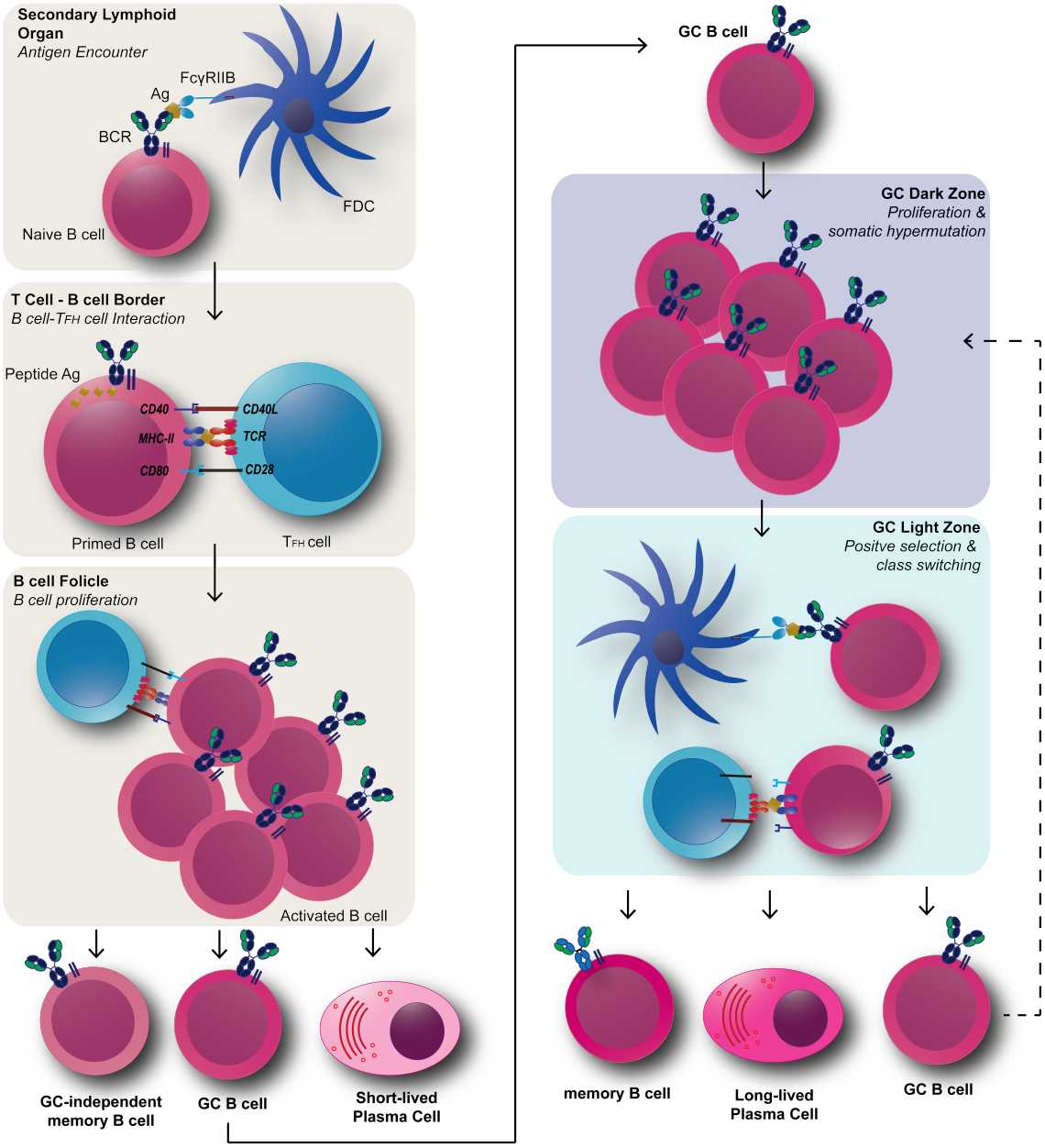

Figure 1.4: The generation of B cell memory
Naive B cells enter secondary lymphoid organs and encounter antigens (Ag) presented by follicular dendritic cells (FDCs) on receptors such as FcγRIIB. The antigen activates the B cell receptor (BCR), is internalised and processed to be presented to T cells via MHC-II at the T cell-B cell border. MHC-II-TCR binding forms signal one, co-stimulation via interactions such as CD40-CD40L and CD80-CD28 forms signal two. This activation causes B cells to proliferate and differentiate forming independent memory B cells, Germinal Centre (GC) B cells or short-lived plasma cells. GC B cells then go on to form the GC and undergo proliferation and somatic hypermutation within the dark zone. GC B cells then enter the light zone where they encounter the antigen presented on FDCs - strong interactions drive pro-survival signalling, whilst weak interactions will cause apoptosis of the B cell. GC B cells also interact with T cells where they receive stimulatory signals and can undergo antibody class switching. GC B cells then exit the GC and either re-enter the Dark zone, or terminally differentiate into memory B cells or long-lived plasma cells. Adapted from Akkaya et al [71].

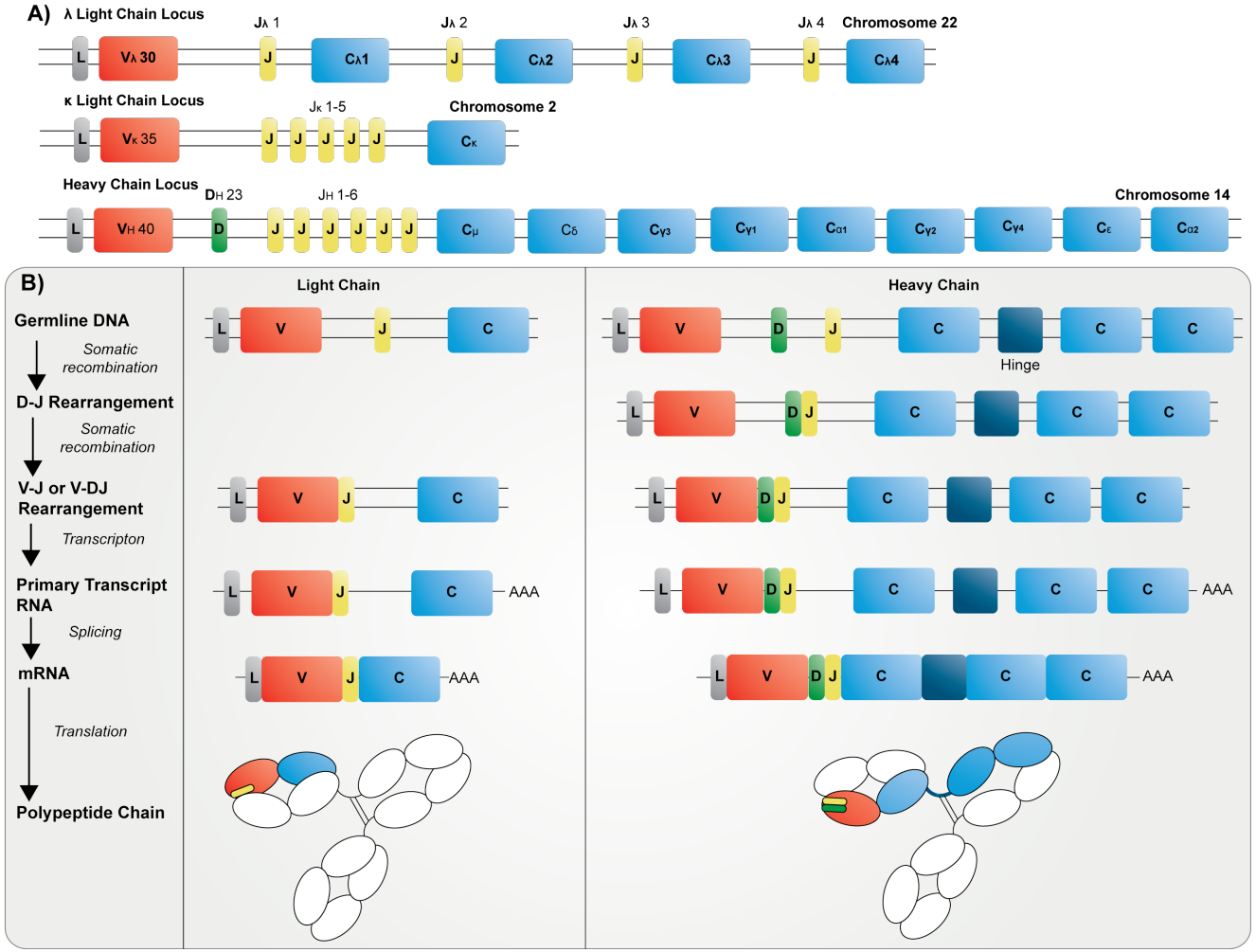

Figure 1.5: The process of VDJ recombination to form an antibody
A) The light chain and heavy chain gene locus for human antibodies. B) The process of VDJ recombination to form a functional antibody. L = leader sequence, V = variable region, D = diversity region, J = joining region, C = constant region. Adapted from Murphy et al [19].

1.3 Antibodies

Antibodies are glycoproteins secreted by plasma cells in response to an antigen. They have several effector mechanisms that enable them to destroy pathogens via interactions with innate immune effector systems [72]. Due to their specificity and efficacy, antibodies underpin multiple clinical and diagnostic applications. Some examples include the induction of active vaccination by the production of an immunological B cell memory response or passive vaccination using serum from convalescent patients. Recombinant mAbs can also be generated for diagnostic purposes such as for pregnancy tests or as targeted therapeutics in diseases ranging from cancer to autoimmunity [72].

1.3.1 Antibody structure

Antibodies are part of the Ig superfamily with a molecular weight of around 150-180 KDa [73]. They are made of two domains, the fragment antigen-binding (F(ab)) responsible for epitope recognition, and the fragment crystallisable (Fc) responsible for the engagement of the immune system [74]. Antibodies are formed of two heavy chains that are linked to the light chains with disulphide bonds and other non-covalent interactions. The light chain is approximately 25 KDa. The N terminus forms the variable region, responsible for epitope binding and the C terminus forms the constant region that can be classed as κ or λ. Not much is known about the influence of κ or λ upon antibody biology, however changes in the ratio of κ:λ have been used to detect human B cell malignancies [19]. The heavy chain is approximately 50 KDa and can consist of either μ, δ, γ, α, or ϵ constant domains held together by an intrachain disulphide bond. Dependent on the isotype, the heavy chain can consist of three or four constant domains, with a hinge to provide flexibility and a variable domain to provide specificity (Figure 1.6).

The V region is the area of the antibody that is responsible for providing its antigen specificity. The light chain and heavy chain V region (V_L and V_H) come together to form six hypervariable loops, known as the complementarity determining regions (CDRs). The V_L and V_H fold to bring three CDR regions together each to create an antigen-binding site – also known as the paratope [75]. The diversity of the paratope is created through the total of the random combination of Ig gene rearrangements (e.g. through VDJ selection and rearrangement) and somatic hypermutation as described earlier (Section 1.2.2.2). These processes result in antibodies with a high affinity and specificity for the resultant epitope.

The bivalent nature of an antibody is another means by which antibodies have increased binding strength for their target through higher avidity. Antibodies can bind to multiples epitopes on one target to enhance binding strength. For example, IgM relies on avidity for it typically binding because it has low-affinity for the epitope on each F(ab) arm, however the multiple binding sites on the pentameric form of IgM gives it high avidity [74] (Figure 1.6).

1.3.2 Antibody isotype

In humans, antibody isotype is dictated by the expression of either μ (IgM), δ (IgD), γ (IgG), α (IgA), or ϵ (IgE) constant chains [74]. Each isotype has a unique structure and function and binds to its cognate ligands such as Fc receptor(s) to elicit function. Each isotype also differs in hinge flexibility, the number of heavy chain constant domains, glycosylation pattern and oligomeric state (Figure 1.6).

IgA is the most abundantly produced antibody isotype within the body and is predominantly found in mucosal secretions such as within the respiratory tract and breast milk [74]. IgA can be found as a dimer associated with a J chain and secretory component in the mucosal regions or as a monomer in serum where it makes up 15% of total Ig [77]. IgA has two subclasses, IgA1 which has a longer and therefore more flexible hinge region, and IgA2. IgA is critical for neutralising or preventing binding of toxins, viruses, and bacteria at the mucosal regions. Serum IgA interacts with its cognate receptor, FcαR, found on myeloid cells such as neutrophils and macrophages [78].

IgM accounts for 5% of total Ig in the serum [77] and is usually found in a pentameric form, linked by a disulphide bond formed between the CH_4 domain of each monomeric unit [74]. The polypeptide J chain (also found in IgA) also binds to two monomers and facilitates secretion at mucosal surfaces by binding to poly Ig receptors [79]. IgM antibodies typically have low affinity as described above, but the pentameric structure gives the molecule high avidity as well as effective opsonisation of targets and complement activation. IgM binds to the FcμR found on B cells to potentiate B cell activation [80].

IgD forms 0.2% of circulating Ig [77] and has a short serum half-life due to its long flexible hinge region leaving it susceptible to proteolysis [74]. The physiological role of IgD has not been determined but has been found to bind to specific bacterial proteins and elicit B

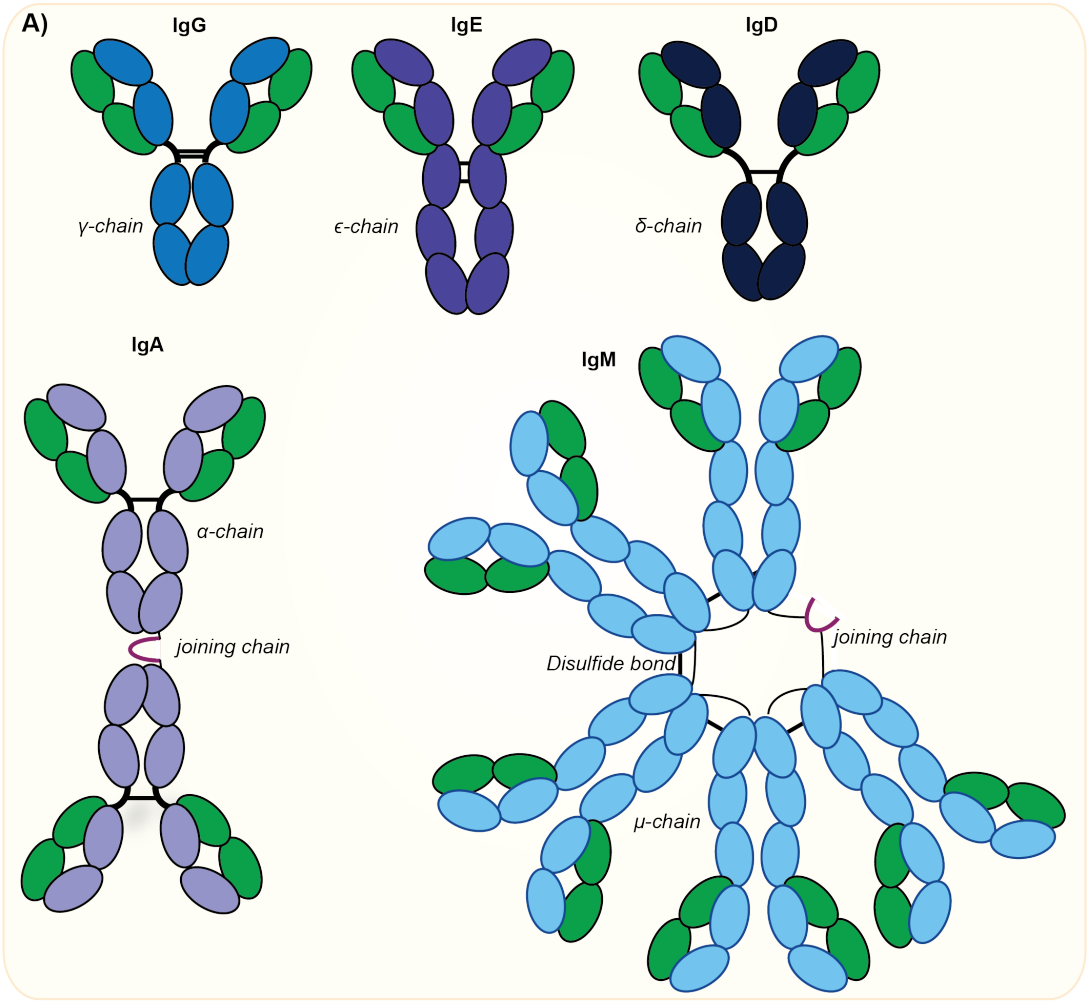

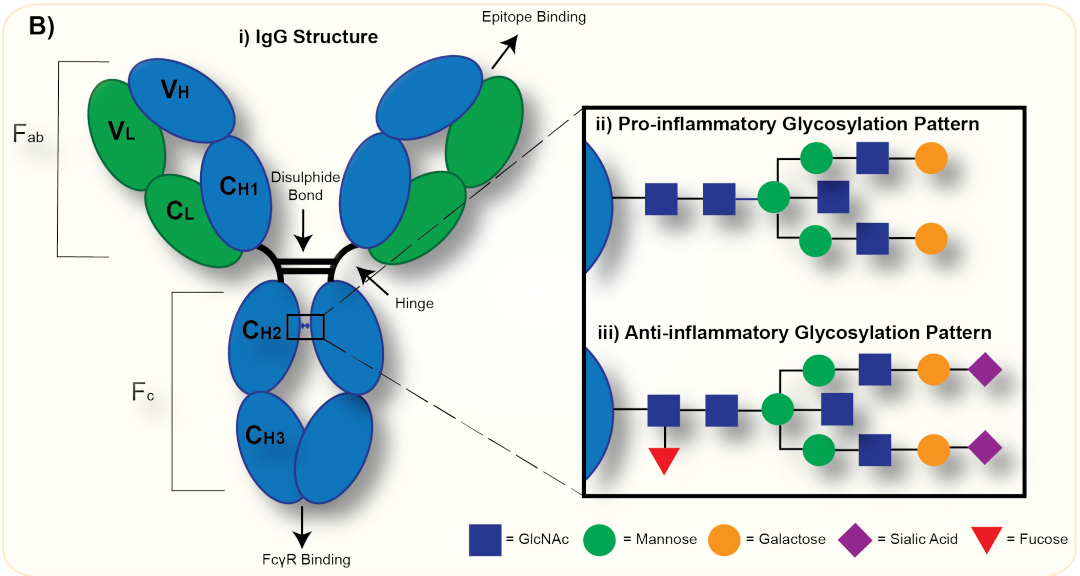

Figure 1.6: Structure of Human Ig Isotypes
A) The structure of different human Ig isotypes. The Light chain is coloured in green, the different coloured heavy chains show the different Ig architecture of IgG, IgE, IgD, IgA and IgM. The J chain is in purple, disulphide bonds in black. B) The schematic of an IgG molecule. i) The heavy chain is shown in blue and light chain in green. ii) The typical glycosylation pattern of a 'pro-inflammatory' antibody. iii) The typical glycosylation pattern of an 'anti-inflammatory' antibody. Endogenous antibodies have shown up to 30 different glycan profiles Adapted from Shade et al [76].

cell stimulation via FcδR [81]. IgD is also found in the membrane of B cells where it forms part of the BCR on mature B cells, it is often co-expressed with IgM.

IgE has the lowest serum concentration at 0.05% and has the shortest serum half-life, however its effector functions are very potent. IgE is thought to be produced in response to allergens and parasitic worm infections. It binds to FcϵRI with such high affinity it effectively remains bound to the receptor without the need to first bind antigen. When it encounters an antigen, it results in the degranulation of basophils, eosinophils, mast cells and Langerhans cells to elicit hypersensitivity reactions through the release of molecules such as histamine, serotonin and prostaglandins. Some reactions can be severe enough to cause anaphylactic shock [82].

1.3.2.1 IgG

IgG is the most abundant antibody in human serum, accounting for 80% of total Ig [83] and can be categorised into four subclasses based on differences in the heavy chain: (in decreasing abundance) IgG1, IgG2, IgG3 and IgG4. They each have a unique profile of effector functions that are determined through differences in their constant region, namely the hinge and CH_2 domain which alter binding to FcγRs and the first component of the complement cascade, C1q (Table 1.2) (Figure 1.7). Their production is skewed by the type of antigen presented (e.g. protein or polysaccharide), the route of presentation (T-dependent or T-independent) and absence/presence of an inflammatory environment which helps to fulfil their different effector functions. IgG1 and IgG3 are produced in response to soluble and surface-bound antigens and produce a pro-inflammatory response [83]. IgG2 is predominantly produced in response to carbohydrate antigens and demonstrates a weaker affinity for FcγRs than IgG1 and IgG3 [84]. Despite the weaker interactions of IgG2 with FcγRs, deficiencies in IgG2 are associated with susceptibility to bacterial infections [85]. IgG3 has a shortened half-life (approximately 1 week) due to its extended hinge region making it susceptible to proteolytic degradation and the presence of the common R435H polymorphism reduces pH-dependent binding to the neonatal Fc receptor (FcRn) (which mediates IgG half-life) [86]. IgG4 binds weakly to all FcγRs except for FcγRI, however it still demonstrates weaker affinity than IgG1 and IgG3. Long term exposure to antigens (and allergens) tends to result in the production of IgG4 and is associated with the induction of immune tolerance [83]. IgG4 also has the unique ability to undergo F(ab) arm exchange *in vivo*, swapping F(ab) arm specificities with other IgG4

molecules, thereby producing monovalent, bispecific antibodies, decreasing their avidity and ability to cross-link target antigens [87].

Mice also express four subclasses of IgG - IgG1, IgG2a or IgG2c (strain-dependent), IgG2b and IgG3 (Table 1.3, Figure 1.7). IgG1 is produced in response to the T-dependent activation of B cells and can effectively neutralise toxins and viruses. However, it demonstrates poor antibody-mediated effector functions. It cannot fix complement efficiently and has moderate affinity for the inhibitory FcγRII and the activatory FcγRIII, and poor affinity for the activatory FcγRI and FcγRIV [88]. IgG3 is highly flexible and produced in response to T-independent and carbohydrate-based antigens. It can fix complement but cannot stably bind to any FcγR. IgG2b antibodies are also produced in response to both T-dependent and T-independent antigens and induce antibody effector functions through moderate interactions with all FcγRs. IgG2a is produced in response to viral infections and is very similar to IgG2b in terms of effector functions, but has a higher affinity for all activatory FcγRs and a lower affinity for the inhibitory FcγRII. This means IgG2a can elicit the strongest antibody effector functions [89]. It is worth noting that IgG2a (found in BALB/C mice, IgH-1a haplotype) and IgG2c (found in C57BL/6 and NOD mice, IgH-1b haplotype) are assumed to be paralogues with comparable function in the different strains [88] [90].

Human antibody class switching normally results in a mixture of B cells producing different Ig isotypes against a particular antigen. In contrast, it has been shown in mice that in response to infection, B cells will typically switch to only one isotype (e.g. IgG) and produce each subclass of that isotype in a coordinated fashion. This was highlighted in regard to the murine IgG isotype and is known as the quartet model of IgG function and is thought to work as follows. IgG3 is generated first and self-aggregates on the target driving a strong complement response, enabling the recruitment of immune cells. IgG2b works in conjunction with IgG3 to engage activatory FcγR effector functions, IgG2a then further enhances antigen clearance through even stronger engagement of activatory FcγRs. IgG1 then functions to temper and control the inflammatory response through engagement of the inhibitory FcγRII [88].

IgG-FcγR interactions are well characterised. However, IgG from both humans and mice can bind to several other receptors. These include FcRn which is responsible for regulating antibody half-life and Tripartite motif-containing protein 21 (TRIM21), an intracellular receptor that can elicit antibody-mediated degradation of bound non-enveloped viruses

[91]. IgG has also been reported to bind to dendritic Cell-Specific Intercellular adhesion molecule-3-Grabbing Non-integrin (DC-SIGN), an inhibitory receptor found on DCs and macrophages that is believed to elicit anti-inflammatory effects [92], although, this observation is disputed in the literature with later research suggesting IgG is not able to bind DC-SIGN [93].

IgG-receptor interactions are mediated by the structure of the Fc domain, this can dictate the affinity to different FcγRs. Critically, these interactions are stabilised by the glycans present at position N297 in the Fc which can alter the binding profile, and therapeutic efficacy of the IgG.

	IgG1	**IgG2**	**IgG3**	**IgG4**
Molecular mass (KDa)	146	146	170	146
Amino acids in hinge	15	12	62	12
Half life in humans (days)	21	21	7	21
Half life in mice (days)	6.5	11	2.5	3
Mean serum levels (g/L))	6.98	3.8	0.51	0.56
Antibody response to:				
Proteins	++	+/-	++	++
Polysaccharides	+	+++	+/-	+/-
Allergens	+	-	-	++
Complement activation				
Complement binding (C1q)	++	+	+++	-

Table 1.2: Properties of human IgG subclasses
Properties of human IgG subclasses, how they respond to different antigens and activate complement. Adapted from [83] [94].

	IgG1	**IgG2a**	**IgG2b**	**IgG3**
Molecular mass (KDa)	160	160	160	160
Half life in mice (days)	6-8	6-8	4-6	6-8
Mean serum levels (g/L)	0.28	0.7	1.22	0.18
Complement activation				
Complement binding (C1q)	-	++	++	++++

Table 1.3: Properties of mouse IgG subclasses
Mouse IgG half-life and strength of complement activation. IgG2c is considered equivalent to IgG2a. Adapted from [95] [96] [97].

1.3.2.2 IgG N-linked glycosylation

Proteins can be glycosylated via a chemical bond between N-acetylglucosamine and the amino acids asparagine (N-linked) or serine/threonine (O-linked). IgG glycosylation of asparagine 297 (N297) within the CH_2 domain of human IgG1 has been extensively studied due to how it changes the biology of IgG. This glycosylation pattern can determine

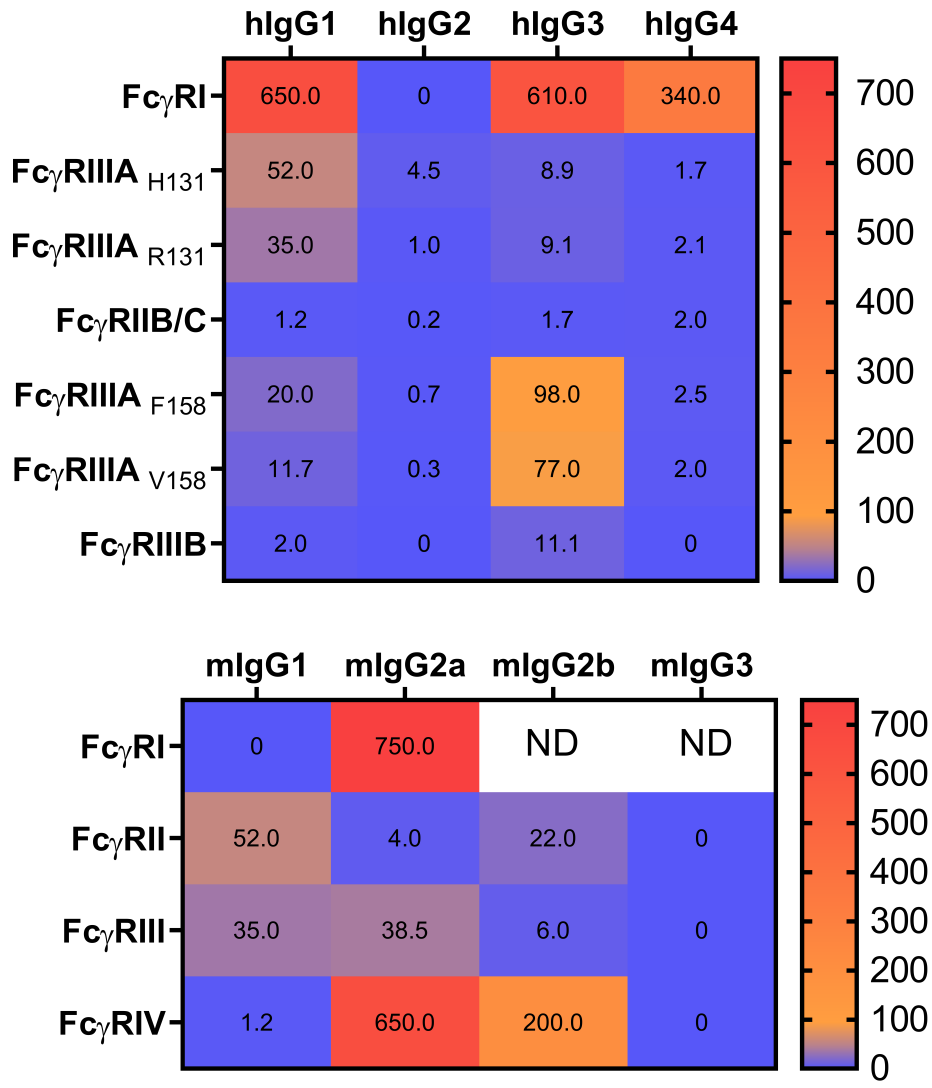

Figure 1.7: Relative binding affinities of human/mouse IgG subclasses to FcγRs.
The binding of IgGs to FcγRs as determined by surface plasmon resonance. Binding affinities = KA x 10^5 M^{-1}. ND = not determined. Adapted from [98] [99].

interactions with FcγRs and complement proteins, ultimately defining the inflammatory (or immunosuppressive) effects of the antibody. During protein folding, a high mannose glycan is added to the heavy chain as it folds within the endoplasmic reticulum which is then trimmed and altered as it passes through the Golgi. The core glycosylation pattern consists of two sequential N-acetylglucosamine (GlcNAc) attached to a mannose and a further two mannose antennae each capped with a GlcNAc [100] [101]. These can be further modified with fucose, galactose, sialic acid and mannose residues. So far, 30 post-translational glycan profiles of antibodies have been identified by nuclear magnetic resonance (NMR) [102] (Figure 1.6). Glycosylation is highly ordered and conserved but can be modulated in an inflammatory setting, such as during an infection. Studies from

patients with HIV and autoimmune conditions have shown an enrichment of agalactosylated antibodies displaying a more inflammatory profile which seem to be regulated in an antigen specific manner [103]. Glycosylation profiles are also influenced by factors such as monosaccharide availability and Golgi pH as well as environmental factors such as age, sex and pregnancy. Whilst the glycosylation pathway is well characterised, the immunological mechanisms that control and change glycosylation are poorly understood. It has long been established that IgG glycosylation heavily influences binding to FcγRs [104].

IgG antibodies now commonly undergo glycoengineering to alter binding profiles and antibody biology. One such common technique involves aglycosylation of N297 to reduce FcγR and C1q binding where effector functions are considered detrimental to the mechanism of action of the antibody [103]. One of the simplest ways to aglycosylate IgG is to mutate N297 to another amino acid (e.g. glutamine), this destabilises binding to the low affinity FcγRs leading to a near complete loss of binding [105]. This technique is now commonly employed for checkpoint inhibitor mAbs, such as those directed against PD-1 or PD-L1 [106]. This is because mAbs directed against these targets aim to abrogate signalling and do not need to engage immune effector functions. Indeed, depletion of PD-1/PD-L1 positive cells may lead to the loss of CTLs, resulting in reduced clinical efficacy. Atezolizumab is directed against PD-L1 and contains the N297A mutation to reduce FcγR mediated effector functions [106]. However, atezolozumab easily forms aggregates, leading to the development of anti-drug antibodies (ADA) in 41% of patients so engineering strategies have been developed to stabilise the mAb using short linker sequences within the hinge region [107].

Alternatively, the glycan profile can be altered to enhance inflammatory or immunosuppressive effects. It is widely recognised that afucosylation of the N297 glycosylation site enhances antibody-dependent cellular cytotoxicity (ADCC) by increasing binding to human FcγRIIIA by up to 50-fold [108]. X-ray crystallography studies suggest that fucosylated IgG sterically hinders the antibody from forming additional hydrogen bonds and van der Waals contacts with FcγRIIIA. Removal of the fucose glycans allows optimal interactions to occur between the antibody and receptor [109] [110]. Although interestingly this effect was found to be limited to IgG1 and IgG3 subclasses when bound to FcγRIIIA on NK cells. Macrophages, which express multiple FcγRs, did not have increased effector functions in the presence of hypo-fucosylated IgG [109]. mAb afucosylation was

employed for the clinically approved anti-CCR4 mAb mogamulizumab and the anti-CD20 mAb obinutuzumab to enhance ADCC [111] [112].

IgG can also be manipulated so their glycosylation pattern is terminally sialylated resulting in an anti-inflammatory profile [113]. It was found that sialylated IgG decreases interactions with activatory FcγRs and decreases binding to cell surface antigens [111]. The mechanism of action is not fully understood but is thought to be due to steric hindrance between FcγRs and sialylated IgG structures binding to immunomodulatory receptors such as CD22 [114]. As a proof-of-concept, the anti-HER2 mAb pertuzumab was enzymatically desialylated and was found to increase ADCC, complement dependent cytotoxicity (CDC) and enhanced FcγRIIIA binding (see Section 1.3.5 for further information on effector functions). Conversely, the half-life of the mAb was reduced, highlighting how Fc modifications can often have multiple effects [115].

Recent real world studies have shown how glycosylation patterns of circulating IgG are dynamically modulated in infectious diseases. A recent study of patients infected with COVID-19 showed a correlation between severe disease and an increase in afucosylated IgG1 that demonstrated enhanced ADCC and production of inflammatory cytokines from monocytes [116]. Other studies have also found that anti-spike IgG produced in severe COVID-19 patients had low fucosylation of their Fc, which could be responsible for increased inflammation of pulmonary tissue and thrombosis seen in these patients [117] [118]. Larsen et al eluded as to why this may be the case - the production of afucosylated antibodies was found to be driven by antigens on the surface of enveloped viruses, as is the case of COVID-19 [119]. Glycosylation can also be used as a read out for the effectiveness of vaccines. 26 volunteers were immunised with the trivalent subunit influenza vaccine and it was found that responders and non-responders could be identified purely on their glycosylation pattern. Responders were identified based on increased levels of galactosylation and high mannose containing glycoforms of IgG specific to the vaccine [120].

As previously discussed, manipulating the glycosylation pattern of IgG is now commonly used when engineering antibodies for clinical use and has become a critical part of fine-tuning antibody biological for maximal clinical efficacy. Routinely these antibodies are monoclonal.

1.3.3 Generation of monoclonal antibodies

Monoclonal antibodies (mAb) are lab generated antibodies that are routinely utilised in the clinic for a broad range of indications. In 1975, the first hybridomas (a fusion of a B cell and immortal myeloma cell) were reported to produce a bivalent mAb with a single specificity [121]. This technology was used to develop the first licensed mAb, muromonab (OKT3) [122]. mAb development has since grown from a very laborious process to an economically viable large scale model for biological therapeutics. As of 2018, mAbs had a market value of approximately $115.2 billion dollars a year, with this value projected to grow to $300 billion by 2025 [123]. Today there are 100 mAbs approved for clinical use by the Federal Drug Agency (FDA) with approximately 40% of those approved for the treatment of cancer [124] (Table 1.4).

The hybridoma technique developed by Milstein and Köhler relies on animal immunisation with a specific antigen. After a robust immune response has developed, the splenic or lymphatic B cells are isolated from the animals to form a pool of polyclonal B cells [112]. The B cells are then fused with an immortal myeloma cell to generate an immortal hybridoma cell capable of producing a single antibody specificity. Unfused B cells will not replicate in culture, whilst an unfused myeloma cell requires a functional Hypoxanthine-guanine phosphoribosyltransferase (HGPRT) enzyme (inherited from the unfused cell) to survive in the hypoxanthine-aminopterin-thymidine (HAT) medium they are cultured in [112]. After single-cell cloning, each hybridoma is screened for the specificity required. mAbs produced in this manner are effective but have some drawbacks. These include the potential genetic instability of a hybridoma which can lead to lower mAb quality, yields and altering of the mAb structure. However, one of the major drawbacks of hybridoma technology is the potential immunogenicity of the animal IgG as well as sub-optimal engagement with the human immune system. This was evident with the first approved clinical mAb, muromonab which was used to suppress rejection of kidney transplants in recipients. It was found that 38% of patients developed blocking antibodies to the murine components that reduced the effectiveness of treatment [125]. These factors can limit commercial and therapeutic use of mAbs generated from hybridomas [126]. Strategies have since been developed to overcome these issues. For example, through the advent of molecular biology and recombinant DNA technology, animal IgG can be chimerised with human IgG. This is achieved through fusing the F(ab) domains of the mAb generated from a hybridoma with human IgG Fc domains to make a mAb that is $\geq$70% of human origin. These chimeric mAbs are considerably less immunogenic and more efficient at eliciting antibody effector

functions in the recipient species [127]. Antibodies can be taken one step further and humanised. This involves taking a human antibody isotype and removing the endogenous CDR regions. These are then replaced with the CDRs from the mAb produced by the hybridoma. This results in a mAb that is 85-90% human and even less immunogenic than a chimera [127].

More recently, techniques have been developed to completely negate the use of animals in the generation of mAbs. One of the most common techniques is known as phage display. In this approach, human B cells are isolated from peripheral blood and their mRNA is extracted and converted into cDNA. PCR is then used to amplify all the V_L and V_H regions. These DNA segments are cloned into bacteriophages as a small chain variable fragment (ScFv). A bacteriophage can subsequently infect *E.coli* bacteria to generate a library of *E.coli* expressing a unique V_L and V_H ScFv. To generate the mAb of interest, ScFv are screened against an antigen. Positive *E.coli* clones are isolated and sequenced to be grafted onto the relevant IgG constant domains. mAbs produced by phage display can be obtained at a quicker pace than hybridomas with no immunisation protocol required [128]. However, phage display lacks the physiological process of affinity maturation so genetic engineering of the CDRs ("affinity maturation") is sometimes required to produce a mAb of high affinity. One of the main benefits of phage display is that mAbs produced in this fashion can be fully human and are unlikely to be immunogenic. Phage display also generates a large number of potentially unique ScFvs against a variety of epitopes, that have not been limited by either negative selection or immunodominance [128]. However, phage display has some limitations that include the high cost associated with generating highly diverse ScFv libraries. These libraries then require screening to ascertain biological activity and suitability which can be very expensive and laborious [129].

Once the unique ScFvs/CDRs have been identified (from phage display or immunisation), the mAb can be expressed recombinantly within an established expression system. mAbs require the folding machinery and post-translational modifications afforded by mammalian cells to generate biologically active molecules. These requirements are typically fulfilled by Chinese hamster ovary (CHO) cells [130]. This is because they are approved by regulators and are used on an industrial scale with approximately 70% of therapeutic proteins produced in CHO cell variants [131]. The specific cell lines used and culture conditions can be further manipulated to change mAb production rate and specific glycosylation pattern. For example, CHO cells can be genetically engineered themselves to alter mAbs, for example knocking out the FUT8 gene produces a completely afucosylated mAb [132].

A complementary approach to phage display for generating fully human mAbs involves using transgenic humanised mice that have the mouse V gene repertoire replaced with the human IgG gene repertoire. These mice can then be directly immunised to produce antibodies with human V regions and the hybridoma technique can be used to produce a mAb of interest. Alternatively individual antigen-specific B cells can be sequenced and their antibodies produced recombinantly. This process naturally allows the antibodies to undergo affinity maturation to form a 'mature' mAb [122]. As of 2020, 9 clinically approved fully human mAbs have been produced by phage-display whilst 19 were produced using transgenic humanised mice [133]. mAbs produced using these techniques have been critical to improving the outcomes of patients in a broad spectrum of disease.

mAb name	Brand name	Format	Target	Indication	FDA approval
Isatuximab	Sarclisa	Chimeric IgG1	CD38	Multiple myeloma	2020
Tafasitamab	Monjuvin	Humanised IgG1	CD19	Diffuse large B cell lymphoma	2020
Naxitamab	Danyelza	Humanised IgG1	GD2	Neuroblastoma	2020
Belantamab mafodotin	BLENREP	humanised IgG1 ADC	BCMA	Multiple myeloma	2020
Polatuzumab vedotin	Polivy	Humanized IgG1, ADC	CD79B	Diffuce large B cell lymphoma	2019
Moxetumomab pasudotox	Lumoxiti	Murine IgG1 dsFv immunotoxin	CD22	Hairy cell leukemia	2018
Cemiplimab	Libtayo	Human mAb	PD-1	Cutaneous squamous cell carcinoma	2018
Durvalumab	IMFINZI	Human IgG1	PD-L1	Bladder cancer	2017
Gemtuzumab ozogamicin	Mylotarg	Humanized IgG4, ADC	CD33	Acute myeloid leukemia	2017
Avelumab	Bavencio	Human IgG1	PD-L1	Merkel cell carcinoma	2017
Atezolizumab	Tencentriq	Humanised IgG1	PD-L1	Bladder Cancer	2016
Olaratumab	Lartruvo	Human IgG1	PDGFRα	Soft tissue sarcoma	2016
Nectimumab	Portazza	Human IgG1	EGFR	Non-small cell lung carcinoma	2015
Daratumumab	Darzalex	Human IgG1	CD38	Multiple myeloma	2015
Dinutuximab	Unituxin	Chimeric IgG1	GD2	Neuroblastoma	2015
Nivolumab	Opdivo	Human IgG4	PD1	Melanoma, non-small cell lung cancer	2014
Blinatumomab	Blincyto	Murine bispecific tandem scFv	CD19, CD3	Acute lymphoblastic leukaemia	2014
Pembrolizumab	Keytruda	Humanised IgG4	PD1	Melanoma	2014
Ramucirumab	Cyramza	Human IgG1	VEGFR2	Gastric cancer	2014
Obinutuzumab	Gazyva	Humanised IgG1	CD20	Chronic lymphocytic leukaemia	2013
Ado-trastuzumab emtansine	Kadcyla	Humanised IgG1, ADC	Her2	Breast cacner	2013
Pertuzumab	Perjeta	Humanised IgG1	Her2	Breast cancer	2012
Brentuximab vedotin	Adcetris	Chimeric IgG1, ADC	CD30	Hodgkin lymphoma	2011
Ipilimumab	Yervoy	Human IgG1	CTLA-4	Metastatic melanoma	2011
Ofatumumab	Arzerra	Human IgG1	CD20	Chronic lymphocytic leukaemia	2009
Panitumumab	Vectibix	Human IgG2	EGFR	Colorectal cancer	2006
Bevacizumab	Avastin	Humanised IgG1	VEGF	Colorectal cancer	2004
Cetuximab	Erbitux	Chimeric IgG1	EGFR	Colorectal cancer	2004
Tositumomab-I131*	Bexxar	Murine IgG2a	CD20	Non-Hodgkin lymphoma	2003
Ibritumomab tiuxetan	Zevalin	Murine IgG1	CD20	Non-Hodgkin lymphoma	2002
Trastuzumab	Herceptin	Humanised IgG1	Her2	Breast cancer	1998
Rituximab	MabThera, Rituxan	Chimeric IgG1	CD20	Non-Hodgkin lymphoma	1997

Table 1.4: Approved clinical antibodies in a cancer setting
Approved antibodies currently in the clinic for use in a cancer setting. Adapted from JM Reichert; The Antibody Society [134] (Updated January 2021).

1.3.4 Monoclonal antibodies in the clinic

The advances in molecular biology and mAb production techniques described above have made it increasingly viable to develop mAbs for clinical intervention. As described above, over 100 mAbs have been approved for clinical use, these mAbs can be broadly characterised into two groups: direct targeting and immunomodulatory. Direct targeting mAbs, as their name suggests, bind directly to cellular targets such as on a tumour cell and often elicit their therapeutic response through antibody effector functions such as antibody dependent cellular phagocytosis (ADCP) and ADCC [135]. Immunomodulatory mAbs by contrast bind to cells other than the target, such as immune cells, in an attempt to enhance the immune response. These mAbs typically either block inhibitory molecules/receptors to release immune suppression, termed "checkpoint inhibitors" or agonise immune cells to enhance the immune response, and are described as "immunostimulatory mAbs" [136].

Direct targeting mAbs were the first to be deployed for immunotherapy - being developed to target a specific cell or molecule to obviate it's function or to destroy the target cell. For example, trastuzumab targets HER2, a receptor found overexpressed on some types of breast cancer. It was designed to stop the dimerisation of the HER2 receptor, a process required to initiate pro-survival and proliferative signalling [137]. Further research has shown that trastuzumab also initiates NK cell-mediated ADCC to destroy HER2 expressing cells [138], highlighting the importance of FcγR mediated effector functions. Anti-CD20 mAbs mediate their anti-tumour effect through Fc dependent mechanisms that include a combination of CDC, ADCC, ADCP and also potentially F(ab)-mediated direct cell death (DCD) (See Section 1.3.5.1 for further detail). Indeed, certain mAbs have also been designed with this latter activity as their main mechanism of action, to induce signalling-mediated death of the target cell. Targets investigated have included Fas and TNF-related apoptosis-inducing ligand (TRAIL) receptors, where mAb engagement drives the induction of the extrinsic apoptosis pathway. However, they have made limited headway in the clinic due to associated hepatoxicities [139]. Further information on direct targeting mAbs can be found in Section 1.3.5.

Checkpoint inhibitors do not usually require FcγR engagement for their mechanism of action as they are designed to block ligand interactions. mAbs directed against have been one of the most successful checkpoint inhibitors in the context of cancer immunotherapy [140]. PD-1 is usually upregulated on activated T cells as an immune homeostasis mechanism to limit T cell activation and expansion and to avoid excessive tissue damage [140].

Tumour cells, for example melanoma, are known to upregulate the expression of its ligand, PD-L1, to circumvent the T cell immune response. When PD-1 engages PD-L1, inhibitory signalling within T cells can drive T cell dysfunction, exhaustion and production of immunosuppressive cytokines such as IL-10 [141]. PD-1 mAbs such as pembrolizumab skew T cells from an anergic to an activatory state by binding to PD-1 in an antagonistic fashion and blocking PD-1 mediated inhibitory signalling. These first generation anti-PD-1 mAbs are of the IgG4 subclass in order to minimise FcγR engagement and depletion of T cells [142]. These treatments have been highly successful in cancers with a high mutational burden and good T cell infiltrates such as non-small cell lung carcinoma (NSCLC) [140]. The next generation of PD-1 mAbs, such as atezolizumab are utilising aglycosylated IgG1 to reduce FcγR binding even further [106].

Immunostimulatory mAbs by contrast typically drive activation of a specific receptor on an immune cell, such as T cells or DCs and usually require some degree of crosslinking to cluster the receptor efficiently and elicit activation. In the case of CD40 mAbs, crosslinking can be achieved through engagement of the inhibitory FcγRIIB or through the unique properties of the hIgG2 isotype [143]. In fact many of the members of the tumour necrosis factor receptor (TNFR) super-family can be clustered in this way to deliver powerful T cell activation and anti-tumour effects such as those directed against OX40, 4-1BB and CD40 [144] [145] [146].

However, some mAbs can operate multiple mechanisms of action to achieve therapy. CTLA-4 is expressed as an inhibitory receptor on T cells that out competes the stimulatory CD28 for its ligand CD80 or CD86. CTLA-4 is upregulated upon TCR activation on both CD4+ and CD8+ T cells and is constitutively expressed on T_{reg} cells. Like anti-PD-1 mAbs, Anti-CTLA-4 mAbs were developed to block CTLA-4 interactions with CD28, in an attempt to enhance effector T cell responses in cancer. Anti-CTLA-4 mAbs, such as ipilimumab, have been successful in the treatment of cancers with high mutational burdens (e.g. melanoma) however therapy has been proposed to be elicited through the depletion of T_{reg} cells as well as the blockade of CTLA-4. It has been suggested the high, constitutive expression of CTLA-4 on T_{reg} cells results in their depletion whilst the low and transient expression of CTLA-4 on effector T cells results in receptor blockade rather than depletion [147] [148] [149].

mAbs directed against both 4-1BB and OX40 have also been suggested to have dual mechanisms of action, acting as both a direct targeting and immunostimulatory mAb. Both

T_{reg} cells and CTLs express 4-1BB, a co-stimulatory receptor found on T cells. T_{reg} cells express a high amount of 4-1BB in comparison to CTLs and this difference can be manipulated for therapeutic purposes. mAb depletion of T_{reg} cells using Fc:FcγR dependent mechanisms could relieve the immunosuppressive environment of a tumour. In addition, mAb mediated agonism of 4-1BB on CTLs could drive a strong immune response against the tumour. These findings were then applied to an *in vivo* tumour model to initially drive depletion of T_{reg} cells cells using the mIgG2a subclass and agonism of CTLs using the mIgG1 subclass [145]. A study of OX40 mAbs highlighted a similar story. Both T_{reg} cells and CTLs express OX40, T_{reg} cells at a constitutively high level and CTLs at a lower level when activated. It was found the mIgG2a subclass of OX40 mAbs successfully depleted T_{reg} cells, whilst the mIgG1 subclass optimally activated CTLs. In a tumour setting, both subclasses gave good tumour control, demonstrating a role for both T_{reg} cell depletion and CTL activation for robust tumour control in pre-clinical models at least [150].

Currently, there has been little translation of immunostimulatory mAbs from research into the clinic. The reason for this is unclear as some have failed due to toxicities from an excessively stimulated immune system whereas others have appeared inactive in humans which may reflect a poor understanding of the agonistic target [151]. Clearly, further research is required to understand the target expression profile, epitope binding and dosing regimen to enhance the therapeutic potential of immunostimulatory mAbs.

1.3.5 Direct targeting monoclonal antibody effector mechanisms

Direct targeting mAbs can elicit effector functions through several different mechanisms that utilise components of the innate immune system such as complement and innate effector cells. These mechanisms can be mediated through $F(ab')_2$ binding alone or require Fc engagement and can result in target neutralisation, ADCC, ADCP, CDC and DCD (Figure 1.8).

Neutralisation is a F(ab) mediated effect which is highly important in the prevention of pathogen spread. Here, the antibody binds to a molecule on the target (e.g. a pathogen or toxin) and prevents it from interacting with the host cells. The clearance of the target can be further enhanced through Fc mediated interactions which was demonstrated using anti-anthrax toxin mAbs in preclinical models. It was found that engagement of activatory FcγRs was critical for the neutralising activity of the mAbs and this effect was lost in activatory FcγR knockout mice [152]. The same group had also found that preferential engage-

ment of activatory FcγRs by broadly neutralising anti-HIV antibodies was responsible for reducing viral load [153]. However, FcγR engagement has also been implicated in the enhancement of other viral infections. Antibody-dependent enhancement (ADE) is when the binding of the antibody to a virus can enhance its entry into the host cell, increasing its virulence. This phenomenon is believed to be due to ineffective target neutralisation, leading to subsequent Fc receptor-mediated or complement facilitated internalisation into the cell. Ineffective target neutralisation is usually due to low antibody affinity or avidity resulting in poor target opsonisation and FcγR mediated internalisation [154]. Complement itself has been shown to enhance HIV entry to CD4+ cells by binding to the viral particles, bringing them to complement receptors such as CR3 and CR4 which inadvertently enhance viral gp120 interactions with CD4 [155]. Neutralising antibodies can be used clinically to passively immunise patients using either laboratory-produced mAbs or the serum from convalescent patients. Neutralising mAbs have also been utilised in non-communicable diseases such as autoimmune disorders and cancer to block receptor-based signalling and ligand binding. For example, cetuximab is used clinically to block the dimerisation of EGFR and therefore cell signalling whilst bevacizumab blocks VEGF binding to its receptor inhibiting angiogenesis [156].

Antibodies can also mediate DCD independently of Fc effector functions. It has been shown *in vitro* that tositumomab and obinutuzumab can bind CD20 on the surface of malignant B cells and initiate programmed cell death independently of the normal apoptotic pathways. This is achieved through actin reorganisation, the generation of reactive oxygen species (ROS) and the release of lysosomal proteases resulting in the loss of plasma membrane integrity [157]. Also, as described earlier, receptors such as Fas and DR5 can be targeted with mAbs to trigger apoptosis in the target cell.

In addition to these F(ab) mediated effector functions, mAb can also elicit a host of Fc-mediated effector functions through engagement of FcγRs or the complement system. For example, ADCC relies on immune complexes crosslinking FcγRIIIA on the immune effector cell. This function is associated with NK cells, but evidence has shown that neutrophils, monocytes and macrophages can also elicit ADCC via alternative activatory FcγRs [158] [159]. FcγRIIIA crosslinking on NK cells results in the intracellular signalling cascade that triggers the degranulation of lytic vesicles and the release of perforin and granzyme resulting in target cell destruction [160].

In contrast, ADCP results in the engulfment of the target cell by mononuclear phagocytes

mediated through the activatory FcγRs. Crosslinking results in the initiation of a downstream signalling cascade which leads to the remodelling of the actin cytoskeleton in the phagocyte to extend around the target and form the phagosome [161]. The ingested phagosome fuses with lysosomes containing digestive enzymes, hydrolases and antimicrobial peptides to create a highly oxidative environment that destroys the target cell [162]. Furthermore, ADCP can also result in the release of pro-inflammatory cytokines and can enhance antigen presentation via peptide-MHC-II complexes [163].

Trogocytosis has recently been identified as another method of target cell destruction mediated by neutrophils and macrophages [164]. During this process immune complexes are thought to engage small clusters of activatory FcγRs and result in the 'pinching' out of small fragments of the target cell membrane into the effector cells. In some models, trogocytosis is beneficial in target cell depletion by disrupting the integrity of the target cell membrane and triggering cell death [165]. However, in other cases, trogocytosis can result in antigenic escape, with the removal of the membrane-bound antibody and target leading to a decrease in Fc mediated effector functions such as ADCC, CDC and ADCP [166].

Antibodies can also initiate CDC through the binding of the first component of the complement cascade, C1q, to initiate the classical complement pathway. The subsequent complement cascade can result in the formation of the MAC which when inserted into a cellular membrane can cause direct cell lysis through calcium influx, mitochondrial poisoning and osmotic swelling [167]. Complement by-products can act as opsonins (C3b, iC3b, C4b) to dispose of immune complexes and cellular debris or as anaphylatoxins (C3a, C4a, C5a) to induce a local inflammatory response akin to an allergic reaction, resulting in mast cell and basophil degranulation, increased blood capillary permeability and recruitment of other immune cells [167].

The first therapeutic direct targeting mAb approved for the treatment of cancer was the anti-CD20 mAb rituximab. It's various mechanisms of action will be discussed in detail in the next section.

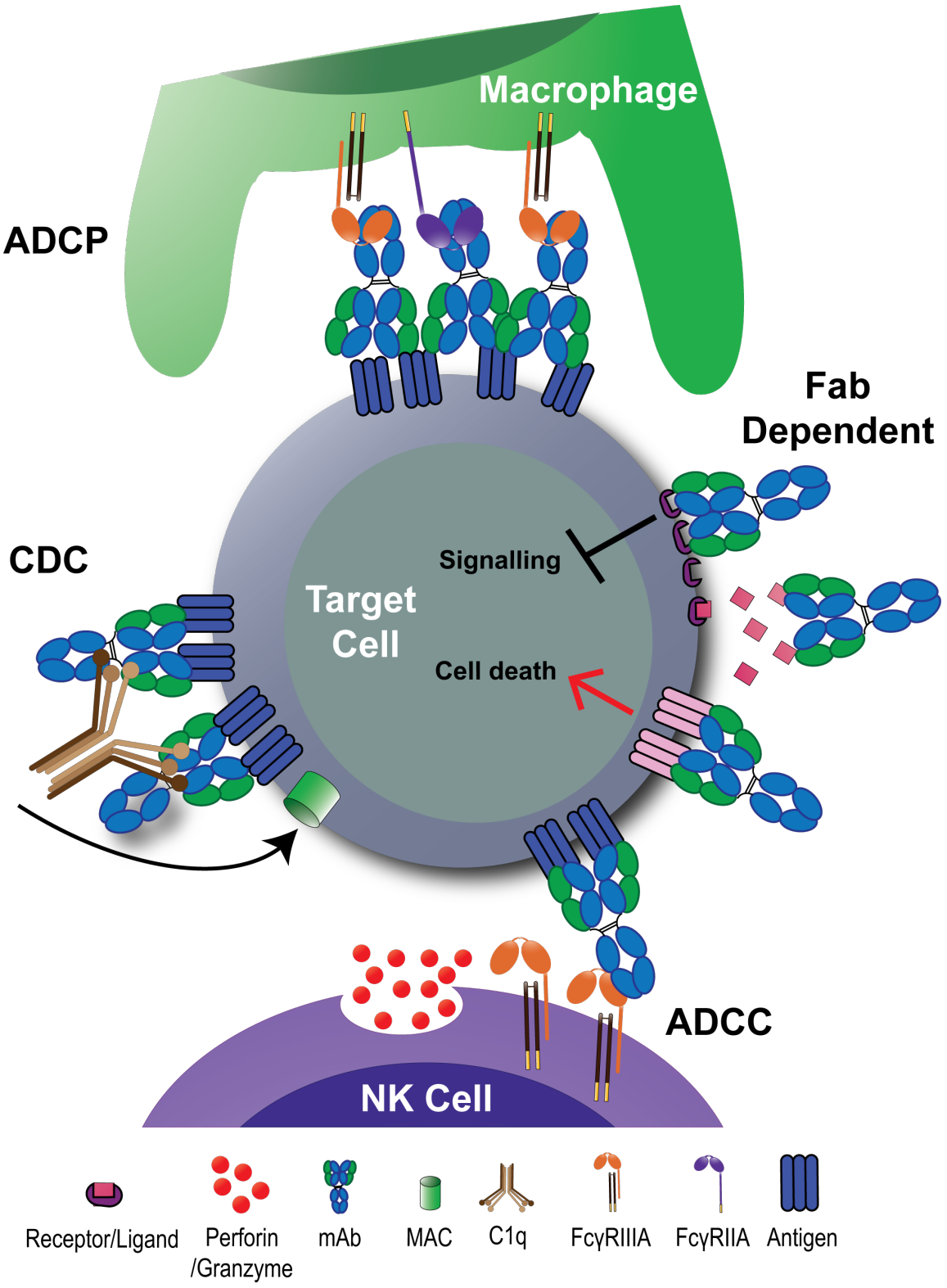

Figure 1.8: Antibody effector mechanisms
Antibodies can elicit various methods to destroy their target. Engagement of FcγRs on NK cells and macrophages activates ADCC or ADCP. C1q can bind to the Fc of an antibody and initiate the complement cascade (resulting in the formation of the membrane attack complex). Apoptotic programs can be activated in an FcγR independent manner by antibodies targeting receptors that activate the apoptosis pathways. Adapted from Overdijk et al [168].

1.3.5.1 CD20 as a therapeutic target

CD20 is a surface expressed phosphoprotein found almost exclusively on healthy and malignant B cells. The physiological role of CD20 is not fully understood, but experimental evidence suggests that CD20 associates with the BCR to drive optimal calcium flux and is required for the generation of a maximal humoral response but the loss of CD20 expression does not seem to have a highly detrimental phenotype [169] [170]. Because CD20 has also been shown to be highly expressed on most malignant B cells, it has also been a successful target for direct targeting mAb therapy [171].

Although expressed on healthy B cells, critically CD20 is not found on pre-B cells, haematopoietic stem cells or terminally differentiated plasma cells [171]. This means that following CD20 depletion, patients still have a level of humoral immunity that does not leave them immuno-compromised, alongside precursors to provide re-population, making it a viable candidate target for the clinic [172]. The structure of CD20 itself also makes it a good target with two exposed extracellular loops that can provide a unique binding site for mAbs [173]. In addition, CD20 itself has been shown to be relatively stable with little shedding from the cell surface and seems to have a relative lack of ligand induced internalisation [174]. The proximity of the extracellular loops to the B cell surface also allows for efficient mAb mediated effector functions such as ADCC and CDC [175]. All these factors make CD20 a highly attractive target for mAb therapy.

As described above, the first CD20 mAb approved for clinical use was rituximab in 1997. Rituximab had a significant effect upon patient survival and catalysed the field of therapeutic mAbs for the treatment of cancer [172]. Decades of research using CD20 mAbs as a paradigm of direct targeting mAbs have furthered our understanding of *in vivo* mAb effector mechanisms but also highlighted mechanisms of resistance. mAbs targeting CD20 can be broadly classed as type I (e.g. rituximab) and type II (e.g. obinutuzumab) based on their ability to redistribute CD20 into lipid rafts within the plasma membrane [176]. Type I mAbs bind to twice as many target molecules compared to type II mAbs. This is due to binding geometry, with two type I mAbs binding to one CD20 molecule compared to one type II mAb per CD20 molecule [177] [178]. In turn, type I mAbs are more vulnerable to internalisation and proteolytic degradation, resulting in decreased CD20 cell surface expression in a process known as antigenic modulation [179]. These geometric differences also drive differences in type I and type II mAb mediated effector functions.

CD20 mAbs are considered capable of inducing ADCC, ADCP, CDC and DCD [172]. Type I mAb-mediated reorganisation of CD20 into lipid rafts has been shown to exhibit a higher level of complement activation due to increased recruitment of C1q [180]. This is thought to be due to more favourable C1q:Fc interactions. Once the mAb Fc's cluster C1q recruitment occurs, with IgG assembling into a hexamer and engaging the 6 globular heads of C1q [181]. Type I mAbs have also been shown to induce an apoptotic cell death through hypercrosslinking of CD20 [182]. However, the high degree of clustering and crosslinking can also result in internalisation of the CD20-mAb complex, reducing the efficacy of other Fc-mediated effector functions. This process of internalisation can be further enhanced by FcγRIIB binding, via a cis interaction on the target cell [179]. Type II mAbs do not efficiently induce CD20 clustering, resulting in decreased C1q binding and CDC but also reduced internalisation of the mAb-CD20 complex [183] allowing sustained Fc-medicated effector functions. Type II mAbs have also been shown to demonstrate a potent DCD response, driving non-apoptotic cell death through actin cytoskeleton remodelling and lysosomal membrane permeabilisation as described earlier [184].

Both type I and type II CD20 mAbs have been shown to elicit FcγR dependent functions such as ADCP and ADCC. In models of absent and dysfunctional FcγR signalling there is a significant decrease in CD20 mAb mediated target cell depletion [185] [186]. The importance of FcγRs to tumour therapy was highlighted in a syngeneic tumour model expressing hCD20, showing the clearance of tumour using anti-CD20 mAbs was dependent on activatory mFcγRs [187]. FcγRs and their importance to antibody mediated effector functions will be discussed in more detail below.

1.4 Fc gamma receptors (FcγRs)

FcγRs are members of the Ig superfamily and are made up of two extracellular domains (except for FcγRI which contains three) that can bind to the Fc region of IgG antibodies [188]. Upon activation, these receptors can elicit either activatory or inhibitory intracellular signalling. Many cells express multiple activatory and inhibitory FcγRs, with the level of expression of each acting as a threshold for cellular activation. These receptors can be further regulated through cellular interactions and the inflammatory state of the microenvironment, skewing the cells to become more activatory or inhibitory [189].

1.4.1 Human FcγRs

Humans have 6 genes that encode FcγRs: FcγRI (CD64), FcγRIIA (CD32A), FcγRIIB (CD32B), FcγRIIC (CD32C), FcγRIIIA (CD16A) and FcγRIIIB (CD16B) [190]. They are able to bind IgG as a monomer or within a multimeric immune complex, with differing affinities. Activatory receptors signal via associated ITAMs, found on the receptors intracellular tail or present on an associated γ chain (Figure 1.9). ITAMs are found on several immunoreceptors (such as FcγRs and the BCR) and facilitate activatory signalling pathways through the phosphorylation of two critical tyrosine residues (See section 1.4.3 for further detail). In contrast, the inhibitory FcγRIIB signals via an intracellular immunoreceptor tyrosine-based inhibitory motif (ITIM). Phosphorylation of the critical tyrosine residue in the ITIM triggers downstream inhibition of the activatory pathways (See section 1.4.4 for further detail) [191]. The relative binding of human IgGs for their human FcγR counterparts can be found in Figure 1.7.

FcγRI is termed the high affinity receptor for IgG and is the only receptor to contain three extracellular Ig domains (Figure 1.9). The high affinity binding is thought to be driven by the receptor providing a unique hydrophobic pocket to interact with Leu235 on the Fc of monomeric hIgG1 [194]. The receptor can also bind to monomers of IgG3 and IgG4 but not IgG2 [195]. To mediate activatory signalling, the receptor associates with the FcR γ chain, which is also essential for stable cell surface expression of the receptor. Under physiological conditions in the presence of serum, the receptor is assumed to be always bound by monomeric IgG which can potentially be displaced by immune complex binding [196]. FcγRI is expressed on granulocytes, most myeloid cells and DCs and demonstrates potent effector functions [197].

FcγRIIA binds to all human subclasses, with the highest affinity to hIgG1 and mediates activatory signalling via the ITAM found in its cytoplasmic tail with signalling reliant on non-covalent dimerisation of FcγRIIA. Mutagenesis studies have shown mutating the dimersation interface of FcγRIIA reduces ITAM phosphorylation and signalling [198]. The receptor has been associated as an important determinant of phagocytosis on neutrophils, monocytes and macrophages and is therefore considered essential for ADCP [199]. For example, the addition of an anti-FcγRIIA blocking mAb was found to reduce the phagocytic potential of neutrophils [198]. FcγRIIA polymorphisms have also been identified in humans, the two most well characterised are at amino acid position 131, encoding either a histidine (H) or arginine (R). The H131 variant shows enhanced binding to hIgG1, hIgG3

Human IgG Receptors

Name	FcγRI	FcγRIIA	FcγRIIB	FcγRIIC	FcγRIIIA	FcγRIIIB	FcRn
CD	CD64	CD32A	CD32B	CD32C	CD16A	CD16B	-

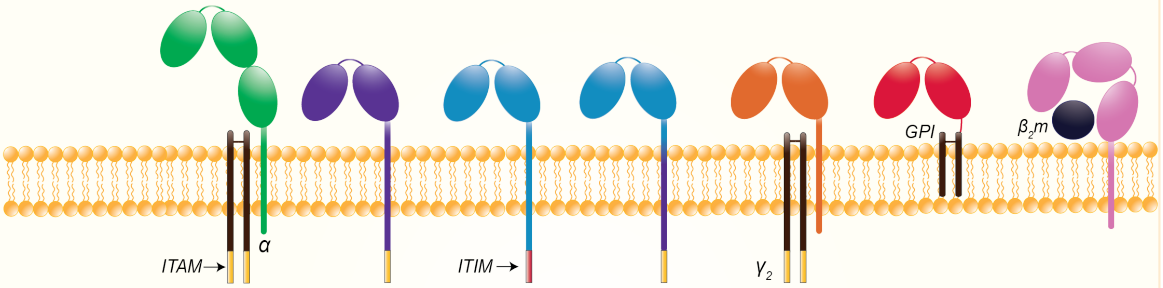

Peripheral Immune Cells							
B cell	-	-	+++	+	-	-	-
T cell	-	+/-	+/-	-	+/-	-	-
NK cell	-	-	-	+	+++	-	-
Classical MO	+++	+++	+/-	+	-	-	+
Non-Classical MO	+	+++	+/-	+	+++	-	+
Neutrophil	-	+++	-	-	+	++++	+
Dendritic Cell	-	++	++	-	-	-	+
Tissue Resident Macrophages (Mθ)							
Splenic Mθ	+/-	+	-	N/A	++	N/A	N/A
Kupffer Cell	+/-	+	+	N/A	++	N/A	N/A
Alveolar Mθ	++	+	-	N/A	++	N/A	N/A
BM Mθ	-	+	-	N/A	++	N/A	N/A

Figure 1.9: Cellular expression of human FcγRs and FcRn
Human FcγRs and FcRn and their expression on human immune cells. - = no expression, -/+ = inducible or expressed on a subset of cells and/or humans, + = low expression, ++ = moderate expression, +++ = high expression, ++++ = very high expression, N/A = not available, MO = monocyte, Mθ = macrophage. FcRn data indicates if the receptor is expressed or not. Adapted from [190] [192] [32] [193].

and is the only receptor able to efficiently bind hIgG2 [200]. This results in a more activatory phenotype and patients carrying this variant have been associated with increased risk of developing autoimmune conditions such as ulcerative colitis and Kawasaki disease [201] [202].

FcγRIIB is the only inhibitory receptor and is critical to modulating the activatory signalling from other FcγRs. It has low affinity for all IgG subclasses and is found most highly expressed on B cells, macrophages and eosinophils [199]. Some essential roles of the receptor include tempering B cell activation, modulating inflammatory responses of macrophages and the removal of small immune complexes from the liver sinusoidal endothelium (LSE) [203]. The function of FcγRIIB will be explored in further detail in Section 1.4.4.

FcγRIIC is the result of an ancestral gene duplication event, generating a gene that encodes for a receptor with the extracellular domain of FcγRIIB and the intracellular domain of FcγRIIA [204]. However, the open reading frame of this receptor is only found in approximately 20% of the European population due to the presence of a stop codon in the third exon, producing a null allele. This receptor is believed to be found on NK cells and B cells, but its physiological function remains unclear. Epidemiological evidence indicates a higher propensity to certain diseases and some *in vitro* evidence suggests an increase in redirected cellular cytotoxicity [205]. However, there is no clear evidence for FcγRIIC enhancing antibody-mediated effector functions in a simple ADCC experiment or in a whole organism [206] [207].

FcγRIIIA demonstrates high affinity for hIgG1 and hIgG3 with lower affinities for hIgG2 and hIgG4. It signals via an associated γ chain and is found on macrophages, monocytes and most importantly NK cells [199]. The receptor is associated with eliciting NK cell mediated ADCC but also has an important role in enhancing ADCP by phagocytes [207] [208]. For example, it was found that blocking FcγRIIIA significantly reduced ADCP of rituximab opsonised target cells by human monocyte-derived-macrophages [209]. Polymorphic variants of FcγRIIIA alter the binding of IgG to the receptor; amino acid position 158 can either be a valine (V) or phenylalanine (F) [210]. The V158 substitution results in an enhanced affinity for all hIgG subclasses (particularly hIgG1) and therefore improved antibody effector functions [211]. In initial studies the high affinity FcγRIIIA allele was associated with better responses to antibody immunotherapy [212]. For example, follicular lymphoma patients found to carry two copies of the V158 mutation had enhanced responses to rituximab therapy, with 90% of patients having an objective response to therapy in comparison to 56% carrying the F158 mutation [213]. However, more recent, larger studies from clinical trials have not supported these initial observations [214] [215].

FcγRIIIB is the only FcγR with no immediate signalling capacity. It has an identical extracellular structure to FcγRIIIA but is bound to the membrane by a GPI anchor. The receptor is highly expressed on neutrophils but is also found on basophils. It has a similar binding pattern to hIgG as FcγRIIIA, with moderate affinities for both hIgG1 and hIgG3 with undetectable binding to hIgG2 and hIgG4, however FcγRIIIA typically binds with higher affinity than FcγRIIIB [98]. Functionally, this receptor is neutral with no direct activatory or inhibitory function. However, despite no specific intracellular domains, studies have suggested that crosslinking of the receptor can cause signalling through associations with FcγRIIA, complement receptor 3 or via lipid rafts [204] [216]. Some studies sug-

gest FcγRIIIB may aid in the clearance of immune complexes and cooperates with other FcγRs during phagocytosis [217], whilst others suggest that the receptor is inert or acts as a decoy receptor to reduce activatory signalling [218].

As described briefly above, IgG can also bind to a second type of Fc receptor, FcRn, a receptor responsible for maintaining the half-life of serum IgG and providing passive immunity to neonates. FcRn is more similar in structure to MHC-I rather than FcγRs, being composed of three α-domains and an associated β2-microglobulin [219]. However, it lacks the diversity of MHC (it is invariant) and does not present antigens. IgG in circulation can be internalised non-specifically and trafficked to the acidic endosome for degradation. If FcRn is present, it will bind to IgG in the acidic environment (pH <6.5) as key residues in the CH_2-CH_3 domain of IgG become protonated, allowing binding to FcRn. This results in the protection and recycling of IgG to the cell surface, preventing lysosomal degradation. Here, where the pH again rises to pH 7.2 - 7.4, FcRn releases the IgG back into the extracellular fluid [219]. This process also protects IgG from degradation by serum proteases. Experimental models of mice lacking FcRn showed that IgG half-life is significantly reduced by 80%, highlighting the importance of FcRn to maintaining the long half-life of IgG. FcRn shows high conservation across all mammals, and like FcγRs, human FcRn shows similarities to FcRn in mice [220].

1.4.2 Mouse FcγRs

Mouse FcγRs can be considered functionally homologous as a family to human FcγRs, but it is difficult to draw direct comparisons between individual receptors due to differences in expression pattern and differing number of receptors. Mice have 4 genes that encode FcγRs: FcγRI (CD64), FcγRII (CD32), FcγRIII (CD16) and FcγRIV (CD16-2). In the mouse, the activatory FcγRs all associate with an ITAM bearing γ chain that is essential for cell surface expression and signalling. Like humans, there is a single inhibitory receptor, FcγRII which signals via an intracellular associated ITIM (Figure 1.10) [89]. The relative binding of mouse IgGs for their mouse FcγR counterparts can be found in Figure 1.7.

FcγRI bears some similarities to its human homologue; it contains 3 Ig domains that can also bind monomeric IgG (mouse IgG2a and IgG2b) but demonstrates no binding to mouse IgG1. It is widely expressed on DCs and has restricted expression on monocytes and macrophages dependent on its immunological niche [221] [193]. Mouse knockout studies have shown FcγRI to be critical for the internalisation of immune complexes by

Mouse IgG Receptors					
Name	FcγRI	FcγRII	FcγRIII	FcγRIV	FcRn
CD	CD64	CD32	CD16	CD16-2	-
	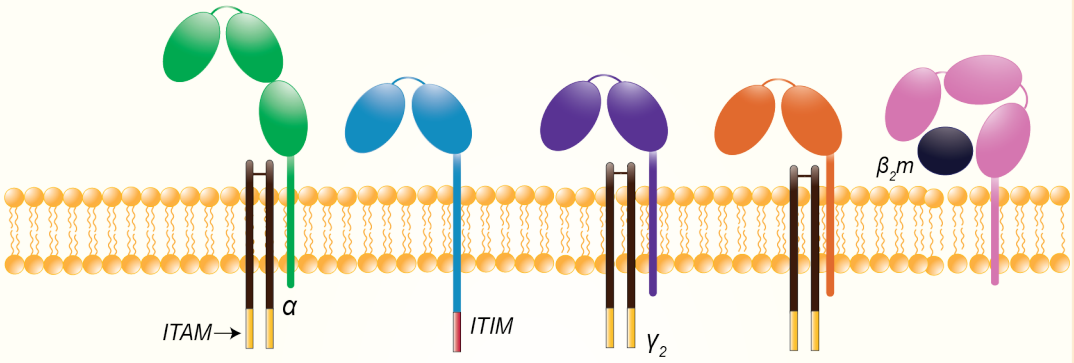				
Peripheral Immune Cells					
B cell	-	++	-	-	-
T cell	-	+/-	-	-	-
NK cell	-	-	+	-	-
Classical MO	++	++	++	+	+
Non-Classical MO	+	++	+	+++	+
Neutrophil	+++	-	+	++	+
Dendritic Cell	+/-	++	++	++	++
Tissue Resident Macrophages (Mθ)					
Splenic Mθ	++	+	++	+++	N/A
Kupffer Cell	++	+	++	+++	N/A
Alveolar Mθ	+++	+++	+++	+++	N/A
Microglia	++	++	+	-	N/A

Figure 1.10: Cellular expression of mouse FcγRs and FcRn
Mouse FcγRs and FcRn and their expression on murine immune cells. - = no expression, -/+ = inducible or expressed on a subset of cells and/or humans, + = low expression, ++ = moderate expression, +++ = high expression, ++++ = very high expression, N/A = not available, MO = monocyte, Mθ = macrophage. FcRn data indicates if the receptor is expressed or not. Adapted from [190] [192] [33].

bone marrow derived macrophages for antigen presentation and mediating ADCP *in vitro*. *in vivo* studies using FcγRI knockout mice have shown reduced inflammatory responses in the Arthus model and increased IgG responses to antigen challenge.

FcγRII is the only inhibitory receptor and has a wide range of expression, on B cells, DCs, basophils, eosinophils monocytes and macrophages. It shows moderate affinity for mouse IgG1 and IgG2b and binds weakly to mouse IgG2a. As in humans it has been

linked to dampening activatory FcγR signalling as well as regulating B cell activation and mediating the removal of small immune complexes [199].

Mouse FcγRIII most closely resembles human FcγRIIA in terms of homology and tissue distribution. It is the most widely expressed activatory receptor and is found on DCs, NK cells, monocytes, macrophages and neutrophils. It has a similar affinity for all mouse IgG subclasses. Blockade of the receptor has revealed its importance in mediating antibody effector functions such as ADCP *in vivo* and can contribute to hypersensitivity reactions such as the Arthus reaction. As expected, based upon its FcγR binding profile (Figure 1.7), mouse IgG1 effector functions are absent in FcγRIII knockout mice [98].

FcγRIV was the most recently discovered activatory FcγR and has a similar tissue distribution to human FcγRIIIA [222]. Its expression pattern is restricted to myeloid cells where it demonstrates strong binding to mouse IgG2a and IgG2b, and residual binding to mouse IgG1. Along with FcγRI and FcγRIII, this receptor is an important mediator of effector functions elicited by mouse IgG2a and IgG2b antibodies such as ADCP and ADCC [199]. Like FcγRIII, knockout studies of FcγRIV have highlighted how the receptor can contribute to autoimmune conditions that include autoimmune arthritis and IgG induced anaphylaxis [223] [224].

FcRn is also found in mice, and is similar in structure and function to human FcRn. One of the main differences is that human FcRn is relatively stringent in binding to human IgG, whilst mouse FcRn shows promiscuity and can bind a wider range of species-specific IgG [225]. Mouse FcRn can maintain mouse and human IgG at a half-life on average of 5 days, whilst human FcRn maintains human IgG half life of approximately 21 days (Table 1.2, 1.3).

1.4.3 Physiological function of activatory FcγRs

In both mice and humans, activatory FcγRs rely on an associated ITAM for intracellular signalling. Receptor cross-linking induced by immune complex binding recruits the Src family kinases (such as Lyn and Fyn) which phosphorylate the two conserved tyrosine residues within the ITAM motif (consensus sequence Yxx[L/I]x(6 to 12)Yxx[L/I]) [226]. The tyrosine kinase Syk is then recruited to the phosphorylated ITAM and activates signalling proteins that include Phospholipase C gamma (PLCγ), Bruton's tyrosine kinase (Btk) and phosphoinositide 3-kinase (PI3K) (Figure 1.12). These signalling pathways result in an in-

creased calcium mobilisation, actin cytoskeleton remodelling, superoxide production and cytokine production (Figure 1.12) [227].

This same common ITAM signalling pathway results in a diverse repertoire of pro-inflammatory functions that are dependent on the cell type engaged (Figure 1.13). Following stimulation of activatory FcγRs, granulocytes exhibit rapid cellular activation with biological effects seen in minutes. These include the generation of ROS, as well as degranulation and the release of antimicrobial peptides [228]. On macrophages, it has been shown that crosslinking of activatory FcγRs predominately drives ADCP (Section 1.3.5). The phosphorylation of FcγR associated ITAMs on macrophages drives signalling pathways that result in the transient increase of Phosphatidylinositol 4,5-bisphosphate (PIP_2) and a sharp decrease in the pseudopods of the phagocytic cup that drives actin disassembly to form a membrane bound vacuole around the opsonised target [229] [230]. The *in vivo* efficacy of some mAbs is thought to be dependent on phagocytosis [228]. Crosslinking of FcγRIIIA on NK cells predominately drives ADCC as discussed in Section 1.3.5.

IgG immune complex engagement of the activatory FcγRIIA on DCs can lead to enhanced maturation, differentiation and antigen presentation [187]. One experimental study demonstrated that the blockade of the inhibitory FcγRIIB on monocyte derived macrophages resulted in spontaneous maturation initiated by IgG binding to the activatory FcγRIIA when incubated with human serum. When challenged with opsonised tumour cells, these DCs were found to drive tumour cell antigen presentation and elicit tumour reactive CD4+ and CD8+ T cells, all mediated by FcγRIIA engagement [231]. This research was then applied to a humanised FcγR mouse model using human CD20 expressing malignant EL4 thymoma cells. When these mice were treated with an anti-CD20 mAb with enhanced binding for FcγRIIA and FcγRIIIA (GASDALIE mutation [232]), 77% survived tumour re-challenge compared to 20% treated with an anti-CD20 mAb with enhanced binding to FcγRIIIA only (ALIE mutation [187]). These data suggest that as FcγRIIA is the key activatory FcγR expressed on human DCs, required to initiate passive adaptive immunity to tumour antigens.

Activatory FcγR signalling has also been shown to alter the phenotypic state of macrophages. As previously mentioned, macrophages demonstrate plasticity and can change states based on their microenvironment. Engagement of activatory FcγRs has been shown to induce the regulatory M2b like state, where macrophages demonstrate

an increased migratory and phagocytic capacity as well as releasing IL-10 and IL-6 [233] [231].

Generally, activatory FcγRs activate the immune response, whilst the inhibitory FcγRIIB down-regulates activatory signalling. However, it has also been shown that FcγRs can elicit non-classical mechanisms to regulate mAb effector functions (Figure 1.11). For example, as already mentioned FcγRIIIB has no direct signalling capacity but experimental evidence suggests it may indirectly elicit signalling (Section 1.4.1). This receptor has also been implicated in downregulating the canonical function of activatory FcγRs. Human neutrophils express high levels of FcγRIIIB as well as FcγRIIA. In a tumour cell killing assay it was found that FcγRIIIB directly competed with FcγRIIA for the engagement of the Fc of the direct targeting mAb, downregulating neutrophil specific ADCC [234]. To rescue ADCC, FcγRIIIB required blocking with a specific F(ab')$_2$, providing evidence of inhibition by FcγRIIIB through competition [234]. Activatory FcγRs can also elicit inhibitory signalling. Low avidity immune complex binding to activatory FcγRIIA and FcγRIIIA has been shown to induce ITAM mediated inhibitory signalling (ITAMi). ITAMi signalling is induced by phosphorylation of the ITAM in a single position, Y536, which then recruits the Src homology region 2 domain-containing tyrosine phosphatase SHP-1. SHP-1 can abrogate activatory signalling pathways, regulating the activation threshold and tempering the development of autoimmunity [227].

Another way in which activatory FcγRs can elicit inhibition of effector functions is through the Kurlander effect. Typically, mAbs are thought to bind in a trans fashion, they interact with their target epitope on one cell and the FcγR on another cell. However, it has also been shown that mAbs can interact in a cis fashion - binding to their target and an FcγR expressed on the same cell [235]. In this experimental system it was found that an antibody could form a heterotrimeric complex with the antigen and the FcγR, with one antibody able to block one FcγR as measured in a binding and blocking assay [236] [235]. The biological effect of the Kurlander effect is to potentially inhibit mAb effector functions through removing the ability of the antibody to bind in trans to the effector cell. It has also been proposed that it could induce cis binding ITAMi signalling to induce an immunosuppresive effect. This potential was demonstrated with a mAb developed against TLR-4, which suppressed LPS activation of myeloid cells. It was found that this effect was dependent on binding to FcγRIIA and not the inhibitory receptor, suggesting a role for ITAMi signalling, however this was not formally demonstrated [237]. Despite these alternate mechanisms of inhibition, FcγRIIB is considered the major regulator of activatory FcγRs.

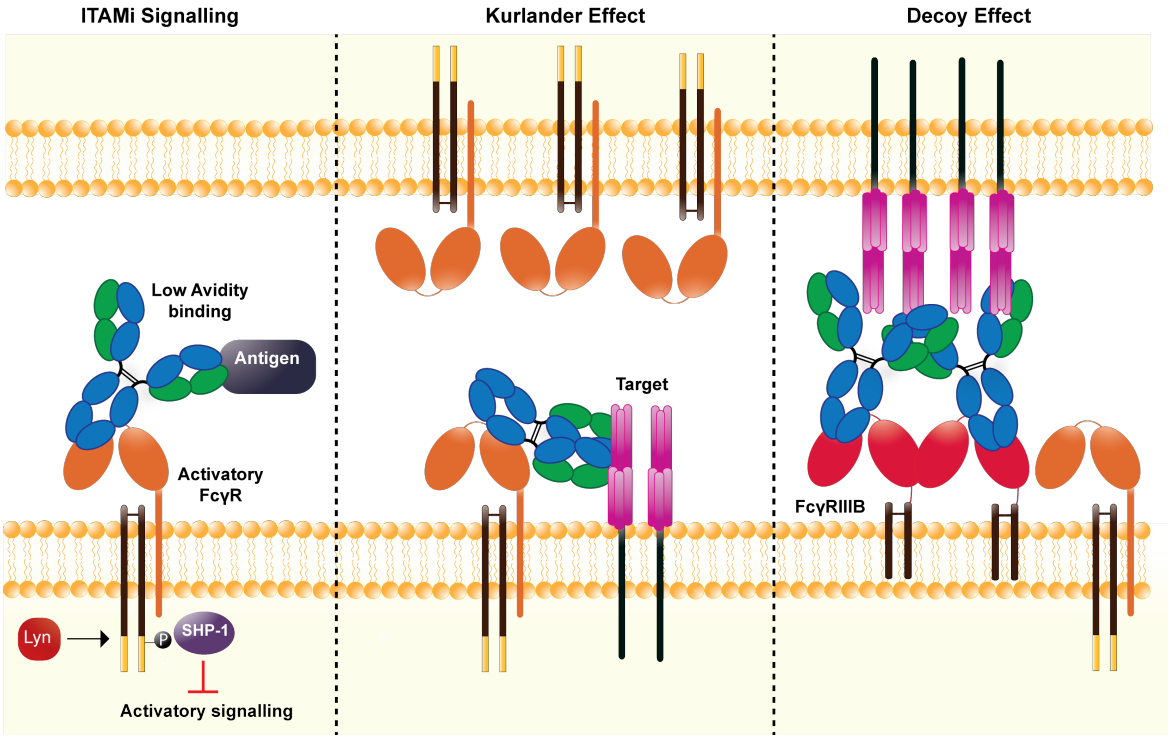

Figure 1.11: Alternative mechanisms of inhibition by FcγRs
FcγRs have been shown to elicit inhibition to antibody effector functions that do not require engaging the inhibitory FcγRIIB. Low avidity binding to activatory FcγRs has been shown to phosphorylate the intracellular ITAM on tyrosine residue 536 only. This allows interactions with the phosphatase SHP-1 which reverses intracellular activatory signalling. Alternatively, the Kurlander effect describes what happens when the antigen and FcγRs are expressed on the same cell, the antibody may bind its target and the FcγR in a cis fashion. This is unlikely to elicit activatory FcγR functions that would be expected from trans binding and may also induce ITAMi signalling. It has been shown that high expression of the GPI-linked FcγRIIIB negatively impacts antibody effector functions by sequestering the Fc of the antibody and has been described to act as a decoy receptor.

1.4.4 Physiological function of FcγRIIB

The sole inhibitory FcγR, FcγRIIB, is the direct regulator of activatory FcγR signalling, but it has important physiological roles that extend beyond its canonical function. FcγRIIB is the most broadly expressed FcγR and can be found in three isoforms, FcγRIIB1 (B1), FcγRIIB2 (B2) and FcγRIIB3 (B3). B1 is the predominant isoform expressed on B cells. The human B1 isoform contains a 19 amino acid insertion (47 amino acids in mice) in the intracellular domain as compared to the B2 isoform [238]. This insertion inhibits the receptors endocytic capacity by disrupting the ability of the receptor to enter into clathrin-coated pits when bound to IgG-immune complexes. The B2 variant is predominantly expressed on myeloid cells as well as liver sinusoidal endothelial cells (LSEC) and it can efficiently endocytose immune complexes due to the presence of a key dileucine motif in the cytoplasmic domain [239] [240]. The B1 variant has been proposed as an important regulator of BCR signalling. Immune complex binding to both the BCR and FcγRIIB negatively regulates BCR signalling, as well as preventing immune complex internalisation and anti-

gen presentation [241]. In contrast, the enhanced endocytic capacity of B2 is utilised by myeloid cells to enhance antigen presentation and by LSECs to remove small immune complexes (SIC) that pass through the liver [242]. The B3 isoform is found cleaved at the extracellular domain to form a soluble decoy receptor. FcγRIIB3 has been shown to bind to IgG complexed antigens in circulation, abrogating activatory FcγR binding on immune cells [243].

The classical inhibitory function of FcγRIIB is propagated through an intracellular signalling ITIM motif (consensus sequence S/I/V/LxYxxI/V/L [244]). When IgG-immune complex engages FcγRIIB and activatory FcγRs, FcγRIIB acts to temper ITAM signalling. Typically, stimulation of activatory FcγR results in activation of Src-kinases and the phosphorylation of the ITAM which recruits the kinase Syk and activates PI3K, converting PIP_2 into Phosphatidylinositol (3,4,5)-trisphosphate (PIP_3). Activated Src-kinases such as Lyn trigger the phosphorylation of the critical tyrosine residue within the ITIM [227]. This phosphorylation event recruits the SH2 domain-containing inositol 5'-phosphatase (SHIP) which catalyses the conversion of PIP_3 into PIP_2 (abrogating activatory signalling pathways). ITIM phosphorylation also recruits Src homology region 2 domain-containing phosphatase-1 (SHP-1), resulting in the de-phosphorylation of co-localised ITAMs and Syk [245] (Figure 1.12).

The importance of the inhibitory FcγR in regulating activatory FcγRs has been demonstrated through genetic deletion of FcγRII in mice. For example, FcγRII deficient macrophages showed enhanced immune complex mediated activation and a more serve phenotype of induced alveolitis [233]. *in vivo*, FcγRII knockout mouse infected with the bacteria Streptococcus pneumoniae showed reduced mortality, which could be due likely due to the release of inhibitory signalling on phagocytosis resulting in their enhanced ability to engulf and remove the pathogen. In a different experimental system, FcγRII knockout mice were vaccinated against Streptococcus pneumoniae. When challenged with live Streptococcus pneumoniae, these mice demonstrated a significant increase in pro-inflammatory cytokines and increased production of IgG, showing stronger immune responses at lower doses of pathogen compared to WT mice. At very high doses of pathogen, FcγRII knockout mice had increased risk of mortality, however the data ultimately shows the loss of FcγRII mediated inhibition resulted in enhanced immune responses [247].

In regard to murine tumour models, FcγRII seems to confer worsened survival outcomes.

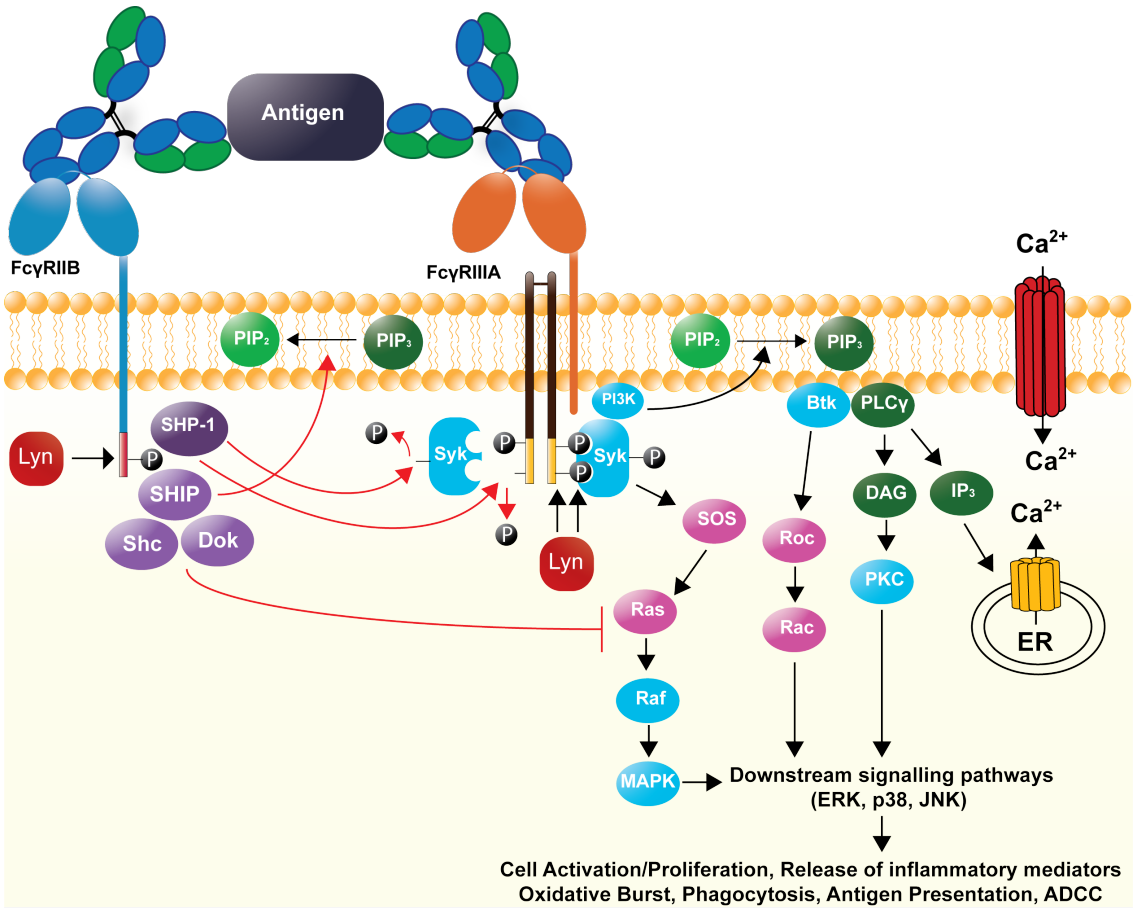

Figure 1.12: ITIM and ITAM intracellular signalling pathways.
Binding of an antigen (Ag)-antibody (mAb) complex to the activatory receptor, FcγRIIIA, results in the clustering of the receptor and phosphorylation of the ITAM's tyrosines by Lyn kinase. This provides a docking site for Syk kinases which is then in turn is phosphorylated and initiates downstream signalling pathways such as phospholipase Cγ and PI3K. PI3K converts PIP_2 into PIP_3 and results in the initiation of activatory pathways and enhanced calcium flux. This can trigger activation, proliferation and phagocytosis. Binding of an immune complex to the inhibitory receptor, FcγRIIB, results in the clustering of the receptor and phosphorylation of the ITIM's tyrosine by Lyn kinase. This provides a docking site for the phosphatases SHIP and SHP-1 which de-phosphorylate the ITAM and Syk kinase. SHIP is also recruited which counteracts PI3K and converts PIP_3 to PIP_2 inhibiting the signalling pathway. SHIP also recruits Shc and Dok to inhibit the activtiy of Ras. Adapted from Nimmerjahn et al, Ivashkiv et al [199] [246].

In one study a breast cancer xenograft model was implanted onto FcγRII deficient mice. When treated with breast cancer specific mAbs, the FcγRII deficient mice had enhanced tumour control as compared to WT mice [185]. Furthermore, another study demonstrated that FcγRII deficient mice had slowed tumour growth, enhanced infiltration of tumour myeloid cells and produced more tumour specific antibodies in the E.G7 tumour model as compared to WT C57BL/6J mice [248]. In contrast, FcγRII provides protection in autoimmune conditions. In a murine arthritis model, it was demonstrated that knocking out FcγRII resulted in severe cartilage destruction and joint inflammation. This was due to increased immune complex deposition, enhanced macrophage activation and the creation of an inflammatory environment created to excessive activation of FcγRII deficient

macrophages within the microenvironment [249]. These data suggest that the inhibitory receptor is an important mediator of inflammation in a wide range of disease states.

As well as modulating activatory FcγRs, FcγRIIB has been shown to regulate B cell activation to control the immune response and maintain immune tolerance [250]. When an immune complex binds to the BCR it initiates intracellular signalling via its associated ITAM motifs. If the BCR co-ligates with FcγRIIB, ITIM mediated inhibitory signalling will reverse ITAM signalling, increasing the threshold required for B cell activation [250]. This effect is mainly elicited through the phosphatase SHIP and to a lesser extent SHP-1. For efficient SHIP binding and phosphorylation, the ITIM motif and the C terminal 16 amino acids are required to fully stabilise the FcγRIIB-SHIP complex [251]. It was also found that mutating the key tyrosine residue into a phenylalanine results in near-complete abrogation of SHIP-FcγRIIB co-localisation [252]. FcγRIIB can suppress co-stimulatory signals provided by APCs as well as reducing antigen internalisation and presentation [203].

Recent evidence has shown FcγRIIB can inhibit BCR activation before ITAM phosphorylation. When presented antigen by APCs, the B cell forms an immunological synapse with the APC. This synapse contains BCR microclusters that are stabilised by membrane lipid rafts to drive strong BCR activation. When the BCR is co-ligated to FcγRIIB, the formation of the immune synapse and BCR microclusters are inhibited by FcγRIIB mediated perturbation of the local lipid membrane. Interestingly this function is independent of the receptor's ability to signal or associate with lipid rafts [253] [254]. It has also been shown that co-ligation of FcγRIIB alone, in the absence of the BCR, can induce apoptosis of the B or plasma cells. This pathway is independent of SHIP and the ITIM; instead cABL kinase interacts with an alternative phosphorylation site (Y264 on FcγRIIB1) resulting in cell cycle arrest and apoptosis. This mechanism is thought to be important in deleting auto-reactive B cells and plasma B cells when immune complexes reach toxic levels [255] [256]. These mechanisms are key to ensuring a controlled and appropriate B cell mediated IgG response. In support of these data, a genome wide association study found people who carried a rare in-frame deletion of FcγRIIB (Asn106del) resulted in a receptor that was unable to bind IgG1. This deletion was associated with increased circulating IgG and an increased risk of developing autoimmunity [257].

Whilst the extracellular domain can inhibit some physiological processes, the intracellular domain of FcγRIIB is considered to be most critical for eliciting receptor function. In regards to signalling, it was found that upon coaggregation of the murine FcγRIIB1 isoform

and the BCR, multiple sites were phosphorylated on the intracellular tail. These include the ITIM Y309 as well as Y290 and Y326, and to a lesser extent Y235 and Y264 [258]. It was found for stable SHIP interaction with the receptor, the ITIM core YSLL residues and the C terminal part of the receptor was required, whilst the LL residues of the ITIM motif were required for interactions with SHP-1 and SHP-2. Mutational studies of residues outside the ITIM significantly affected FcγRII inhibitory function [258]. Internalisation of immune complexes has been found to be modulated by the amino acid sequence of the cytoplasmic tail. As previously discussed, hFcγRIIB1 contains a 19 amino acid insertion that significantly reduces its ability to internalise. Research has indicated that this insertion in hFcγRIIB1 reduces endocytosis irrespective of its location on the cytoplasmic tail. The insertion is thought to functionally exclude hFcγRIIB1 from clathrin coated pits as the receptor displays even less internalisation than FcγRIIB with no cytoplasmic tail [259]. In contrast, the hFcγRIIB2 variant internalises immune complexes with high efficiency, and was found to require the cytoplasmic amino acid residues 18 - 31, which encompass the receptor ITIM. The critical tyrosine within the ITIM residue was found to be partially required for internalisation, slowing the kinetics of internalisation and reducing co-localisation to clarthin pits to 86% of WT hFcγRIIB2 [259]. In contrast, a later study suggests that removal of the ITIM phosphorylation site was completely dispensable, only reducing internalisation by 5% and suggested a C-terminal di-leucine motif is critical for eliciting internalisation [239].

As already described, FcγRIIB has a diverse expression pattern and has several important physiological roles that extend beyond its role as the regulator of FcγR and B cell activation (Figure 1.13). As previously discussed, activatory FcγRs are an important mediator of DC maturation and producing a vaccinal response; FcγRIIB is an important regulator of this process. If an immune complex binds to FcγRIIB instead of activatory FcγRs, this can result in reduced antigen presentation and DC maturation [260]. However, further evidence has shown that FcγRIIB expression on DCs can enhance the T-independent antigen response. Activatory FcγRs can internalise immune complexes and degrade the T-dependent antigen for presentation on MHC-II to activate T cells. In contrast, it was found that FcγRIIB is required for internalisation of immune complexes containing T-independent antigens. FcγRIIB internalises these immune complexes and recycles them to the cell surface to present native antigen to B cells, resulting in B cell priming and activation [261]. FcγRIIB has also been found to be critical to the activation of FDCs that are found within the germinal centre in mice. FDCs ensure the development and selection of high-affinity B cells and antibody responses. Upon germinal centre formation, FDCs

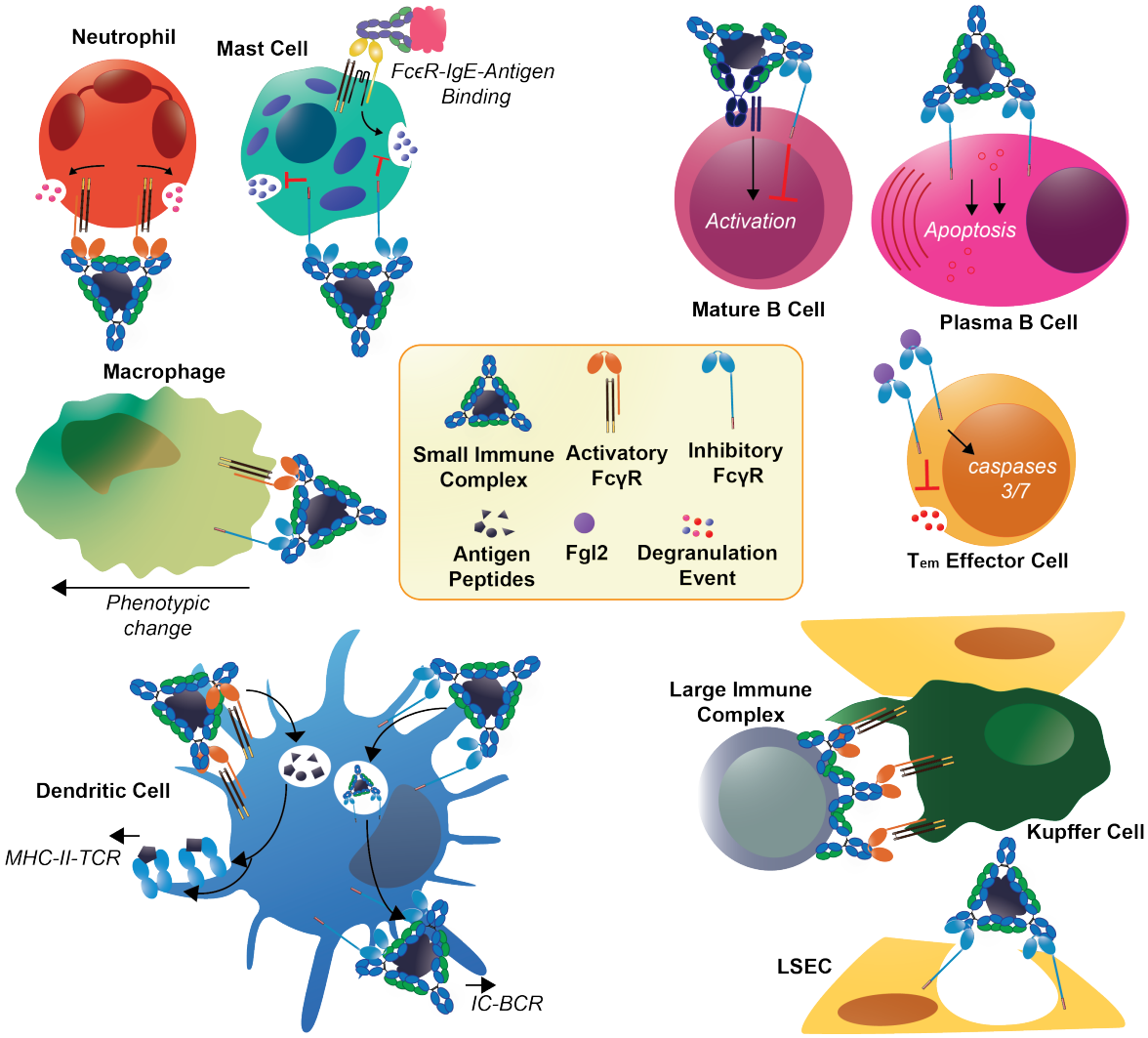

Figure 1.13: FcγR physiological functions.
Engagement of FcγRs elicit several important immune cell functions. Binding of activatory FcγRs on neutrophils can result in their degranulation and activation, whilst binding to FcγRIIB on mast cells can inhibit IgE induced degranulation. Immune complex binding to FcγRs on macrophages has a multitude of effects which includes changing the phenotype (e.g. more or less inflammatory). Immune complex binding to DCs can both enhance the presentation of T independent and T dependent antigens, depending on the engagement of activatory or inhibitory FcγRs. Within the liver, FcγRs are responsible for removing large immune complexes via Kupffer cells and small immune complexes via LSECs. Fgl2 binding to FcγRIIB on Tem cells can inhibit their activity whilst FcγRIIB engagement on B cells can result in their inhibition (Mature B cells) and apoptosis (Plasma cells).

upregulate their expression of FcγRIIB. FcγRIIB can present immune complexes to B cells within the germinal centre which was found to enhance clonal selection and somatic hypermutation (Figure 1.4) [262] [263].

As well as priming the adaptive immune system, FcγRIIB can modulate hypersensitivity reactions. Mast cells express both FcγRIIB and FcεRs. When FcγRIIB associates with FcεRs it has been shown to inhibit degranulation and the release of histamine [264]. This knowledge was recently utilised in an *in vivo* peanut allergy vaccine model. Peanut-sensitised mice were protected from IgE mediated anaphylaxis by vaccinating the mice

against a single peanut allergen (SPA). The allergen generated an IgG response so when the mice were challenged with peanut allergens, IgG-SPA complexes bound to FcγRIIB on mast cells and basophils, inhibiting IgE mediated signals [265].

Expression of FcγRIIB on immune cells is well characterised, but importantly the receptor is also found highly expressed on endothelial cells. These include the villus interstitium of the placenta, skeletal muscle microvascular endothelium and the LSE [266]. The LSE contains LSECs, highly specialised endothelial cells that form the walls of the liver sinusoids. They regulate blood flow, act as a selective barrier to hepatic stellate cells and hepatocytes as well as serving as a waste clearance system in conjunction with Kupffer cells [267]. LSECs have several immune functions that include acting as an adhesion platform for Kupffer cells, lymphoid cells and DCs, presenting antigen and priming naïve CD8 T cells [268]. Kupffer cells are liver resident macrophages associated with the LSE and represent 80-90% of tissue-resident macrophages within the body [269]. They have an important role in providing front line defence against microbial particles derived from the gastrointestinal tract via the portal vein [270]. Kupffer cells were initially thought to be the only liver-specific cell type that expresses FcγRIIB. However, further observations indicated that LSECs express FcγRIIB and it is integral to their role as professional pinocytes, removing small immune complexes from circulation [271]. LSECs have since been found to be one of the highest capacity endocytic tissues in the body, which is partially mediated by FcγRIIB [267]. Moreover, studies within mice have found that 72% of the total pool of FcγRIIB is expressed within the liver, with 90% being present on the LSECs [242]. A recent study even highlighted the significance of FcγRIIB in the removal and degradation of freely circulating HIV-IgG immune complexes within mice. Neutralising mAbs against cell free HIV pseudovirus in human FcγRIIB knock-in mice were found to effectively eliminate the viral particles by binding to FcγRIIB on LSECs, endocytosing the immune complex and trafficking to the lysosome for degradation. [272].

Recently, novel evidence has also been provided to suggest that FcγRIIB can regulate CTL activation in transplant rejection and tumour control independently of binding to IgG immune complexes [273]. The expression of FcγRs on T cells has been controversial but an increasing body of evidence suggests a portion of T cell subsets can express these receptors such as some CD3+ cells expressing FcγRIIIA, CD4+ cells expressing FcγRIIA and CD8+ cells expressing FcγRIIB [274] [275] [276]. In one study, the authors found FcγRIIB was expressed on T effector memory cells (Tem) in both mice and humans. In an allogeneic murine skin graft model, FcγRII deficient Tem mounted a stronger alloimmune

response than FcγRII+ Tem. Here, FcγRII+ Tem expressed higher levels of pro-apoptotic proteins such as caspases 3/7. Interestingly, the ligand for FcγRII+ on Tem cells was found to be fibrinogen-like 2 (Fgl2) and not IgG. Fgl2 is an anti-inflammatory cytokine produced by immune cells that can inhibit DC maturation and induce B cell apoptosis independently of ITIM phosphorylation [277]. These findings from transplant models were also applied to a tumour model, where FcγRII deficient Tem demonstrated better tumour control than FcγRII+ Tem [273]. Further evidence has since suggested that FcγRIIB expression on tumour infiltrating CD8+ in a murine melanoma model contributed to the suppression of the CD8 T cell response and FcγRIIB expression itself was identified on approximately 28% of CD8+ T cells by flow cytometry from patients with melanoma [278].

FcγRIIB has both signalling dependent and independent functions that are typically driven by interactions with IgG immune complexes but also with novel ligands. Overall, FcγRIIB demonstrates a complex biological picture of its mechanisms of action. For example, as previously discussed, FcγRIIB regulation of BCR signalling relies on ITIM phosphorylation. However, inhibition of immune synapse formation is signalling independent - the removal of the cytoplasmic domain did not impair the ability of FcγRIIB to block formation of the BCR immune synapse [254]. These signalling dependent and independent mechanisms will be discussed further in Section 1.4.5.

1.4.4.1 FcγRIIB and Autoimmunity

Autoimmunity is defined as the failure of central and peripheral tolerance mechanisms, leading to the activation of the immune system against self [203]. As a key regulator of immune activation and B cell clonal selection, it is of no surprise that dysregulation in FcγRIIB results in an increased risk of developing autoimmune diseases. Studies within FcγRII deficient mice have shown increased serum IgG, autoantibodies against single-stranded DNA and increased deposition of immune complexes within the glomeruli of the kidneys compared to their WT counterparts [279]. Other studies have shown than FcγRII deficiency increases susceptibility to collagen-induced arthritis and if the sle16 locus (a susceptibility locus for systemic autoimmunity in C57BL/6 mice [280]) is present in conjunction with mFcγRII, these mice can develop lethal lupus [281].

Genetic polymorphisms shed light on the importance of human FcγRIIB in maintaining immune tolerance. The isoleucine (I) 232 threonine (T) polymorphism in the transmembrane domain of hFcγRIIB has been well characterised due to its association with autoim-

mune conditions such as systemic lupus erythematosus (SLE) [282]. FcγRIIB dysfunction has been identified in SLE patients carrying two alleles of the 232T polymorphism and is thought to be a contributing factor to severity of the disease. NB: these patients also have decreased expression of FcγRIIB (although this is not thought to be related to the 232T polymorphism) [203]. An association between hFcγRIIB 232T or a downregulation of FcγRIIB expression on key immune cells (in comparison to healthy patients) has been established in patients with rheumatoid arthritis [283], anti-glomerular basement membrane disease [284], multiple sclerosis [285] and idiopathic thrombocytopenic purpura [286].

The I232T polymorphism is thought to affect hFcγRIIB mediated inhibition in several ways. Firstly, the 232T isoform reduces the propensity of hFcγRIIB to accumulate in lipid rafts. This means the receptor is less able to cluster and induce the intracellular signalling need to inhibit activatory receptors resulting in a more 'active' cellular phenotype. B cells carrying the 232T polymorphism have been shown to have increased proliferative potential and calcium mobilisation, processes usually modulated by hFcγRIIB signalling [287] [288]. Further research showed hFcγRIIB mediated blockade of BCR-mediated immune synapse formation was reduced in the presence of the 232T isoform, and this was shown to be independent of ITIM signalling [254]. Furthermore, molecular dynamic simulations and single-cell FRET assays have indicated that the 232T isoform tilts the receptor's extracellular domain towards the plasma membrane, allosterically inhibiting the binding of ligand [289].

The balance of activatory and inhibitory FcγRs is an important contributor to the pathogenesis of autoimmunity, thus making FcγRs a focus of therapeutic intervention. Intravenous immunoglobulin (IVIG) is a therapeutic product consisting of pooled normal human polyclonal IgG obtained from healthy donors, and is commonly used to treat autoimmune conditions [290]. It is thought to broadly work by interacting with and blocking FcγRs. However, it is expensive and has limited availability, driven by the high doses needed per patient (500 mg/kg). This, alongside its unknown precise mechanism of action have limited its further use, with the latter hampering development of next-generation therapeutics that do not require a diverse pool of healthy donors [290]. hFcγRIIB has been implicated as responsible for some of IVIG's therapeutic effects. When treated with IVIG, human monocytes and B cells showed an upregulation of FcγRIIB expression [291], which was also observed on splenic macrophages of mice treated with IVIG [292]. IVIG may directly stimulate FcγRIIB to induce inhibitory signalling on B cells and immune effector cells [293].

Antibody glycoengineering has been used to try and enhance the efficacy of IVIG. It was found that IVIG enriched for sialylated forms of IgG displayed a 10-fold increase in anti-inflammatory effects compared to standard IVIG therapy [294]. This observation in mice was linked to sialylated IVIG binding to SIGNR1 (the murine ortholog of DC-SIGN) resulting in an indirect upregulation of mFcγRII [295]. However, other groups have contested these results after being unable to reproduce them. These studies have failed to show an upregulation in FcγRIIB expression in response to IVIG and that IVIG's therapeutic effect is independent of sialylation [296]. One study even found that sialylated IgG cannot bind to DC-SIGN [297]. This area of research highlights how findings in murine immunology are not always applicable to human immunology.

Despite the unknown mechanism of action, IVIG has been established as a useful immunosuppressive therapy and FcγRIIB's potential involvement has been investigated as a means to try and develop the next generation of IVIG-like therapeutics. For example, a recombinant soluble form of FcγRIIB, known as valziflocept, was recently developed for SLE and immune thrombocytopenic purpura (ITP) patients. With the understanding that IVIG may work by reducing binding of pathogenic IgG to activatory FcγRs, valziflocept was designed as a decoy receptor, neutralising pathogenic IgG in circulation so it cannot bind. Bi-specific antibodies have also been developed to target FcγRIIB and CD19 as well as FcγRIIB and CD79B. These bi-specifics bind to the components of the BCR and FcγRIIB to sterically inhibit activation of those cells to alleviate symptoms of diseases. Both therapies showed some successes but have not continued beyond Phase II clinical trials [298].

1.4.5 FcγRIIB and immunotherapy

As a greater appreciation of FcγRIIB biology has emerged, it's implications for mAb mediated immunotherapy has become more complex. In some cases, the classical ITIM mediated inhibitory signalling negatively regulates immunotherapy. In others, the signalling independent mechanisms of FcγRIIB have been shown to both positively and negatively regulate antibody-mediated immunotherapy. These varied aspects are detailed below.

1.4.5.1 FcγRIIB and CD20 antibodies

Rituximab, the type-I anti- CD20 mAb, evokes multiple effector functions that include CDC, ADCP and ADCC (as detailed in Section 1.3.5.1). However, these are limited by its propensity to rapidly internalise from the cell surface, which results its reduced effector functions and mAb degradation, a process that is enhanced by the presence of FcγRIIB [299] [300]. Type-II mAbs are more resistant to CD20-FcγRIIB mediated internalisation which is most likely due to their inability to cluster into lipid rafts [179]. Studies have suggested that when type I mAbs bind CD20, the Fc portion of the mAb interacts with FcγRIIB on the same cell in a cis fashion via antibody bipolar bridging (Figure 1.14). The rate of type-I anti-CD20 mAb internalisation can be correlated with the cell surface expression of FcγRIIB [299] and this finding was also found to be applicable to samples from various B lymphoma patients. Specifically, mantle cell lymphoma (MCL) and follicular lymphoma (FL) patients who had high levels of FcγRIIB on their lymphoma cells were associated with high rates of internalization and reduced response to rituximab therapy [299] [301]. Further evidence has shown that this process is signalling independent and does not require the phosphorylation of the FcγRIIB ITIM [300]. A recent clinical study also highlighted how FcγRIIB expression correlated with worsened prognosis when diffuse large B cell lymphoma (DLBCL) patients were treated with rituximab and chemotherapy. When the same analyses was conducted with obinutuzumab, a type-II mAb, FcγRIIB expression did not show a significant correlation with treatment outcome [302].

FcγRIIB may also exert inhibitory effects on immune effector cells. Kupffer cells have been identified as key effector cells for mediating CD20 mAb depletion *in vivo* via FcγRs [303] [304]. FcγRIIB has been shown previously to reduce macrophage effector functions *in vitro* and FcγRII deficient mice display reduced tumour growth and better responses to mAb therapy (Figure 1.14) [233] [248] [185]. It was further shown that in CD20 expressing xenograft and syngeneic tumour models, anti-CD20 mAbs showed enhanced therapeutic efficacy in FcγRII knock out mouse models through optimal engagement with activatory FcγRs on effector populations such as macrophages [305]. This evidence suggests that the expression of FcγRIIB on immune effector cells is also responsible for reducing the efficacy of anti-CD20 mAbs. However, the contribution of FcγRIIB mediated internalisation and FcγRIIB inhibition of immune effector cells remain to be elucidated. In addition, the contribution of ITIM mediated signalling to inhibition of immune effector functions has not been fully explored.

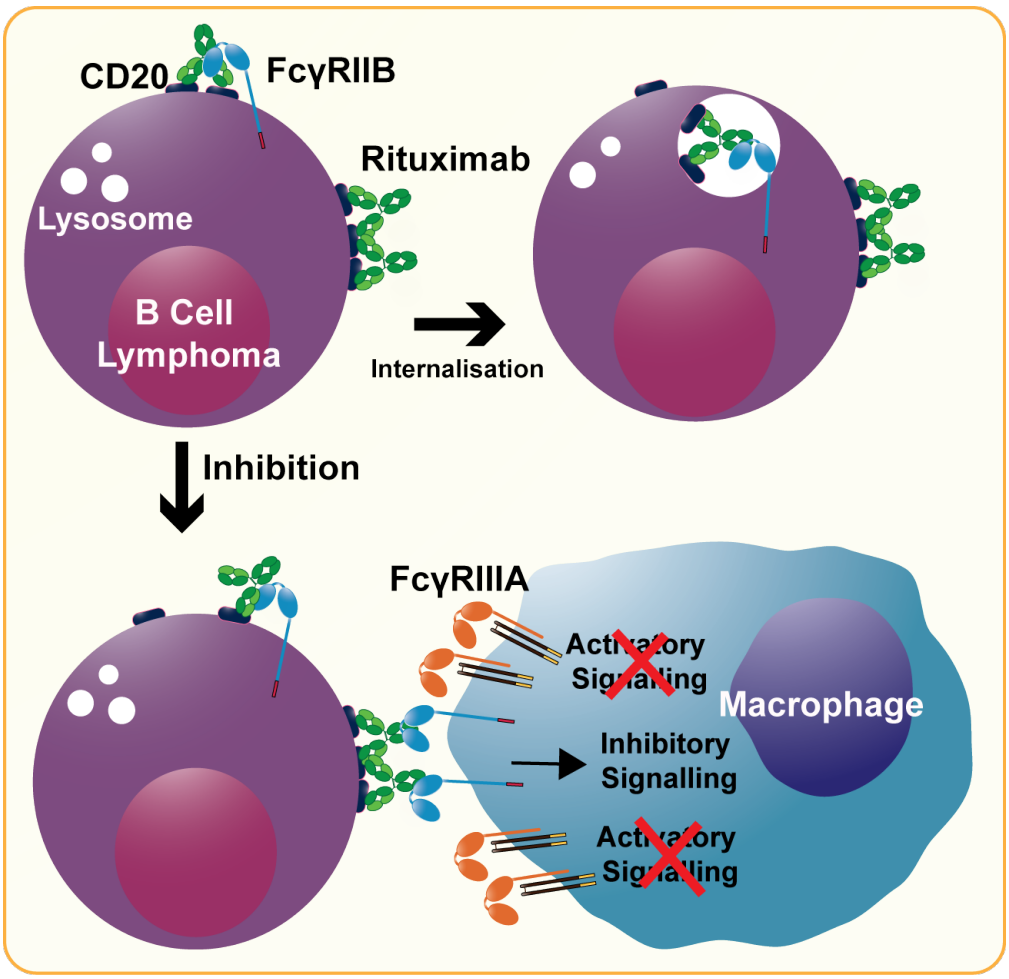

Figure 1.14: FcγRIIB Regulation of CD20 mAb immunotherapy
Rituximab (Type I anti-CD20) can bind to its target on B cells and subsequently be rapidly internalised and marked for degradation by cis binding of FcγRIIB, also known as antibody bipolar bridging. Rituximab may also bind to FcγRIIB on effector cells in a trans fashion and initiate inhibitory signalling resulting in less effective effector mechanisms such as ADCP and ADCC.

1.4.5.2 FcγRIIB and immunostimulatory antibodies

Interactions with FcγRIIB has been shown to be critical for the efficacy of some immunostimulatory mAbs, such as those targeting CD40, a member of the TNFR superfamily. CD40 is type I transmembrane protein expressed on APCs, that interacts with its trimeric ligand, CD40L primarily on activated CD4 T cells. CD40-CD40L binding results in a series of enhanced immune responses that include DC licensing, augmented antigen-cross presentation, enhanced B cell germinal centre formation, differentiation and proliferation [306] [307]. Agonistic CD40 mAbs bind to their target on APCs, acting as a pseudo-ligand in place of CD40L, which results in potent activation of myeloid cells, B cells and DCs [306]. For activation, CD40 requires cross-linking by the CD40 mAbs to mimic the trimeric binding of CD40L. Studies have shown that monovalent F(ab) binding to CD40 does not cause activation, instead, bivalent IgG is routinely required for cross-linking of CD40 and

APC activation, with further cross-linking through some means required. This crosslinking effect was found to be mediated by mFcγRII *in vivo* [308] [309].

In this context, FcγRII is thought to act as a scaffold that binds the Fc domain of the CD40 mAb in a trans fashion on accessory immune cells, providing hyper cross-linking of the receptor to initiate activatory signalling (Figure 1.15). This has been demonstrated *in vivo* by the requirement of mouse IgG1 (which preferentially binds mFcγRII) for maximal therapeutic benefit. In contrast, mouse IgG2a (which binds preferentially to activatory FcγRs) showed a lack of efficacy and when therapy experiments were repeated in situations where FcγRII was blocked and/or absent, the activity of the mIgG1 CD40 mAb was lost [308]. CD40 mAbs have also been utilised as a therapeutic tool in murine carcinoma models, where it was also found that *in vivo* efficacy was dependent on FcγRII expression, specifically within the tumour microenvironment [143]. Immunostimulatory mAbs targeting other TNFRs such as 4-1BB and OX40 have also been identified as requiring FcγRIIB for crosslinking and activation [145] [144].

To dissect the requirements for CD40 agonism, a series of selective knockdown and FcγRIIB signalling studies were conducted. Firstly, to assess the impact of FcγRIIB mediated signalling on CD40 agonism, SHIP deficient mice were treated with CD40 mAbs in an OT-I expansion model. The researchers found little change in OT-I specific expansion compared to a WT mouse, whilst FcγRII deficient mice showed minimal expansion of OT-I cells [310]. These data indicate SHIP mediated signalling is not required for CD40 agonism. Next, to interrogate what cells were responsible for providing FcγRIIB mediated crosslinking of CD40 mAbs, a series of cell-selective FcγRII knockout models, FcγRII heterozygous (reduced receptor expression) and FcγRII homozygous (full receptor expression) mice were developed. It was found that CD40 driven agonism of APCs was lost if FcγRII was selectively knocked out on murine B cells. It was also found that CD40 agonism was significantly reduced in FcγRII heterozygous mice, suggesting that a threshold level of expression is required to induce agonism (Figure 1.15). This finding was also relevant for DR5 mAbs, whereby FcγRII expression on DCs and macrophages within the liver were responsible for eliciting agonism, most likely due to the high expression of DR5 on cholangiocytes [310].

To augment CD40 agonism further, antibodies have been engineered to selectively enhance FcγRIIB binding. Anti-CD40 mAbs displaying the V11 set of mutations (G237D, P238D, H268D, P271G, A330R) [312] showed an enhanced anti-OVA response *in vivo* as

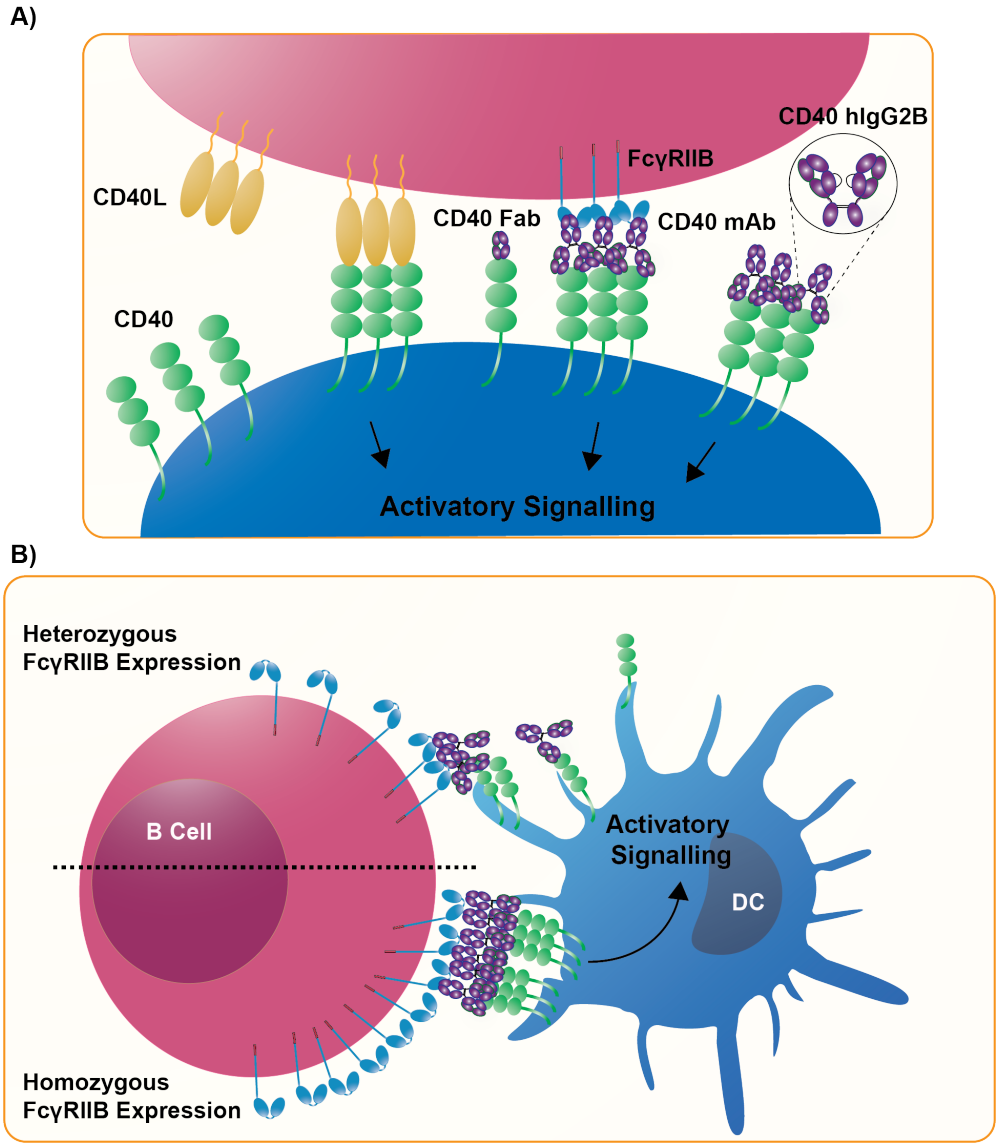

Figure 1.15: FcγRIIB Regulation of CD40 mAb immunotherapy
A) CD40 activation typically requires activation by trimerisation induced by CD40L. anti-CD40 mAbs can bind to their target on effector immune cells (such as dendritic cells) and require hyper cross-linking by FcγRIIB to imitate CD40L binding. Alternatively, the use of hIgG2B antibodies can be used to overcome the requirements for FcγRIIB mediated cross-linking. B) For CD40 mAb activity, there is a requirement for a threshold of FcγRIIB expression on accessory cells within the microenvironment. In a heterozygous FcγRII (-/+) mouse model, CD40 mAbs did not have sufficient cross-linking to initiate signalling and therefore activation. In a homozygous FcγRII (+/+) mouse model CD40 mAbs can sufficiently activate CD40 and initiate activatory signalling [308] [309] [310] [311].

measured by the expansion of OVA specific CD8+ T cells, driven by FcγRIIB cross-linking [313]. However, enhanced efficacy can also increase the toxicities associated with CD40 agonism. Systemic dosing with this anti-CD40 mAb was found to induce hepatotoxicity and thrombocytopenia. In order to maintain therapeutic doses and minimise systemic toxicities, the authors injected lower doses of the mAb directly into tumours, this resulted in significantly improved survival outcomes compared to systemic administration in the MC38 colon tumour model [314].

An alternative route of research has taken the opposite approach and attempted to elicit FcγRIIB-independent agonism. Here the approach is to promote receptor clustering without the need for FcγR involvement. For anti-CD40 mAb this was achieved by isotype switching to the human IgG2 isotype. hIgG2 has a unique hinge structure and so this is proposed to result in a more rigid antibody that is better able to cross-link CD40 independently of FcγRs [311]. Specifically an isoform of hIgG2, termed IgG2B, was shown to deliver FcγR-independent agonism for CD40, even converting CD40 antagonists into strong agonists ([146]). hIgG2 is also able to deliver enhanced cross-linking and agonism for other TNFRs including OX40 and 4-1BB ([315]) as well as some non-TNFR super family members such as CD28 ([311]).

1.4.5.3 Therapeutic Targeting of FcγRIIB

As detailed above, both CD20 and CD40 mAbs highlight how FcγRIIB can be manipulated to modulate antibody-mediated immunotherapy. With direct targeting mAbs, the blockade of FcγRIIB could help improve the depletion of target cells. In contrast, improving the affinity of some immunostimulatory mAbs for FcγRIIB could increase their therapeutic potential as discussed above.

An active area of research to improve mAb therapy has been to introduce mutations into the IgG Fc domain to change FcγR binding profiles. With regards FcγRIIB, a number of mutations have been examined that reduce FcγRIIB binding, improve activatory FcγR binding, or a mixture of both. The G236A mutation of the hIgG1 Fc was found to provide a 6-7 fold enhancement in binding to FcγRIIA, whilst not affecting FcγRIIB binding [316]. Further research has since found that the G236A/A330L/I332E mutation of hIgG1 enhances binding to FcγRIIA and FcγRIIIA whilst reducing binding to FcγRIIB [317]. *in vitro* studies showed that this mutated Fc had superior ADCC capability compared to WT hIgG1 and that *in vivo* depletion of hCD20 transgenic B cells was enhanced. However, the mutations resulted in decreased stability and *in vivo* half-life, making it unsuitable for clinical translation [232] [318]. In contrast, the S239D/I332E hIgG1 mutation that increases binding to both FcγRIIA and FcγRIIB is thought to drive enhanced ADCC and has been adopted into the recently approved anti-CD19 mAb tafasitamab for the treatment of DLBCL and chronic lymphocytic leukaemia (CLL) [319]. How much more active it is than rituximab remains to be seen and how much any improved efficacy relates to the Fc mutations will be difficult to assess. Although mAb engineering has the potential to improve

therapy, the highly homologous FcγR family makes it difficult to selectively improve binding to a single FcγR. Therefore some initiatives aimed at changing the FcγRIIB binding profile have looked at targeting the inhibitory receptor directly using other mAb reagents.

Targeting FcγRIIB directly using mAbs is a relatively new area of research due to the difficulties in finding a specific mAb that distinguishes hFcγRIIB from hFcγRIIA owing to the 96% sequence homology in the extracellular region [320] (Section 1.4.1). Initial murine studies using the more easily targeted mFcγRII showed that blockade of the inhibitory receptor could be a viable strategy to improve direct targeting mAbs. *in vitro* studies showed that directly targeting the mouse FcγRII, using the antibody AT130-2, can result in programmed cell death (PCD) and phagocytosis of lymphoma cells. However, when the mAb was assessed *in vivo* it was quickly cleared from circulation due to FcγRII mediated internalisation and degradation, limiting its efficacy [321].

Anti-human FcγRIIB antibodies have since been produced that are successfully able to distinguish FcγRIIB from FcγRIIA [322] [323] [133]. One of these mAbs (BI-1206/6G11) produced by BioInvent is currently in clinical trials [324] as a human IgG1 variant and a glycoengineered variant that lacks FcγR binding is in pre-clinical testing (BI-1607/6G11-N297Q) [325]. 6G11 has been shown to antagonise FcγRIIB and can augment rituximab therapy through increased ADCP, ADCC and direct cell death of lymphoma cells in pre-clinical xenograft tumour models (Figure 1.16) [323]. Phase I/IIa data currently shows that 6G11 is tolerated in patients and may improve rituximab therapy [326] [327]. The deglycosylated variant, 6G11-N297Q can also antagonise FcγRIIB to improve mAb immunotherapy [323]. Current evidence suggests that 6G11 and 6G11-N297Q have a more stable pharmacokinetic profile in pre-clinical models and humans than seen with AT130-2 targeting mFcγRII, making targeting human FcγRIIB a viable clinical approach. Other companies are now taking an interest in targeting FcγRIIB as a therapeutic strategy. Novartis have developed a FcγRIIB specific mAb with an afucosylated Fc region to enhance Fc mediated effector functions. This represents a different approach to BioInvent, as Novartis aim to potentially use their afuscolyated mAb as a direct targeting agent against FcγRIIB+ tumours, whilst BioInvent aim to enhance rituximab therapy by blocking the negative contributions of FcγRIIB. The Novartis reagent has shown synergy with anti-CD20 mAbs in depleting FcγRIIB+ tumours in xenograft murine models but has not been tested in systems where FcγRIIB is also expressed on cells of the host [133].

In summary, all these data indicate that FcγRIIB modulation of antibody immunotherapy is

complex. To design better direct targeting and immunostimulatory antibodies, the biology of the FcγRIIB requires greater understanding. Such research is required to fully discern the mechanisms through which FcγRIIB inhibits mAb-based therapy and when and how therapeutic blockade of FcγRIIB may enhance antibody-mediated immunotherapy.

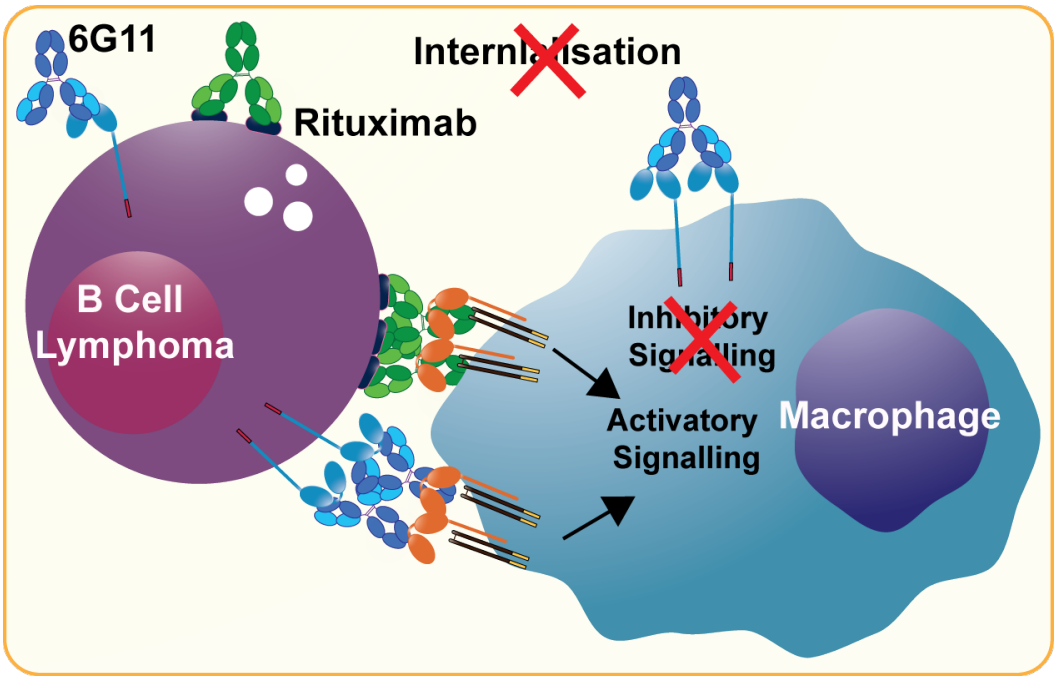

Figure 1.16: FcγRIIB directed immunotherapy
mAb therapy targeting FcγRIIB (6G11) can reduce internalisation of rituximab from the cell surface and enhance opsonisation of the target cell increasing rituximab efficacy

1.5 Hypothesis and Aims

FcγRIIB has been shown to broadly modulate mAb immunotherapy and has increasingly become a focus of antibody research. Antibodies have been engineered to increase or reduce binding to FcγRIIB to enhance their therapeutic benefit and FcγRIIB has even become the target of mAb therapy itself. The research described in this thesis aims to expand our understanding of how FcγRIIB negatively regulates mAb immunotherapy and how therapeutic blockade of the receptor may augment it. Specifically, it addresses whether the signaling from the ITIM is important for the inhibitory effects of the receptor and if it is important to overcome. The initial hypothesis therefore was that the loss of the FcγRIIB ITIM mediated signalling will reduce its inhibitory function and augment mAb immunotherapy. The hypothesis was tested primarily using two transgenic mouse models, a signalling competent human FcγRIIB transgenic mouse (hFcγRIIB Tg) and a novel non-signalling ITIM mutant human FcγRIIB transgenic mouse (NoTIM). The biology of human FcγRIIB was then explored using *in vitro* immunoassays and *in vivo* therapeutic models.

The specific aims of the project were as follows:

1. Characterise the novel NoTIM mouse, assessing the expression of the transgene and its impact upon *in vitro* effector functions
   (a) Confirm the integration and expression of the NoTIM transgene, and compare expression to the hFcγRIIB transgenic mouse model
   (b) Compare the expression pattern of the endogenous murine FcγRs in C57BL/6J, mFcγRII KO, hFcγRIIB Tg and NoTIM mice
   (c) Functionally examine the ability of the NoTIM receptor to elicit inhibitory signalling and how the loss of function effects cell functions *in vitro*

2. Assess the impact of the NoTIM transgene on the efficacy of mAb target cell depletion and mAb target cell agonism *in vivo*
   (a) Use a dose escalation model to assess the differences in depletion of B cells using both anti-CD20 mIgG1 and mIgG2a in C57BL/6J, mFcγRII KO, hFcγRIIB Tg and NoTIM mice
   (b) Dissect the contribution of FcγRIIB mediated internalisation, mAb half life and cell specific expression to the inhibition of direct targeting anti-CD20 mAb depletion

(c) Examine if blockade of hFcγRIIB using mAb directed strategies can improve target cell depletion of CD20+ target cells

(d) Deplete circulating lymphocytes in mFcγRII KO, hFcγRIIB Tg and NoTIM mice using specific mAbs to understand if previous observations are unique to the depletion of CD20+ B cells

(e) Utilise the ovalbumin (OVA) antigen and OT-I adoptive transfer model to confirm that FcγRIIB drives mAb mediated agonism of CD40 independently of inhibitory signalling

3. Apply the understanding of FcγRIIB mediated inhibition of direct targeting mAb therapy to murine tumour models

(a) Examine the impact of hFcγRIIB on direct targeting mAb therapy in the Eμ-T cell leukemia-1 oncogene (TCL1) malignant B cell model

(b) Examine the impact of hFcγRIIB on the depletion of T regulatory cells E.G7 tumour bearing mice

Chapter 2

Methods and materials

2.1 Molecular biology

2.1.1 Generation of the NoTIM mouse

The NoTIM transgenic mouse model was generated by Dr. Yury Bogdanov at the University of Southampton in collaboration with Cyagen US Inc. Details of production are below.

The human FCGR2B2 gene was isolated and generated as previously described ([323]). In brief, the full length FCGR2B2 coding region was amplified from the human Burkitt's lymphoma cell line Raji cell cDNA and ligated with the native FCGR2B promoter through overlapping PCR. The DNA construct was cloned into a pBluescript plasmid using the restriction enzyme location sites NotII/SmaII/PvuI. The ITIM mutation (Y273F, TAT to TTT) and an additional mutation (Y254F, TAC to TTT) was introduced using back-to-back primers containing the DNA mutation that were subsequently ligated into the DNA construct and sequenced to select the correct clone.

Cyagen US Inc then microinjected the purified expression cassette into the pronuclei of C57BL/6J zygotes. C57BL/6J NoTIM founder mice were then rederived into the animal unit and backcrossed with mFcγRII$^{-/-}$ to remove the endogenous mouse inhibitory receptor. The resulting progeny were screened by PCR (amplifying genomic DNA) and flow cytometry of peripheral blood to check for expression of the transgene.

2.1.2 Isolating DNA from murine ear tips

Murine ear punches were collected and placed in 1.5 mL tubes containing 97.5 μL ear lysis buffer (50 mM Tris pH 8.9, 12.5 mM $MgCl_2$, $6H_2O$, 0.5% Tween-20) and 2.5 μL proteinase K (ThermoFisher Scientific). Tips were placed in a PTC-200 thermocycler (MJ Research) overnight at 55°C for digestion. The resultant lysates were then maintained at -20°C until ready for analysis by PCR.

2.1.3 Polymerase chain reaction (PCR)

Specific primers were used to amplify regions of interest. A full list of primers can be found in Table 2.1. Ear tip lysate were then added to the following reaction mix containing the primers of interest in order to amplify NoTIM DNA:

- 10 μM forward and reverse primers
- 100 mM Deoxynucleotide triphosphates (Promega)
- 10x Pfu buffer (200 mM Tris-HCl, 100 mM KCl, 100 mM $(NH_4)_2SO_4$, 20 mM $MgSO_4$, 1% Triton X-100, 1 mg/mL nuclease-free BSA) (Promega)
- 2-3 u/μL Pfu Enzyme (Promega)
- 500 ng ear tip lysate
- Milli-Q H_2O to a total volume of 25 μL

The reactions were mixed well and then placed into Bio-rad C1000 thermocycler using the following program:

1. 95°C for 5 minutes
2. 95°C for 30 seconds
3. 60°C for 1 minute
4. 72°C for 2 minutes
5. Repeat steps 2-4, 32 times
6. 72°C for 10 minutes
7. 4°C until further notice

PCR samples were then run through a 1% agarose gel using electrophoresis to visualise any PCR products (Section 2.1.4).

Primer	Sequence 5'-3'
NoTIM Screen F	AGAAGCTTGCTGGTGCACGCTGTCCTGCATCAC
NoTIM Screen R	TGTCCCAGCAACAGGAGCCAGGAATAGCACAGCTGT
Tyr Mutation F	AGGCTGACAAAGTTGGGGCTGAGAACACAATCACCTTTTCA CTTCTCATGCACCCGGATGC
Tyr Mutation R	GTTGCTGCTGTAGTGGCCTTGATCTTTTGCAGGAAAAAGCGG ATTTCAGCCAATCCCACTAATCCTGATG
NoTIM Mut	CTCATCCAAGCCTGTGACCATCAC

Table 2.1: Table of primer sequences
NoTIM Screen = primers used to screen NoTIM progeny, Tyr mutation = primers used to introduce NoTIM mutations. NoTIM Mut = primers used to identify NoTIM mutations. F = Forward. R = Reverse.

2.1.4 DNA gel electrophoresis

3 μL of 6x orange DNA loading dye (Thermo Scientific) was added to each DNA sample and then run on a 1% agarose gel containing 0.05% GelRed™ (Biotum) in tris(hydroxymethyl) aminomethane (TAE) buffer (40 mM TRIS (base), 20 mM acetic acid and 1mM Ethylenediaminetetraacetic acid [EDTA]). O'Gene Lader 100bp and 1kb molecular markers (Thermo Scientific) were used as molecular weight markers to evaluate size of DNA fragments. The samples were run at 140V for 50 minutes and imaged using a BioRad UV imager.

2.1.5 DNA gel extraction

DNA was excised from agarose gels using a scalpel and the QIAquick Gel Extraction Kit (Qiagen) was used to purify the DNA by following the manufacturer's instructions. The kit uses bind-wash-elute procedure that removes impurities from DNA samples using a series of high and low salt buffers. The purified DNA was quantified by absorbance readings at 260nm on a NanoDrop 1000c (ThermoFisher).

2.1.6 DNA sequencing

DNA samples were diluted to 10 ng/μL using TAE buffer and sent to Source Biosciences (Nottingham) for Sanger Sequencing along with the relevant primers (Table 2.1). Sequencing data was analysed using SeqManPro Software (DNASTAR Laser-gene).

2.2 Cell culture

2.2.1 Cell thawing

Cells stored in liquid nitrogen were removed from storage and immediately placed on ice. To thaw cells, 5 mL of pre-warmed sterile media was gently added to cells using a Pasteur pipette and then placed into a universal tube. The cells were then centrifuged at 250 x g for 10 minutes and the supernatant was poured off. The pelleted cells were resuspended in 1 mL of media and a cell count was carried out (Section 2.2.3). Cells were then typically resuspended to a concentration of $0.5x10^6$ cells/mL and incubated at 37°C and 5% CO_2 in a New Brunswick Galaxy 170R incubator.

2.2.2 Cell line maintenance

Cells were maintained in media as detailed in 2.2. The murine E.G7-OVA cell line (derivative of EL4 parental cell line) was maintained in supplemented Roswell Park Memorial Institute 1640 Media (RPMI) (ThermoFisher), also known as R10 media, with the addition of 500 μg/mL Geneticin (Gibco) to maintain selection for cells expressing OVA. The cells were maintained at a density of $0.25\text{-}0.5x10^6$ cells/mL. Cells were removed from Geneticin selection 24 hours prior to injection *in vivo*. Murine π-BCL_1 cells were cultured in R20 media and maintained at $0.25\text{-}0.5x10^6$ cells/mL.

For sub-culturing, E.G7 suspension cells were aspirated from the flask into a universal and then centrifuged at 250 x g for 5 minutes before being resuspended in an appropriate volume of media. Murine π-BCL_1, a semi-adherent cell line, required the aspiration of media and then the addition of enough PBS to cover the cell surface. Cells were then lifted using a cell scraper (Fisher Scientific) and the PBS-cell mixture was then added to the aspirated media and centrifuged as above. Cells were sub-cultured every 2-3 days to maintain the optimal density. All cells were incubated at 37°C and 5% CO_2 in a New Brunswick Galaxy 170R Incubator.

Media	Components	Cells
R10	RPMI media (ThermoFisher), 10% Foetal Calves Serum (FCS) (Sigma-Aldrich), L-glutamine (200 μM), sodium pyruvate (100 μM), penicillin (100 U/mL), streptomycin (100 μg/mL), β-mercaptoethanol (2-ME) (55μM) (Sigma-Aldrich)	Primary mouse cells, E.G7 cell line
R20	RPMI media (ThermoFisher), 20% Foetal Calves Serum (FCS) (Sigma-Aldrich), L-glutamine (200 μM), sodium pyruvate (100 μM), penicillin (100 U/mL), streptomycin (100 μg/mL), 2-ME (55μM), amphotericin B (2μg/mL)	π-BCL_1 cell line
L929 Conditioned Media	Dulbecco's Modified Eagle Medium (DMEM) media, 10% FCS (Sigma-Aldrich), 1% HEPES, penicillin (100 U/mL), streptomycin (100 μ/mL), macrophage-colony stimulating factor (m-CSF)	BMDMs

Table 2.2: Mammalian cell culture media

2.2.3 Determining cell concentration and viability

The concentration of cells was determined using either a Coulter Counter Z1 particle counter (Beckman Coulter) or a Cell Drop FL cell counter (DeNovix). For the Coulter counter, 20 μL of cell suspension was placed diluted with 10 mL isoton II diluent (Beckman Coulter), with two drops of Zap-OGLOBIN (Beckman Coulter) to lyse any red blood cells (RBC). The Coulter Particle Counter (Beckman Coulter) was then used to determine the cell concentration.

For the Cell Drop FL, 5 μL of cells were mixed with 5 μL of acridine orange and propidium iodide (AO/PI) viability solution (DeNovix) and then the 10 μL solution was pipetted into the cell counting chamber. AO is permeable to both live and dead cells, staining all nucleated cells to generate green fluorescence and exclude RBCs from cell counts. PI is only permeable to cells with compromised cellular membranes and stains dying cells with red fluorescence. The Cell Drop allowed the quantification of cells and the percentage viability of the sample by calculating the number of AO stained cells and AO/PI stained cells.

2.3 Antibodies for *in vitro* and *in vivo* experimentation

2.3.1 Antibody quality control

Antibodies produced in-house by the Antibody & Vaccine Group production team were produced using either from hybridomas, transient expression in ExpiCHO-S cells or stable expression in CHO-K1S cells. Antibodies were then checked for aggregation, protein impurities, and endotoxin contamination before use in experimentation.

Antibodies were checked for aggregation by using a size exclusion high performance liquid chromatography (SE-HPLC) system. Protein samples were loaded onto a gel filtration column and attached to an HPLC infinity system (Agilent). Only samples with less than 1% aggregation were collected.

Capillary electrophoresis sodium dodecyl sulphate-polyacrylamide gel electrophoresis (CE SDS-PAGE) was used to ascertain protein purity and also to evaluate any unexpected protein behaviours. A size exclusion column was then used to remove any impurities.

Finally, antibodies were subject to an endotoxin assay (Charles River) to measure the contamination of antibody samples. Samples were prepared according to the manufacturers instructions and analysed using Endosafe-PTS cartridge and Endotoxin cartridge reader (Charles River). The assay utilises limulus amebocyte lysate to recognise endotoxin and samples are quantified using a chromogenic readout. Samples of <1 EU/mg were used in experiments.

2.3.2 Determining antibody concentration

The concentration of a protein sample was determined with a NanoDrop spectrophotometer 1000c (ThermoFisher) by measuring absorbance at 280 nm. The nanodrop was blanked with the appropriate buffer before the loading of a 2 μL protein sample. The absorbance was recorded and the final concentration was determined by adjusting for the extinction coefficient of the relevant protein using the following equation:

$$\text{Concentration} = \frac{\text{Absorbance (A280)}}{\text{Extinction Coefficient x Path Length}}$$

Clone	Target	Isotype	Method	Experiment
18B12 [328]	mCD20	mIgG1	Stable	*in vivo*, internalisation
18B12 [328]	mCD20	mIgG2a	Transient	*in vivo*
1D3 [329]	mCD19	mIgG1	Transient	*in vivo*
1D3 [329]	mCD19	mIgG2a	Stable	*in vivo*
YTS169.4 [330]	mCD8	mIgG1	Transient	*in vivo*
YTS169.4 [330]	mCD8	mIgG2a	Transient	*in vivo*
PK136 [331]	mNK1.1	mIgG2a	Hybridoma	*in vivo*
PC61 [332]	mCD25	rIgG1	Hybridoma	*in vivo*
3/23 [332]	mCD40	mIgG1	Stable	*in vivo*
AT107-2	CD79B	rIgG1	Hybridoma	*in vivo*
OX86 [333]	mCD134	mIgG2a	Transient	*in vivo*
AT130-2 [321]	mCD32	mIgG1 N297A	Stable	ADCP
AT130-5 [321]	mCD32	rIgG1	Transient	IF
4D5 [334]	hHER2	mIgG1 N297A	Transient	ADCP
Rituximab	hCD20	mIgG1	Stable	*in vivo*
Rituximab	hCD20	mIgG2a	Stable	*in vivo*
KB4 [146]	OVA	mIgG1	Hybridoma	ELISA

Table 2.3: Antibodies produced in-house for *in vitro* and *in vivo* experiments
Transient cells expressing antibodies were made by transfecting ExpiCHO-S cells. Stable cells expressing antibodies were produced by transfecting CHO-K1S Cells. Hybridomas were made by fusing B cells from spleen of immunised mouse with the NS-1 cell line. m = mouse, r = rat, h = human, OVA = ovalbumin, ADCP = antibody-dependent cellular phagocytosis, WB = western blot, Ca^{2+} flux = calcium flux assay, IF = immunofluorescence

Clone	Target	Isotype	Source	Experiment
Rituximab	hCD20	hIgG1	UHS	*in vivo*, ADCP
Cetuximab	hEGFR	hIgG1	UHS	*in vivo*
6G08-NQ	hCD32B	hIgG1 N297Q	BioInvent	WB, Ca^{2+} flux
6G/BI-1206	hCD32B	hIgG1	BioInvent	*in vivo*
6Q/BI-1607	hCD32B	hIgG1 N297Q	BioInvent	*in vivo*, ADCP, Ca^{2+} flux
FITC8	FITC	hIgG1 N297Q	BioInvent	ADCP, WB, Ca^{2+} flux
EP888Y	hCD32B	rbIgG	Abcam	WB, IF
EP926Y	hCD32(-P)	rbIgG	Abcam	WB
3941S	mSHIP1(-P)	rbIgG	CST	WB
2728S	mSHIP1	rbIgG	CST	WB
AB221544	AF488	rbIgG	Invitrogen	Internalisation
A9044	mIgG	rbIgG-HRP	Sigma	ELISA
AB2337831	hIgG	gIgG	Jackson	Internalisation
AB2339874	mIgM	$gF(ab')_2$	Jackson	Ca^{2+} flux

Table 2.4: Commercial antibodies used *in vitro* and *in vivo* experiments
m = mouse, r = rat, h = human, rb = rabbit, g = goat, (-P) = phosphorylated, CST = Cell signalling technologies, ADCP = antibody-dependent cellular phagocytosis, WB = western blot, Ca^{2+} flux = calcium flux assay, IF = immunofluorescence, UHS = University Hospital Southampton pharmacy

2.4 Flow cytometry

2.4.1 Direct staining

To assess the cell surface expression of proteins, 20 μL of human or mouse blood (and 80 μL of PBS) or 100 μL single-cell suspension were transferred to FACS tubes (BD Biosciences) and incubated with fluorescently labelled antibodies at 4°C for 30 minutes in the dark (Table 2.5). 1 mL of 1x erythrolyse RBC lysing buffer (BioRad) or Ammonium-Chloride-Potassium (ACK) lysis buffer (150 mM NH_4Cl, 10 mM $KHCO_3$, 0.1 mM Na_2EDTA) were added to the cells and allowed to lyse for 2 minutes at RT. The cell suspensions were centrifuged at 450 x g for 5 minutes and the supernatant aspirated. 3 mL of fluorescence-activated cell sorting (FACS) wash (PBS, 1% BSA, 10 mM sodium azide) was added per tube and samples were centrifuged as before. Tubes were stored at 4°C in the dark until ready for analysis using FACSCalibur or FACSCanto II (BD Biosciences). Data analysis was performed using FCS Express Version 3 (De Novo Software) or Flo Jo Version 10 (Tree Star Inc) and plotted using Graph Pad Prism Version 9 (Graph Pad Software).

Antibodies made in-house were used at a final concentration of 10 μg/mL, commercial antibodies were used at the concentration recommended by the manufacturer.

2.4.2 Secondary staining

Cell suspensions were incubated with 10 μg/mL (unless otherwise stated) of unlabelled antibody for 30 minutes at 4°C. These cells were then washed in 3 mL FACS wash and spun at 450 x g for 5 minutes. This process was repeated once more and then the cells were stained using a fluorescently labelled anti-IgG. Antibodies against cell surface markers were also added, before cells were washed and analysed as in Section 2.4.1.

2.4.3 Intracellular staining

Cell suspensions were incubated with fluorescently labelled antibodies specific for membrane bound markers at 4°C for 30 minutes in the dark (Table 2.5). 1 mL of 1x RBC lysing buffer (BioRad) was added to the cells and allowed to lyse for 2 minutes at RT. The cell

suspensions were centrifuged at 450 x g for 5 minutes and the supernatant aspirated. 300 μL of diluted FIX & PERM Cell Fixation solution (Invitrogen) was added to the cells and left at 4°C for 1 hour in the dark. 1 mL of diluted Permeabilization Buffer (Invitrogen) was added to samples and then washed at 450 x g for 5 minutes. Samples were resuspended in 1 mL of diluted Permeabilization Buffer (Invitrogen) and then washed again at 450 x g for 5 minutes. Intracellular fluorescent mAbs was then added to the cells at 4°C for 1 hour in the dark. 3 mL of FACS wash was added to the samples and they were washed at 450 x g for 5 minutes. Samples were analysed as in Section 2.4.1.

Antigen	Isotype	Clone	Fluorophore	Source
mCD19	rIgG2a	1D3	APC, PE	Biolegend
mCD20	rIgG2b	SA275A11	PE	Biolegend
mCD20	mIgG1	18B12	AF488	in-house
mCD11B	rIgG2b	M1/70	PE	Biolegend
$mBCL_1$	rIgG1 $F(ab')_2$	MC106A5	FITC	in-house
mCD3	rIgG2a	KT3.1.1	PE	Biolegend
mCD4	rIgG2b	GK1.5	PE, APC/Cy7, APC	Biolegend
mB220	rIgG2a	RA3-6B2	PerCP, APC	Biolegend
mCD5	rIgG2a	53-7.3	PerCP Cy5.5	Biolegend
mCD45.2	mIgG2a	104	PE-Cy7	Biolegend
mCD45	rIgG2b	30-F11	BV510	Biolegend
mCD8α	rIgG2a	53-6.7	PB, APC	Biolegend
mNK1.1	mIgG2a	PK136	APC	Biolegend
mNKp46	rIgG2a	29A1.4	PE/Cy7	Biolegend
mCD23	rIgG2a	B3B4	PE/Cy7	Biolegend
mCD44	rIgG2b	IM7	APC/Cy7	Biolegend
mCD62L	rIgG2a	MEL-14	PerCP Cy5.5	Biolegend
mCD146	rIgG2a	ME-9F1	PE	Biolegend
mMHC-II	rIgG2b	M5/114.15.2	AF488	Biolegend
mF4/80	rIgG2b	Cl:A3-1	APC	BioRad
mF4/80	rIgG2b degly	Cl:A3-1	AF647	in-house
mLy6C	rIgG2c	HK1.4	PerCP-Cy5.5	Biolegend
mLy6G	rIgG2a	1A8	APC-Cy7	Biolegend
mFOXP3	rIgG2a	FJK-16s	APC	Invitrogen
mKi67	mIgG1	B56	AF647	BD Biosciences
mIgG	$F(ab')_2$	AB2338861	AF647	Jackson
mFcγRI	rIgG2a $F(ab')_2$	AT 152-9	FITC	in-house
mFcγRII	mIgG2a $F(ab')_2$	AT 130-2	FITC	in-house
mFcγRIII	rIgG2b $F(ab')_2$	AT 154-2	FITC	in-house
mFcγRIV	hamIgG	9E9	FITC	in-house
hFcγRII	mIgG1 $F(ab')_2$	AT 10	FITC	in-house
hCD16	mIgG1	3G8	PE	in-house
hCD14	mIgG2a	M5E2	PB	Biolegend
hCD19	mIgG1	HIB19	APC	Biolegend
hCD56	mIgG1	5.1h11	APC-Cy7	Biolegend
hFcγRIIB	hIgG1	6G11	AF488	Bioinvent
hHer2	mIgG1	4D5	AF488	in-house
hIgG	gIgG	AB2337831	AF488	Jackson
H2-Kb SI-INFEKL	MHC-I Tetramer	N/A	PE	in-house

Table 2.5: Fluorescently labelled antibodies used for flow cytometry
h = human, m = mouse, ham = hamster, r = rat Cy = cyanine, AF = Alexa Fluor, PB = Pacific Blue

2.5 *In Vitro* experimental methods

2.5.1 Collection of human blood

Informed consent was given following ethics committee approvals under the Declaration of Helsinki. Ethical approval for the use of clinical samples was obtained by the Southampton University Hospitals' NHS trust from the Southampton and South West Hampshire Research Ethics Committee. Whole blood was obtained from healthy anonymous donors with consent, placed in vacutainers containing EDTA (BD Biosciences) and stored on ice until ready for processing. Research was conducted under the University's Ethics and Research Governance Online (ERGO) Code: 19660.

2.5.2 Culturing and differentiation of bone marrow progenitor cells

Bone marrow was harvested from schedule I culled mice. Both hind limbs (femurs and tibias) of the mouse were collected and bone marrow progenitor cells were flushed out with R10 media. Cells were then spun at 450 x g and plated out at a density of $0.8x10^6$ cells/mL in R10 media with 20% L929 conditioned media containing m-CSF (Table 2.2). The cells were cultured for 7 days at 37°C (5% CO_2) in a New Brunswick Galaxy 170R incubator. The media was changed every 2-3 days.

2.5.3 Preparing BMDMs for flow cytometry

On day 8, the media was aspirated and the cells were washed in sterile PBS. 2 mM PBS-EDTA was added to each well and the plate was placed on ice for 10 minutes. A cell scraper (Fisher Scientific) was used to detach the cells from the plate surface and the cell suspension was collected and centrifuged at 250 x g for 5 minutes. The cells were re-suspended in 1 mL PBS and then adjusted to a concentration of $1x10^6$ cells/mL.

2.5.3.1 Antibody-dependent cellular phagocytosis (ADCP) assay

On day 8, BMDMs were harvested (Section 2.5.3) and seeded at a concentration of $5x10^4$ cells per 100 μL R10 media with 20% L929 conditioned media into a flat bottomed 96 well

plate (Thermo Scientific). The following day target B cells were isolated from the spleens of mFcγRII $^{-/-}$ x human CD20 transgenic C57BL/6J mice (hCD20Tg$^{+/-}$) mice were harvested and processed into a single cell suspension by passing through a 100 μm cell strainer. B cells were isolated using a negative selection B cell isolation kit (Miltenyl Biotec) according to the manufacturers instructions. The B cells were centrifuged at 250 x g for 5 minutes and then re-suspended in FCS-free RPMI media.

B cells were labelled with 5 μM of Carboxyfluorescein succinimidyl ester (CFSE) (Life Technologies) and incubated for 10 minutes in the dark at room temperature (RT). An equal volume of FCS was then added to quench the CFSE and the cells were centrifuged and resuspended in R10 media. In some experiments, the plated BMDMs were incubated with a mFcγRII or hFcγRIIB blocking mAb at 37°C for 30 minutes (Table 2.3, Table 2.4). The B cells (at a concentration of 5x10^6 cells/mL) were incubated with rituximab (or an isotype control) at 4°C for 30 minutes to opsonise them. 50 μL of B cells was then added to the plated BMDMs to achieve a 5:1 target effector ratio of B cells to macrophages and incubated at 37°C for 60 minutes.

Anti-F4/80 APC at 1μg/mL was added per well to identify macrophages and then incubated at RT in the dark for 30 minutes. The media was removed from the plate and wells were washed twice in 200 μL PBS. 200 μL of FACS wash was then added per well and cells were transferred into FACS tubes. Samples were analysed on FACSCalibur (BD Bioscience) to assess the percentage of F4/80+ cells and F4/80+CFSE+ cells. Each condition was repeated using triplicate wells. The percentage of ADCP was calculated using the formula below. The phagocytic index was calculated from the percentage of ADCP. This was worked out by dividing the percentage of phagocytic macrophages (CFSE+F480+) under the test condition by the percentage of phagocytic macrophages co-cultured with unopsonised B cells.

$$\%\ \text{ADCP} = \left(\frac{\%\ \text{Gated F4/80}^{+}\text{CFSE}^{+}\ \text{cells}}{\%\ \text{Gated F4/80}^{+}\text{CFSE}^{-}\ \text{cells} + \%\ \text{Gated F4/80}^{+}\text{CFSE}^{+}\ \text{cells}} \right) \text{x100}$$

2.5.4 Western blot

Cells for western blotting were isolated as detailed. B cells were isolated from the spleens of mice as previously described (Section 2.5.3.1). BMDMs from hFcγRIIB Tg and NoTIM

mice were harvested and cultured as previously described (Section 2.5.2). Cells were then centrifuged at 250 x g for 5 minutes and re-suspended in 3 mL of RPMI media ready for experiment specific cellular stimulation.

Cells were centrifuged at 250 x g for 5 minutes and re-suspended in 1mL cold PBS and then centrifuged again and re-suspended in 50 μL ONYX lysis buffer (50 mM NaF, 2 mM Na_3VO_4, 6 μL protease inhibitor cocktail (Sigma-Aldrich), in 10 mM Tris-HCl pH 7.4, 67.5 mM NaCl, 0.5 mM $MgCl_2$, 0.5 mM ethylene glycol tetraacetic acid (EGTA), 0.5% Triton X-100 and 5% glycerol) and placed on ice for 30 minutes. Suspensions were then centrifuged at 15000 x g for 15 minutes to pellet nuclear content. Lysates were transferred to a clean tube and stored at -20°C until ready for use.

Lysate protein concentration was determined colourimetrically using the Bradford Assay. 200 μL of 1:4 diluted Bradford reagent was added to 5 μL of lysate, the intensity of the sample was measured at 570 nm on an Epoch plate reader (Biotek) and protein concentration was determined using a BSA standard curve. 25 - 50 μg of protein was added to 5 μL of reducing-Laemlli buffer (60 mM Tris-HCl, 2% sodium dodecyl sulphate [SDS], 10% glycerol, 5% 2-ME, 0.01% bromophenol blue) and ddH_2O was added to make each sample up to 20 μL. Each sample was then incubated at 95°C for 5 minutes to induce denaturation of proteins. The samples was then loaded onto pre-made 10%, 1.5 mm x 10 well, bis-tris gels (ThermoFisher) and passed through the gel at 120V for 75 - 90 minutes in MOPS buffer (5 mM MOPS, 70 mM SDS, 5mM Tris, 1 mM EDTA). Proteins were transferred onto a nitrocellulose blotting membrane using the iBlot 2 Dry blotting system (Invitrogen), following the manufacturer's instructions.

The blots were subsequently washed in Tris-buffered Saline (TBS) (10 mM Tris, 150 mM NaCl pH 7.6) with 0.05% Tween-20 (TBS-T). The membrane was blocked in 5% BSA TBS-T, 0.01% azide solution for 60 minutes. Primary antibodies (Table 2.4) were added at a dilution recommended by the manufacturer in 5% BSA TBS-T and left overnight at 4°C on rollers. The following day, the blots were washed in 5% BSA TBS-T, 0.01% azide solution 3 times for 5 minutes and then incubated with horseradish peroxidase (HRP)-linked secondary antibodies (Table 2.4) for 1 hour in 5% BSA TBS-T solution. ECL Western Blot Substrate (Pierce) was used to detect HRP activity and imaged using the Imager Chemi Doc-it Imaging system (UVP) and the VisionWorks LS software (UVP).

2.5.5 Sectioning snap frozen tissue

Mice were humanely culled by a Schedule I method, with tissues (e.g. spleens and livers) immediately harvested. Tissues were put into OCT solution (Cell Path) and frozen in a bath of isopentane (Sigma-Aldrich) on dry ice. Samples were stored at -80°C until further use. Samples were then mounted onto a cryostat and 7 μm thick sections were cut at -17°C. Sections were placed onto Superfrost Plus slides (ThermoFisher) and left to dry overnight.

2.5.6 Staining tissue sections for immunofluorescence microscopy

Sections were fixed in 100% dry acetone for 10 minutes and left to air dry for 5 minutes. Sections were marked with ImmEdge Pen (Vector Labs) and next rehydrated with 1x PBS. Sections were then washed with PBS-0.05% Tween 20 and incubated with 100 μL 2.5% Normal Goat's Serum in PBS-0.05% Tween 20 for 30 minutes to reduce non-specific binding. The sections were covered with 100 μL of 1 μg/mL of primary antibody in PBS-0.05% Tween 20 overnight at 4°C in a dark humid chamber (Table 2.6).

The next day sections were washed 3 times with PBS-0.05% Tween 20. Sections were then covered in secondary AlexaFluor 488 labelled antibodies specific for the primary antibody isotype in PBS-0.05% Tween 20 for 1 hour at RT in a dark humid chamber. Sections were then washed 3 times with PBS-0.05% Tween 20 and covered with 1 μg/mL anti-mouse cell marker in PBS-0.05% Tween 20 for 2 hours at RT in a dark humid chamber. Sections were washed 3 times with PBS-0.05% Tween 20 and covered in secondary AlexaFluor 647 labelled antibodies specific for the mouse cell marker antibody isotype in PBS-0.05% Tween 20 for 1 hour at RT in a dark humid chamber. Sections were washed 3 times with PBS-0.05% Tween 20 and then covered in 100 μL of 1:5000 DAPI in 1x PBS-0.05% Tween 20 for 10 minutes at RT in a dark humid chamber. Sections were washed in PBS and then dried.

Coverslips were mounted with 1 drop of Vectorshield Hard Set (Vector Labs) on top of each section avoiding the introduction of air bubbles. Slides with coverslips were left to dry in the dark for 1 hour at RT and stored in the dark at 4°C until ready for use. Sections were imaged using an Olympus CKX41 microscope at 10x and 40x objectives. Antibodies used can be found in Table 2.6.

Antigen	Isotype	Clone	Fluorophore	Source
Hu FcγRIIB	Rab IgG	EP888Y	N/A	Abcam
Mo FcγRII	Rat IgG1	AT 130-5	N/A	In-house
Mo B220	Rat IgG2a	RA3-6B2	N/A	BD Biosciences
Mo CLEC4F	Hu IgG1	4M23	N/A	In-house
Rab IgG	Go IgG	AB143165	AlexaFluor488	Invitrogen
Rat IgG	Go IgG	AB2534074	AlexaFluor488	Invitrogen
Rat IgG	Go IgG	AB141778	AlexaFluor647	Invitrogen
Hu IgG	Go IgG	AB2337813	DyLight 549	Jackson

Table 2.6: Antibodies used for Immunofluorescence
Hu = Human, Rab = Rabbit, Mo = Mouse, Go = Goat

2.5.7 Enzyme-linked immunosorbent assay

To determine the concentration of analyte, the enzyme-linked immunosorbent assay (ELISA) was used. 96-well Nunc MaxiSorp plates (ThermoFisher) were coated with the appropriate protein at the required concentration in coating buffer (0.015 M Na_2CO_3, 0.035 M $NaHCO_3$) and 100 μL was added to each well. Plates were incubated for 2 hours at 37°C. Coating buffer was then discarded and 150 μL of 1% BSA-PBS was added per well and incubated at 4°C overnight.

Plates were washed 3 times with PBS 0.05% Tween20 (Sigma-Aldrich) using a Skan-washer 300 (Skatron). Serum was added to the plate at a dilution of 1 in 200 in 1% BSA-PBS and diluted 2 fold across the plate. A matched standard was used and also diluted 2 fold across the plate. Plates were incubated at 37°C for 90 minutes and washed 3 times. The HRP conjugated detection antibody was diluted in 1% BSA-PBS and 100 μL was added to each well. Plates then were incubated for 1 hour at 37°C.

Plates were washed 5 times and 100μL of substrate (o-Phenylediamine dihydrochloride tablet (Sigma-Aldrich)) dissolved in 24.7 mL ELISA citrate (stock: 0.02M BDH succinate salt; (FisherScientific)), 25.3 mL Na_2PO_4 (0.2M Na_2PO_4 stock (FisherScientific)), 50 mL dH_2O and 40 μL 30% hydrogen peroxide (Merck Millipore) was added to each well. The ELISA was allowed to develop and after sufficient colour change, 2M H_2SO_4 (VWR) was added to each well to stop the reaction. Absorbance was measured at 492nm on an Epoch plate reader (Biotek). Analysis was performed using Excel 2016 (Microsoft Office), linear regression was used to calculate the unknown values from the linear range of the plotted standard curve determined from the known concentration of the standard.

To detect OVA within the serum of mice, 100 μg/mL of OVA (Sigma) was used to coat plates. The mAb KB4 (ant-OVA IgG) was then used as a matched standard (starting concentration of 1 μg/mL). The HRP conjugated rabbit anti-mouse IgG (Sigma) detection antibody was added at a dilution of 1:2000 (Table 2.3, Table 2.4).

2.5.8 B cell monoclonal antibody internalisation assay

B cells were isolated from the spleens of mice as previously described (Section 2.5.3.1). 2x10^5 cells/mL were incubated with 5 μg/mL AlexaFluor488 labelled mAb in a 96 well round-bottomed plate. Samples were incubated at 37°C and 5% CO_2 and either taken immediately or after 2 hours, 6 hours or 24 hours of incubation with mAb. The excess antibody was removed by washing at 300 x g for 5 minutes and samples were split into 'quenched' and 'unquenched' tubes. Anti-Alexa Fluor 488 antibody (Invitrogen) (Table 2.4) was then added to the 'quenched' tube to quench the fluorescence of surface-bound antibody. Samples were washed as before and then analysed using FACSCalibur (BD Biosciences. The surface accessible mCD20 was calculated as below, percentages were then inverted to show the proportion of internalised antibody.

$$\% \text{ accessible mCD20} = \left(\frac{\text{Pre-quench Geo Mean - Post-quench Geo Mean}}{\text{Pre-quench Geo Mean}} \right) \text{x100}$$

2.5.9 B cell heat aggregated human IgG internalisation assay

Human IgG was treated at 62°C for 30 minutes to induce aggregation. Heat aggregated human IgG (ahIgG) was then separated from the monomeric fraction by size exclusion HPLC. The ahIgG was then incubated with cells as follows.

B cells were isolated from the spleens of mice as previously described (Section 2.5.3.1). 1x10^6 cells/mL were treated with 20 μg/mL ahIgG for 30 minutes at 4°C. The cells were then washed in R10 media and centrifuged at 250 x g for 5 minutes and divided into three. One third was maintained at 4°C (time 0 fraction), one third was maintained at 37°C for 30 minutes and 4 °C for 30 minutes (time 30 fraction) and one third was maintained at 37°C for 60 minutes (time 60 fraction). Cells were washed 250 x g for 5 minutes and stained with AlexaFluor488 labelled polyclonal goat anti-human IgG (Jackson ImmunoResearch

Laboratories) at 4 °C for 30 minutes. Cells were then washed again. Samples were run on the FACS Calibur and internalisation was quantified using the following formula:

$$\left(\% \text{ cell surface ahIgG internalisation} = \frac{\text{MFI of time 30/60 fraction}}{\text{MFI of time 0 fraction}}\right) \text{x}100$$

2.5.10 π–BCL_1 cell binding assay

To ascertain the concentration of murine anti-mCD20 IgG in serum, a π-BCL_1 cell binding assay was used. 100 μL of R20 media was pipetted into a 96 well round-bottomed plate. Mouse serum was then added to the plate at an initial dilution of 1:40, with matched standards added at an initial concentration of 10 μg/mL. Samples were serially diluted 2 fold down the plate. 100 μL of 0.5-1x10^6 cells/mL was then added to the plate and cells were incubated with the diluted serum for 15 minutes at RT. Samples were then washed at 250 x g for 5 minutes and resuspended in 100 μL of FACS wash. Next, cells were stained with an anti-mouse Fc-FITC conjugated F(ab')$_2$ antibody (Jackson Laboratories) for 30 minutes at 4°C. Cells were then washed as before and resuspended in 150 μL of FACS wash. Samples were examined on the FACSCanto II plate reader (BD Biosciences). Analysis was performed using Excel 2016 (Microsoft Office), linear regression was used to calculate the unknown values from the linear range of the plotted standard curve.

2.5.11 B cell calcium flux assay

B cells were isolated from mice as previously described (Section 2.5.3.1). 1x10^7 cells/mL were washed in serum free RPMI at 250 x g for 5 minutes. 10 μM Fluo-3-AM dye in 0.002% Pluronic F-127 DMSO solution (Thermo Fisher) was added to the resuspended cells and incubated in the dark at 37°C. Cells were washed as before and resuspended in 1 mL serum free RPMI. If appropriate, cells were pre-incubated with specific mAbs which were rested for 15 minutes in the dark prior to analysis (Table 2.3, Table 2.4). Live cell events were collected as identified by FSC and SSC parameters on the FACSCalibur (BD Biosciences). 250 μL aliquots were assessed for 15 seconds on the flow cytometer before the addition of PBS or 20 μg/mL anti-IgM polyclonal F(ab')$_2$ (Jackson Laboratories) and assessed for a further 2 minutes and 45 seconds. 0.65 μM ionomycin was added after 3 minutes and data recorded for another 1 minute to observe maximal calcium flux.

2.6 *In Vivo* experimental methods

2.6.1 Animals

C57BL/6J WT mice were bred in-house, C57BL/6J mFcγRII KO mice were a kind gift from Dr. Sjef Verbeek [281], C57BL/6J human (h)FcγRIIB (hFcγRIIB Tg) mice were generated in-house [323], C57BL/6J hFcγRIIB NoTIM (NoTIM) mice were previously described (Section 2.1.1), hCD20 mice were backcrossed onto C57BL/6J background in-house [335], C57BL/6J γ-chain KO mice were a kind gift from Dr. Sjef Verbeek and C57BL/6J OT-I TCR transgenic mice [336] were a kind gift of Dr. Matthias Merkenschlager. hFcγRIIB NoTIM/hCD20 and C57BL/6J mFcγRII KO/hCD20 were crossed and maintained in-house.

Animals used throughout these experiments were maintained in conventional barrier facilities or individually ventilated cages (IVC), with constant access to food, water, appropriate husbandry with a 12 hour light/dark cycle. All procedures carried out were approved by the local Animal and Welfare Ethics Review Body and performed under the Animals (Scientific Procedures) Act 1986 (ASPA) and Home Office licenses PPL P4D9C89EA and PIL I8D0C1A01. Procedures were performed to best practice guidelines by competent trained PIL holders. Experiments were performed following the NC3Rs and Animal Research: Reporting of *in vivo* Experiments (ARRIVE) guidelines.

2.6.2 Mouse blood and serum collection

Blood was collected in 0.5 mL microfuge tubes containing 20% heparin sodium 5,000 I.U/mL (Wockhardt) by tail-tipping or lancing with the application of lidocaine according to best practice guidelines. Blood was then processed for flow cytometry (Section 2.4.1).

For the collection of serum, blood was collected in 0.5 mL microfuge tubes without heparin. Blood was allowed to clot at RT for 30 - 60 minutes. Clotted blood was then centrifuged at 15000 x g for 5 minutes with serum collected and stored at -20°C until required.

2.6.3 Harvesting murine tissue

Spleen and inguinal lymph nodes (iLN) were harvested from schedule I culled mice. Spleen and iLN were mechanically homogenised with PBS and passed through a 100 μm cell strainer (BD Biosciences) to produce a single-cell suspension.

Livers were harvested from schedule I culled mice and dissected into small pieces and placed into gentleMACS C tubes (Miltenyi Biotec) with 5 mL of R10 media. A liver dissociation kit (Miltenyi Biotec) was then used according to the manufacturer's instructions and samples were digested using the gentleMACS Octo Dissociator with Heaters (Miltenyi Biotec). The cell suspension was then filtered a 100 μm cell strainer (BD Biosciences) and washed with PBS at 250 x g for 10 minutes. The suspension was then carefully layered on a 25/50% Percoll gradient (GE Healthcare) and centrifuged at 800 x g for 30 minutes with the brake turned off. The non-parenchymal layer between the 25/50% gradient was removed and washed in PBS at 250 x g for 5 minutes. Samples were then processed for flow cytometry.

Murine tumours were harvested from schedule I culled mice. Tumours were mechanically disrupted using razor blades to increase overall surface area before the addition of 1 WÃ$\frac{1}{4}$nsch (units/mL) of Liberase TL (Roche) per tumour. Samples were then placed in a shaking incubator at 37 °C to aid tumour digestion. 1 mL of FCS was added per sample to neutralise Liberase activity. Tumours were mechanically homogenised with PBS and passed through a 100 μm cell strainer (BD Biosciences) to produce a single-cell suspension. Samples were then processed for flow cytometry (Section 2.4.1).

Bone marrow was harvested as previously described (Section 2.5.2). Cells were subsequently differentiated into bone marrow-derived macrophages (BMDMs) (Section 2.5.2) or processed for flow cytometry (Section 2.4.1).

2.6.4 Depletion of circulating lymphocytes

Mice were tail bled at least 24 hours before dosing with lymphocyte depleting mAb reagents to obtain the baseline peripheral cell percentages using flow cytometry. Once the baseline had been determined, sterile filtered antibody was administered I.V. or I.P. in PBS and further tail bleeds were conducted as appropriate to assess depletion. On

the final day, mice were bled and culled using a suitable Schedule I method. Mice were dissected for spleens and/or iLNs and analysed by flow cytometry. Depletion were calculated as a percentage of the target cells within the lymphocyte gate (based on FSC/SSC) as compared to baseline.

For depletion of CD20+ B cells, mice were treated with increasing doses of 18B12 mIgG1 or mIgG2a I.V and cells were identified based on CD19+/B220+ expression. For depletion of CD19+ B cells, mice were treated with increasing doses of 1D3 mIgG1 or mIgG2a I.V. and cells were identified based on CD20+/B220+ expression. For depletion of NK1.1+ NK cells, mice were treated with increasing doses of PK136 mIgG2a I.V. and cells were identified based on CD3-/NKp46+ expression. For depletion of CD8+ T cells, mice were treated with increasing doses of YTS169.4 mIgG1 or mIgG2a I.V. and cells were identified based on CD3+/CD4- expression. For depletion of CD25+ T_{reg} cells, mice were treated with 250 μg PC61 or AT 107-2 rIgG1 I.P. and cells were identified based on CD4+/FOXP3+ expression

2.6.5 18B12 mIgG1 pharmacokinetics study

Mice were tail bled at least 24 hours before dosing to obtain the baseline peripheral B cell percentage. Once the baseline had been determined, 50 μg of sterile-filtered anti-mCD20 (clone 18B12) mIgG1 was administered by I.V. injection. Tail bleeds were conducted at 1 hour, 6 hours, 24 hours, 48 hours and 96 hours following injection to collect un-coagulated blood for flow cytometry analysis of cell components and serum for 18B12 pharmacokinetic analysis (Section 2.5.10). At the end of the experiment, mice were terminally bled and culled using a suitable Schedule I method and blood was either processed for serum or analysed using flow cytometry.

Pharmacokinetic parameters were generated using the PKSolver tool developed by Zhang et al. [337]. In brief, parameters were calculated for each mouse based on the serum concentration of mAb as calculated using the π-BCL_1 cell binding assay for the 1 hour, 6 hours, 24 hours, 48 hours and 96 hours time points. A non-compartmental analysis using an I.V. bolus model was then utilised to provide the parameters.

2.6.6 Adoptive B cell transfer depletion experiments

To assess depletion of a specific cell population *in vivo*, the adoptive B cell transfer system was utilised. Labelled cells expressing a specific antigen (targets, high CFSE) are transferred with the same labelled cells not expressing the antigen (non-targets, low CFSE) into recipient mice. The recipients are then treated with an agent that will specifically deplete the target, and the level of depletion can be ascertained by comparing the ratio of labelled target to labelled non-target cells in the recipient.

Mice were harvested for non-target and target splenocytes and then processed into a single-cell suspension using a 100 μm cell strainer. Cell suspensions were washed in PBS, spun at 450 x g for 5 minutes and resuspended at $2x10^7$ cells/mL. The target splenocytes were stained with 5 μM CFSE (Life Technologies) and the non-target splenocytes stained with 0.5 μM to achieve high and low CFSE stained splenocytes respectively. After the addition of CFSE, splenocytes were incubated for 10 minutes at RT in the dark on a roller. CFSE was then quenched using an equal volume of FCS for 1 minute. Splenocytes were washed in PBS as before and resuspended in 1 mL of PBS, a cell count was performed and the largest cell count was diluted down to achieve equal concentrations. The CFSE low and high cells were mixed at a 1:1 ratio and staining was checked by flow cytometry to ensure that the cells were at the correct ratio. The cell mixture was administered into mice I.V. at a concentration of $5\text{-}10x10^6$ splenocytes/mL.

Mice were subsequently treated with isotype control or experiment specific target depleting antibody. 18-24 hours after the last treatment, mice were terminally bled under non-recoverable isoflurane anaesthesia. Mice were harvested for spleens and bone marrow progenitor cells were extracted and analysed using flow cytometry to assess the remaining CFSE labelled cells. CFSE labelled B cells were identified as CD19+B220+ and then further identified based on CFSE fluorescence, producing a low (non-target) and high (target) fluorescing population. CFSE low and high cells were gated the target:non-target cell ratio was calculated. The ratio for each experimental condition was then normalised to the control group, with control assigned a ratio of 1. The expression of FcγRs was then analysed on key immune effector cell populations within the spleen and bone marrow of recipient mice.

Adoptive transfer experiment using mFcγRII KO (non-target) and mFcγRII KO x hCD20 Tg (target) splenocytes transferred into mFcγRII KO and NoTIM recipient mice

C57BL/6J mFcγRII KO and C57BL/6J NoTIM mice were adoptively transferred with mFcγRII KO (non-target) and mFcγRII KO x hCD20 Tg (target) splenocytes on Day 0. On Day 1, 20 mg/kg of sterile-filtered hIgG1 6G11, hIgG1 6G11-NQ or isotype control (cetuximab), was administered via I.P injection. On Day 2 am, 20 mg/kg of sterile-filtered hIgG1 6G11, hIgG1 6G11-NQ or cetuximab was administered via I.P. injection. On Day 2 pm, 2 mg/kg of sterile-filtered hIgG1 rituximab or cetuximab was administered via I.V. injection. Mice were culled and harvested on Day 3.

Adoptive transfer experiment using mFcγRII KO (non-target) and mFcγRII KO x hFcγRIIB NoTIM x hCD20 Tg (target) splenocytes transferred into mFcγRII KO recipient mice

C57BL/6J mFcγRII KO mice were adoptively transferred mFcγRII KO (non-target) and mFcγRII KO x hFcγRIIB NoTIM x hCD20 Tg (target) splenocytes on Day 0. On Day 1 pm, 2 mg/kg of sterile-filtered hIgG1 6G11, hIgG1 6G11-NQ or isotype control (cetuximab), was administered via I.P injection. On Day 2 am, 2 mg/kg of sterile-filtered hIgG1 rituximab or cetuximab was administered I.V. injection. Mice were culled and harvested on Day 3.

2.6.7 OT-I adoptive transfer model with OVA immunisation and mCD40 agonism *in vivo*

A spleen from a C57BL/6J OT-I TCR transgenic mouse [336] was harvested and then processed into a single-cell suspension using a 100 μm cell strainer (BD Biosciences). Cell suspensions were washed in PBS, spun at 450 x g for 5 minutes and resuspended at $5x10^5$ OT-I cells/mL. The activation status of OT-I cells was assessed using flow cytometry to ensure no prior activation, using a cut off $<$10% CD44 positive and $>$90% CD62L positive OT-I cells. If the OT-I cells met these requirements, 100 μL were injected I.V. into mice. 24 hours later mice were given 500 μg OVA (Sigma-Aldrich) and 100 μg antibody (anti-mCD40 3/23 mIgG1 or anti-hCD20 rituximab mIgG1) in 200 μL PBS via I.P. injection.

Mice were tail bled on Day 4, 7, 14 and 28 according to the experimental schedule to assess OT-I expansion and the anti-OVA IgG response. Blood samples were processed for flow cytometry and stained with for CD8 positivity and SIINFEKL tetramer (Table 2.5) to identify OT-I cells as a percentage of total CD8 T cells. Flow cytometry was also used to assess CD62L and CD44 expression on endogenous CD8+ cells as well as CD23 expression on B cells. On Day 35, mice were re-challenged with 50 μg of OVA if OT-I lymphocytes were deemed to be <1% of total lymphocytes and <10% of CD8 cells. Mice were then tail bled 4, 7, 14 and 28 days later according to the experimental schedule to assess OT-I expansion. The anti-OVA IgG response was monitored by isolating serum from mouse blood and analysed using an ELISA (Section 2.6.2, Section 2.5.7).

2.6.8 Depletion of malignant B cells in the Eμ-TCL1 tumour model *in vivo*

Eμ-TCL1 splenocytes [338] were screened for the presence of murine pathogens before use in mice by Envigo. Screened Eμ-TCL1 splenocytes were thawed, washed in PBS, spun at 450 x g for 5 minutes and resuspended at $2x10^7$ cells/mL in sterile PBS. Mice were then given 500 μL of cells via I.P. injection. Tumour load was monitored every 7 days by assessing the percentage of Eμ-TCL1 cells in peripheral blood. In brief, mice were tail bled and were assessed for the percentage of CD19+CD5+B220lo cells as a percentage of total lymphocytes by flow cytometry. When tumour load reached 10-20% of lymphocytes, mice were treated with 100 μg antibody (anti-mCD20 18B12 mIgG2a or anti-hCD20 rituximab mIgG2a as an isotype control) via I.P. injection. Mice were then bled on Day 2 and Day 7 to monitor tumour load. Mice were bled once a week from treatment until experimental endpoint was reached which was defined as 2 of the three following criteria being met: Eμ-TCL1 cells as a percentage of lymphocytes exceeding 80%, a white blood cell count of $>5x10^7$ cells/mL and a splenomegaly score of 3 or above (approximately 3 cm long). Eμ-TCL1 cells were monitored using flow cytometry, the white blood cell count was also monitored by flow cytometry using Precision Count Beads (Biolegend) according to the manufacturers instructions. Splenomegaly was monitored by trained animal technicians three times a week once Eμ-TCL1 cells as a percentage of lymphocytes exceeded 50%.

The depletion of endogenous B cells was also monitored throughout the experiment. Two days following treatment with 18B12, serum was isolated from mice and the concentration of mAb was analysed using the π-BCL_1 cell binding assay (Section 2.5.10).

2.6.9 Depletion of T regulatory cells in the syngeneic E.G7 tumour model *in vivo*

The E.G7 cell line [339] were screened for the presence of murine pathogens before use in mice by Envigo. $5x10^5$ screened E.G7 tumours cells in 100 μL PBS were injected subcutaneously (S.C) into the right hand flank of mice. Tumours were measured using electronic calipers (Draper), once palpable (5x5 - 7x7 mm^2), mice were treated with 2x 200 μg shots of antibody (anti-mOX40 OX86 mIgG2a or anti-hCD20 rituximab mIgG2a as an isotype control) on Day 0 and Day 2 via I.P. injection. Mice were then bled on Day 2 and Day 4 to ascertain T_{reg} depletion within the periphery. Briefly, blood was analysed by flow cytometry and stained for CD4+, CD8+, FOXP3+ and Ki67+. T cell populations were enumerated using Precision Counting Beads (Biolegend) according to the manufacturer's instructions. Mice kept for long term survival were also bled on Day 9. Tumour size was monitored 3 times a week until experimental endpoint was reached as determined by a tumour size of 15x15 mm^2. Surviving mice were culled around day 50 because the majority of mice remained tumour free approximately 3 weeks after complete regression.

For analysis of T_{reg} cell depletion in different tissue compartments, mice were bled on Day 2 and culled for harvest on Day 4. T_{reg} cell depletion and myeloid infiltrate were characterised by flow cytometry in the blood, spleen and tumours of each mouse. The T cell compartments were analysed based on CD4+, CD8+, FOXP3+ and Ki67+ expression. Myeloid cells were identified based on a CD11B+, F4/80+, Ly6C+ and Ly6G+ and enumerated using Precision Counting Beads (Biolegend).

2.7 Statistics

Statistical Analysis was performed using GraphPad Prism Version 9. Statistical significance between two factors was analysed using a two-tailed unpaired t-test. Statistical significance between groups was assessed by using a one way ANOVA and two way ANOVA test unless otherwise stated. To test for the normality of distribution, the D'Agostino-Pearson normality test was utilised and then subsequently determined the use of parametric or non-parametric analyses. Multiple comparison tests were used as appropriate and are detailed in figure legends. The statistical significance in long term survival

experiments was analysed using Kaplan-Meier survival test with the Mantel-Cox test used to assess significance between groups (*$\leq$ 0.05, **p$\leq$0.01, ***p$\leq$0.001, ****p$\leq$0.0001).

Chapter 3

Characterisation of the hFcγRIIB ITIM signalling mutant (NoTIM) mouse model

3.1 Chapter Introduction

As detailed in the introduction to this thesis, FcγRIIB biology is complex, with inhibition of biological processes shown to be achieved through functions that are dependent or independent of ITIM signalling [266]. Prior research has heavily relied on using cell lines artificially expressing hFcγRIIB and/or murine models to investigate how mFcγRII mediated inhibition, with parallels then drawn to human FcγRIIB. Advances in the production of transgenic mouse models has allowed the direct investigation of hFcγRIIB *in vivo* and more recently the advent of murine models expressing all human FcγRs have shown promise in furthering our understanding. However, further work is needed to ascertain exactly how hFcγRIIB mediates inhibition of antibody therapeutics.

In a seminal paper by Clynes et al. it was shown that the genetic knockout of mFcγRII in BALB/c nude mice resulted in the improved efficacy of direct targeting cancer mAb therapy [185]. It is assumed that this improvement was due to the loss of mFcγRII mediated signalling, but has not been formally investigated. In later years, a growing body of evidence has shown that FcγRIIB can provide inhibition independently of the ITIM signalling motif such as inhibition of BCR signalling through disruption of BCR microclusters on the cell

surface [254]. FcγRIIB has also been shown to accelerate target dependent internalisation of CD20 mAbs independently of signalling, with high FcγRIIB expression correlating with worsened survival in some lymphoma cohorts [300] [309] [301]. In contrast, several TNFR targeted agonistic mAbs have been shown to be reliant on FcγRIIB binding to elicit efficacy. This has been shown for mAbs targeting CD40, OX40 and 4-1BB and is independent of ITIM signalling [309] [308] [144] [145].

As previously mentioned, the majority of these studies have relied on the manipulation and overexpression of hFcγRIIB in cell lines and primary cells as well as probing mFcγRII *in vivo*. However, there are some limitations to these models. Cell lines *in vitro* cannot replicate the complexities and cross talk of the immune system. FcγRIIB is known to be expressed on a multitude of different cells *in vivo*, and so studying one cell type in isolation may not recapitulate cross-talk between different cells. Studies utilising mFcγRII have proved insightful, showing how the inhibitory receptor regulates activatory FcγRs and is an important suppressor of some forms of autoimmunity [281]. However, sequence alignment using Uniprot blast search shows that mFcγRII B2 and hFcγRIIB B2 share 59% in sequence homology with differences in both the intracellular and extracellular regions, meaning the murine receptor is unlikely to fully recapitulate the biology of the human receptor [340]. Studies utilising transgenic hFcγRIIB mouse models have opened new avenues, such as allowing valuable preclinical validation of targeting hFcγRIIB as a cancer therapy [323] which has lead to clinical trials in humans [327]. Human FcγR research has since evolved to examine murine models that only express human FcγRs. These models have been utilised to study antibody therapy in the context of cancer and anaphylaxis and go some way to recapitulating the expression pattern of human FcγRs on murine immune cells [341] [342].

However, questions remain about individual FcγRs and their contribution to mAb therapy and disease states. One of these questions centres around the contribution of hFcγRIIB mediated ITIM signalling in the inhibition of direct targeting mAb therapy. To formally investigate this question, an hFcγRIIB non-signalling ITIM mutant transgenic mouse model (named NoTIM) was developed. This mouse model has had two tyrosine residues within the intracellular tail mutated into a phenylalanine, Y254F and Y273F, to prevent intracellular ITIM signalling. This chapter aimed to characterise the NoTIM mouse to understand the transgenic expression pattern, how it compares to human whole blood and how the overall FcγR expression pattern compares with other related mouse models (C57BL/6J,

mFcγRII KO, hFcγRIIB Tg). The lack of ITIM mediated signalling was then investigated in NoTIM mice to understand it's impact upon immune effector cell functions *in vitro*.

3.2 Generation of the NoTIM Mouse

The NoTIM mouse was produced on a C57BL/6J background, with the mutated human FcγRIIB (B2 isoform) transgene inserted into it's genome. The NoTIM construct was designed and produced by Dr. Yury Bogdanov, inserted into a pcDNA 3.0 expression plasmid and injected into WT C57BL/6J zygotes (Cyagen Biosciences). The gene was inserted via random integration under the control of the human FcγRIIB promoter (approximately 400bp upstream of the hFcγRIIB gene [343]). Once founder mice were produced they were crossed with C57BL/6J mice that lack mouse FcγRII (mFcγRII KO) due to genetic deletion [281]. The resulting offspring had the NoTIM construct integrated into their genome and lack the homologous mouse receptor. The presence of the NoTIM mutations in these mice was confirmed using Sanger sequencing of DNA generated from murine ear tissue. Results showed the presence of the expected cytoplasmic Y254F and Y273F mutations (Source Bioscience) (Figure 3.1). These mice were subsequently bred with mFcγRII KO mice and maintained as heterozygous for the hFcγRIIB NoTIM transgene.

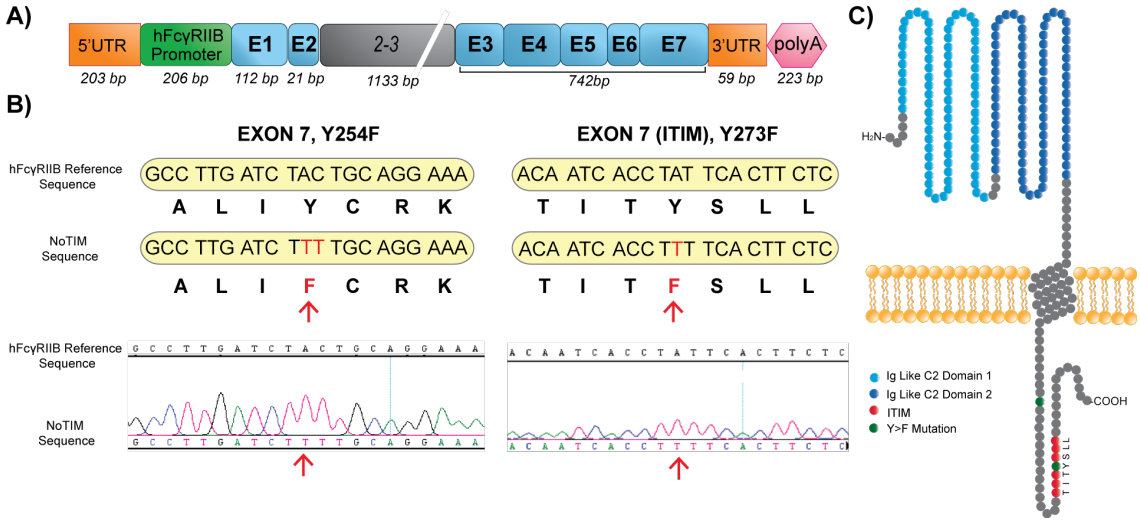

Figure 3.1: The NoTIM transgene, intended mutations and cartoon representation of the receptor
A) The NoTIM transgene was randomly integrated into the zygote of a C57BL/6J mouse under the control of the human FCGR2B promoter. Untranslated regions (UTR) = orange, exons (E) = blue, introns = grey, polyA tail = pink. B) Murine DNA was isolated from ear biopsies of positive NoTIM progeny. The presence of the NoTIM mutations was confirmed by using specific primers to amplify the region of DNA containing the mutations. Sanger sequencing was then used to confirm the presence of the Y254F and Y273F mutations. C) A cartoon representation of the NoTIM hFcγRIIB with the subsequent mutations (in green).

3.2.1 Genotyping NoTIM Mice

NoTIM mice required screening for the presence of the NoTIM transgene due to the maintenance of the colony as heterozygous for the transgene. PCR was performed with NoTIM specific primers to determine if the hFcγRIIB signalling mutant was present in murine DNA generated from ear biopsies of progeny. The products were assessed on an agarose gel and examined for a positive band of 536 base pairs. As an example, figure 3.2 shows that progeny D2, E2, E3 and E4 as well as the positive control (RG1) produced a band at the expected size for the NoTIM transgene. D1 and E1 produced no detectable band as seen with the negative control, taken from the WT C57BL/6J mouse. Overall this demonstrates that this PCR assay could accurately identify the mice containing the NoTIM transgene.

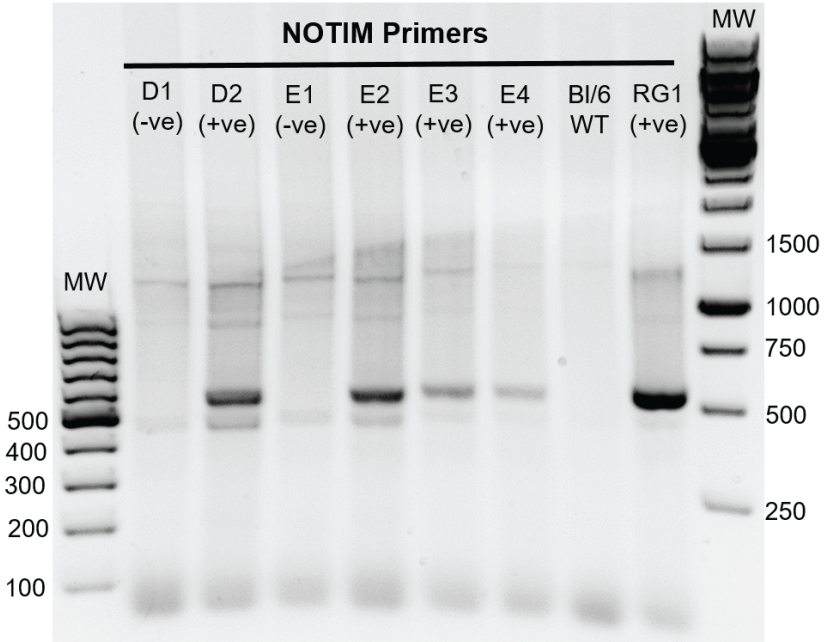

Figure 3.2: Genotyping NoTIM transgenic mice
PCR was performed on DNA extracted from NoTIM progeny ear biopsies using specific primers that produce an expected band of 536bp on an agarose gel (identified against the molecular weight ladder (MW)). C57BL/6J WT lysate was used as the negative control (Bl/6 WT) and DNA from a NoTIM transgenic mouse was used as a positive control (RG1). +ve = positive band for the NoTIM transgene, -ve = negative for the NoTIM transgene.

3.2.2 Immunophenotyping NoTIM mice

Once it was established the transgene was present and was inherited by progeny, peripheral blood was screened for hFcγRIIB protein expression. Peripheral blood was extracted and stained with fluorescently labelled mAbs against specific markers for different cell lineages along with an antibody specific for hFcγRII (AT 10) [344]. This mAb can detect both

hFcγRIIA and hFcγRIIB, and as the progeny do not express hFcγRIIA, this was sufficient for the purpose of screening. Flow cytometry was then used to determine if the transgene was being expressed and to evaluate the cellular expression pattern.

Anti-mouse CD19 and anti-mouse CD11B were used to identify B cells and myeloid cells respectively (Figure 3.3 A). B cells from positive progeny showed clear expression of hFcγRIIB compared to isotype control whilst myeloid cells showed a positive population and a negative population compared to isotype control (Figure 3.3 B). The two peaks shown for NoTIM +ve monocytes indicate there are two populations: one expressing hFcγRIIB and the other not. This is potentially expected, as CD11B+ is not specific to monocytes, NK cells also express CD11B+ and would not be expected to express hFcγRIIB [190]. The expression of mFcγRII was assessed using AT 130-2 and showed no expression on CD19+ B cells in either the positive or negative progeny for the NoTIM transgene (Figure 3.3 C). The expression of the NoTIM hFcγRIIB on CD11B+ lineages was investigated in further detail later on. Interpreting this and subsequent breeding data, it was ascertained that the NoTIM gene was inherited equally across males and females in the progeny indicating that typical Mendelian inheritance was observed (data not shown).

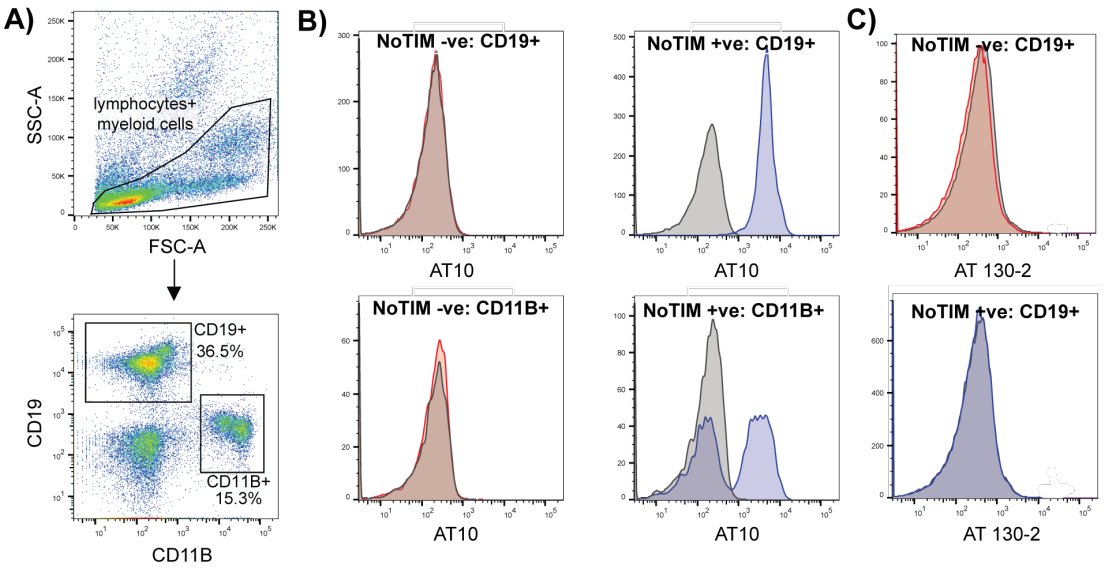

Figure 3.3: Gating Strategy to Identify NoTIM positive progeny
A) Lymphocytes were identified from murine peripheral blood using flow cytometry, B cells were CD19+ and myeloid cells CD11B+. B) NoTIM -ve lymphocytes were negative for hFcγRIIB expression, whilst NoTIM +ve lymphocytes were positive for hFcγRIIB. This was apparent from the shift in fluorescence compared to isotype control (in grey). C) CD19+ lymphocytes were also screened for mFcγRII expression, both NoTIM -ve and NoTIM +ve were negative, confirming the absence of the mFcγRII.

3.3 FcγRIIB expression in human whole blood

In order to subsequently assess if the NoTIM expression pattern mimicked that in humans, whole blood was first collected from three separate healthy human donors and analysed by flow cytometry to ascertain FcγRIIB expression across B cells (CD19+), classical monocytes (CD14+,CD16+), non-classical monocytes (CD14+, CD16-) and NK cells (CD56+). The resultant histograms showed that B cells had the highest expression of FcγRIIB (mean MFI: 5000) followed by non-classical monocytes (mean MFI: 700) and classical monocytes (mean MFI: 400). NK cells showed little expression compared to isotype control (Figure 3.4). The pattern of expression was consistent with previous findings, validating our staining protocols and reagents [192].

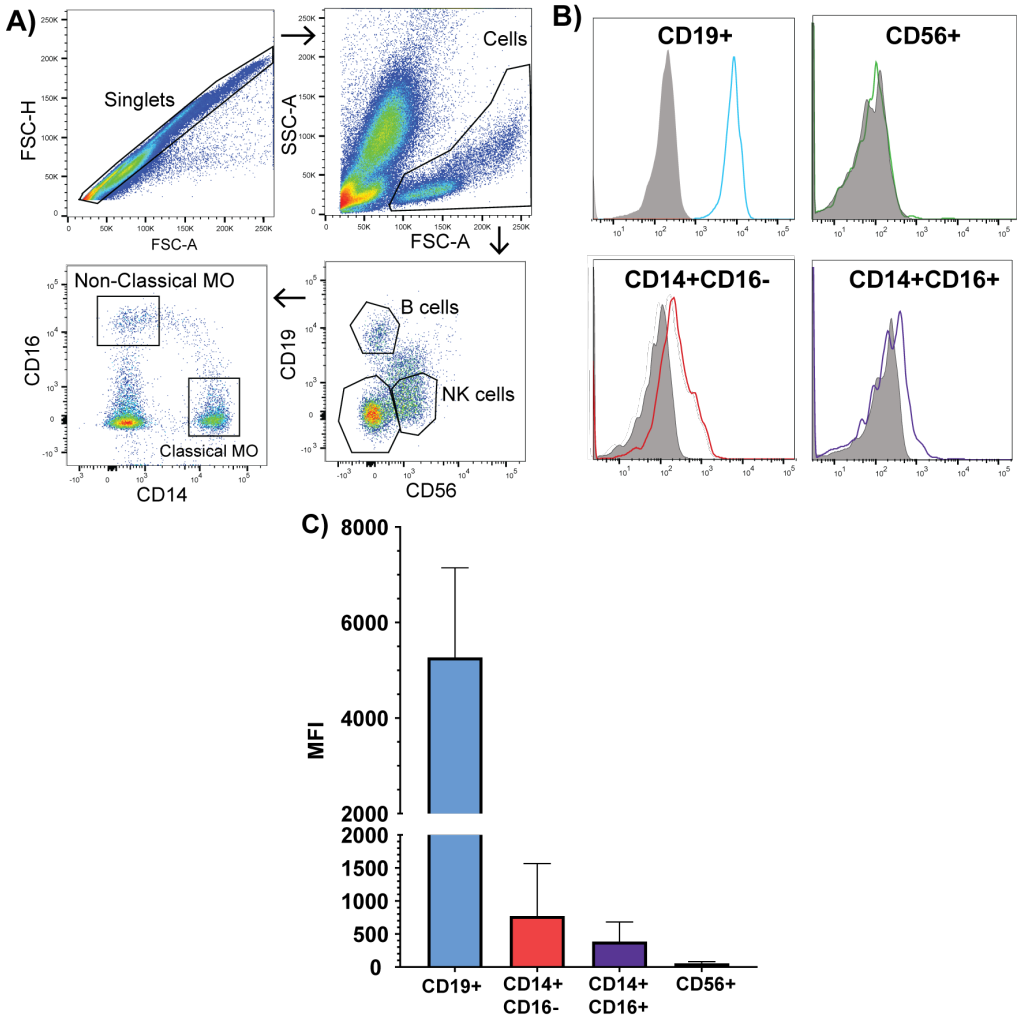

Figure 3.4: FcγRIIB expression on immune cells within human whole blood
A) Human whole blood was extracted from anonymous donors and stained using fluorescent antibodies to detect cell surface expression of hFcγRIIB using flow cytometry. The gating strategy used to pick out each cell type was based on CD19 (B cells), CD56 (NK cells), CD14+/CD16+ (non-classical monocytes [MO]) and CD14+/ CD16- (classical MO). B) Representative histograms of hFcγRIIB expression on key cell types from one donor compared to isotype control (Grey). C) The average MFI for each cell type (N = 3 +SD).

3.4 Comparison of FcγR expression in C57BL/6J, mFcγRII KO, hFcγRIIB Tg and NoTIM mice

After identifying the successful integration and expression of the NoTIM transgene, a comprehensive analysis of mFcγRs and hFcγRIIB was carried out in the NoTIM mouse in comparison to other related mouse models (C57BL/6J, mFcγRII KO and hFcγRIIB Tg). The expression of activatory and inhibitory FcγRs is often finely balanced on effector cells to give an appropriate threshold of activation. Therefore it was important to establish if the deletion of the endogenous mFcγRII, and/or the introduction of hFcγRIIB (without a functional ITIM) resulted in any compensatory changes in activatory mFcγR expression. Flow cytometry was used to examine FcγR expression on key lymphocytic and myeloid cells in the periphery, spleen and iLN. The gating strategy for individual cell populations is shown in Table 3.1 and Figure 3.5. Example data from the NoTIM mouse is then shown, followed by composite data from the 4 different mouse strains.

Cell Type	**Markers**
B Cells	CD45.2+B220+
NK Cells	CD45.2+ NK1.1+
CD4+ T Cells	CD45.2 CD4+
CD8+ T Cells	CD45.2+CD8+
Ly6C High Monocytes	CD45.2+ CD11B+ Ly6C high
Ly6C Low Monocytes	CD45.2+ CD11B+ Ly6C Low
Macrophages	CD45.2+ CD11B low F4/80+
Neutrophils	CD45.2+ CD11B+ Ly6C+ Ly6G+

Table 3.1: Flow cytometry panel of cellular markers used to identify murine immune cells

3.4.1 FcγR expression on immune cell populations within the spleens of C57BL/6J, mFcγRII KO, hFcγRIIB Tg and NoTIM mice

The spleen was most rich in lymphocytes and myeloid cells allowing for a detailed analysis of FcγR expression patterns. The expression pattern was consistent across three independent experiments as shown in Figure 3.6 (lymphocytes), Figure 3.7 (myeloid cells) and Figure 3.8 (composite data within the spleen from N = 3 experiments). mFcγRII showed a low level of consistent binding on most cell populations, such as CD4+ and CD8+ cells which are known not to express the receptor [98]. As the expression was consistent across mouse models and cell types, the staining observed is most likely due to non-specific binding of the mAb and it can be concluded that mFcγRII was not expressed in the mFcγRII

KO, hFcγRIIB Tg and NoTIM models. It has been previously noted that batches of the mAb (AT 130-2) can sometimes lead to non-specific binding (Kerry Cox, personal communication) on negative populations but the 'real' expression can be discerned above this. Increased fluorescence of mFcγRII stained cells was seen on appropriate populations (e.g. B cells) in C57BL/6J mice indicating expression.

mFcγRIII was expressed on NK cells, both monocyte populations, macrophages and neutrophils at similar levels across all mouse models. mFcγRIV was expressed on subsets of Ly6C low and high monocytes, macrophages and neutrophils equally across all models. The NoTIM mice showed high levels of hFcγRIIB on B cells, monocytes and macrophages. The hFcγRIIB Tg mice showed a similar expression pattern on the same cell types as NoTIM mice, however they had a lower geometric mean (as assessed on hFcγRIIB+ populations) and some populations (B cells, monocytes) displayed a mosaic expression pattern [323].

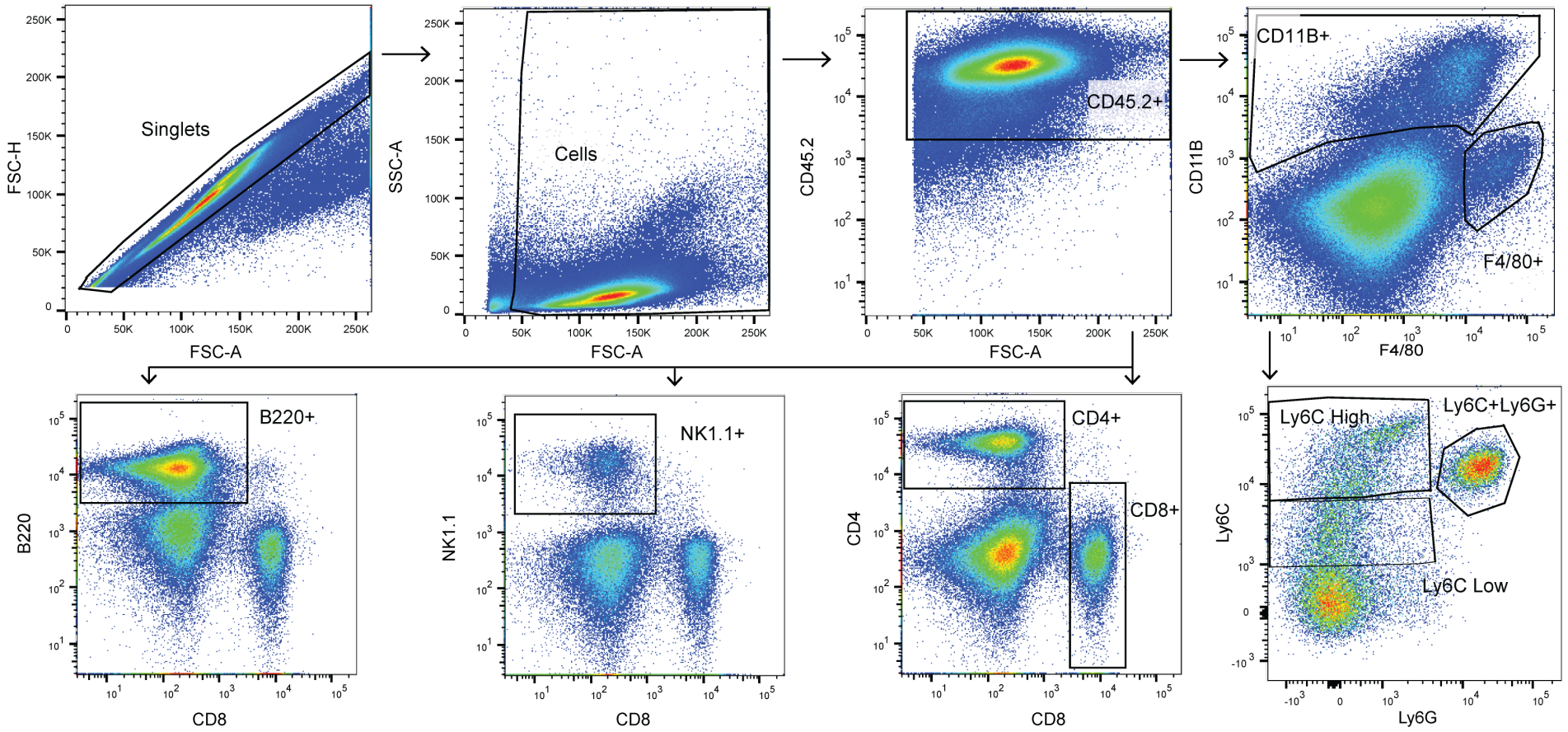

Figure 3.5: Example gating for lymphocyte and myeloid cells from mouse spleen
Spleens were processed into single cell suspensions and stained with fluorescently conjugated antibodies against specific cell markers. Cellular populations were then analysed by flow cytometry. Gating was initially based on forward and side scatter to distinguish singlets and cells. Lymphocytes were identified by CD45.2+ cells which were then further distinguished using B220+ (B cells), NK 1.1+ (NK cells) or CD4+/CD8+ (T cells). Myeloid cells were identified as CD45.2+ and the further distinguished by CD11Blo/F480+ (macrophages), CD11B+/Ly6Clo (Ly6C low monocytes), CD11B+/Ly6C+ (Ly6C high monocytes) and CD11B+/Ly6C+/Ly6G+ (neutrophils).

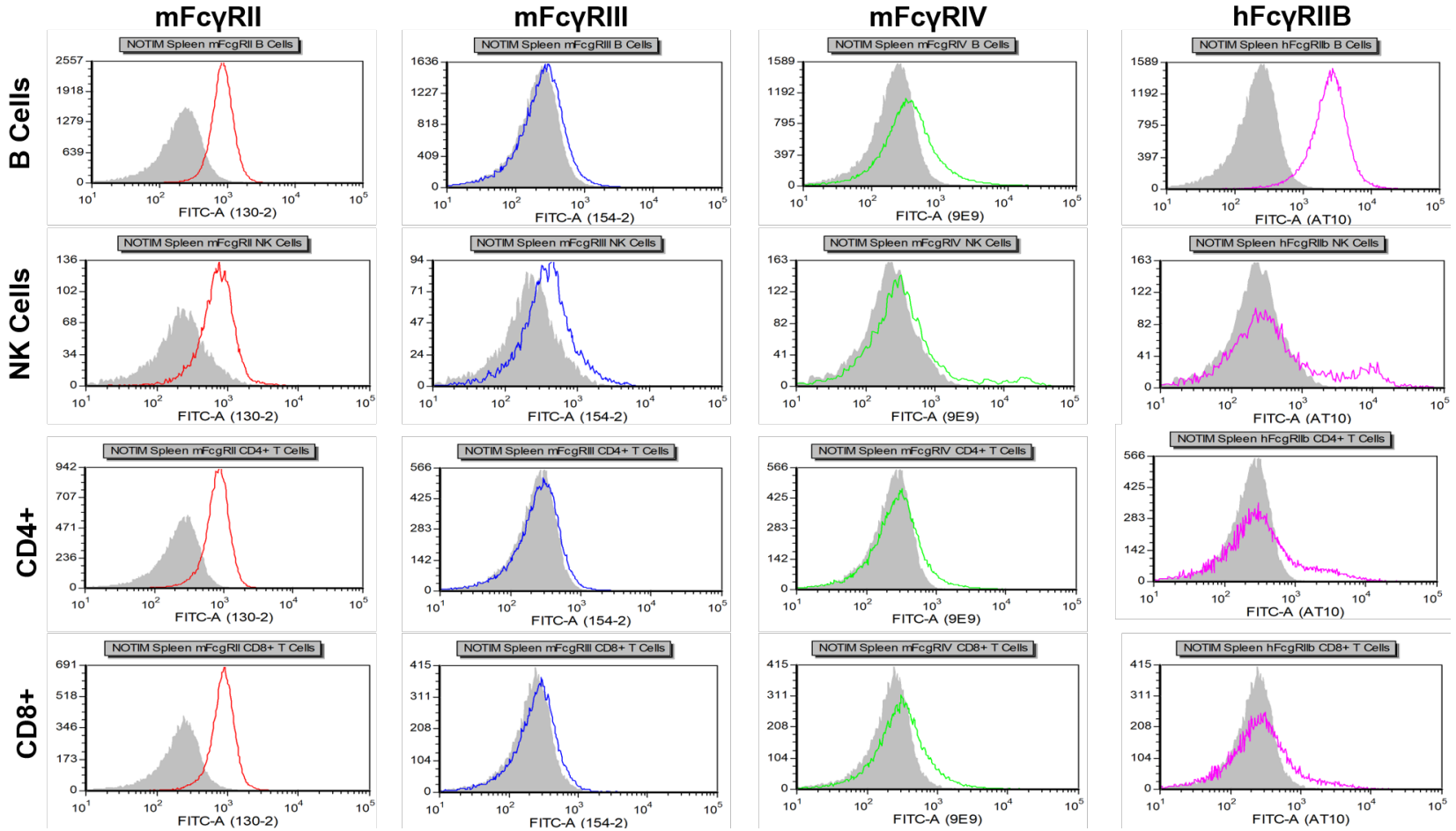

Figure 3.6: Splenic Lymphocyte FcγR Expression in NoTIM mice
Spleens were processed into single cell suspensions and stained with fluorescently conjugated antibodies against specific cell markers. Cellular populations were then analysed by flow cytometry as previously described. Lymphocytic populations were further stained with antibodies specific to the mouse FcγRs and human FcγRIIB. Grey = isotype, Purple = mouse FcγRI, Red = mouse FcγRII, Blue = mouse FcγRIII, Green = mouse FcγRIV, Pink = human FcγRIIB. Representative staining of FcγRs from NoTIM mice from one experiment.

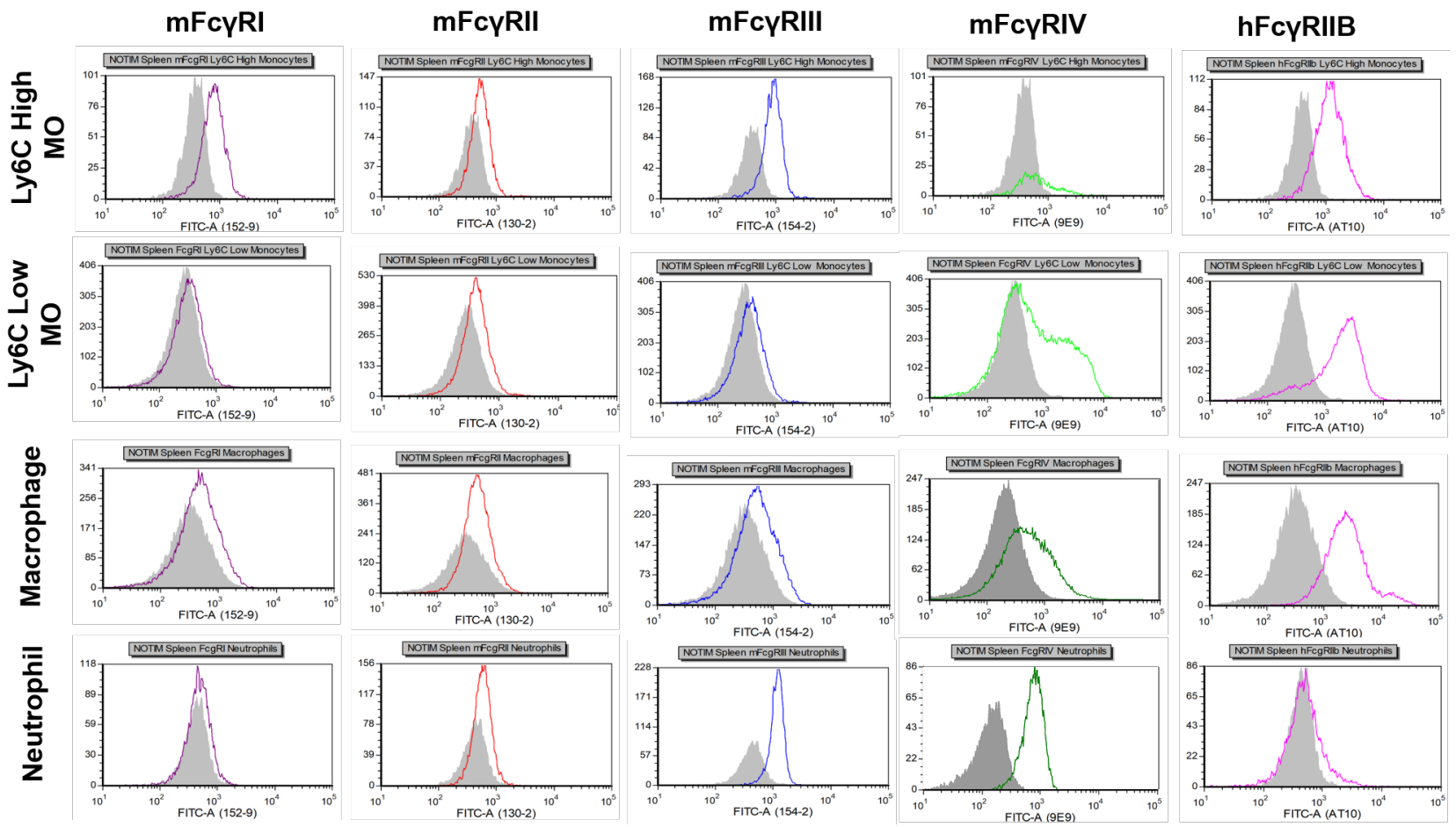

Figure 3.7: Splenic Myeloid FcγR Expression in NoTIM mice
Spleens were processed into single cell suspensions and stained with fluorescently conjugated antibodies against specific cell markers. Cellular populations were then analysed by flow cytometry as previously described. Myeloid populations were further stained with antibodies specific to the mouse FcγRs and human FcγRIIB. Grey = isotype, Red = mouse FcγRII, Blue = mouse FcγRIII, Green = mouse FcγRIV, Pink = human FcγRIIB, MO = monocyte. Representative staining of FcγRs from NoTIM mice from one experiment.

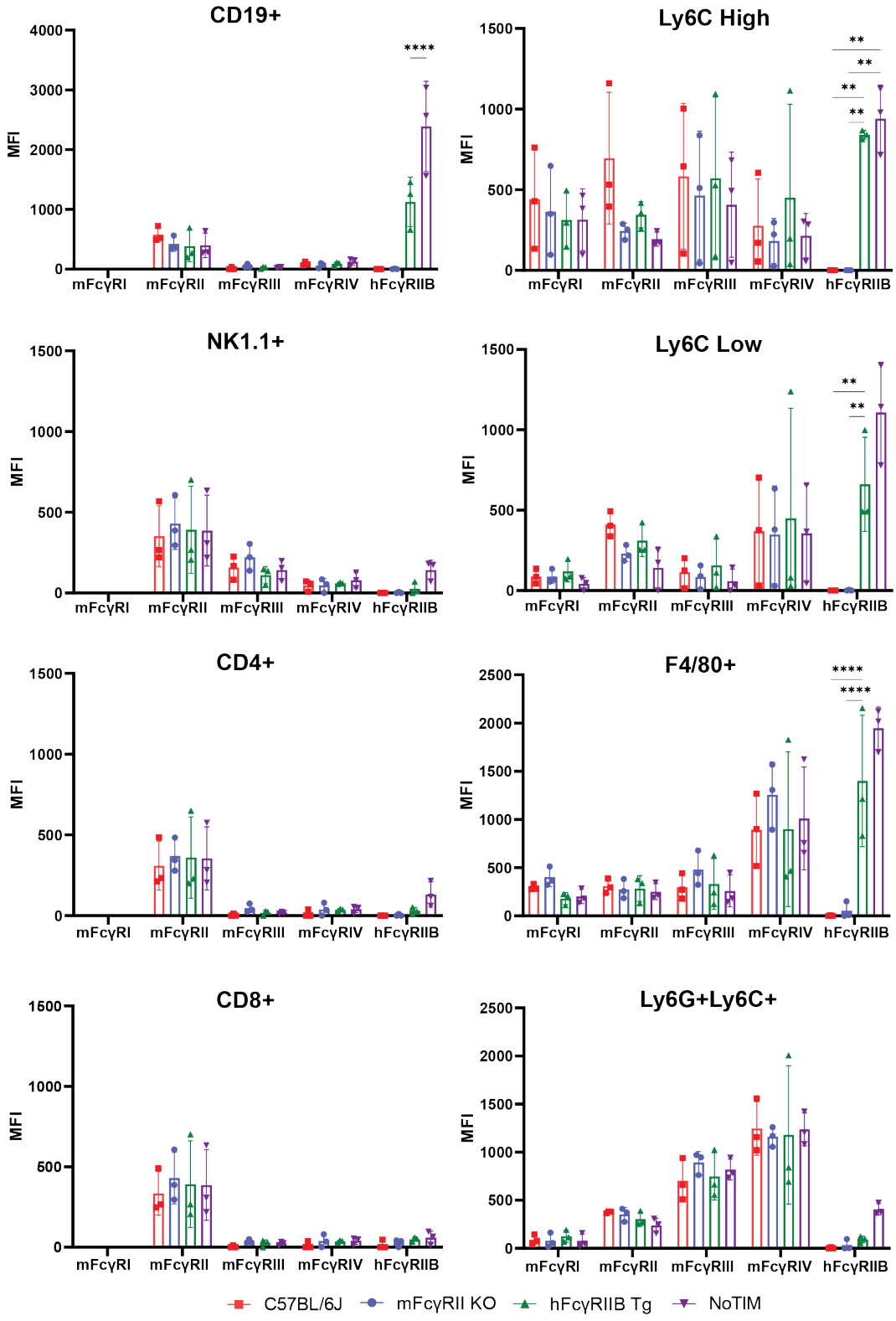

Figure 3.8: Expression of mouse FcγRI, FcγRII, FcγRIII, FcγRIV and hFcγRIIB on cells within the spleen of C57BL/6J, mFcγRII KO, hFcγRIIB Tg and NoTIM mice
Spleens were processed into single cell suspensions and stained with fluorescently conjugated antibodies against specific cell markers. Cellular populations were then analysed by flow cytometry as previously described. The FcγRs on B cells, NK cells, CD4+/CD8+ T cells, Ly6C high monocytes, Ly6C low monocytes, macrophages and neutrophils were analysed. The result of three independent experiments (n = 1 per experiment). Line = mean ± SD. Statistical analyses conducted using a one-way ANOVA with Tukey's multiple comparison test. * = $P \leq 0.05$, ** = $P \leq 0.01$, *** = $P \leq 0.001$, **** = $P \leq 0.0001$. NB: batches of the mAb (AT 130-2) can sometimes lead to non-specific binding (personal communications) on negative populations but the 'real' expression can be discerned above this.

3.4.2 FcγR expression on immune cell populations within the inguinal lymph nodes of C57BL/6J, mFcγRII KO, hFcγRIIB Tg and NoTIM mice

Having established the expression in the spleen, the iLN was then assessed as it is an important migratory centre for immune cells that are known to express FcγRs. As seen in the spleen, mFcγRII had high expression on the expected cell types in WT mice (CD19+ B cells, Ly6C+ monocytes, F4/80+ macrophages). There was apparent non-specific binding on cell populations across each mouse model when examining mFcγRII expression as described for the spleen. mFcγRI, mFcγRIII and mFcγRIV geometric mean fluorescence intensity was consistent across different strains of mice suggesting no compensatory changes in the expression of these receptors. hFcγRIIB had a greater MFI in NoTIM populations in comparison to hFcγRIIB Tg (Figure 3.6, Figure 3.7 and Figure 3.9).

3.4.3 FcγR expression on immune cell populations within the blood of C57BL/6J, mFcγRII KO, hFcγRIIB Tg and NoTIM mice

The blood contains a number of migratory immune cells and can be compared to human whole blood and so was examined in a similar manner to spleen and iLN. mFcγRII had high expression on the expected cell types in WT mice with none present on mFcγRII KO, hFcγRIIB Tg and NoTIM mice. The expression of mFcγRII was lowest within the blood (for example, comparing CD19+ cells within the blood and spleen or LN) and also displayed the lowest level of non-specific binding. mFcγRI and mFcγRIII geometric mean fluorescence intensity was broadly consistent across groups. hFcγRIIB was expressed more strongly on the NoTIM B cells compared to the hFcγRIIB Tg mouse B cells. The myeloid cells had more comparable expression than seen in the spleen or iLN of hFcγRIIB between NoTIMs and hFcγRIIB Tg mice (Figure 3.6, Figure 3.7 and Figure 3.10).

The FcγR expression data generated from splenic populations was most robust, therefore a heat map was produced to compare expression of each FcγR across mouse models. The data shows that activatory FcγRs are expressed similarly across mouse models suggesting no compensatory changes in expression (Figure 3.8). Once the expression pattern had been established *in vivo*, the expression of FcγRs was examined *ex vivo* on BMDMs.

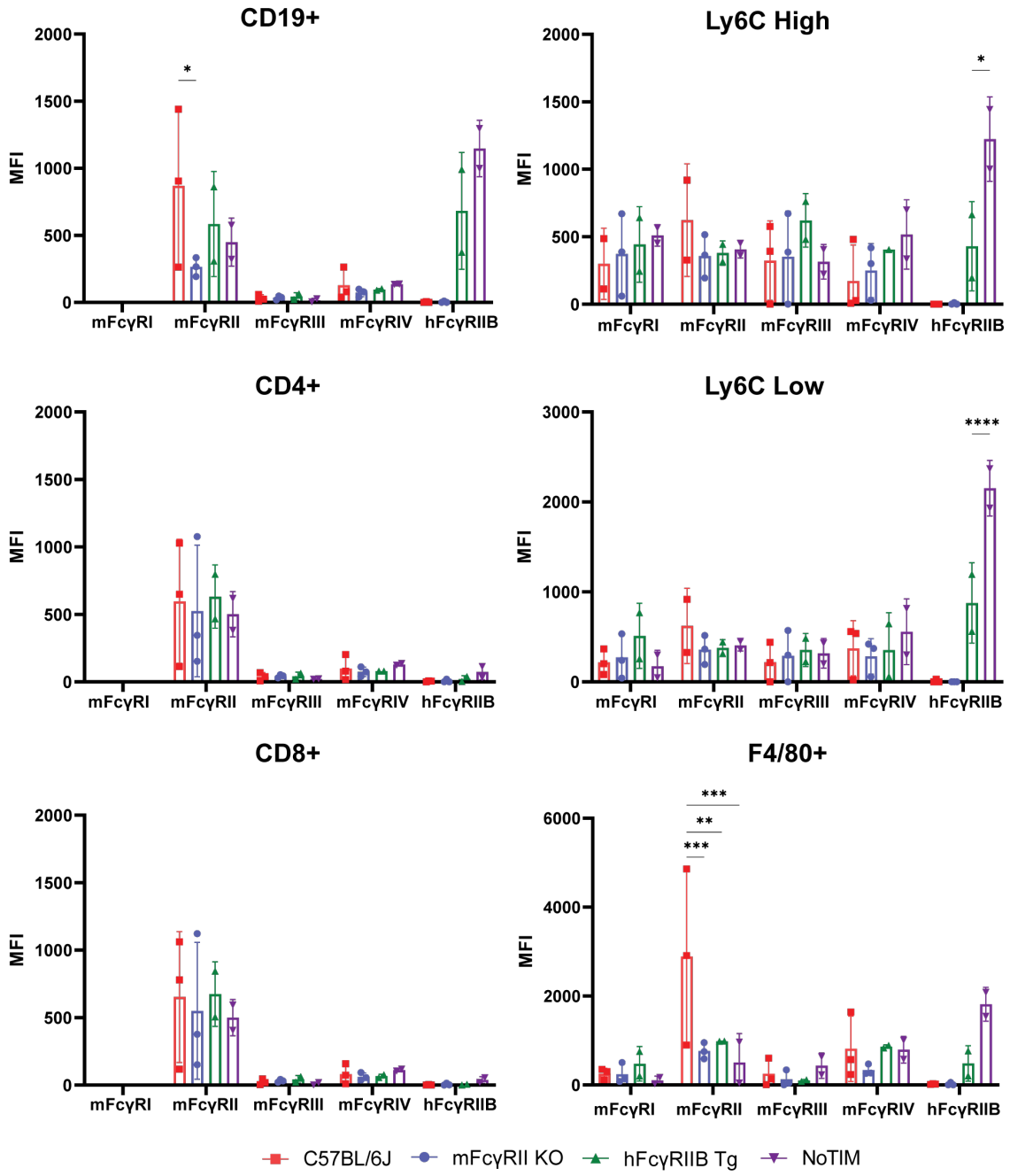

Figure 3.9: Expression of mouse FcγRI, FcγRII, FcγRIII, FcγRIV and hFcγRIIB on cells within the inguinal lymph nodes of C57BL/6J, mFcγRII KO, hFcγRIIB Tg and NoTIM mice
Spleens were processed into single cell suspensions and stained with fluorescently conjugated antibodies against specific cell markers. Cellular populations were then analysed by flow cytometry as previously described. The FcγRs on B cells, NK cells, CD4+/CD8+ T cells, Ly6C high monocytes, Ly6C low monocytes, macrophages and neutrophils were analysed. The result of two - three independent experiments (n = 1 per experiment). Line = mean ± SD. Statistical analyses conducted using a one-way ANOVA with Tukey's multiple comparison test. * = $P \leq 0.05$, ** = $P \leq 0.01$, *** = $P \leq 0.001$, **** = $P \leq 0.0001$. NB: batches of the mAb (AT 130-2) can sometimes lead to non-specific binding (personal communications) on negative populations but the 'real' expression can be discerned above this.

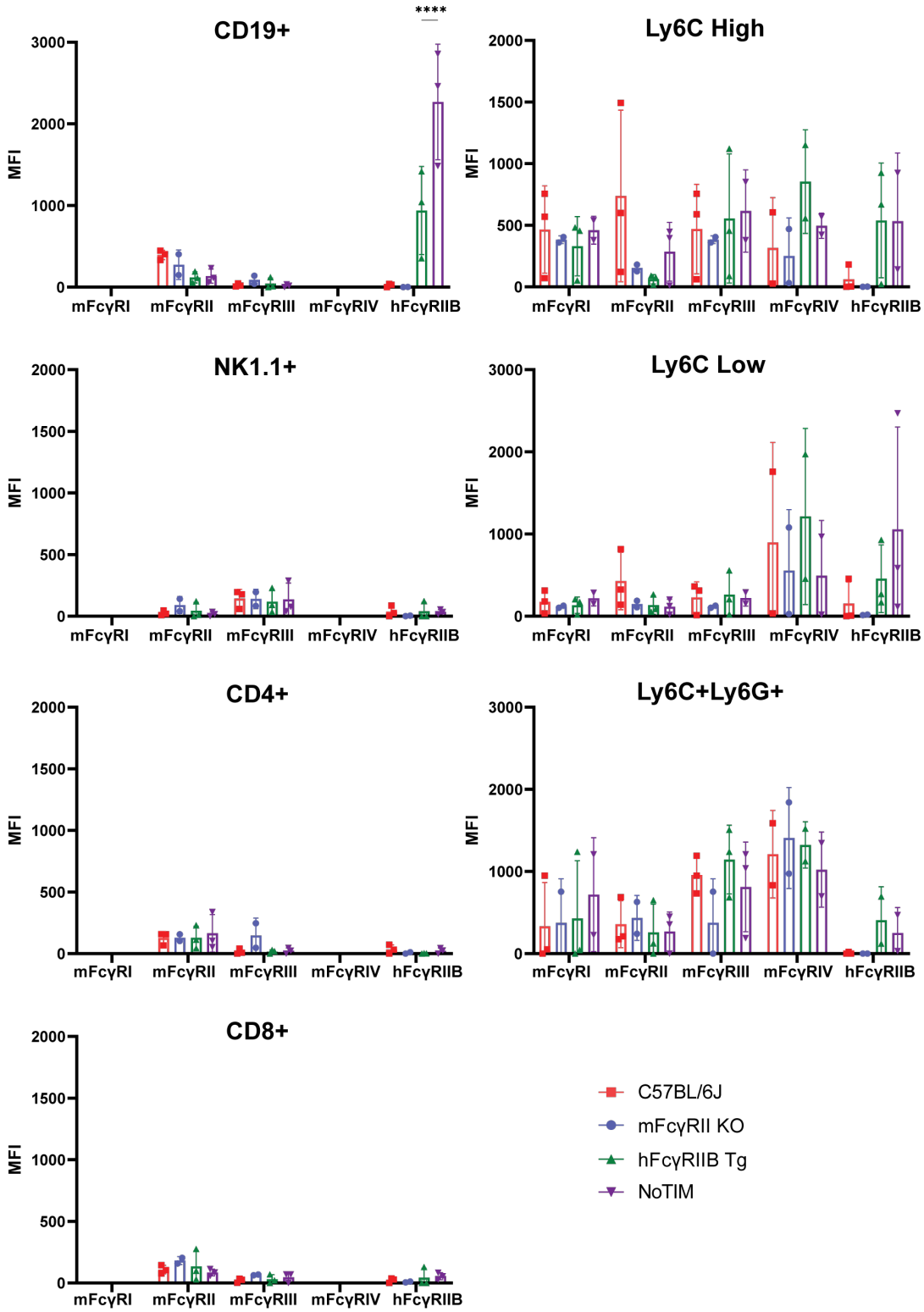

Figure 3.10: Expression of mouse FcγRI, FcγRII, FcγRIII, FcγRIV and hFcγRIIB on cells within the blood of C57BL/6J, mFcγRII KO, hFcγRIIB Tg and NoTIM mice
Spleens were processed into single cell suspensions and stained with fluorescently conjugated antibodies against specific cell markers. Cellular populations were then analysed by flow cytometry as previously described. The FcγRs on B cells, NK cells, CD4+/CD8+ T cells, Ly6C high monocytes, Ly6C low monocytes, macrophages and neutrophils were analysed. The result of two - three independent experiments (n = 1 per experiment). Bar = mean ± SD. Statistical analyses conducted using a one-way ANOVA with Tukey's multiple comparison test. * = $P \leq 0.05$, ** = $P \leq 0.01$, *** = $P \leq 0.001$, **** = $P \leq 0.0001$. NB: batches of the mAb (AT 130-2) can sometimes lead to non-specific binding (personal communications) on negative populations but the 'real' expression can be discerned above this.

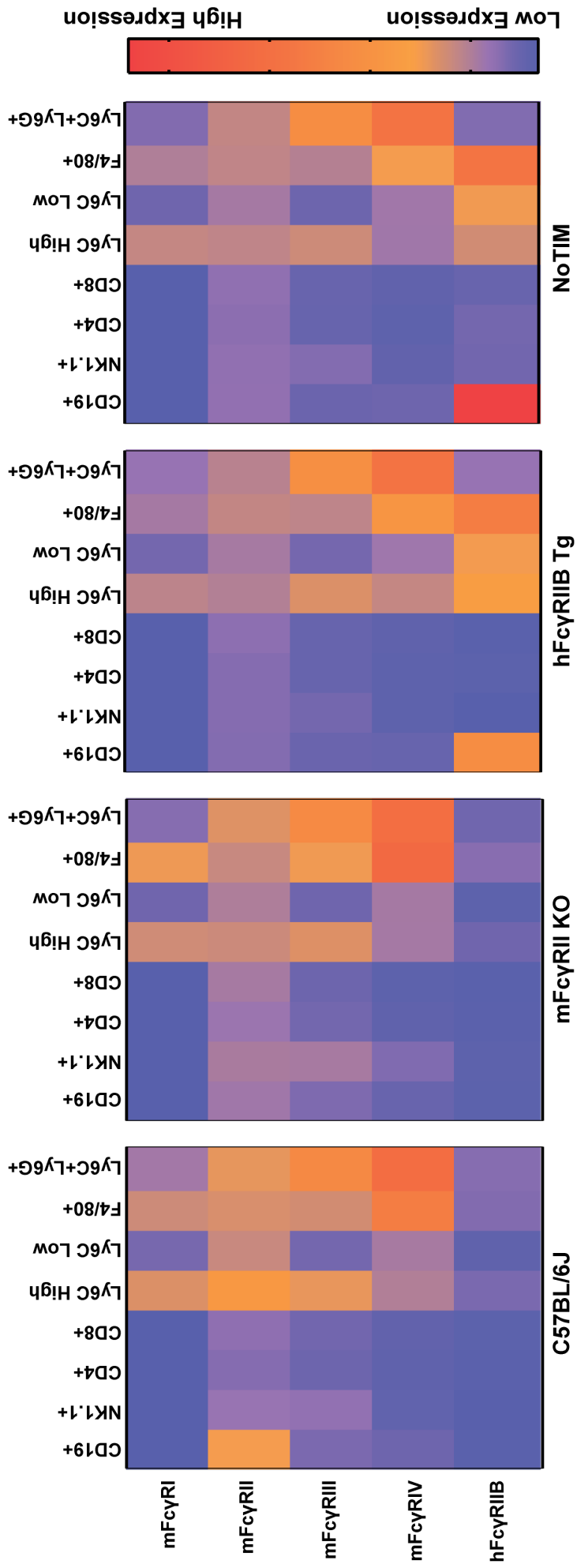

Figure 3.11: Relative expression of each FcγR on key immune cells across C57BL/6J, mFcγRII KO, hFcγRIIB Tg and NoTIM mice
The relative expression of each mouse FcγR and the transgenic hFcγRIIB receptor in each mouse model was determined on key cell types based using flow cytometry data generated from mouse spleen. Within each mouse, FcγR expression level was normalised across every mouse model so that the highest MFI was plotted in red as 'high expression'. The result of three independent experiments.

3.4.4 FcγR expression on bone marrow derived macrophages

Macrophages are integral to the study of mAb effector functions as they express all FcγRs and have a central role in antibody-mediated target cell depletion [345]. To study the function of macrophages, BMDMs are routinely utilised due to their ease of generation, relative abundance and similarities to *in vivo* macrophages. Therefore to study *ex vivo* macrophage effector functions from each mouse model, it was important to establish that these cells sufficiently express each respective FcγR.

To examine FcγR expression on BMDMs, bone marrow progenitor cells were collected from the femurs and tibias of mice and differentiated *ex vivo* into macrophages in the presence of L929 conditioned media (containing m-CSF). BMDMs were then analysed using flow cytometry to examine the expression pattern of FcγRs. Mouse FcγRI had similar expression between all mouse models, mFcγRIII and mFcγRIV was similar between mFcγRII KO, hFcγRIIB Tg and NoTIM but was expressed at higher levels in the C57BL/6J BMDMs, albeit not statistically significant. mFcγRII was expressed on C57BL/6J BMDMs but was absent in mFcγRII KO, hFcγRIIB Tg and NoTIM BMDMs as expected. Human FcγRIIB expression was mosaic in hFcγRIIB Tg BMDMs whilst NoTIMs had slightly higher expression as measured by MFI but this was not statistically significant (Figure 3.12).

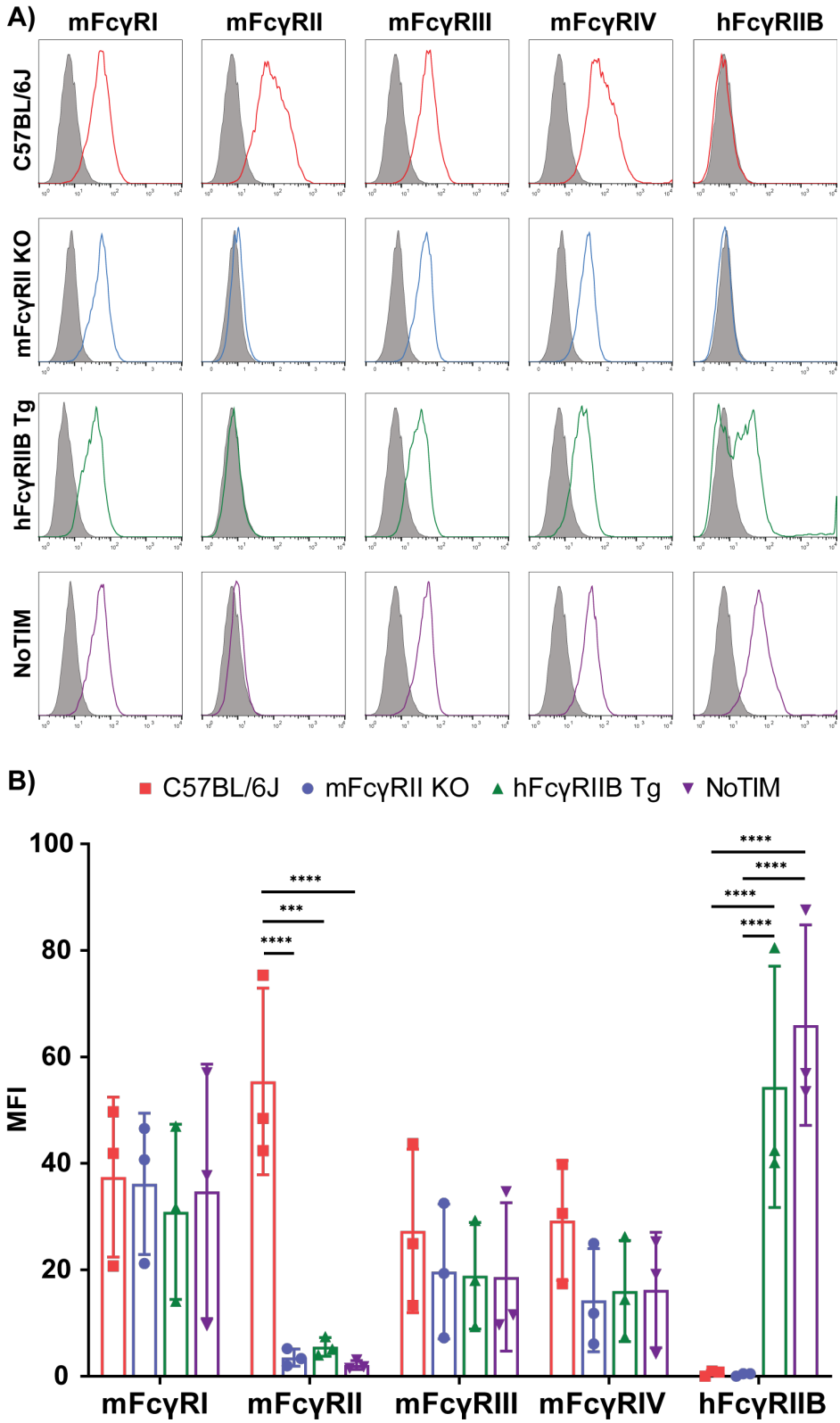

Figure 3.12: The mean fluorescent intensities of FcγR expression on C57BL/6J, mFcγRII KO, hFcγRIIB Tg and NoTIM BMDMs

Bone marrow progenitor cells were taken from each mice and differentiated *ex vivo* into BMDMs in the presence of L929 media for 7 days. BMDMs were then stained with antibody-fluorescent conjugates specific for FcγRs and analysed using flow cytometry. Mean fluorescence intensity was then calculated by geometric mean minus isotype control. The result of three independent experiments (n = 1 per experiment). Bar = mean ± SD. Statistical analyses conducted using a one-way ANOVA with Tukey's multiple comparison test. *** = $P \leq 0.001$, **** = $P \leq 0.0001$.

3.4.5 Analysis of mosaic expression in hFcγRIIB Tg mice

As previously described, hFcγRIIB Tg mice show a mosaic expression pattern of hFcγRIIB on some key cell types. To assess differences between expression in hFcγRIIB Tg and NoTIM mice, the expression of hFcγRIIB was directly compared from splenic cell populations. B cells, and Ly6C high monocytes displayed a similar level of mosaicism, with approximately 70% of cells expressing the transgene in the mice analysed. In NoTIM mice, all cells expressed the receptor. Ly6C low monocytes had a heterogeneous expression on both hFcγRIIB Tg and NoTIM mice. However, NoTIM mice had a higher percentage of expressing cells (42.3%) compared to hFcγRIIB mice (24.9%). Interestingly, all macrophages in both mouse models expressed the receptor however the shift in the histograms compared to isotype control suggest NoTIM macrophages express higher levels of the receptor than hFcγRIIB Tg mice.

This data shows that hFcγRIIB in hFcγRIIB Tg and NoTIM mice is expressed on the same cells, but to differing extents with hFcγRIIB Tg mice displaying less expression of the receptor than the NoTIM mice. The reason for this is unclear, but most likely a result of the integration sites of the transgene in each mouse model. Nevertheless, expression is sufficient to draw comparisons between the transgenic mouse models with the caveat of differing expression levels taken into account.

Once hFcγRIIB had been analysed by flow cytometry, a comparison of mFcγRII and hFcγRIIB within the architecture of the spleen and liver were assessed by immunofluorescence.

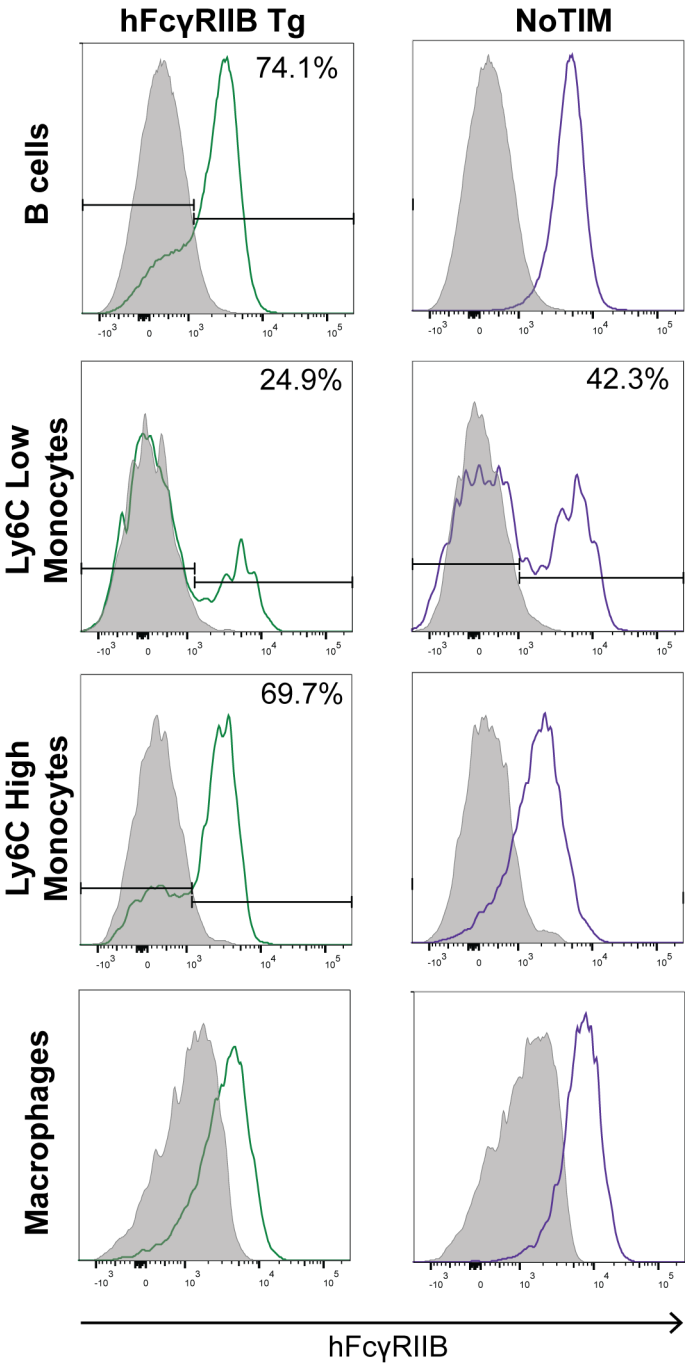

Figure 3.13: Expression of hFcγRIIB on key splenic cell types in hFcγRIIB Tg and NoTIM mice
Spleens were processed into single cell suspensions and stained with fluorescently conjugated antibodies against specific cell markers. Cellular populations were then analysed by flow cytometry as previously described. A representative example of expression taken from one hFcγRIIB Tg and NoTIM mouse.

3.4.6 Immunofluorescence analysis of hFcγRIIB expression in spleen and liver

To visualise the distribution of mFcγRII and hFcγRIIB in the transgenic mice and assess whether it differed to other strains, immunofluorescence was used to examine key cell types within the spleen and liver.

Spleen sections were stained for B cells (B220+) and mFcγRII or hFcγRIIB. C57BL/6J spleens were stained for mFcγRII using AT 130-5 and showed co-localisation with B220+ cells as expected (Figure 3.14). At 10x magnification it was possible to resolve the architecture of the spleen using B220 positivity and identify areas that were likely to be B cell follicles. The staining also highlighted expression of mFcγRII on non-B cells (most likely macrophages, monocytes or FDCs). As expected, the mFcγRII KO spleen showed no staining with AT 130-5 (Figure 3.14).

hFcγRIIB Tg spleens stained using the anti-hFcγRIIB mAb EP888Y showed more punctate staining than mFcγRII staining in C57BL/6J mice. At 10x magnification there was some identification of the follicular architecture and at 40x magnification, hFcγRIIB showed clear co-localisation with B220+ cells. However, hFcγRIIB was not co-localised with every B220+ cell which likely reflects the mosaic expression pattern within the hFcγRIIB Tg mice. The NoTIM spleen stained strongly for hFcγRIIB and showed clear co-localisation with B220+ cells. At 40x magnification hFcγRIIB expression matched the pattern of the B220+ staining. Other hFcγRIIB+ cells that did not co-localise with B220 were likely other populations such as macrophages and monocytes (Figure 3.15).

Overall the immunofluorescence images showed a similar staining pattern between mFcγRII and hFcγRIIB on splenic B cells with equivalent splenic architecture. This suggested that the introduction of the (signalling or non-signalling) hFcγRIIB transgene did not alter expression of activatory FcγRs.

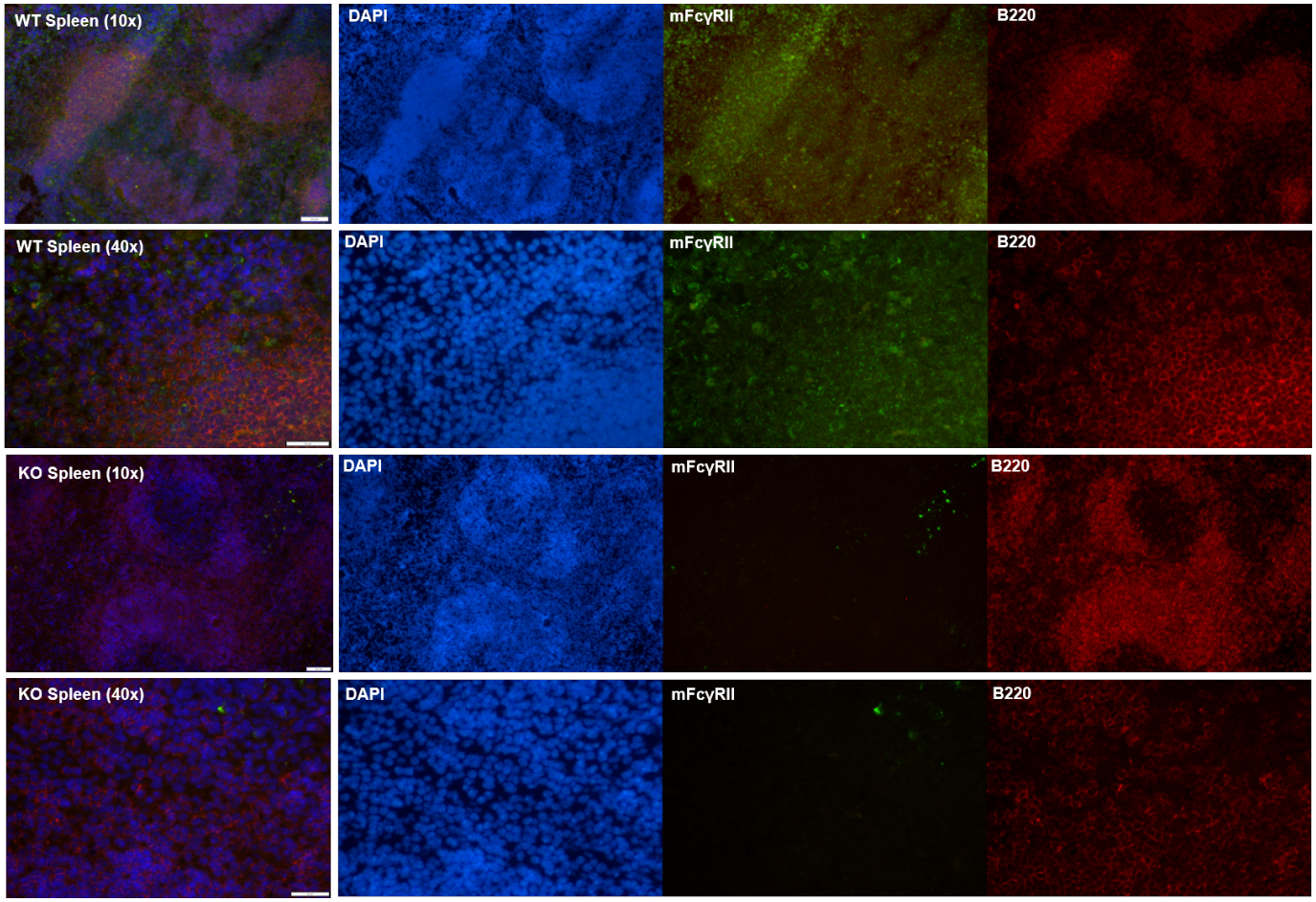

Figure 3.14: Immunofluorescence staining mFcγRII and B220 within spleens taken from C57BL/6J and mFcγRII KO mice
Spleens from C57BL/6J and mFcγRII KO mice were snap frozen in OCT and sectioned on a cryostat. Sections were then stained using primary antibodies to detect the antigen and fluorescently labelled secondary antibodies to amplify the signal. DAPI shows cell nuceli (blue), B220+ to identify B cells (red) and AT 130-5 to identify mFcγRII (green). 10x scale bar = 50 μm, 40x scale bar = 20 μm.

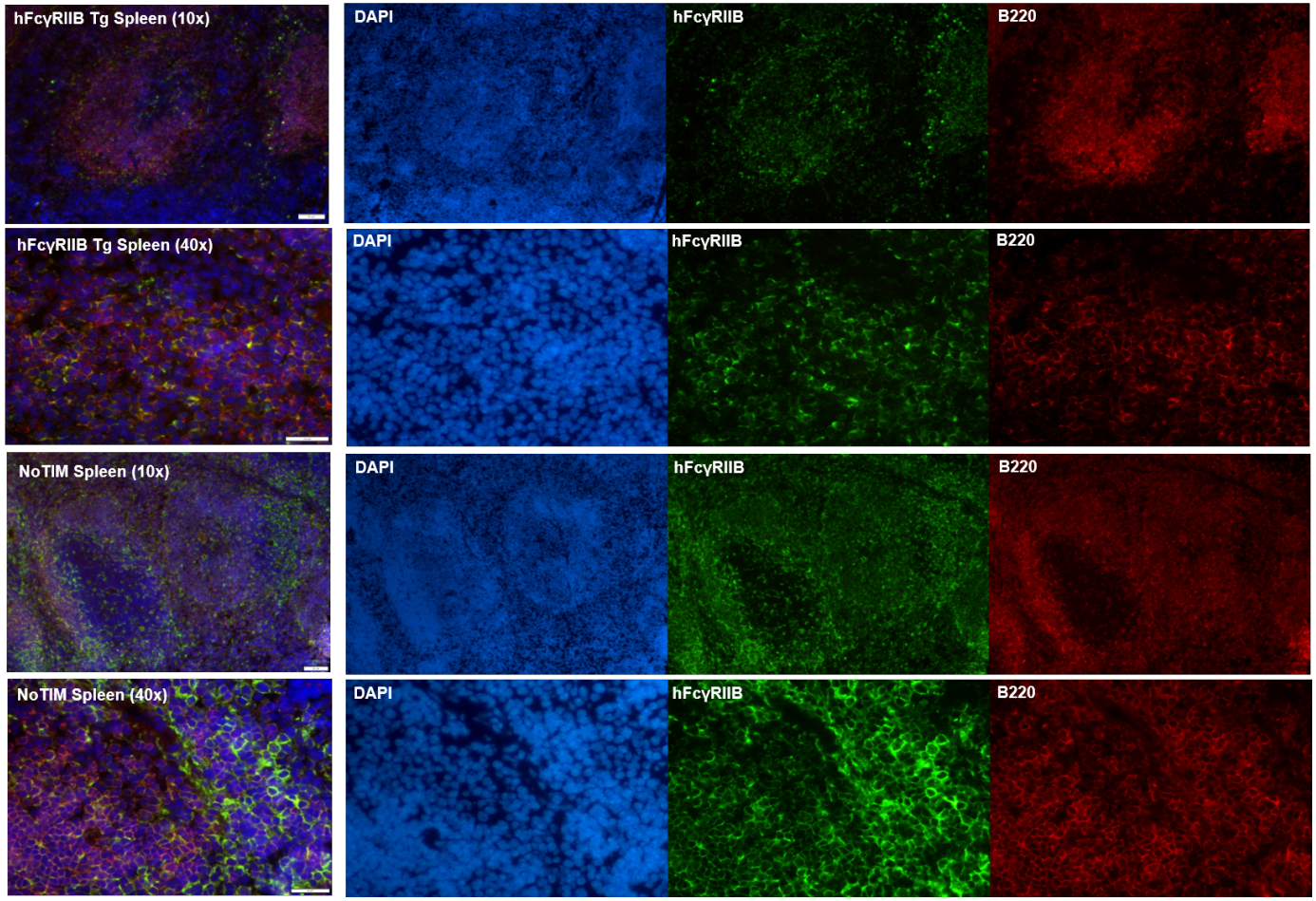

Figure 3.15: Immunofluorescence staining hFcγRIIB and B220 within spleens taken from hFcγRIIB Tg and NoTIM mice
Spleens from hFcγRIIB Tg and NoTIM mice were snap frozen in OCT and sectioned on a cryostat. Sections were then stained using primary antibodies to detect the antigen and fluorescently labelled secondary antibodies to amplify the signal. DAPI shows cell nuclei (blue), B220+ to identify B cells (red) and EP888Y to identify hFcγRIIB (green). 10x scale bar = 50 μm, 40x scale bar = 20 μm.

mFcγRII and hFcγRIIB are known to be expressed on key cell populations within the liver such as LSECs and Kupffer cells [242]. Therefore, mFcγRII and hFcγRIIB were assessed for expression on CLEC4F+ cells (Kupffer cell marker) due to their importance in mediating depletion of opsonised cells *in vivo* [346] [304]. Livers from C57BL/6J mice showed strong expression of mFcγRII throughout, however there was limited co-localisation with CLEC4F+ cells. These data suggest there is some expression on the Kupffer cell population whilst the majority of mFcγRII was expressed on another cell type, most likely LSECs. As expected, the mFcγRII KO liver showed no staining for mFcγRII (Figure 3.16).

hFcγRIIB expression in hFcγRIIB transgenic livers showed a distinct pattern of expression compared to mFcγRII. hFcγRIIB Tg liver sections showed a greater degree of co-localisation as indicated by yellow staining created from the coincidence of CLEC4F+ (red) and hFcγRIIB expression (green). Not every CLEC4F+ cell showed co-localisation with hFcγRIIB which is likely due to the mosaic expression pattern. NoTIM liver sections had even stronger co-localisation, which is likely due to the complete penetrance of the NoTIM transgene (Figure 3.17). The percentage of co-localisation was calculated by examining the overlap of CLEC4F+ and mFcγRII or hFcγRIIB from each respective mouse model in a blinded manner (Figure 3.18 A). It was found that C57BL/6J liver sections had significantly less co-localisation of CLEC4F/mFcγRII than CLEC4F/hFcγRIIB in the hFcγRIIB transgenic mouse models, suggesting that the inhibitory FcγR is differentially regulated dependent on if the receptor is of mouse or human origin.

One reason for the lack of co-localisation in C57BL/6J mice between CLEC4F+ cells and mFcγRII expression may be due to weak staining by the mAb. Therefore, flow cytometry was also used to interrogate expression of mFcγRII and hFcγRIIB on non-parenchymal liver cells (Figure 3.18 B). Livers were harvested from mice and subjected to enzymatic digestion, before separating non-parenchymal cells using a percoll gradient. C57BL/6J livers had expression of mFcγRII on both the LSEC (CD45-/CD146+) and Kupffer cell (CD45+/CD11B+/F4/80++) populations [347]. mFcγRII KO non-parenchymal cells did not express mFcγRII as expected. The C57BL/6J Kupffer cell population had both a low and high expressing mFcγRII population, indicating that potentially only the high population was registered by immunofluorescence. Both hFcγRIIB Tg and NoTIM livers had some expression of hFcγRIIB on LSECs with a much greater expression of hFcγRIIB on Kupffer cells; hFcγRIIB Tg Kupffer cells also displayed a mosaic expression of the receptor. Once the expression pattern had been analysed *in vivo*, the functional consequences of the NoTIM mutations were assessed *ex vivo*.

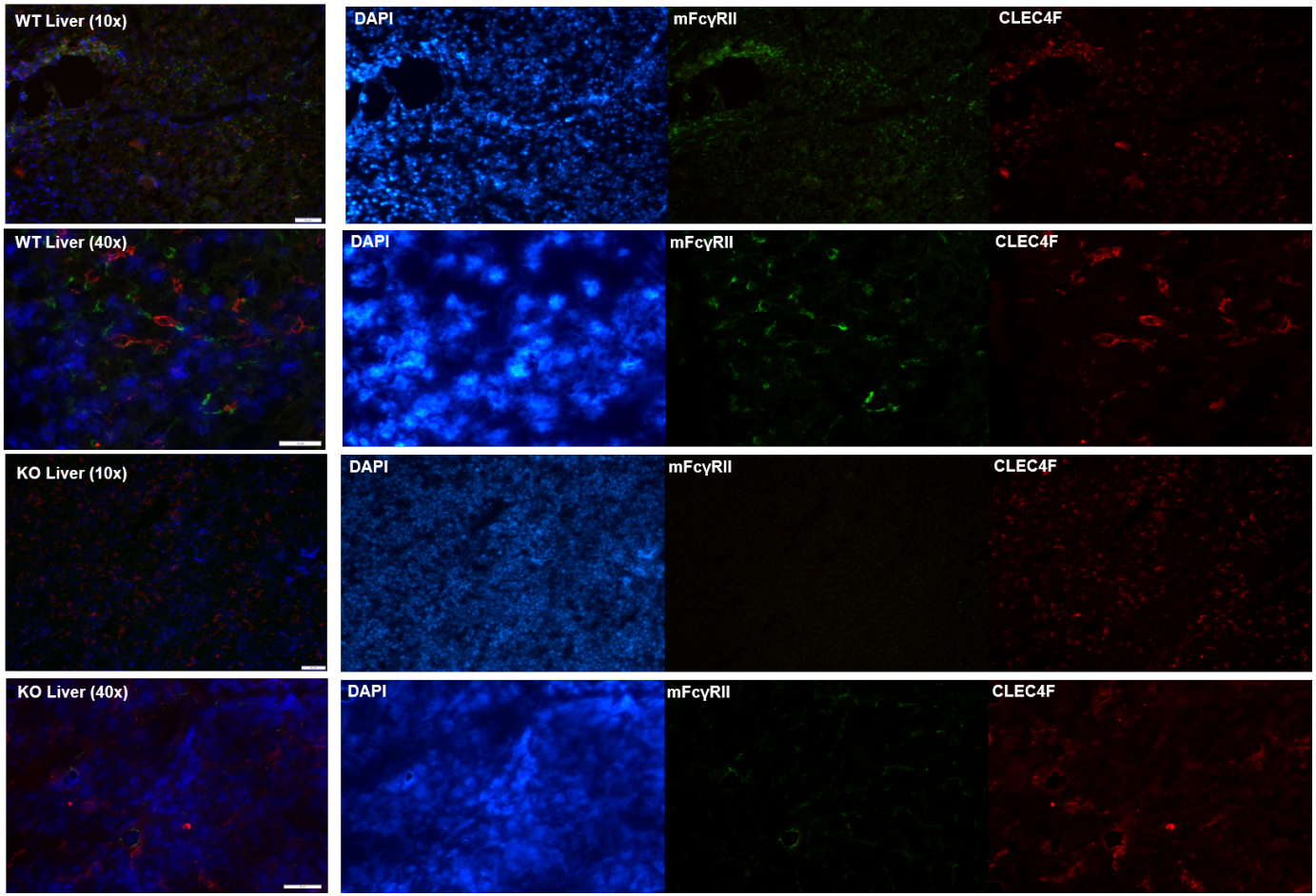

Figure 3.16: Immunofluorescence staining mFcγRII and CLEC4F+ within livers taken from C57BL/6J and mFcγRII KO mice
Livers from C57BL/6J and mFcγRII KO mice were snap frozen in OCT and sectioned using a cryostat. Sections were then stained using primary antibodies to detect the antigen and fluorescently labelled secondary antibodies to amplify the signal. DAPI shows cell nuclei (blue), CLEC4F+ to identify Kupffer cells (red) and AT 130-5 to identify mFcγRII (green). 10x scale bar = 50 μm, 40x scale bar = 20 μm.

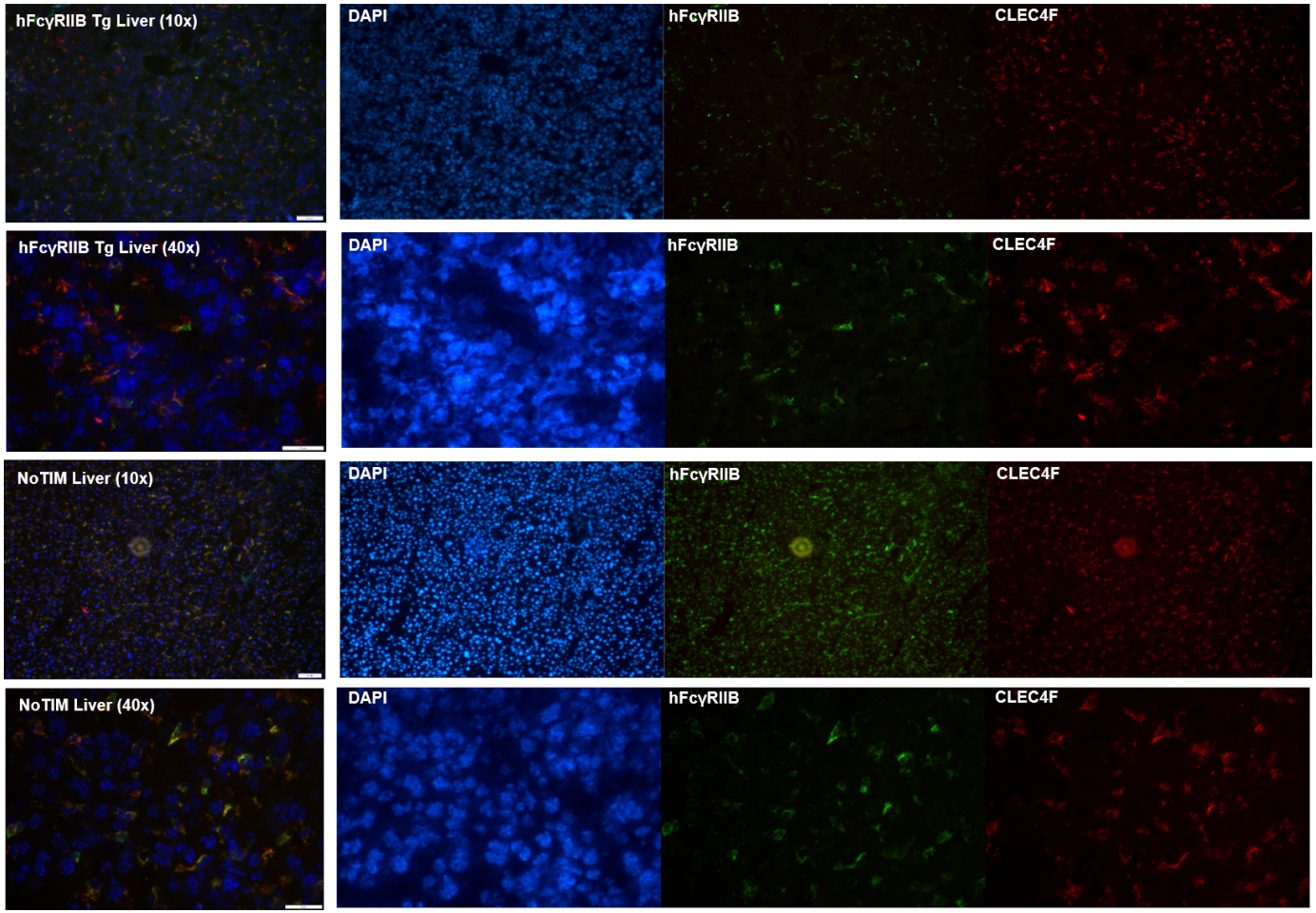

Figure 3.17: Immunofluorescence staining hFcγRIIB and CLEC4F+ within livers taken from hFcγRIIB Tg and NoTIM mice
Livers from hFcγRIIB Tg and NoTIM mice were snap frozen in OCT and sectioned using a cryostat. Sections were then stained using primary antibodies to detect the antigen and fluorescently labelled secondary antibodies to amplify the signal. DAPI shows cell nuclei (blue), CLEC4F+ to identify Kupffer cells (red) and EP888Y to identify hFcγRIIB (green). 10x scale bar = 50 μm, 40x scale bar = 20 μm.

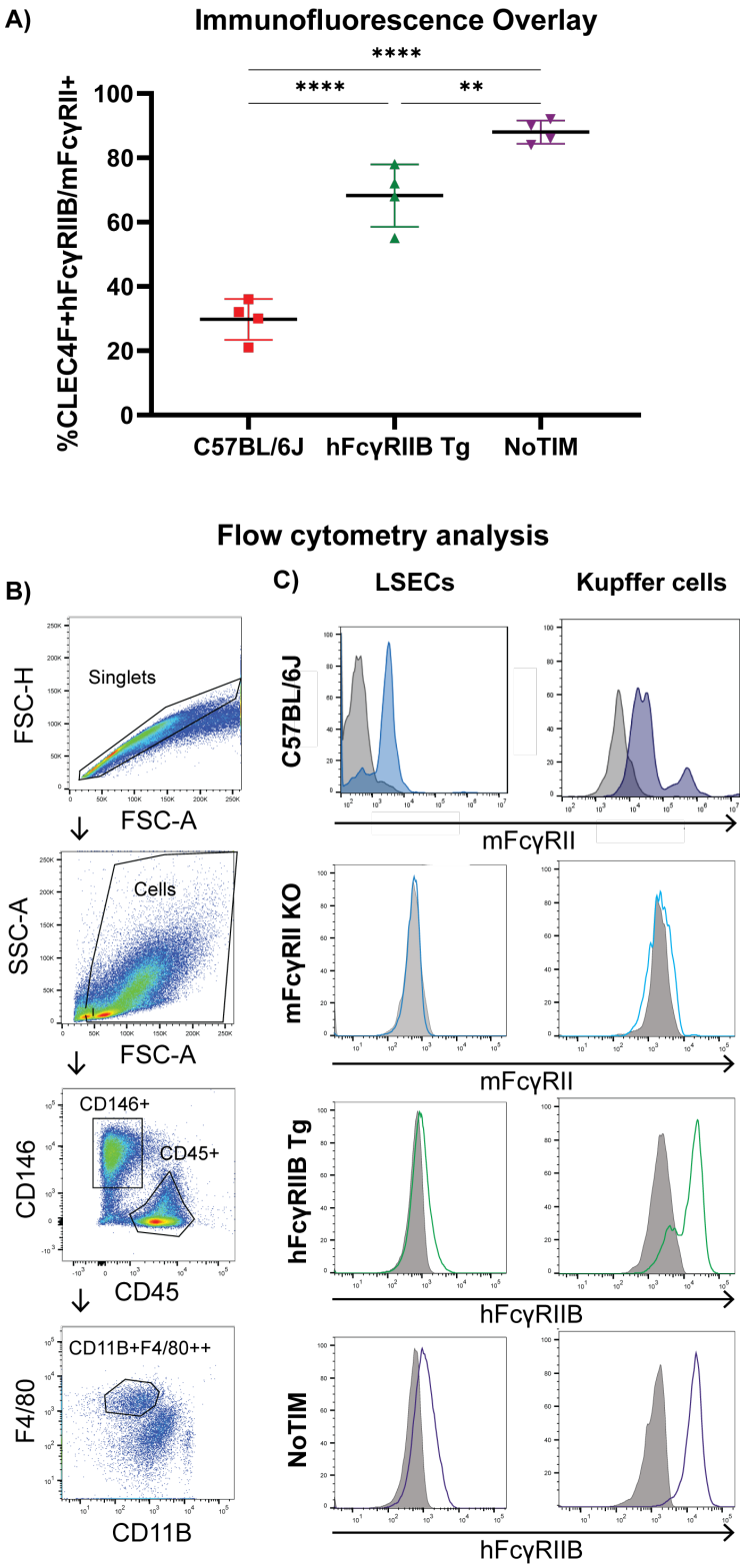

Figure 3.18: Expression of mFcγRII and hFcγRIIB on liver associated non-parenchymal cells C57BL/6J, mFcγRII KO, hFcγRIIB Tg and NoTIM mice
A) Four different sections from livers were taken and stained for CLEC4F+ and mFcγRII or hFcγRIIB using immunofluorescence. Images were taken at 40x magnification and overlapping CLEC4F+/mFcγRII/hFcγRIIB were calculated manually as a percentage of total CLEC4F+ cells in a blinded manner. The result of 4 independent experiments. Line = mean ± SD. Statistical analyses conducted using a one-way ANOVA with Tukey's multiple comparison test. ** = $P \leq 0.01$, **** = $P \leq 0.0001$. B) Non-parenchymal cells were isolated from each respective mouse model using a 25/50% percoll gradient and then assessed using flow cytometry. The gating strategy used to identify LSECs (CD146+/CD45-) and liver resident Kupffer cells (CD45+/CD11B+/F4/80++) based on [347]. C) Flow cytometry plots of mFcγRII and hFcγRIIB on LSECs and Kupffer cells from each mouse model. The result of 1 independent experiment.

3.5 Functional analysis of the non-signalling hFcγRIIB

After investigating expression pattern, it was important to establish if the NoTIM mutation resulted in a non-functional ITIM. To do this a series of assays were carried out to analyse the ITIM signalling pathway. Specifically, hFcγRIIB induced internalisation of immune complex, the inhibition of BCR induced calcium flux and the regulation of ADCP were assessed.

3.5.1 Phosphorylation of the NoTIM receptor

ITIM phosphorylation is critical to initiating FcγRIIB mediated ITIM signalling [244]. Upon immune complex binding, FcγRIIB clusters with other FcγRs to form an intracellular signalling platform for tyrosine phosphorylation by Lyn kinase [227]. The NoTIM mutation was designed to abrogate this event by mutating out the tyrosine residue that would normally be phosphorylated. To test if NoTIM immune cells were unable to elicit inhibitory signalling, splenic B cells and BMDMs were isolated from hFcγRIIB Tg and NoTIM mice. These cells were then stimulated with either of three different mAbs, FITC8 (isotype control), 6G08 (hFcγRIIB agonist) or 6G11 (FcγRIIB antagonist). FcγR binding disabled variants (containing the Fc N297Q mutation) were used to minimise interactions with other FcγRs which could induce cross-linking, so hFcγRIIB could be assessed in isolation. Cells were then subsequently lysed and protein lysates assessed in a western blot to probe for total and phosphorylated hFcγRIIB as well as total and phosphorylated SHIP-1, downstream of the hFcγRIIB ITIM.

In both hFcγRIIB Tg BMDMs and splenic B cells, mAb induced agonism of hFcγRIIB with 6G08 resulted in phosphorylation of the intracellular ITIM (Figure 3.19 A, B). Antagonising the receptor or using an isotype control did not produce a band indicative of phosphorylation. NoTIM BMDMs and splenic B cells showed no band when hFcγRIIB was agonised using a specific mAb. This indicates that the ITIM domain within the NoTIM receptor is not phosphorylated when agonised. In both mouse models, total hFcγRIIB was blotted for, with NoTIM cells producing a stronger band than hFcγRIIB Tg cells likely reflecting the higher expression seen in NoTIM mice when conducting flow cytometry.

SHIP-1 is downstream of the ITIM signalling pathway and interacts with phosphorylated hFcγRIIB to propagate inhibitory signalling. Splenic B cells were probed for phospho-

rylated SHIP-1. hFcγRIIB Tg B cells showed a band for phosphorylated SHIP-1 after stimulation with the agonist 6G08 (Figure 3.19 B). In contrast, agonised NoTIM splenic B cells had no phosphorylated SHIP-1 providing further evidence that the ITIM signalling pathway was non-functional. Antagonised B cells in both groups showed no band for phosphorylated SHIP-1. Interestingly, isotype treated hFcγRIIB Tg B cells showed the presence of a phosphorylated SHIP-1 band whilst NoTIM B cells did not. This could be due to an experimental artifact or the presence of non-specific IgG aggregates agonising hFcγRIIB. After confirming the NoTIM receptor cannot be phosphorylated, the mutation was functionally probed to ascertain the impact upon cellular functions.

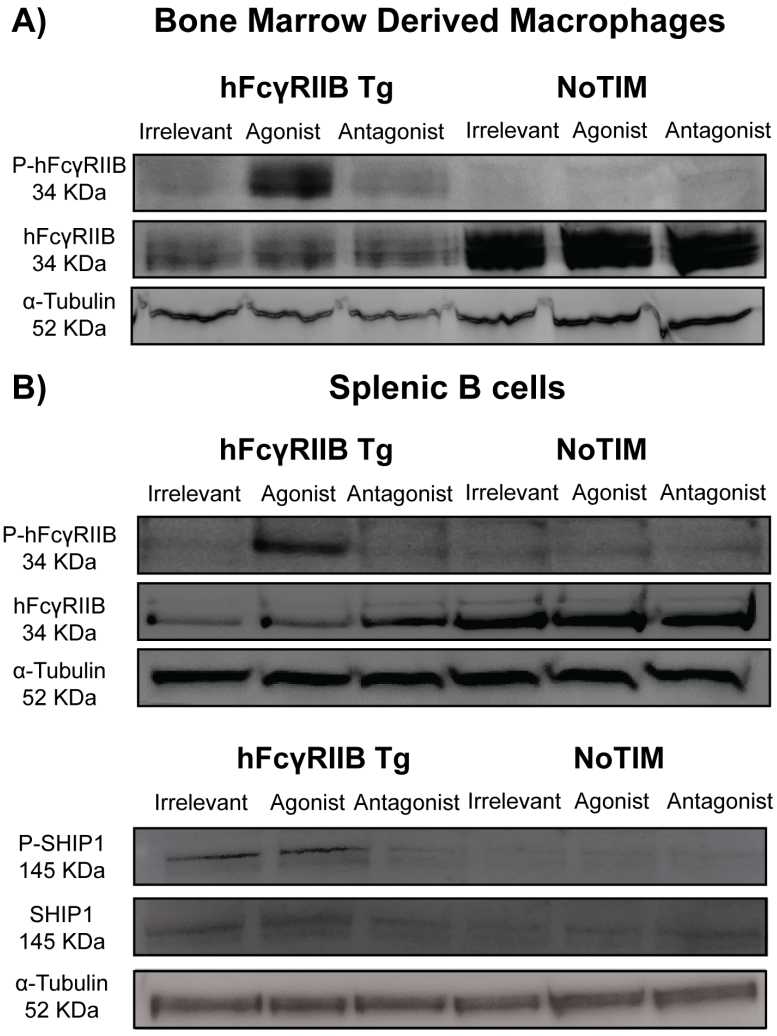

Figure 3.19: Probing for phosphorylated hFcγRIIB and SHIP1 following stimulation with hFcγRIIB agonist or antagonist in hFcγRIIB Tg and NoTIM B cells and macrophages
A) BMDMs were isolated from hFcγRIIB Tg and NoTIM mice and were treated with 10 μg/mL irrelevant, hFcγRIIB agonist mAb or hFcγRIIB antagonist mAb (N297Q Fc null mutation) for 15 minutes. Cells were then lysed and a western blot performed to probe for phosphorylated hFcγRIIB (P-hFcγRIIB), total hFcγRIIB and α-tubulin. B) Splenic B cells were isolated from hFcγRIIB Tg and NoTIM mice and were treated with an irrelevant, hFcγRIIB agonist mAb or hFcγRIIB antagonist mAb (N297Q Fc null mutation) for 30 minutes. Cells were then lysed and a western blot was performed for P-hFcγRIIB, total hFcγRIIB and α-tubulin. They were also probed for phosphorylated SHIP1 (P-SHIP1), total SHIP-1 and α-tubulin. A molecular weight ladder was used to ascertain the apparent size of the protein resolved on the blot. The result of 2 independent experiments.

3.5.2 hFcγRIIB inhibition of BCR induced calcium flux

hFcγRIIB mediated inhibition of BCR activation has previously been well characterised [250]. To assess if the NoTIM receptor was able to inhibit BCR signalling, B cells were isolated from each respective mouse model and labelled with a fluorescent calcium reporter dye. These cells were then incubated with an isotype control, hFcγRIIB agonist or hFcγRIIB antagonist (6G08 and 6G11 [323]) and then stimulated with a polyclonal $F(ab')_2$ anti-IgM to agonise the BCR. BCR signalling results in the intracellular release of calcium, which binds to the probe and increases fluorescence which can be detected using flow cytometry. Responses were quantified and graphed by determining the peak fluorescence response of B cells with fluorescence intensity above the unstimulated threshold (defined as the 85th percentile of the fluorescence intensity of unstimulated cells as performed previously [348]).

Crosslinking the BCR of mFcγRII KO B cells with anti-IgM resulted in robust calcium flux, which was unaffected by the addition of the hFcγRIIB agonist. hFcγRIIB Tg B cells had robust calcium flux after BCR crosslinking but showed a delayed calcium flux when hFcγRIIB was also agonised. In contrast, BCR cross linking of NoTIM B cells in both the absence and presence of the hFcγRIIB agonist gave a strong calcium flux (Figure 3.20 A, B).

The experiment was repeated again with the addition of the hFcγRIIB antagonist prior to BCR stimulation. mFcγRII KO B cells had a similar calcium response in the absence and presence of the hFcγRIIB agonist and antagonist. hFcγRIIB Tg B cells had enhanced calcium flux in the presence of the antagonist and diminished calcium flux in the presence of the agonist when compared to BCR cross-linking alone. NoTIM B cells had similar calcium flux irrespective of the agonist or antagonist (Figure 3.20 C). These data demonstrate that hFcγRIIB agonism inhibits calcium flux and hFcγRIIB antagonism increases calcium flux in hFcγRIIB Tg B cells whilst binding of the NoTIM receptor with the same reagents does not affect calcium flux.

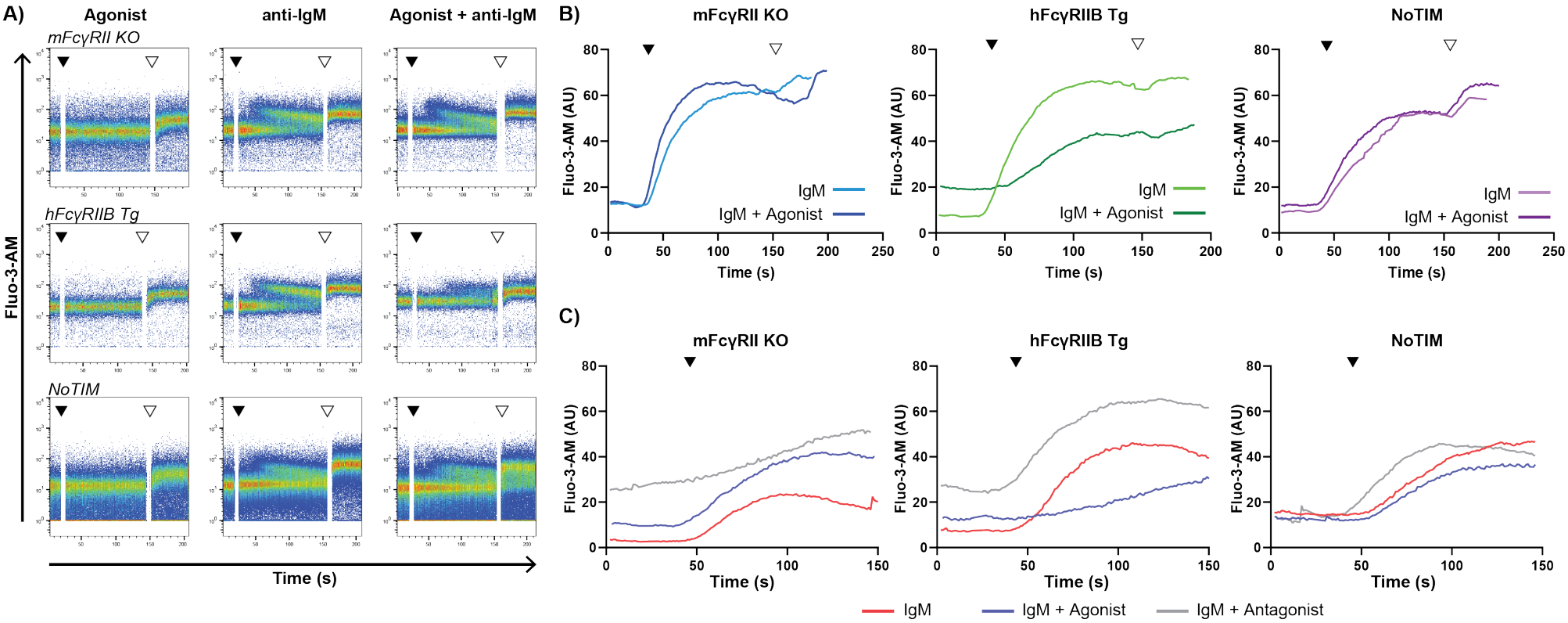

Figure 3.20: FcγRIIB mediated inhibition of BCR induced calcium flux on splenic B cells isolated from mFcγRII KO, hFcγRIIB Tg and NoTIM mice
A) B cells were isolated from each respective mouse model and then labelled with a fluorescent calcium probe Fluo-3-AM for 30 minutes. Cells were then incubated with either 10 μg/mL hIgG1 (N297Q mutation) isotype control, a hFcγRIIB specific agonist or antagonist for 15 minutes, before stimulating the BCR with 20 μg/mL polyclonal anti-IgM F(ab')$_2$ (black arrow). Change in calcium flux were measured using flow cytometry. Ionmycin (0.65 μM) was added as a positive control (white arrow). B) Responses were quantified by determining the peak fluorescence response of B cells with fluorescence intensity above the unstimulated threshold (defined as the 85th percentile of unstimulated cells) for the FACS plots shown in A). C) A second experiment was conducted comparing BCR stimulated calcium flux in the presence of the hFcγRIIB agonist or antagonist, quantified by determining the peak fluorescence response of B cells with fluorescence intensity above the unstimulated threshold.

3.5.3 hFcγRIIB mediated internalisation of ahIgG by murine B cells

Previous studies have suggested the hFcγIIB ITIM may have an impact on the internalisation of immune complexes [259] [239]. To investigate if the NoTIM receptor impacted immune complex internalisation, murine B cells were isolated from mFcγRII KO, hFcγRIIB Tg and NoTIM mice and then incubated with heat aggregated IgG (ahIgG) for 30 - 60 minutes.

mFcγRII KO mice showed no internalisation of ahIgG over the experiment. This was expected as the cells expressed no inhibitory receptor. B cells only express the inhibitory FcγRII, with no activatory receptors on their surface, and so these cells cannot internalise ahIgG. hFcγRIIB Tg B cells did show internalisation of ahIgG, with an average of 29% reduction in cell surface ahIgG at 30 minutes and 44% reduction after 60 minutes. NoTIM B cells showed an average of 2% reduction at 30 minutes and a 21% reduction after 60 minutes. hFcγRIIB Tg B cells had internalised significantly more ahIgG than mFcγRII KO at both time points and significantly more than NoTIM B cells at 30 minutes (Figure 3.21). These data demonstrate that within the first 30 minutes, an intact hFcγRIIB ITIM results in a significantly enhanced internalisation of ahIgG compared to the ITIM mutant hFcγRIIB. By 60 minutes, hFcγRIIB Tg B cells showed further internalisation of ahIgG, however the difference is no longer significant when compared to NoTIM B cells.

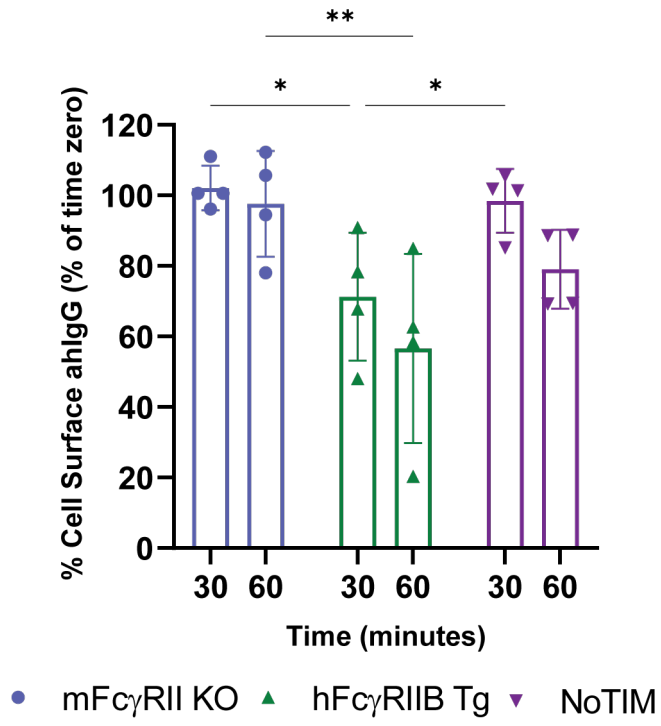

Figure 3.21: FcγRIIB mediated internalisation of heat-aggregated IgG (ahIgG) by murine B cells from mFcγRII KO, hFcγRIIB Tg and NoTIM mice
A) B cells were isolated from each respective mouse model and then incubated with 20μg/mL ahIgG for 30 - 60 minutes. The surface level of ahIgG was detected using a labelled secondary antibody against ahIgG by flow cytometry. Results were normalised to a sample from 0 minutes from the same mouse model and plotted as percentage of cell surface ahIgG. The result of four independent experiments repeated in triplicate. Bar = mean ± SD. Statistical analyses conducted using a two-way ANOVA with Tukey's multiple comparison test. * = P $\leq$ 0.05, ** = $\leq$ 0.01.

3.5.4 Regulation of ADCP by mFcγRII and hFcγRIIB

ADCP is an important mAb mediated effector mechanism that relies on interactions with activatory FcγRs on phagocytes to deplete the target cell. mFcγRII had been reported to downregulate the level of ADCP by macrophages [233], and so the contributions of both mFcγRII and hFcγRIIB to inhibition of ADCP were examined. BMDMs were differentiated from each mouse model and pre-incubated with a mFcγRII/hFcγRIIB blocking mAb (again Fc-null, N297Q or N297NA, to reduce impacts on Fc-binding to other FcγRs). They were then co-cultured with rituximab opsonised hCD20 Tg B cells as target cells. Flow cytometry was used to identify F4/80+ cells (macrophages) that had phagocytosed rituximab opsonised CFSE+ labelled hCD20 Tg B cells; the percentage of double positives was used to plot the percentage of ADCP (Figure 3.22).

Comparing C57BL/6J and mFcγRII KO BMDMs, little change in ADCP was observed regardless of the concentration of opsonising mAb used. When BMDMs were pre-treated

with the mFcγRII Fc null blocking mAb, there was a modest decrease in ADCP in the C57BL/6J BMDMs compared to rituximab. The mFcγRII KO BMDMs level of ADCP was unaffected by the addition of the blocking mAb (Figure 3.23).

In contrast, rituximab (0.1 μg/mL) induced a greater level of ADCP with the NoTIM mouse (non-signalling receptor) BMDMs than the wild type (signalling competent) hFcγRIIB Tg BMDMs. This effect was also seen at 1.0 μg/mL and 10 μg/mL of rituximab. When BMDMs were pre-treated with the Fc null hFcγRIIB blocking mAb, the level of ADCP in the hFcγRIIB Tg macrophages was partially restored to levels seen in the NoTIM BMDMs. At 1.0 μg/mL rituximab, hFcγRIIB Tg BMDMs treated with blocking mAb had the greatest increase in ADCP compared to hFcγRIIB Tg BMDMs treated with 0.1 μg/mL and 10 μg/mL rituximab, respectively. At 10 μg/mL rituximab, blocking hFcγRIIB partially improved ADCP compared to rituximab alone, whilst 0.1 μg/mL rituximab with blocking mAb made no difference (Figure 3.24). Blocking hFcγRIIB on NoTIM BMDMs did not alter levels of ADCP.

The most pronounced differences were seen with the sub-optimal dose of 1 μg/mL of rituximab. These data were converted into a phagocytic index to normalise for the variability seen across several experiments and to make direct comparisons, with 1 being set as the background phagocytosis with unopsonised B cells (Figure 3.25). When looking at mFcγRII inhibition, mAb specific blockade did not improve ADCP in C57BL/6J BMDMs (Figure 3.25 A). In contrast, mAb specific blockade of hFcγRIIB partially restored the level of hFcγRIIB Tg BMDM phagocytosis to that seen in NoTIM BMDMs. In the presence of rituximab alone, NoTIM BMDMs had a significantly higher level of ADCP (compared to hFcγRIIB Tg BMDMs) that was not improved with mAb specific blockade suggesting that the loss of inhibitory signalling resulted in more efficient ADCP (Figure 3.25 B).

Together, these results suggested that inhibitory signalling by hFcγRIIB negatively impacts ADCP to a modest extent in BMDMs.

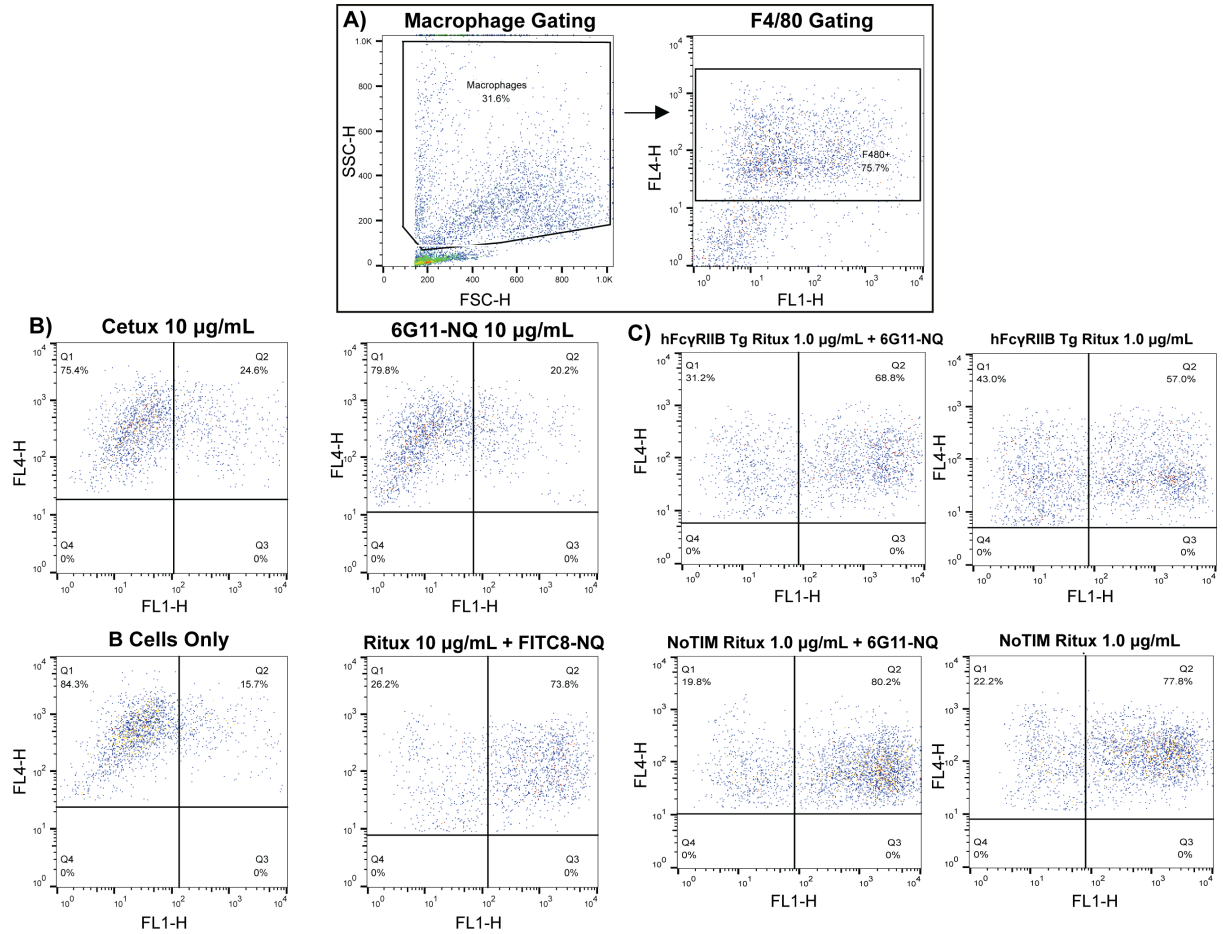

Figure 3.22: Gating strategy used to identify phagocytosed B cells in ADCP assay.
A) The gating strategy for the ADCP assay. NoTIM macrophages were gated on their forward and side scatter, they were then further identified as F4/80+. Dot plots were set out for each condition plotting APC (F4/80) vs CFSE (B cells). Macrophages that had phagocytosed B cells would be positive for F4/80 and CFSE (appearing on the top right of the plot). B) shows the plots of controls used for the ADCP assay from hFcγRIIB Tg mice - Cetuximab, 6G11, unopsonised B cells and rituximab + FITC8. C) shows the gating used to determine the level of phagocytosis for each condition in the NoTIM and hFcγRIIB Tg mice.

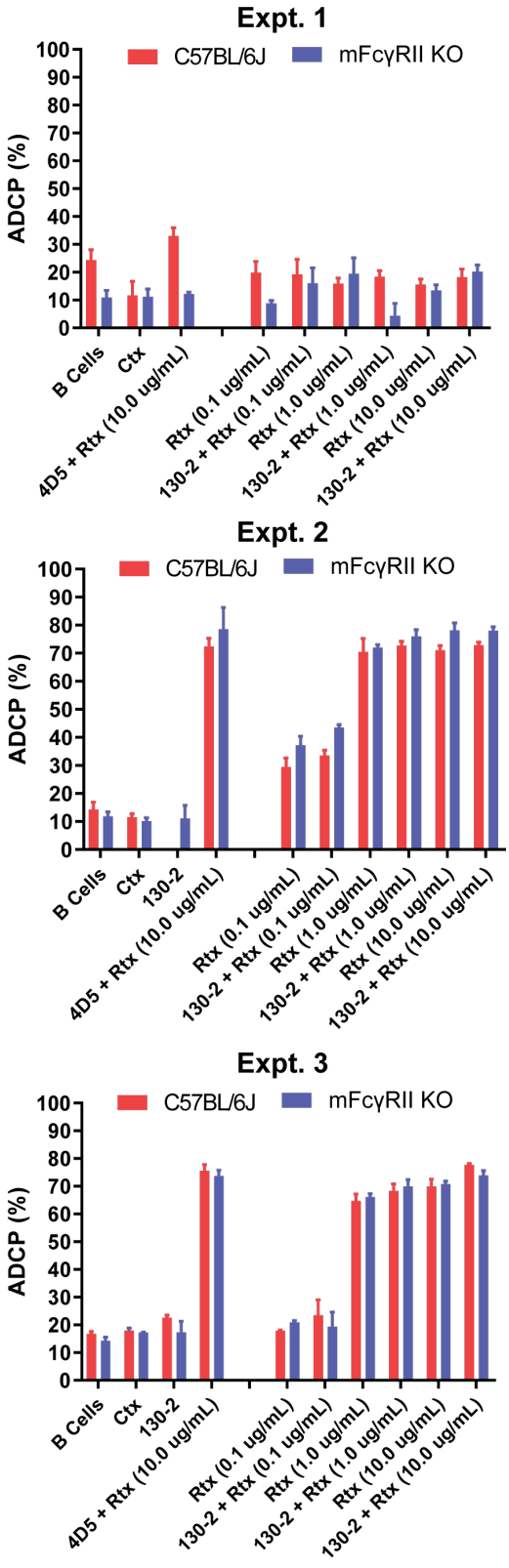

Figure 3.23: ADCP in C57BL/6J and mFcγRII KO BMDMs
BMDMs were differentiated from each mouse model and pre-incubated with (or without) 10μg/mL mFcγRII blocking mAb for 15 minutes. They were then co-cultured with rituximab opsonised hCD20 Tg B cells at a ratio of 5:1 for 30 minutes. Flow cytometry was then used to identify F4/80+ cells that had phagocytosed rituximab opsonised CFSE+ labelled hCD20 Tg B cells, the percentage of double positives was used to plot the percentage of ADCP. ADCP in WT and mFcγRII KO macrophages across 3 different experiments in the absence and presence of AT 130-2 NA (mFcγRII Fc null blocking mAb). Ctx = cetuximab (hIgG1 isotype control), 4D5 = AT 130-2-NA isotype control, Rtx = rituximab. Error bars = +SEM of 3 replicates

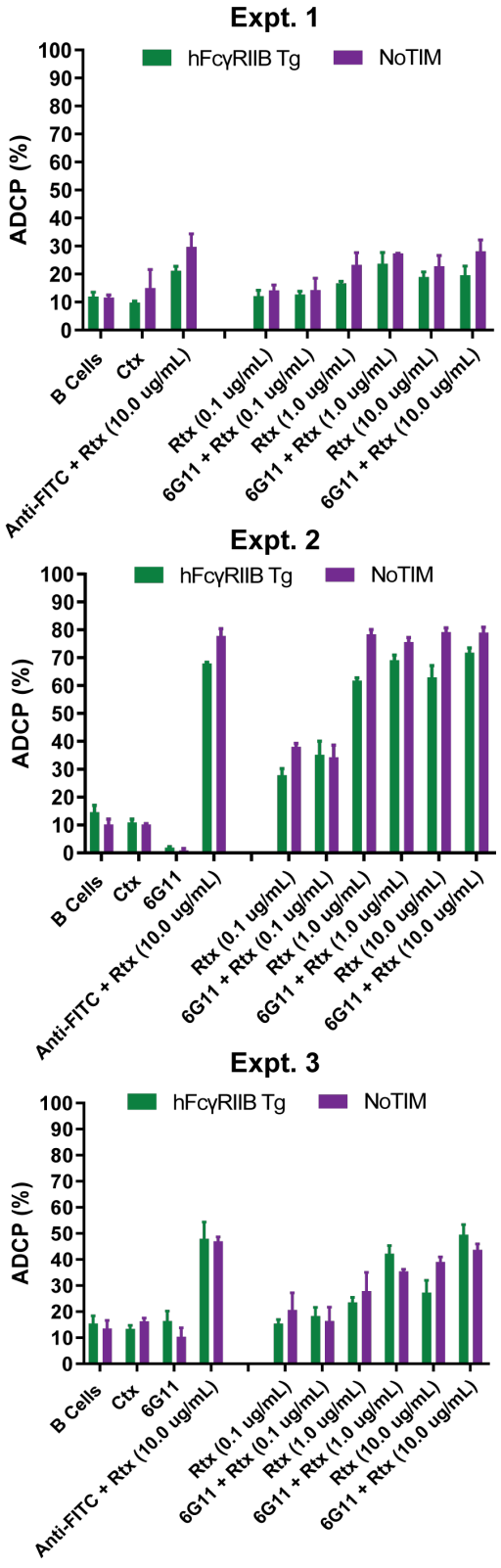

Figure 3.24: ADCP in hFcγRIIB Tg and NoTIM BMDMs
BMDMs were differentiated from each mouse model and pre-incubated (or not) with 10 μg/mL hFcγRIIB blocking mAb for 15 minutes. They were then co-cultured with rituximab opsonised hCD20 Tg B cells at a ratio of 5:1 for 30 minutes. Flow cytometry was then used to identify F4/80+ cells that had phagocytosed rituximab opsonised CFSE+ labelled hCD20 Tg B cells, the percentage of double positives was used to plot the percentage of ADCP. ADCP in hFcγRIIB Tg and NoTIM macrophages across three different experiments in the absence or presence of 6G11-NQ (hFcγRIIB Fc null blocking mAb). Ctx = cetuximab (hIgG1 isotype control), Rtx = rituximab, FITC = 6G11-NQ isotype control. Error bars = +SEM of 3 replicates

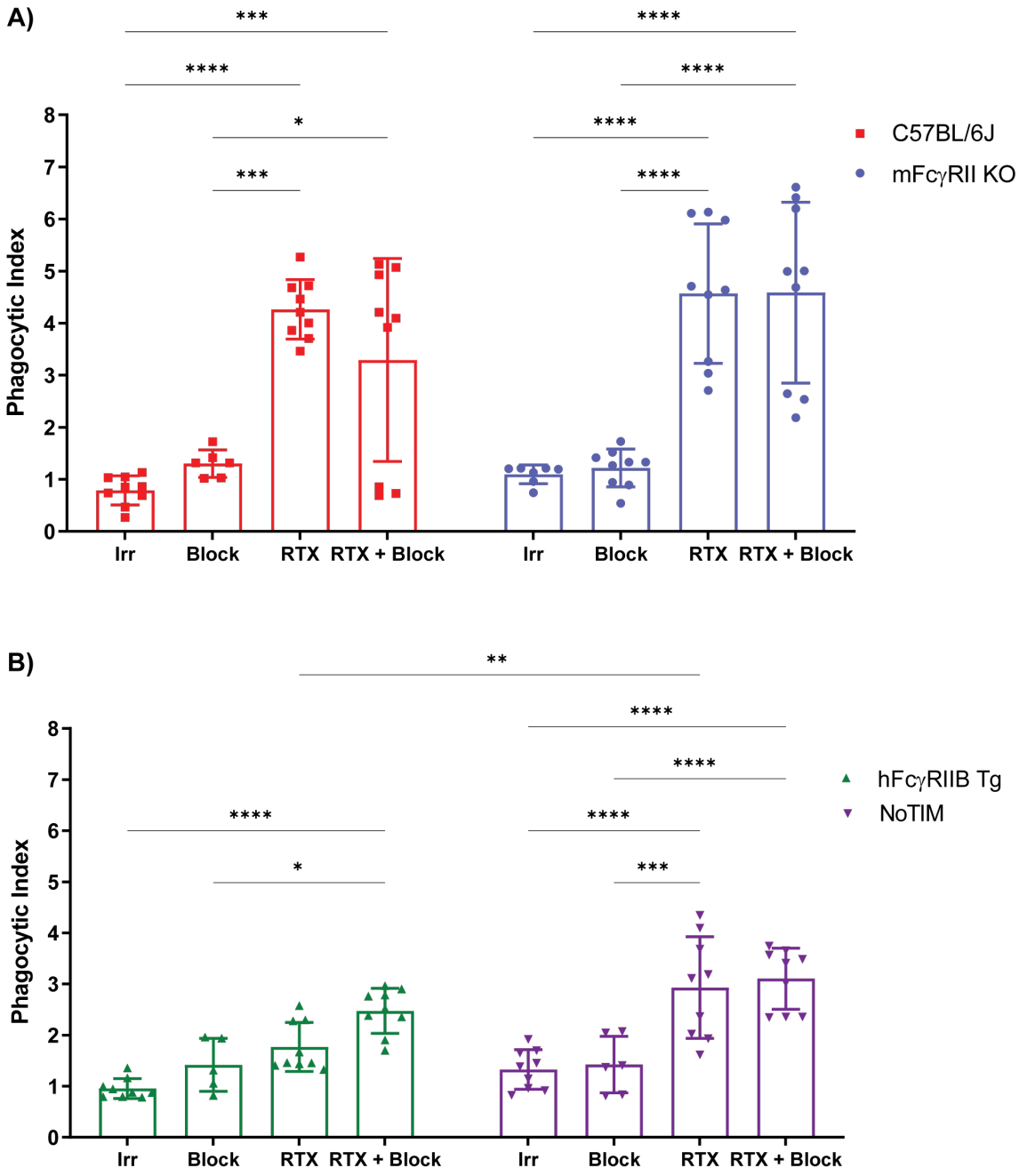

Figure 3.25: Phagocytic index comparing ADCP cumulatively across experiments from each mouse model BMDMs were differentiated from each mouse model and pre-incubated with (or not) 10 μg/mL mFcγRII/hFcγRIIB blocking mAb for 15 minutes. They were then co-cultured with 1 μg/mL rituximab opsonised hCD20 Tg B cells at a ratio of 5:1 for 30 minutes. Flow cytometry was then used to identify F4/80+ cells that had phagocytosed rituximab opsonised CFSE+ labelled hCD20 Tg B cells, the percentage of double positives was used to plot the percentage of ADCP. A cumulative analysis of all experiments shown in Figure 3.23 and 3.24. A) ADCP of hCD20 Tg B cells in C57BL/6J and mFcγRII KO BMDMs in the absence and presence of AT 130-2 NA (mFcγRII blocking antibody). B) ADCP of hCD20 Tg B cells in hFcγRIIB Tg and NoTIM BMDMs in the absence or presence of 10μg/mL 6G11 NQ opsonised BMDMs (hFcγRIIB blocking mAb). Irr = cetuximab (hIgG1 isotype control), Block = blocking mAb (AT 130-2 NA or 6G11 NQ), RTX = rituximab. The result of three independent experiments (n = 1 per experiment, repeated in triplicate). Bar = mean ± SD. Statistical analyses conducted using a two-way ANOVA with Tukey's multiple comparison test. * = P ≤ 0.05, ** = ≤ 0.01, *** = ≤ 0.001, **** = ≤ 0.0001

3.6 Chapter Discussion

hFcγRIIB biology has proved to be complex with a role that extends beyond inhibitory signalling [266]. Herein, a non-signalling hFcγRIIB transgenic model (NoTIM) was generated and characterised to assist in separating signalling dependent and signalling independent mechanisms of action of hFcγRIIB. Specifically, signalling through the ITIM was assessed.

First, the expression of hFcγRIIB was characterised in human whole blood and compared to the expression on key immune cell types within the NoTIM transgenic mouse model. Genomic integration of the NoTIM transgene was confirmed and protein expression analysed as well as visualised within tissues. The key mutation within the ITIM of the NoTIM mouse was verified by Sanger sequencing and western blotting to show that the critical residue within the ITIM is no longer able to be phosphorylated. Finally, the functional consequence of the NoTIM mutation was studied by looking at the internalisation of ahIgG, inhibition of BCR induced calcium flux and inhibition of ADCP, confirming that the NoTIM mutation confers the loss of ITIM mediated inhibitory signalling.

Initial analysis of human whole blood highlighted that hFcγRIIB is strongly expressed on B cells, moderately expressed on classical monocytes, with weaker expression on non-classical monocytes whilst NK cells had no expression (Figure 3.4). This is broadly consistent with the literature [322] [192] and was used as a reference point to compare expression within the NoTIM mouse. Analysis of the expression profile of mFcγRII using flow cytometry on a WT C57BL/6J mouse showed a different profile from the expression of the human homologue. Murine B cells and Ly6C high monocytes expressed a relatively high level of mFcγRII and Ly6C low monocytes expressed a low level of mFcγRII (Figure 3.11). The expression profile of mFcγRII also agrees with the literature [349] [192]. Comparing the expression profile of hFcγRIIB between NoTIM mice and human whole blood showed similarities. Both NoTIM mice and humans have the highest expression on B cells with some expression on monocytes. NoTIM Ly6C high monocytes showed moderate expression of hFcγRIIB (akin to human classical monocytes) with little expression on Ly6C low monocytes (akin to human non-classical monocytes) however it is hard to compare murine and human monocytes like-for-like due to differing physiological functions. Murine Ly6C high monocytes are typically pro-inflammatory migratory monocytes requiring inhibitory regulation whilst Ly6C low monocytes are typically patrolling, immuno-suppressive cells and do not require the same regulation [350]. Human monocytes are a more heteroge-

neous population. Despite classifications into CD14+CD16- and CD14+CD16+ there are intermediate populations that likely blur the boundaries of discrete functional differences [350].

The insertion of a human transgene into the mouse genome offers the opportunity to study *in vivo* biology in a way that would not be possible in humans. However, the insertion of a transgene could also alter the expression or regulation of the introduced receptor in such a way that the system is no longer applicable to human biology. The NoTIM transgene essentially acts as a pseudo-receptor, acting in place of the inhibitory mFcγRII but without a ITIM signalling function. It is also know that the expression of activatory and inhibitory FcγRs is tightly regulated on the cell surface of immune cells to elicit a threshold of cellular activation, regulating the effector functions of IgG [351]. Therefore it was important to determine if the NoTIM transgene appropriately expressed hFcγRIIB and if the insertion of the non-signalling human hFcγRIIB altered the expression levels of the activatory mFcγRs.

When examining the expression profile of hFcγRIIB in NoTIM mice, it was clear that they have a higher and more uniform expression pattern than hFcγRIIB Tg mice. hFcγRIIB Tg mice showed weaker expression and a heterogenous population of cells that expressed hFcγRIIB (Figure 3.13). The reason for these key differences remains to be understood. Screening of the hFcγRIIB Tg progeny across the period of study showed a highly variable penetrance of the transgene, from 10% to 90% transgenic positive lymphocytes (albeit with the majority expressing >45-70%), whilst NoTIM mice were 100% penetrant. Transgene integration analysis of hFcγRIIB Tg mice by our collaborators at GSK had mapped the integration site to chromosome 14 (chr14:116,698,211-116,777,674), in an unannotated part of the genome. The transgene was estimated to have a copy number of >5 however this does not explain the heterogenous mosaic expression observed. The insertion point of the NoTIM transgene is unknown.

Interestingly, despite the majority of expressing cells showing mosaicism (e.g. B cells, monocytes, Kupffer cells) some cells appeared to have higher penetrance, namely LSECs and splenic macrophages (Figure 3.13, Figure 3.18). These observations suggest that within some cell types, certain factors may drive the inactivation of the gene - this could be due to transcriptional silencing by incorporation into heterochromatin regions leading to epigenetic regulation, or the presence of truncated locus control regions which can result in unstable expression [352]. It is also possible that the transgene integration may

have occurred beyond the one cell embryo stage resulting in non-uniform uptake of the transgene. Alternatively, a low concentration of transgene used during injection could have resulted in poor uptake by the embryonic cells [353]. Despite these differences between hFcγRIIB Tg and NoTIM mice, broadly the expression pattern of hFcγRIIB was deemed to be equivalent.

From the data generated, there was no strong evidence for substantial changes in activatory FcγR expression in the presence or absence of a functional inhibitory receptor. The spleen acts as a reservoir of immune cells, allowing for the collection of a substantial number of flow cytometry events for analysis (5,000+ myeloid cells, 10,000+ lymphocytes). The lymph nodes and blood do not contain all the cell populations in a sufficient amount to be as confident with the analysis as with the spleen but provides a good indication of expression across key tissues. The activatory mouse FcγRs were expressed broadly to the same extent across all key cells in each mouse strain. Published research had suggested that mFcγRII KO mice had a compensatory increase in expression of mFcγRIV [98] [190], however this was not observed in our mice. This expression pattern was consistent with the literature and overall showed no evidence of compensatory activatory mFcγR expression in the presence or absence of a functional inhibitory FcγR [222] [190] [192].

mFcγRIV was broadly similar across strains, except for on splenic macrophages which showed large variation between experiments. This may be explained by the open-top conventional mouse caging used at the time to house the mice used in this experiment. These open top cages could result in exposure to a variety of pathogens that would be mitigated by the use of IVC caging. At the time, the animal unit had also suffered from a pinworm infection outbreak, resulting in the universal dosing of all mice with ivermectin. If mice used in these phenotyping experiments were infected with pinworm, it would be expected that exposure to this pathogen may result in the increased production inflammatory molecules such as IFN-γ, upregulating activatory FcγRs expression [222] [354] [281]. Ivermectin has also been shown to modulate the immune system, which could result in differential expression of activatory FcγRs between experiments [355].

mFcγRII was expressed within the C57BL/6J mice as expected, with expression on B cells, Ly6C high monocytes, Ly6C low monocytes, macrophages and neutrophils. Figure 3.11 showed lower but consistent staining of mFcγRII across all cells types in mice that do not express mFcγRII (mFcγRII KO, hFcγRIIB Tg and NoTIM mice). As explained earlier, the mAb AT 130-2 is anecdotally known from batch to batch to have increased

background binding. Fortunately, specific binding to mFcγRII allows for detection of the receptor beyond the relatively high background.

FcγR expression on BMDMs mirrored the expression pattern seen on splenic macrophages (Figure 3.12). hFcγRIIB was expressed highly in both hFcγRIIB Tg (albeit with mosaic expression) and NoTIM BMDM samples. mFcγRI was equally expressed across BMDMs from all mice, however mFcγRIII and mFcγRIV showed non-significantly lowered expression in mFcγRII KO, hFcγRIIB Tg and NoTIM mice compared to C57BL/6J BMDMs. These findings may be related to the proximity of the mFcγRII gene to both the mFcγRIII and mFcγRIV genes [190]. Genetic deletion of mFcγRII could have disrupted the regulation of mFcγRIII and mFcγRIV resulting in downregulated expression. However, this observation seems to be BMDM specific and was not observed when on other cell types *in vivo* so is unlikely to be the cause. The differences in expression are small, and unlikely to affect BMDM effector functions.

Comparison of immunofluorescence images generated from tissues taken from the NoTIM mice reflect a different expression profile of hFcγRIIB compared to mFcγRII within the liver. Sections taken from C57BL/6J mice showed mFcγRII expression was diffuse and not highly localised with the Kupffer cell marker, CLEC4F (Figure 3.16). Ganesan et al. had reported that as little as 10% of mFcγRII in the liver is expressed on Kupffer cells with the remainder found on liver sinusoidal endothelial cells [242]. In contrast, both hFcγRIIB transgenic models showed increased co-localisation between hFcγRIIB and CLEC4F (Figure 3.17, Figure 3.18). These observations were further assessed by flow cytometry analysis. Analysis of non-parenchymal liver cells from C57BL/6J mice showed expression of mFcγRII on LSECs, with two sub populations of expressing Kupffer cells. The majority of Kupffer cells expressed a low level of mFcγRII, with a small population expressing a high level of receptor. This may explain why immunofluorescence indicated a low level of co-localisation between Kupffer cells and mFcγRII - because only the high expressing Kupffer cells are detected by this less sensitive technique. In contrast, the expression of hFcγRIIB in NoTIM and hFcγRIIB Tg mice showed some expression on LSECs, with stronger expression on the Kupffer cells (Figure 3.18). LSECs had notably lower hFcγRIIB expression in hFcγRIIB Tg mice compared to NoTIM mice, whilst the hFcγRIIB+ population of hFcγRIIB Tg Kupffer cells had a similar shift in fluorescence to NoTIM Kupffer cells. The differences in expression of mFcγRII and hFcγRIIB could be due to the transgene being under control of the human promoter, driving a different expression pattern in the context of LSECs and Kupffer cells. However to confirm these findings, a

detailed analysis of human liver would be required. So far, this area of research has been limited. Some studies have suggested subsets of both LSECs and Kupffer cells can be identified based on hFcγRII expression, but the studies did not separate hFcγRIIA from hFcγRIIB [356] [357]. A single cell RNA sequencing analysis of human liver did specifically show heterogeneous expression of hFcγRIIB whilst hFcγRIIB expression was not identified on Kupffer cells [358]. Further work is needed to increase the experimental numbers analysing inhibitory FcγR expression in these mouse models. A comparison of the similarities and differences in hFcγRIIB expression between the transgenic mouse models and humans would also help understand if the human promoter recapitulates hFcγRIIB in the transgenic mice.

Taken together, the NoTIM mouse had strong expression of hFcγRIIB with close resemblance to the expression of hFcγRIIB in human whole blood. Both hFcγRIIB Tg and NoTIM mice had a similar pattern of expression and distribution on the expected immune cells as has been previously been observed [190] [192]. The hFcγRIIB Tg mice had more varied expression of the transgene and exhibited mosaicism on some cell types which was important to consider during further *in vivo* experiments. The expression of activatory mFcγRs was broadly consistent across C57BL/6J, mFcγRII KO, hFcγRIIB Tg and NoTIM mice. The distribution and expression of mFcγRs was as expected [192] and despite the loss of ITIM signalling in NoTIM mice, it had a minimal impact on expression of other receptors. These data reflect similar observations made in the non-signalling γ-chain NOTAM mouse produced by DeHaij et al. where the expression pattern of endogenous mFcγRs was also unaffected [186].

To further power these findings and understanding if the human promoter recapitulates human FcγRIIB expression rather than mouse, it would be helpful to compare expression within murine and human tissues. Human blood gives an indication of expression, however it is well established that immunological niches drive differential FcγR expression in both mouse and human [56] [32] [33]. To therefore extrapolate the expression pattern of FcγRIIB within human blood to transgenic murine tissues may not be representative of human expression, however there are difficulties in obtaining human tissue. Generally, tissue is removed from diseased patients which could skew FcγR expression profiles (as seen in mice [359] [323]). These tissues can undergo extensive cellular stress to retrieve samples and often little is provided for analysis within the lab. Currently, detailed human FcγR analyses have relied on histological staining to observe expression patterns in tissue. These techniques can be limited by poor sample processing and only allows

for a qualitative analysis of expression. Currently, we have an understanding of differential expression of FcγRs on human macrophage populations based on histology [32] and mRNA analyses of different FcγR expression across different human tissues [360], however further work is required to produce a data set more applicable to murine models.

Next it was important to determine if the NoTIM hFcγRIIB transgene was non-functional. The ITIM mutation (Y273F) was integral for abolishing ITIM mediated signalling; with the second upstream mutation (Y254F) introduced as a fail-safe to ensure intracellular signalling was abrogated. Previous evidence has shown that the intracellular tail of mFcγRII can be phosphorylated in several places which may serve in aiding inhibitory signalling [251]. The homologous residue of hFcγRIIB B2 Y254 in mFcγRII B1 is Y290 and had been shown to be phosphorylated upon receptor activation however it was not deemed to have any signalling effect. Despite these findings, as a precaution it was decided the second mutation would be introduced to ensure ITIM signalling was abrogated. Sanger sequencing confirmed the presence of both mutations, with single base pair changes identified using primers that flanked the ITIM region (Figure 3.1).

To show the mutation successfully translated into the abrogation of ITIM signalling, hFcγRIIB was agonised on B cells and BMDMs using specific monoclonal antibodies [323]. Western blotting showed that the hFcγRIIB Tg receptor could be phosphorylated, whilst the NoTIM receptor could not (Figure 3.19). The impact was investigated further downstream, and within B cells it was demonstrated that an important mediator of ITIM signalling, SHIP-1, was not phosphorylated in NoTIM mice. SHIP-1 is the main mediator of ITIM signalling and results in the conversion of PIP_3 into PIP_2, arresting the propagation of intracellular activatory signalling and the activation of the RAS pathway [361]. The lack of SHIP-1 activation further confirms the success of the NoTIM mutations, indicating it cannot propagate ITIM signalling. In agreement with these results, the impact of the Y273F hFcγRIIB mutation was also tested in a cell reporter assay by Stopforth et al. The authors found the mutation successfully abrogated the recruitment of SHIP-1 to the receptor, mitigating inhibitory signalling [252]. In future experiments it would be useful to probe other proteins in the signalling pathway (such as phosphorylated SHP-1) and to look at total cellular phosphorylated tyrosine to further analyse how the NoTIM mutations affect cellular signalling pathways.

Several assays were then conducted to understand how the loss of ITIM mediated inhibitory signalling modulated the cellular response. The regulation of BCR signalling by

FcγRIIB has been extensively characterised. The binding of antigen to the BCR results in ITAM activatory signalling, if FcγRIIB also binds in proximity to the BCR, as a result of immune complex formation, it has been shown to inhibit this signalling pathway [250]. Calcium flux is an important downstream signalling event of BCR signalling, it is also a temporal event that can be examined using flow cytometry [348]. To examine the impact of the NoTIM receptor on BCR signalling, splenic B cells were activated with anti-IgM antibodies in the presence of a specific hFcγRIIB agonist or antagonist. mFcγRII KO B cells showed no change in calcium flux in the presence of a hFcγRIIB agonist or antagonist, as expected. Agonising hFcγRIIB and the BCR on hFcγRIIB Tg B cells resulted in a delayed and suppressed calcium flux that was not observed in NoTIM B cells. When hFcγRIIB Tg B cells were treated with a hFcγRIIB antagonist along with anti-IgM, calcium flux was enhanced whilst again the NoTIM B cells showed no change. These experiments provide robust evidence that the NoTIM receptor is not able to elicit ITIM signalling.

hFcγRIIB has also been show to play an important role in antigen internalisation and processing [261]. To investigate this, murine B cells from each mouse model were incubated with a surrogate for immune complex, ahIgG, and the kinetics of internalisation were assessed (Figure 3.21). Within the first 30 minutes, the presence of a functional ITIM on hFcγRIIB Tg B cells allowed higher levels of internalisation of ahIgG compared to NoTIM B cells which showed negligible internalisation. By 60 minutes, the extent of internalisation in the NoTIM B cells was higher but still lower than with hFcγRIIB Tg B cells after 30 minutes. The precise molecular mechanism behind the reduced internalisation kinetics by the NoTIM receptor is unknown.

Interestingly, mutational studies conducted in the 1990s indicated the phosphorylation site within the ITIM had minimal to no impact on the internalisation of immune complex. Instead, the authors of these studies found that other components of hFcγRIIB intracellular tail (e.g. the di-leucine motif of the ITIM) were significantly linked to internalisation [259] [239]. However, these studies have some short comings and may have overlooked the contribution of the ITIM phosphorylation site to clathrin dependent internalisation. The key papers published by Miettinen et al. and Budde et al., devised systems using immortalised cell lines (the murine A20.IIA cell line and CHO cell line) transfected with hFcγRIIB B2. These cells may may display non-physiological functions due to their transformed nature [259] [239]. Another group, Mousavi et al., used rat LSECs to probe how they internalised immune complex and found ITIM phosphorylation (achieved through artificially cross-linking of rat FcγRII rather than by immune complex binding) was not required for

internalisation [362]. Taken together these data suggest ITIM dependence of internalisation may depend on cell-type and the nature of the reagent used to elicit internalisation. The ahIgG system used in this thesis utilises murine B cells with an immune complex like reagent (ahIgG) which may be more physiologically relevant, however the contribution of both the Y254F and Y273F mutations are unknown and require further investigation.

Next, it was examined how the NoTIM receptor influenced mAb mediated ADCP. As previously discussed phagocytosis is a key antibody effector mechanism, it has been demonstrated to be critical to rituximab mediated B cell depletion and is dependent on tissue resident macrophages [363] [304] [346]. Macrophages are known to express all FcγRs which means the execution of ADCP requires a balance between activatory and inhibitory FcγR signals [233]. In theory, by blocking the inhibitory FcγRIIB, there should be a relative increase in activatory signals increasing the overall A:I ratio and the level of ADCP. The hFcγRIIB Tg and NoTIM models were used to address the contribution of ITIM mediated signalling to inhibition of ADCP.

mFcγRII KO BMDMs showed an modest increase in ADCP when compared to WT BMDMs (Figure 3.23, Figure 3.25). This effect seemed to be most pronounced at 1 μg/mL rituximab with little improvement at 10 μg/mL probably due to receptor saturation. In C57BL/6J BMDMs where ADCP would have been expected to have been improved with the mFcγRII blocking mAb AT 130-2 NA, there was little difference in ADCP which was surprising. Previous experiments published in the literature show that pre-incubation of BMDMs with AT 130-5 mIgG1, a weaker affinity mFcγRII specific mAb, did enhance ADCP by 10% [321]. However, both AT 130-2 and 130-5 were classed as agonistic mAbs and questions the ability of both mAbs to simply block mFcγRII [321]. In those studies, the agonistic potential of the mAbs was tested using whole IgG, where it was found a functional Fc domain was required for agonism. In the ADCP assay presented in this thesis, AT 130-2 was used as an Fc null N297A variant and therefore should not be able to agonise mFcγRII [318]. Further investigations within the lab have proceeded to show that AT 130-2 N297A (the same clone as used in the ADCP assay) does not phosphorylate mFcγRII (Robert Oldham, unpublished data). The reasons as to why blocking mFcγRII did not augment ADCP as observed in the literature [321] are unknown.

When examining hFcγRIIB expressing BMDMs, it was clear NoTIM BMDMs had enhanced ADCP at every concentration of rituximab compared to the hFcγRIIB Tg BMDMs (Figure 3.24, Figure 3.25). The 6G11 NQ (N297Q mutation) Fc null mAb, a hFcγRIIB an-

tagonist, was used to block hFcγRIIB [323]. When hFcγRIIB Tg BMDMs were treated with rituximab and 6G11 NQ, there was an increase in ADCP across all three concentrations. 6G11 NQ did not enhance the ADCP of NoTIM BMDMs and matched the percentage seen with rituximab alone. This suggests that the hFcγRIIB ITIM signalling negatively regulates ADCP, and that abrogating ITIM phosphorylation improves ADCP. The variation seen across experiments in ADCP when analysing hFcγRIIB Tg BMDMs could be due to the mosaic expression pattern of the transgene and should be taken into consideration for future experiments. Dependent on the transgene penetrance, there will be a subset of BMDMs that do not express any inhibitory receptor. In these cells the A:I ratio would intrinsically be skewed towards an activatory phenotype with no enhancement seen with the addition of 6G11 NQ. Future experimentation could sort hFcγRIIB+ transgenic BMDMs from those negative for the transgene to mitigate for this effect.

To summarise, a hFcγRIIB non-signalling ITIM mutant transgenic mouse model was successfully produced. The expression pattern of both the transgene and the endogenous murine FcγRs met expectations and were sufficient to proceed towards further *in vivo* experimentation.

Chapter 4

Role of FcγRIIB signalling in the modulation of antibody effector mechanisms

4.1 Chapter Introduction

In the previous chapter, the NoTIM hFcγRIIB transgenic mouse model was shown to be a viable *in vivo* model, suited to studying the ITIM signalling independent mechanisms of hFcγRIIB. *in vitro* analysis of immune cell effector functions influenced by hFcγRIIB signalling have shown that the ITIM mutant cells exhibit reduced immune complex internalisation and can no longer inhibit BCR induced calcium flux or ADCP. To examine the impact of ITIM mediated signalling by hFcγRIIB *in vivo*, the NoTIM mouse was investigated in the context of antibody mediated target cell depletion and immune stimulation.

Direct targeting antibody immunotherapy relies on eliciting effector functions through FcγR-dependent and FcγR-independent mechanisms that include ADCP, ADCC, CDC and PCD [168]. Activatory FcγRs are critical for most FcγR-dependent functions which FcγRIIB negatively regulates to temper the immune response. In regards to mAb therapy for cancer, FcγRIIB regulation of activatory FcγRs can be detrimental to therapeutic outcome by limiting effector cell functions [185]. CD20 mAbs are often used as a paradigm for analysing FcγRIIB inhibition to direct targeting mAb therapy, and in the context of the

anti-CD20 mAb rituximab, FcγRIIB is thought to elicit at least two different mechanisms of inhibition.

Firstly, FcγRIIB has been shown to accelerate the internalisation of type-I CD20 mAbs, like rituximab, through antibody bipolar bridging on malignant and autoimmune B cells [179] [299] [300], limiting all Fc-mediated effector functions. Secondly, it has been assumed that FcγRIIB engagement on immune effector cells elicits inhibitory signalling, reducing target cell depletion. Studies using mice deficient in murine FcγRII showed that mAb mediated depletion of malignant cells was enhanced in these mice and this effect was presumed to be due to the loss of ITIM signalling [233] [185] [305] [248]. However, there is currently no published research that has dissected the contribution of ITIM signalling to this mechanism of action.

The NoTIM transgenic mouse model was developed to investigate this. To explore the mechanism of FcγRIIB mediated inhibition *in vivo*, a series of mice exhibiting different FcγRIIB status were treated with mAbs targeting murine CD20, CD19, NK1.1, CD8 and CD25 and then relative depletion of lymphocytic populations assessed. The mechanism of inhibition was then evaluated using a series of adoptive transfer models and pharmacokinetic studies.

In addition to impairing target cell depletion, FcγRIIB has been implicated in modulating the adaptive immune response and boosting immunostimulatory mAb. Some early evidence suggested if an immune complex binds to hFcγRIIB instead of activatory FcγRs, it can result in reduced antigen presentation and DC maturation [260]. However later evidence suggested that FcγRIIB was critical to producing a strong T cell independent immune response; with the notion that hFcγRIIB can internalise unprocessed antigens for presentation on the surface of B cells [261]. Moreover, in the context of immunostimulatory mAbs, FcγRIIB expression has been reported to be critical for the agonistic effect of certain mAbs, such as mAbs directed against CD40. Here, they have been found to require hFcγRIIB for crosslinking and target receptor activation [308] [309].

Therefore, to assess the impact of the hFcγRIIB ITIM on the agonistic activity of immunostimulatory mAbs NoTIM mice were used, and compared to mFcγRII and hFcγRIIB Tg mice with immune stimulation assessed using anti-CD40 mAb in an OT-I adoptive transfer model. First the impact of the different inhibitory FcγR models on mAb-mediated target cell depletion of target cells was assessed.

4.2 Depletion of endogenous CD20+ B cells

To evaluate the impact of the different hFcγRIIB receptors on direct targeting mAbs *in vivo*, murine B cells were depleted using the anti-mCD20 mAb 18B12. In these experiments it was expected that B cell depletion would be more effective in NoTIM mice due to the absence of inhibitory signalling. To test this hypothesis mice from the strains characterised in the previous chapter were treated using a 5-fold dose escalation regimen of 18B12, beginning with 2 μg and ending with 50 μg (Figure 4.1 A). First, mice were pre-bled to establish the percentage of B cells in the periphery using flow cytometry (CD19+/B220+). At subsequent time points mice were bled to analyse the percentage of B cells following the administration of mAb, this was then normalised to the pre-treatment B cell percentage baseline to ascertain depletion (Figure 4.1 B). Both the mIgG1 and mIg2a subclass were utilised in separate experiments as they exhibit altered levels of FcγR interactions (Figure 4.1 C) and so allow the assessment of the hFcγRIIB in different contexts.

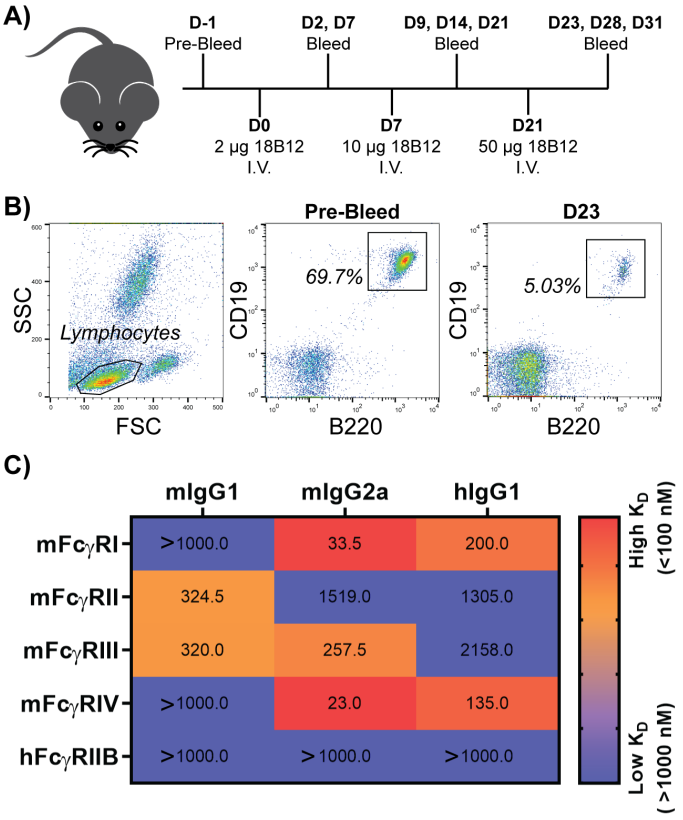

Figure 4.1: Experimental Plan for 18B12 B Cell Depletion Experiment
A) The dose escalation regimen for the depletion of CD20+. C57BL6J, mFcγRII KO, hFcγRIIB Tg and NoTIM mice were pre-bled to establish the percentage of B cells at baseline (100%). Mice were then administered 18B12 I.V. and bleed regularly to monitor B cell depletion/recovery. B) The gating strategy used to identify B cells (CD19+/B220+) as a percentage of total lymphocytes. C) The dissociation constants for mouse IgG1, mouse IgG2a and human IgG1 for all mouse FcγRs and the human FcγRIIB. Data generated in-house by Dr. Ian Mockridge by surface plasmon resonance (unpublished).

4.2.1 18B12 mIgG1 Depletion

For the first set of experiments, 18B12 mIgG1 was utilised due to it's sub-optimal engagement of activatory FcγRs and therefore allowed the identification of any subtle differences in depletion between strains (Figure 4.2). 2 μg of 18B12 is a relatively small dose of mAb, however mFcγRII KO mice were responsive showing a mean decrease of 20% compared to baseline on Day 2. No clear depletion was observed in any of the other mouse strains, suggesting that the presence of an inhibitory receptor stopped depletion at this dose. After treatment with 10 μg 18B12 mIgG1, mFcγRII KO mice showed a mean 75% decrease in B cells, whilst C57BL/6J and hFcγRIIB Tg mice dropped by 40%. Unexpectedly, the NoTIM mice remained resistant with a smaller 20% drop in the percentage of B cells. By Day 21 (7 days after 10 μg of mAb), C57BL/6J and hFcγRIIB Tg showed a strong increase in mean percentage B cells (77% and 67% B cells of baseline, respectively) whilst mFcγRII KO remained depressed (43% of baseline) and NoTIM mice remained unchanged. After 50 μg, B cells were efficiently depleted in C57BL/6J, mFcγRII KO and hFcγRIIB Tg mice whilst NoIM mice continued to show resistance to depletion.

On Day 31 (10 days after 50 μg mAb), the mice were culled and harvested to assess depletion in the secondary lymphoid organs (spleen and iLN), key reservoirs of B cells within mice (Figure 4.3). As seen within the periphery, B cell depletion was blunted in both the spleen and iLN in NoTIM mice when compared to the other groups. hFcγRIIB Tg and mFcγRII KO mice had similar percentage of B cells within the spleen, with C57BL/6J lowest whilst hFcγRIIB Tg mice appeared to be slightly more resistant to depletion than the C57BL/6J and mFcγRII KO mice in the iLN. Notably, the NoTIM mice were shown to be most resistant to B cell depletion, despite the receptor being unable to elicit ITIM mediated signalling.

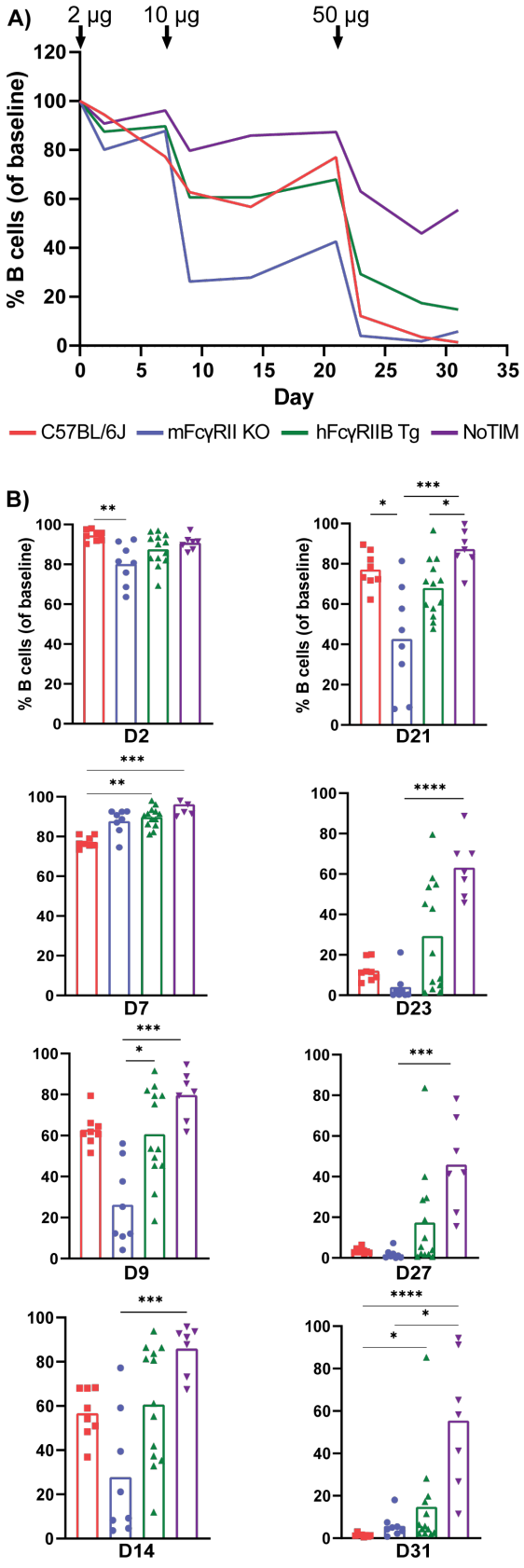

Figure 4.2: Depletion of peripheral CD20+ B cells using 18B12 mIgG1
A) C57BL6J, mFcγRII KO, hFcγRIIB Tg and NoTIM mice were pre-bled to establish the B cells as a percentage of lymphocytes (100%) and then subsequently treated with increasing doses of 18B12 mIgG1 via intravenous injection as indicated (2 µg, 10 µg and 50 µg). Mice were bled in-between doses to ascertain the percentage of B cell depletion. Line = mean. B) Depletion of peripheral B cells at each time point. The result of 3 independent experiments (7 - 12 mice per group). Bar = mean. Statistical analyses conducted using the Kruskal-Wallis test with Dunn's multiple comparison test. * = $P \leq 0.05$, ** = ≤ 0.01, *** = $P \leq 0.001$, **** = $P \leq 0.0001$.

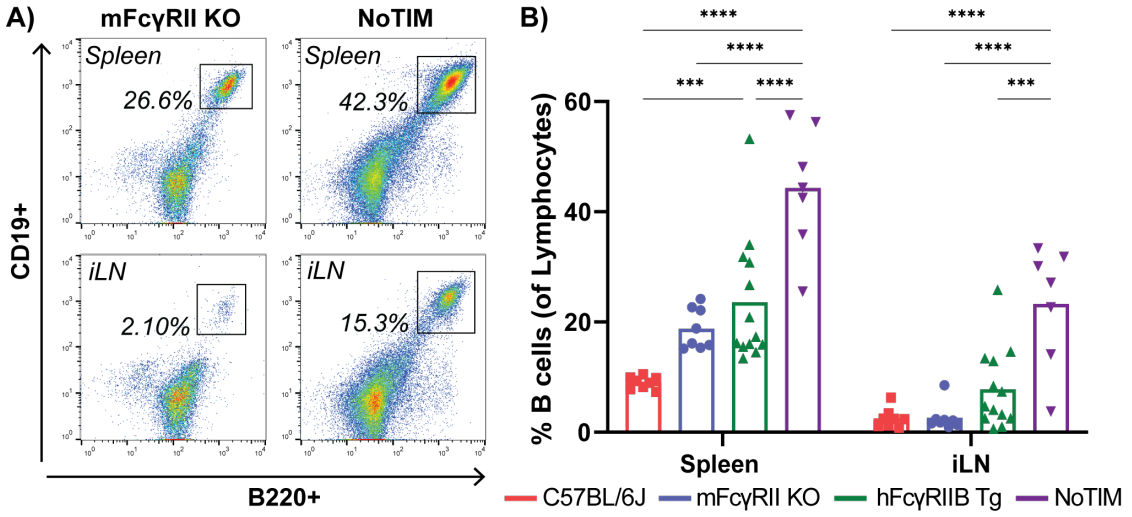

Figure 4.3: Depletion of splenic and lymph node CD20+ B cells using 18B12 mIgG1
A) C57BL6J, mFcγRII KO, hFcγRIIB Tg and NoTIM mice were treated with increasing doses of 18B12 mIgG1 via intravenous injection using a dose escalation regimen (2 μg, 10 μg and 50 μg). Mice were then culled on Day 31 (10 days after 50 μg dose) and depletion of CD20+ B cells was analysed in the spleen and inguinal lymph nodes (iLN) using flow cytometry. B) B cells within the spleen and iLN expressed as a percentage of lymphocytes on Day 31. The result of 3 independent experiments (7 - 12 mice per group). Bar = mean. Statistical analyses conducted using a one-way ANOVA with Tukey's multiple comparison test. *** = $P \leq 0.001$, **** = $P \leq 0.0001$.

4.2.2 18B12 mIgG2a Depletion

To assess if the former observation was subclass dependent, the dose escalation experiments were repeated using 18B12 mIgG2a. The mIgG2a subclass engages the activatory mFcγRI and mFcγRIV with much higher affinity than mIgG1, therefore it would be expected that inhibition elicited by hFcγRIIB would not be as strong (Figure 4.1).

On Day 2, after 2 μg of 18B12 mIgG2a, all groups had a mean 10-15% drop in B cells except for NoTIM mice where the decrease was only 5% (Figure 4.4). B cell levels had recovered by Day 7 in all mice, but two days after 10 μg of 18B12 (Day 9), NoTIM mice were significantly more resistant to depletion than C57BL/6J and mFcγRII KO mice. This trend continued at Day 14 with NoTIM mice B cell percentage (mean 84%) recovering significantly faster than C57BL/6J (43%), mFcγRII KO (39%) and hFcγRIIB Tg mice (49%). Two days after 50 μg 18B12 (Day 23), there was substantial depletion of peripheral B cells in all mice, however NoTIM mice remained most resistant to depletion and recovered fastest through to Day 31.

A harvest conducted on Day 31 showed that NoTIM mice were most resistant to B cell depletion, with a significantly higher proportion of B cells in the spleens of NoTIM mice than both mFcγRII KO and hFcγRIIB Tg mice (Figure 4.5). Within the iLNs, C57BL/6J,

hFcγRIIB Tg and NoTIM mice had similar percentage of B cells. mFcγRII KO had a lower mean B cell percentage than the other groups but this was not significantly different. This suggests that the differences observed in depletion in the blood are also reflected in the lymphoid tissues with respect to NoTIM mice.

Together, these experiments demonstrate that depletion of CD20+ B cells using both 18B12 mIgG1 and mIgG2a mAb was least effective in the non-signalling hFcγRIIB NoTIM mouse. These data infer that inhibition of direct targeting mAb therapy by hFcγRIIB is independent of ITIM signalling.

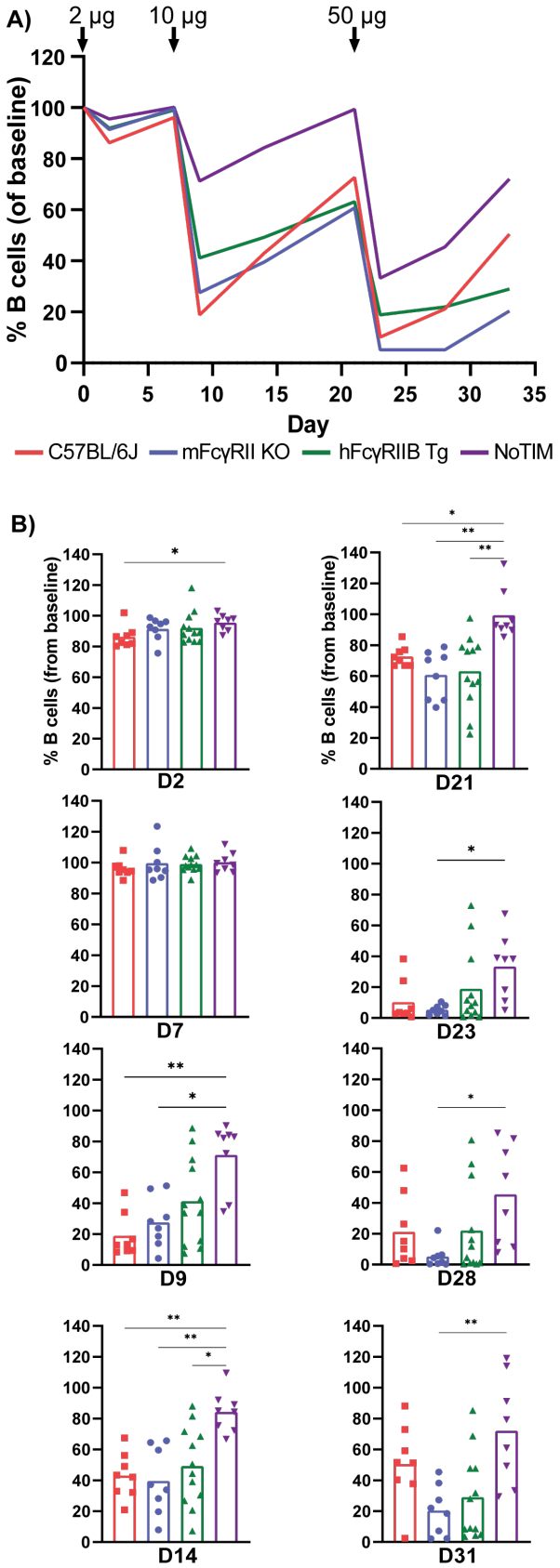

Figure 4.4: Depletion of peripheral CD20+ B cells using 18B12 mIgG2a
C57BL6J, mFcγRII KO, hFcγRIIB Tg and NoTIM mice were pre-bled to establish the B cells as a percentage of lymphocytes (100%) and then subsequently treated with increasing doses of 18B12 mIgG2a via intravenous injection (2 µg, 10 µg and 50 µg). Mice were bled in-between doses to ascertain the percentage of B cell depletion. Line = mean. B) Depletion of peripheral B cells at each time point. The result of 2 independent experiments (8 - 12 mice per group). Bar = mean. Statistical analyses conducted using the Kruskal-Wallis test with Dunn's multiple comparison test. * = $P \leq 0.05$, ** = ≤ 0.01, *** = $P \leq 0.001$, **** = $P \leq 0.0001$.

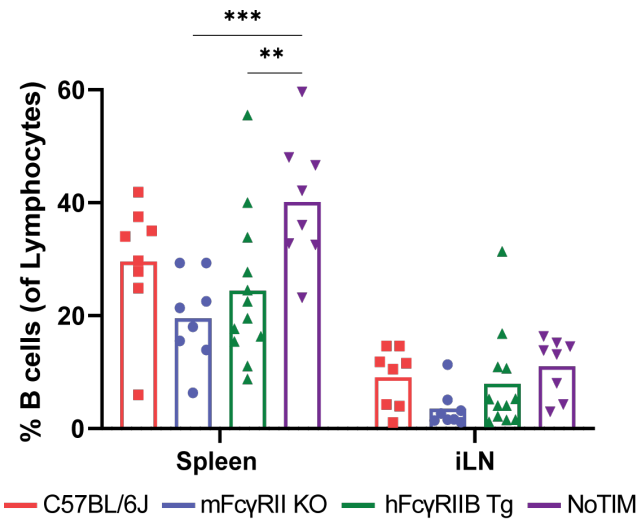

Figure 4.5: Depletion of splenic and lymph node CD20+ B cells using 18B12 mIgG2a
C57BL6J, mFcγRII KO, hFcγRIIB Tg and NoTIM mice were treated with increasing doses of 18B12 mIgG2a via intravenous injection using a dose escalation regimen (2 μg, 10 μg and 50 μg). Mice were then culled on Day 31 (10 days after 50 μg dose) and depletion of CD20+ B cells was analysed in the spleen and inguinal lymph nodes (iLN) using flow cytometry. The result of 2 independent experiments (8 - 12 mice per group). Bar = mean. Statistical analyses conducted using a one-way ANOVA with Tukey's multiple comparison test. ** = $\leq$ 0.01, *** = P $\leq$ 0.001.

4.2.3 Internalisation of 18B12 mIgG1

Within the literature hFcγRIIB mediated internalisation of type I hIgG1 mCD20 mAbs has been well characterised and linked to a reduction in mAb efficacy and worsened survival outcomes in lymphoma patients [299] [302] [301]. However, there is a lack of information regarding the internalisation of mAbs directed towards mCD20, including 18B12. As such, differences in the rate of 18B12 mAb internalisation may have been responsible for the differences in mAb mediated B cell depletion seen above. To investigate this, splenic B cells were isolated from each mouse strain and incubated with fluorescently labelled 18B12 mIgG1. At key time points, a quenching mAb was used to abrogate the fluorescence of any cell surface bound mAb. Anything internalised would not be quenched. By comparing quenched and unquenched samples to samples taken at 0 hours, the percentage of mAb internalisation can be estimated.

After two hours, there was little internalisation of 18B12 across cells from each mouse model (Figure 4.6). After incubation for 6 hours, C57BL/6J, hFcγRIIB Tg and NoTIM B cells showed a higher rate of internalisation than mFcγRII KO B cells. This trend continued at the 24 hour time point, with no significant difference in the internalisation rate between strains.

These data suggest that the presence of the mFcγRII or hFcγRIIB enhances the internalisation of 18B12 mIgG1 compared to when there is no inhibitory receptor. However, the differences between the groups were non-significant and the maximal internalisation over a 24 hour time period was only 40% suggesting that internalisation is unlikely to affect mAb efficacy in a substantial manner.

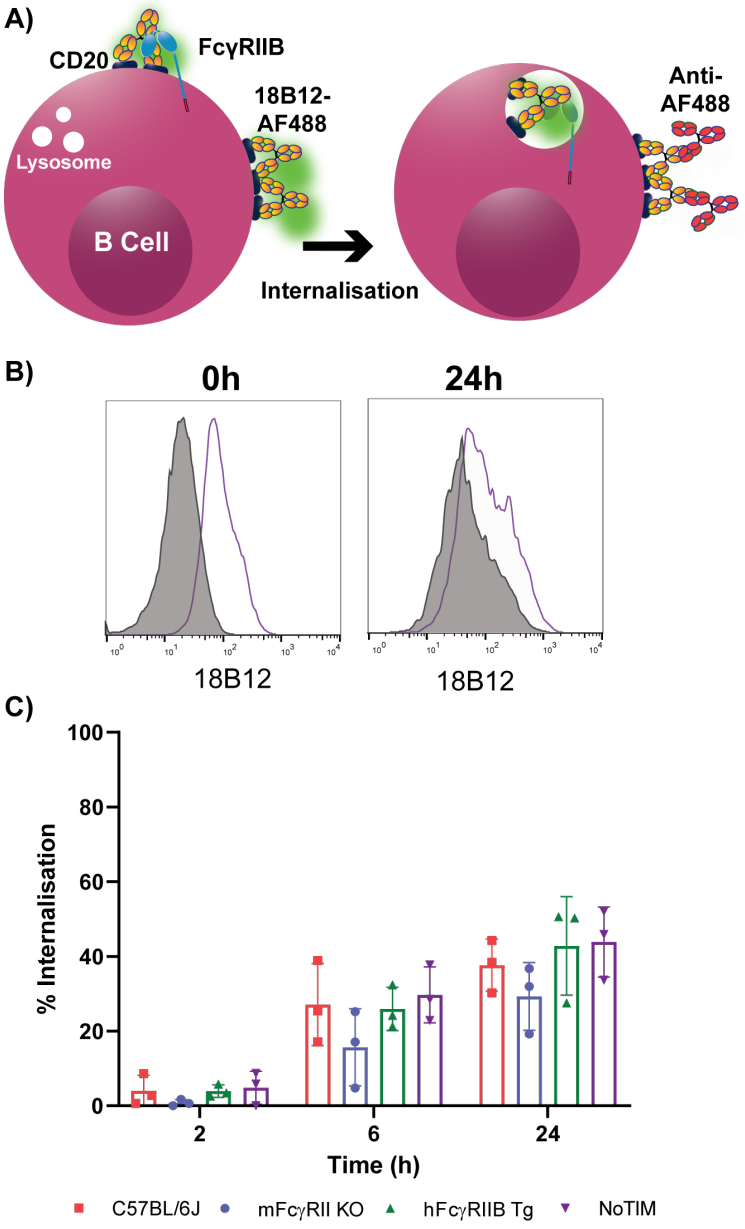

Figure 4.6: Internalisation of 18B12 mIgG1 by isolated splenic B cells from different mouse strains
A) Splenic B cells were isolated from C57BL6J, mFcγRII KO, hFcγRIIB Tg and NoTIM mice and were incubated with 5 μg/mL of AF488 labelled 18B12 mIgG1 for 2, 6 or 24 hours. At each time point samples were taken and split into quenched (where cells were labelled with a quenching mAb against AF488) or unquenched. Samples were then assessed by flow cytometry to determine the percentage of internalisation (quenched-unquenched) compared to a sample taken at 0 hour. B) Representative flow cytometry profiles to show quenched (grey) vs unquenched (purple) at 0 hour and 24 hour from NoTIM B cells. C) The internalisation of 18B12 mIgG1 over a 24 hour time period. The result of 3 independent experiments (repeated in triplicate). Bar = mean $\pm$ SD. Statistical analyses conducted using a one-way ANOVA with Tukey's multiple comparison test. Groups were not statistically significant.

4.2.4 Pharmacokinetics of 18B12 mIgG1

hFcγRIIB has also been implicated in the regulation of mAb half life. This is broadly related to expression on LSECs, which play a critical role in the removal of small immune complexes [242]. It has also been shown that NOD-SCID mice (which exhibit decreased FcRn expression and the absence of circulating IgG) have decreased mAb half life for certain IgG isotypes/subclasses, due to an effect of mFcγRII [364]. Therefore, it was considered that differential expression levels of mFcγRII and hFcγRIIB within the mouse models could have resulted in differential regulation of mAb half life and there in target cell depletion.

To investigate this, mice were given a bolus of 50 μg 18B12 mIgG1 via intravenous injection and serially bled over a five day period to ascertain the concentration of free 18B12 mIgG1 in the sera. B cell depletion was assessed using flow cytometry and 18B12 mIgG1 concentration was analysed using a bioassay (π-BCL$_1$ cell line binding assay).

Depletion of B cells within the periphery followed a similar pattern to that observed in the dose escalation experiments (Figure 4.7 A and C). At the 1 hour time point, all groups experienced substantial B cell depletion. By 6 hours, the NoTIM and hFcγRIIB Tg B cells had recovered towards baseline whilst C57BL/6J and mFcγRII KO B cells recovered but to a lesser extent. At 24 hours post treatment, C57BL/6J peripheral B cells had made a significant recovery, with similar percentage to NoTIM and hFcγRIIB Tg mice, whilst mFcγRII KO remained depleted. At 48 and 96 hours, peripheral B cells in the NoTIM mice continued to remain resistant to depletion whilst peripheral B cells in the C57BL/6J and hFcγRIIB Tg mice continued to be depleted.

Analysis of mAb concentration within the serum showed that the presence of either the mFcγRII or hFcγRIIB reduced the levels of circulating 18B12 mIgG1 compared to levels in mFcγRII KO mice (Figure 4.7 B and D). At 1 hour, there was similarly high levels of 18B12 mIgG1 across all mice. From 6 hours onward, C57BL/6J, hFcγRIIB Tg and NoTIM mice had similar concentrations of 18B12 within the periphery, whilst mFcγRII KO mice had notably more. At 6 hours, NoTIM mice had significantly less 18B12 mIgG1 in the periphery than mFcγRII KO mice. Statistical significance was then lost between groups until the 96 hour time point where both C57BL/6J and NoTIM mice had significantly less 18B12 mIgG1 in the serum than in mFcγRII KO mice.

To investigate links between depletion and mAb concentration, pharmacokinetic parameters were calculated for each mouse (Figure 4.8 A). The half life ($t_{1/2}$) of 18B12 mIgG1 was consistent across groups, with C57BL/6J mice having a slightly lower average $t_{1/2}$ than other mice. The area under the curve ($AUC_{0\text{-}t}$) gives an indication of the exposure to mAb throughout the experiment. Again, C57BL/6J mice had a slightly lower AUC suggesting a lower overall exposure compared to other groups, however the range of values overlapped. mFcγRII KO mice had the highest $AUC_{0\text{-}t}$ but this was not significantly different compared with other groups. The volume of distribution (V_z) indicates the distribution of mAb across tissues and was found to be equal across mice. The mAb clearance (CL) was greater in C57BL/6J and NoTIM mice compared to mFcγRII KO and hFcγRIIB Tg mice. Overall, these data suggest that both mFcγRII and hFcγRIIB may be driving greater clearance of 18B12 mIgG1 compared to mice which lack any inhibitory receptor but the differences are not sufficient to explain the effects on depletion.

Correlating peripheral B cell depletion and concentration of 18B12 mIgG1 at key time points showed no relationship (Figure 4.8 B). This was clear at both 6 hours and 48 hours, with the relationship between parameters weak with low R^2 values. To assess whether the concentrations of mAb in the serum were sufficient to saturate binding of mCD20, a dose-response of the binding of 18B12 mIgG1 to murine splenic B cells was analysed by flow cytometry (Figure 4.8 C). It is clear that in mFcγRII KO, hFcγRIIB Tg and NoTIM mice that 18B12 binds equally between groups and saturates at 2.5 μg/mL. This suggests that despite mFcγRII KO having a slightly higher peripheral blood (serum) concentration of 18B12 mIgG1, binding sites were likely to be equally saturated across all mice across the 96 hour period. Finally, to explore the relationship between receptor expression and half-life, the geometric mean of hFcγRIIB+ B cells was correlated to mAb $t_{1/2}$ in hFcγRIIB Tg and NoTIM mice (Figure 4.8 D). It was found that there was no relationship between these two factors suggesting that mAb half life was not related to hFcγRIIB expression level.

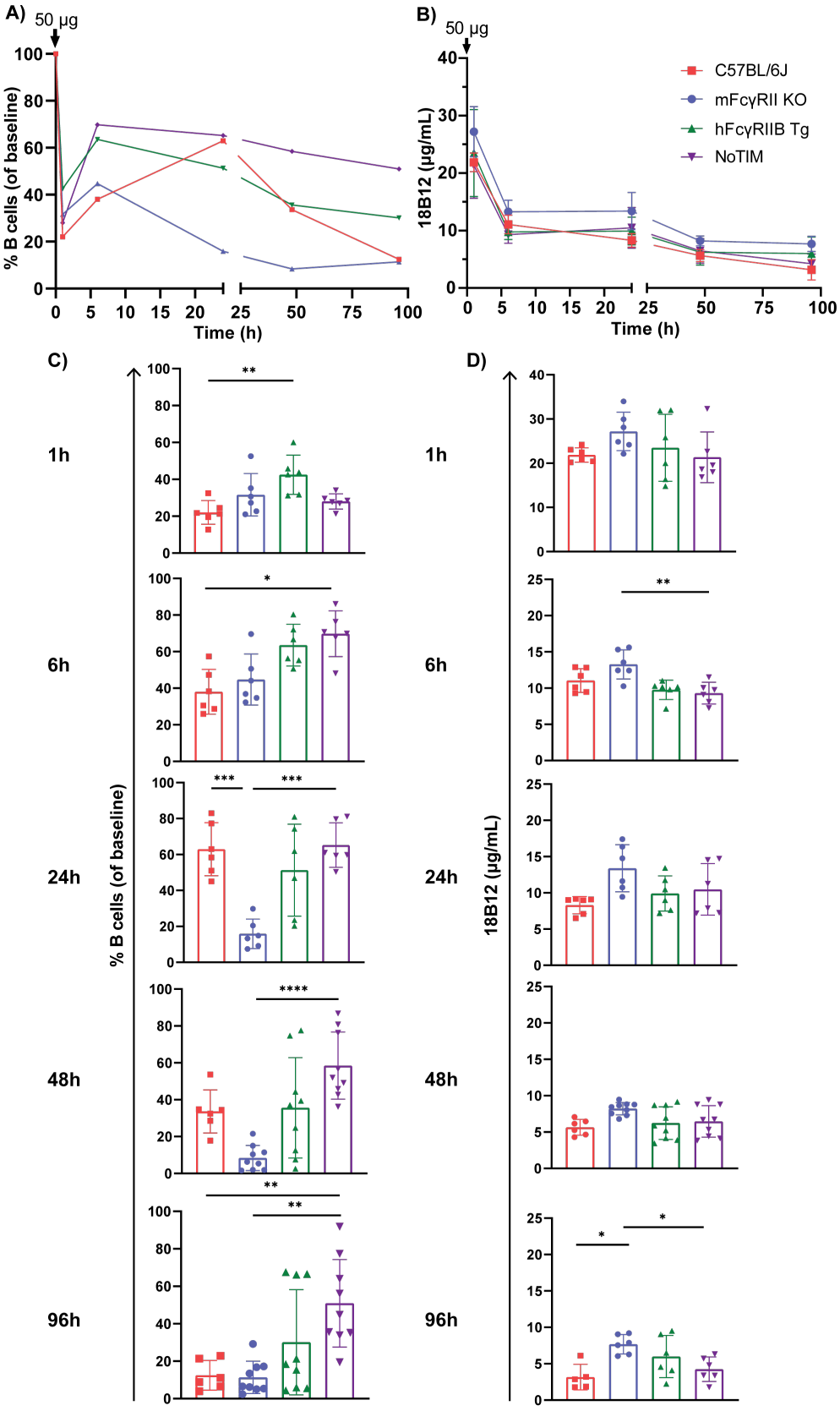

Figure 4.7: The kinetics of 18B12 mIgG1 mediated depletion and availability within peripheral blood
A) C57BL6J, mFcγRII KO, hFcγRIIB Tg and NoTIM mice were treated with an intravenous bolus of 50 µg 18B12 mIgG1 and then bled at 1, 6, 24, 48 and 96 hours to assess depletion by flow cytometry. Line = mean. B) 18B12 mIgG1 concentration was also assessed using the π-BCL_1 cell binding assay to calculate serum concentration of 18B12. Line = mean ± SD. C) The depletion at each individual time point across groups. Bar = mean ± SD. D) The 18B12 concentration at each time point. The result of 2-3 independent experiments (6 - 9 mice per group). Bar = mean ± SD. Statistical analyses conducted using the Kruskal-Wallis test with Dunn's multiple comparison test * = $P \leq 0.05$, ** = ≤ 0.01, *** = $P \leq 0.001$, **** = $P \leq 0.0001$.

A)

Parameter	Unit	C57Bl/6J mean ±SD (Range)	mFcγRII KO mean ±SD (Range)	hFcγRIIB Tg mean ±SD (Range)	NoTIM mean ±SD (Range)
$t_{1/2}$	h	39.52 ±12.64 (29.66 - 61.10)	63.06 ±10.96 (50.95 - 77.71)	64.08 ±22.05 (37.54 - 71.53)	47.99 ±16.57 (28.80 - 71.53)
AUC_{0-t}	µg/ml*h	662.13 ±68.72 (584.36 - 767.58)	991.72 ±88.04 (893.28 - 1123.39)	802.08 ±220.14 (491.22 - 1065.65)	723.20 ±167.73 (541.32 - 986.58)
V_z	(µg)/(µg/ml)	3.27 ±0.37 (2.80 - 3.47)	2.75 ±0.21 (2.60 - 2.99)	3.50 ±0.77 (2.48-4.42)	3.46 ±0.65 (3.15 - 4.21)
CL	(µg)/(µg/ml)/h	0.0607 ±0.0136 (0.0382 - 0.0751)	0.0309 ±0.0052 (0.0232 - 0.0366)	0.0429 ±0.0217 (0.0203 - 0.0816)	0.0541 ±0.0171 (0.0305 - 0.0766)

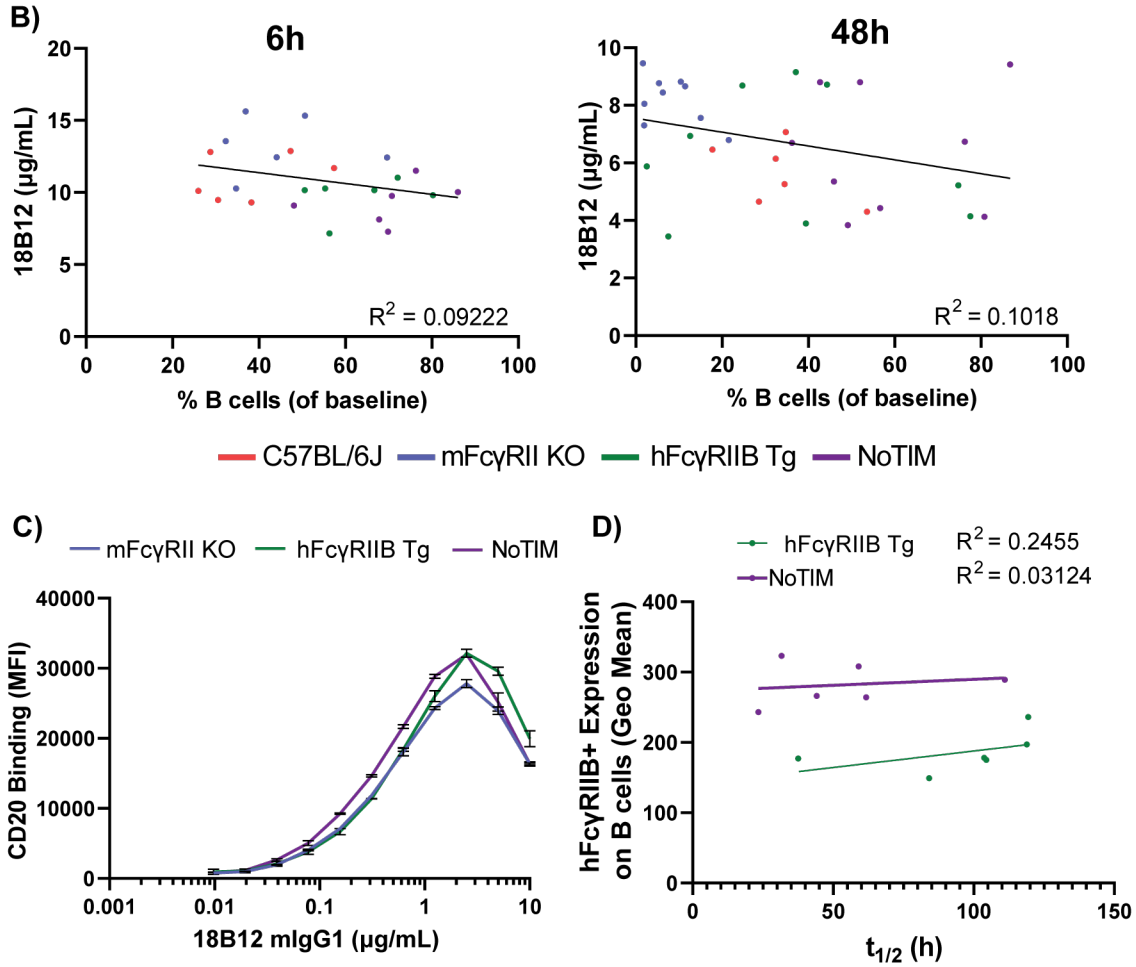

Figure 4.8: Pharmacokinetic parameters of mice treated with 18B12 mIgG1
A) C57BL6J, mFcγRII KO, hFcγRIIB Tg and NoTIM mice were treated with an intravenous bolus of 50 µg 18B12 mIgG1 and then bled at 1, 6, 24, 48 and 96 hours to assess depletion and peripheral 18B12. Pharmacokinetic parameters for each mice were calculated using PKSolver based on an I.V. model with non-compartmental analysis [337]. $t_{1/2}$ = half-life, AUC_{0-t} = Area under curve, V_z = volume of distribution, CL = clearance. B) Correlation data of 18B12 within the periphery against B cell depletion at 6 hour and 48 hour time point. C) B cells were isolated from each respective mouse model and incubated with varying concentrations of 18B12 mIgG1. Bound 18B12 was then detected using a specific fluorescently labelled mAb by flow cytometry. The binding curve of 18B12 mIgG1 on splenic B cells isolated from mFcγRII KO, hFcγRIIB Tg and NoTIM mice. D) Correlation of 18B12 half-life and the geometric mean of hFcγRIIB on positive B cells from hFcγRIIB Tg and NoTIM mice. The result of 2 - 3 independent experiments (6 - 9 mice per group).

4.2.5 hFcγRIIB expression and inhibition of CD20+ B cell depletion

As a result of these last two experiments, the differences seen in the depletion of CD20+ B cells in each mouse model were considered unlikely to be linked to internalisation of 18B12 or modulation of half-life *in vivo*. A retrospective analysis of the dose escalation experiments highlighted some interesting findings. In both the mIgG1 and mIgG2a data, it was clear that two and nine days after the 10 μg dose of mAb (D9 and D14), that hFcγRIIB Tg mice split into two groups (Figure 4.2, Figure 4.4). One group, termed 'responders', had a depletion profile similar to that seen in mFcγRII KO mice. The other group termed 'non-responders', had a depletion profile similar to NoTIM mice. This effect was most pronounced using mIgG1, most likely due to the sub-optimal depletion of CD20+ B cells.

As discussed in Chapter 3, hFcγRIIB Tg mice have a mosaic expression pattern on most cell types and tend to have a lower expression of hFcγRIIB compared to NoTIM mice as measured using the fluorescence geometric mean. Taking the D14 time point for hFcγRIIB Tg mice treated with 18B12 mIgG1 and correlating depletion with both transgene expression and geometric mean, the data suggests that the higher the geometric mean of the hFcγRIIB+ population, the more resistance there is to B cell depletion (Figure 4.9 B). The R^2 value of 0.6072 suggests that there is a moderate correlation. When correlating the percentage transgene expression on B cells with B cell depletion, a relationship between these two factors suggests the higher the proportion of transgene expressing cells, the more resistance there is to depletion (R^2 0.5019). This relationship was also observed at D9 and D23 (data not shown).

The mIgG2a subclass is more efficient at eliciting target cell depletion due to its ability to better engage activatory FcγRs. As a result the difference between 'responders' and 'non-responders' was not as stark and the correlations in these experiments were not as robust (Figure 4.9 D).

Due to the intensive bleed schedule in the dose escalation experiments it was not possible to collect enough blood to also examine the myeloid population. Because the myeloid population drive mAb effector functions, hFcγRIIB expression on these cells is likely to influence mAb depletion more than expression on B cells. Therefore to see how relevant the expression of hFcγRIIB on B cells are to the myeloid population, a retrospective analysis of immunophenotyping data was conducted on hFcγRIIB mice (Figure 4.9 E). It was found that the percentage transgene expression on CD11B+ cells correlated strongly with

the transgene expression as measured on CD19+ cells (R^2 = 0.7558). This suggests that transgene expression on B cells equates to that seen on CD11B+ myeloid cells. To understand if this was the same with geometric mean, the hFcγRIIB+ population from hFcγRIIB Tg mice on both splenic Ly6C high monocytes and B cells were correlated (Figure 4.9 F). It was found that there was a positive relationship between both factors, indicating the higher the MFI on B cells, the higher the MFI on Ly6C high monocytes.

Taken together, these data suggested that hFcγRIIB inhibits anti-mCD20 mAb therapy independently of ITIM signalling. Differences in depletion seen between hFcγRIIB Tg and NoTIM mice are unlikely to be due to differences in mAb internalisation or mAb pharmacokinetics. Rather, inhibition appeared to be driven by the level of expression - the higher the geometric mean and/or the transgene expression, the more resistant hFcγRIIB Tg mice were to B cell depletion.

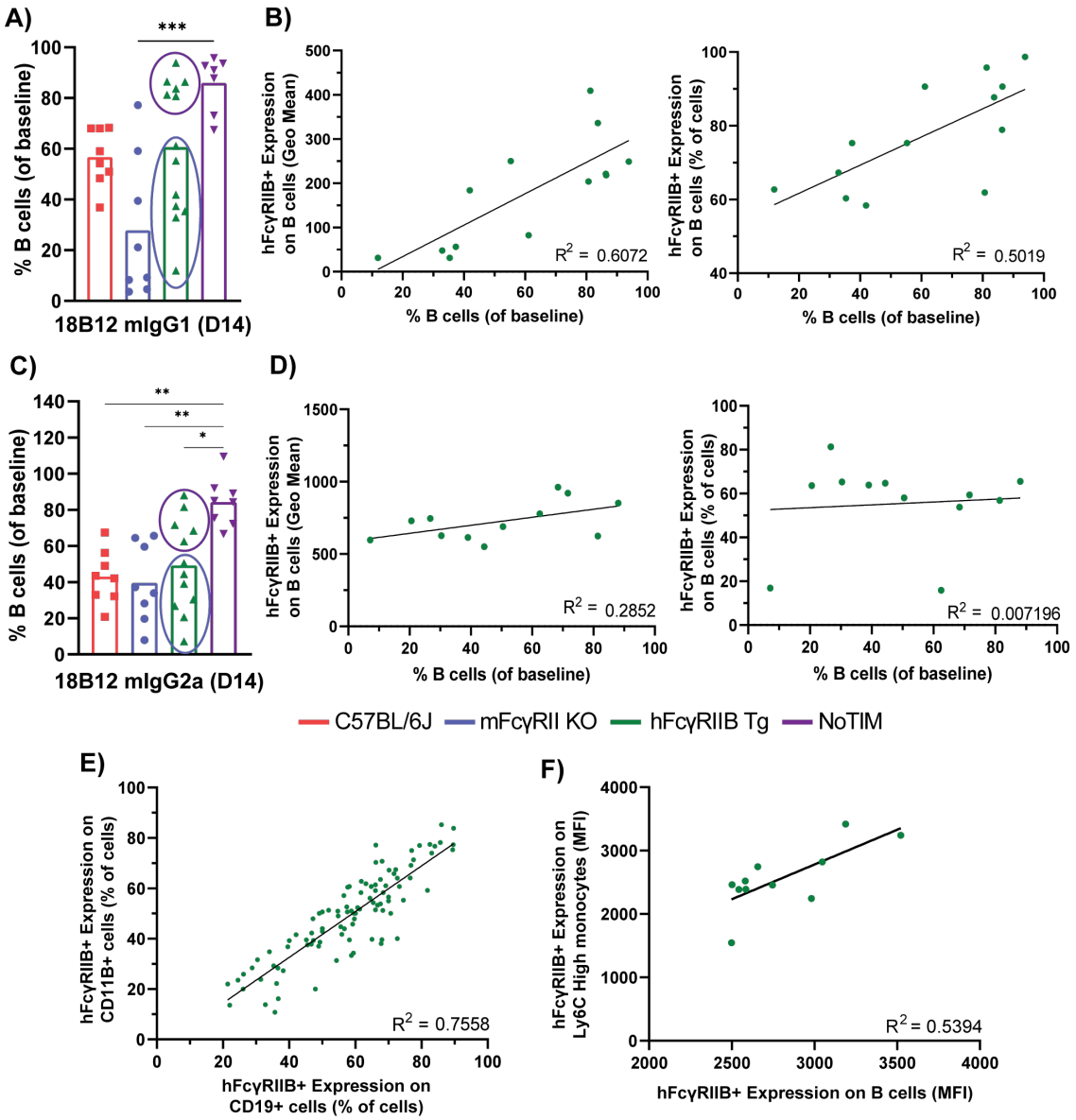

Figure 4.9: Correlation between transgene expression, geometric mean of hFcγRIIB and depletion in hFcγRIIB Tg mice

A) C57BL6J, mFcγRII KO, hFcγRIIB Tg and NoTIM mice were pre-bled to establish the B cells as a percentage of lymphocytes (100%) and then subsequently treated with increasing doses of 18B12 mIgG1 via intravenous injection (2 μg, 10 μg and 50 μg). Mice were bled in-between doses to ascertain the percentage of B cell depletion. The depletion on Day 14, 7 days after treatment with 10 μg of mAb (result of 3 independents experiments, 7- 12 mice per group). Purple circle indicates 'responders', blue circle indicates 'non-responders'. Line = Mean. B) The correlation between B cell depletion and geometric mean of hFcγRIIB+ positive cells and transgene expression on peripheral B cells from mice treated with 18B12 mIgG1. C) Mice were treated as above but with 18B12 mIgG2a. Depletion on Day 14. 7 days after treatment with 10 μg of mAb (result of 2 independents experiments, 8 - 12 mice per group). Purple circle indicates 'responders', blue circle indicates 'non-responders'. Line = Mean. D)The correlation between B cell depletion and geometric mean of hFcγRIIB+ positive cells and transgene expression on peripheral B cells from mice treated with 18B12 mIgG2a. E) The correlation between transgene expression on CD19+ cells and CD11B+ cells from immunophenotyped hFcγRIIB Tg mice. F) The correlation between hFcγRIIB+ MFI on splenic Ly6C high monocytes and splenic B cells. Statistical analyses conducted using the Kruskal-Wallis with Dunn's multiple comparison test. * = $P \leq 0.05$, ** = ≤ 0.01, *** = $P \leq 0.001$, **** = $P \leq 0.0001$.

4.3 Adoptive B cell transfer models to elucidate the mechanism of hFcγRIIB mediated inhibition of direct targeting mAb therapy

In the previous experiments detailed above, it was established that the non-signalling hFcγRIIB was able to inhibit the direct targeting mAb 18B12 from depleting B cells independently of ITIM signalling.

To expand these observations to other mAbs and deduce if inhibition was driven by expression of hFcγRIIB on effector cells or target cells, two adoptive B cell transfer models were developed (Figure 4.10). In the first set of experiments, murine B cells expressing both the NoTIM receptor and hCD20 were adoptively transferred into mFcγRII KO recipients. This was to assess the contribution of hFcγRIIB on target cells to inhibition of depletion with the clinically relevant anti-hCD20 mAb rituximab. In the second set of experiments, murine B cells expressing hCD20 but deficient in mFcγRII were adoptively transferred into mFcγRII KO and NoTIM hosts to understand the contribution of hFcγRIIB on effector cells.

4.3.1 Importance of hFcγRIIB expression on target cells for inhibition of direct targeting mAb therapy

In the first system, mFcγRII KO mice were adoptively transferred with target B cells expressing NoTIM hFcγRIIB/hCD20 and non-target B cells from mFcγRII KO mice on day 0 (Figure 4.11 A). This system was designed to show if the NoTIM receptor is only expressed on the target cells, does it elicit inhibition. On day 1, mice were then treated with 2 mg/kg of 6G11 hIgG1 (6G) (hFcγRIIB blocking mAb), 6G11 NQ (6Q) (hFcγRIIB blocking mAb, Fc null variant) or isotype control to target the NoTIM receptor to assess if these mAbs could improve target cell depletion. On day 2, mice were then treated with 2 mg/kg rituximab hIgG1 (RTX) (anti-hCD20) to deplete hCD20 expressing target cells.

On day 3 a harvest was conducted to assess depletion of the adoptively transferred cells by examining the target:non-target (T:NT) ratio (Figure 4.11 C). It was found depletion was similar across the blood, spleen and bone marrow (Figure 4.11 B). RTX alone resulted in depletion of approximately half of all target cells, indicating that NoTIM expression on the

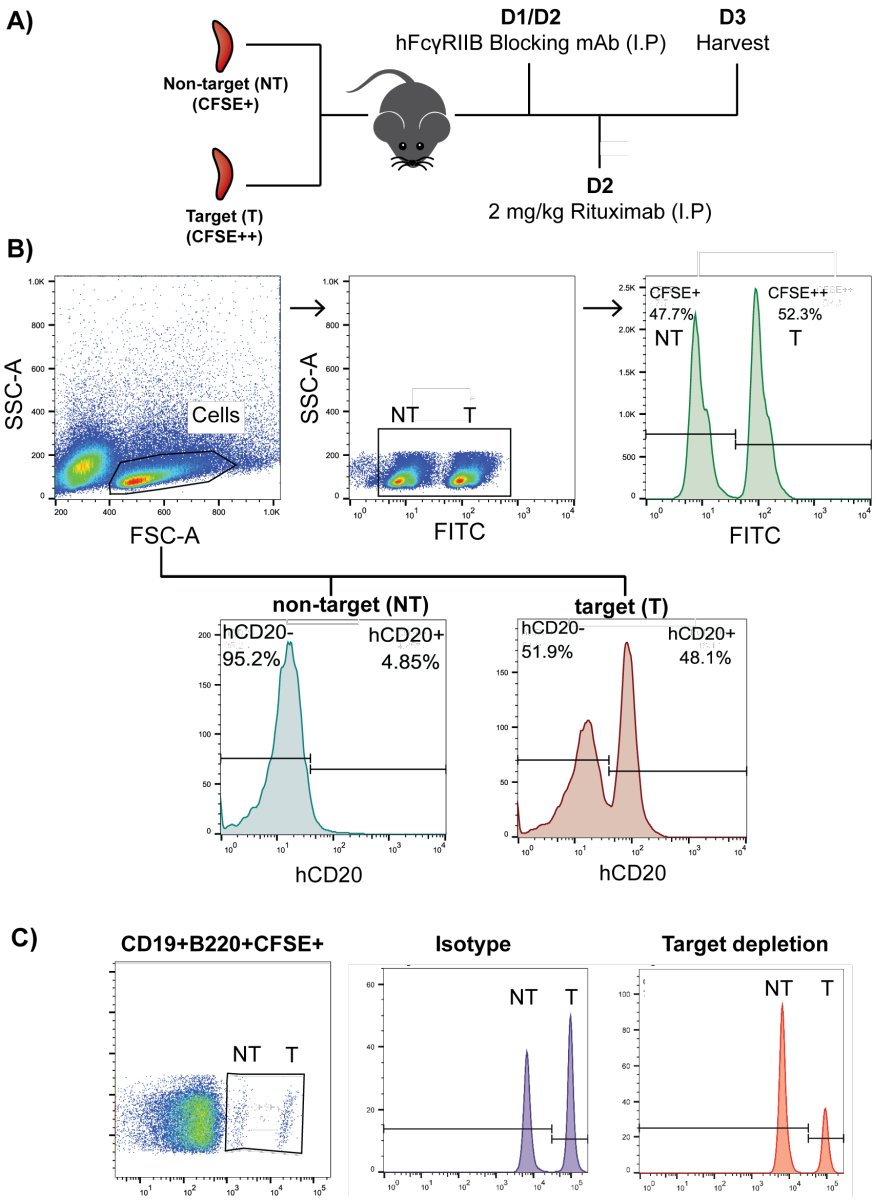

Figure 4.10: Adoptive B cell transfer experimental setup
A) Mice were adoptively transferred non-target (NT) and target (T) (expressing hCD20) splenocytes labelled with low (+) and high (++) levels of CFSE respectively at a 1:1 ratio. On Day 1/Day 2 , mice were treated with a hFcγRIIB blocking antibody via I.P injection. The following day (or later that day) mice were treated with 2 mg/kg rituximab. Target cell depletion was then assessed on Day 3. B) On Day 0, NT and T cells were labelled with low and high levels of CFSE and checked by flow cytometry to ensure at a 1:1 ratio and that they expressed hCD20. C) At harvest, NT and T B cells were identified by expression of CD19+/B220+/CFSE+. Isotype mice approximately maintained a 1:1 ratio, target depletion resulted in a decrease in the T population.

target cells does not inhibit target cell depletion. 6G alone resulted in the near complete depletion of all target cells, indicating that hFcγRIIB may be a good target for mAb mediated depletion. In contrast, 6Q monotherapy had little effect. The combination of 6G with RTX did not improve depletion as 6G was so effective as a monotherapy. The addition of 6Q to RTX did not improve depletion after RTX alone. This data suggests that 6G works effectively as direct targeting mAb in this system. This is likely due to the mAb being a WT hIgG1 and having the ability to engage activatory mFcγRs. hFcγRIIB is also expressed highly on target cells, providing plenty of F(ab) binding sites. In contrast, 6Q did not im-

prove target cell depletion most likely because the Fc null mutation (N297Q) abrogates interactions with activatory mFcγRs. Also, it is unlikely in this experimental system that hFcγRIIB mediated internalisation of RTX had any potential negative impact, hence 6Q did not impact depletion.

The expression of activatory mFcγRs was also analysed on key immune effector cells within the spleen and bone marrow (Figure 4.11 C and D). Across each treatment group, there was no difference in the detection of activatory mFcγRs, suggesting they are available equally to interact with direct targeting mAbs in each scenario. These data suggest that hFcγRIIB expression on target cells is not responsible for inhibition of anti-hCD20 mAb mediated depletion in the NoTIM mouse.

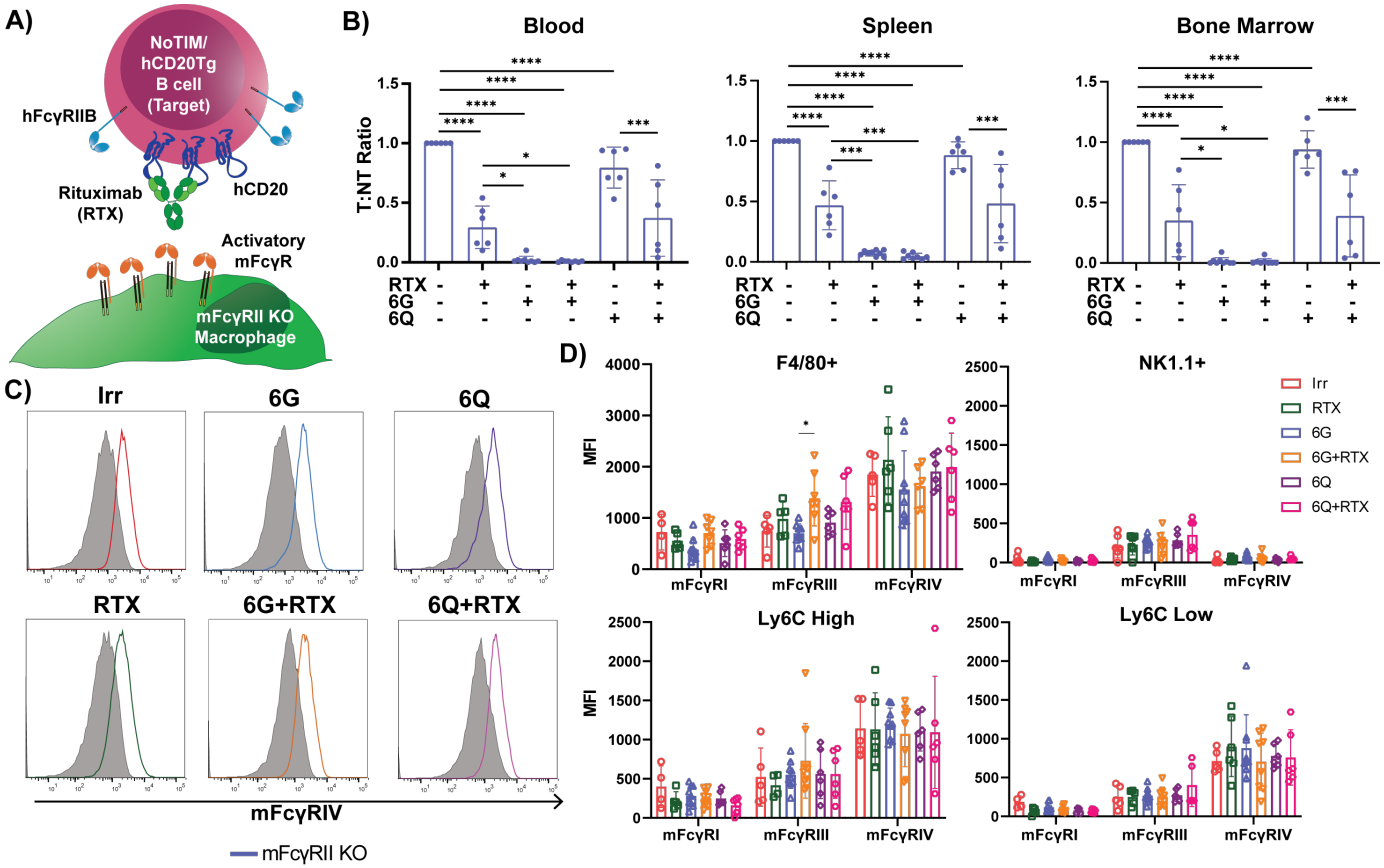

Figure 4.11: Adoptive transfer of mFcγRII KO B cells and NoTIM/hCD20 B cells into mFcγRII KO recipients followed by treatment with hFcγRIIB blocking mAbs and rituximab
A) mFcγRII KO B cells (non-targets) and NoTIM/hCD20 B cells (targets) labelled with low or high CFSE respectively were adoptively transferred into mFcγRII KO recipients on Day 0. On Day 1, mice were treated with either 2 mg/kg of hFcγRIIB blocking mAb hIgG1 (6G), N297Q mutation (6Q), or isotype. On Day 2, mice were treated with 2 mg/kg rituximab hIgG1 or isotype control (Irr) and then harvested on Day 3 to assess depletion of target cells. B) The Target:Not-Target (T:NT) ratio of depletion in the blood, spleen and bone marrow. The result of two independent experiments (6 mice per group). Line = mean ±SD. Statistical analyses conducted using a one-way ANOVA with Sidak's multiple comparison test. Significance was compared between isotype/rituximab monotherapy and other treatment groups C) Representative expression profile of mFcγRIV on splenic macrophages from each treatment group. D) The plotted MFI of each activatory mFcγR from key immune cells within the spleen. Bar = mean ±SD. Statistical analyses conducted using a one-way ANOVA with Tukey's multiple comparison test. * = $P \leq 0.05$, *** = $P \leq 0.001$, **** = $P \leq 0.0001$.

4.3.2 Importance of hFcγRIIB expression on effector cells for inhibition of direct targeting mAb therapy

In the second system, mFcγRII KO and NoTIM mice were adoptively transferred with target mFcγRII KO B cells expressing hCD20 and non-target mFcγRII KO B cells (Figure 4.12 A). This was to assess if the NoTIM receptor on effector cells was responsible for inhibition of target cell depletion. On day 1 and day 2, mice were then treated with 20 mg/kg of 6G, 6Q or isotype control to systemically block the NoTIM receptor throughout mice. 6 hours later, mice were then treated with 2 mg/kg RTX to opsonise hCD20 expressing target cells for depletion. On day 3, a harvest was conducted to assess the T:NT ratio.

In mFcγRII KO mice, RTX depleted approximately half of all target cells (Figure 4.12 B) - akin to that seen in the previous experiment. When repeated in NoTIM mice, RTX therapy reduced the ratio to approximately 0.75 - 0.80, showing clear resistance to depletion. Both 6G and 6Q monotherapy depletion resulted in no target cell deletion due to the lack of hFcγRIIB on the target cells. When 6G was combined with RTX, there was no improvement over RTX alone. However, when 6Q was combined with RTX, depletion of target cells was restored to the same level as seen in mFcγRII KO mice, suggesting that 6Q overcomes hFcγRIIB mediated inhibition of depletion in NoTIM mice.

As before, activatory mFcγRs were examined on immune effector cells. The addition of 6G (as a monotherapy or in combination) resulted in a significant drop in the detection of both mFcγRIII and mFcγRIV on key immune cells (Figure 4.12 C and D). These included splenic and bone marrow derived populations, with the effect most notable on splenic macrophages and Ly6C low monocytes (Figure 4.12 D). In the bone marrow, a significant decrease in the detection of activatory mFcγRs was noted on macrophages, Ly6C high monocytes and Ly6C low monocytes (Figure 4.13). The same effects were not observed with the 6Q mAb, nor in mFcγRII KO recipient mice.

Taking these data together, it was concluded that inhibition of target cell depletion was elicited by hFcγRIIB expression on immune effector cells. The addition of 6G did not improve RTX therapy, despite blocking hFcγRIIB. This is most likely because 6G is a hIgG1 with a functional Fc that is able to concurrently block hFcγRIIB and activatory mFcγRs, reducing interactions with RTX. In contrast, 6Q overcomes hFcγRIIB mediated inhibition because it blocks the inhibitory receptor and does not block any additional FcγRs, enabling RTX to bind efficiently with activatory mFcγRs and elicit target cell depletion.

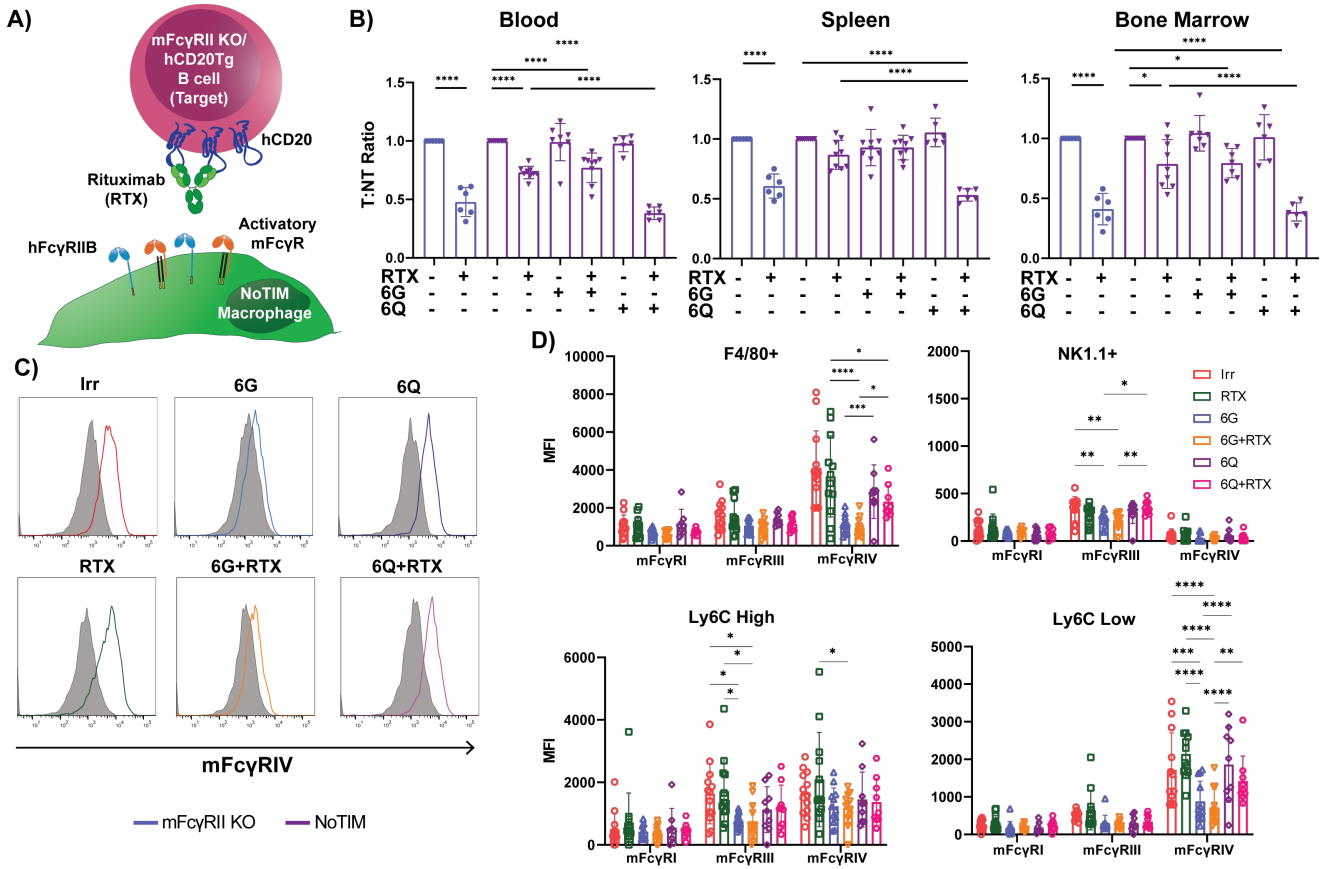

Figure 4.12: Adoptive transfer of mFcγRII KO B cells and mFcγRII KO/hCD20 B cells into mFcγRII KO and NoTIM recipients followed by treatment with hFcγRIIB blocking mAbs and rituximab

A) mFcγRII KO B cells (non-targets) and mFcγRII KO/hCD20 B cells (targets) labelled with low and high CFSE respectively were adoptively transferred into mFcγRII KO and NoTIM recipients on Day 0. On Day 1 and Day 2 am, mice were treated with 20 mg/kg of either hFcγRIIB blocking mAb hIgG1 (6G), N297Q mutation (6Q), or isotype. 6 hours later, mice were treated with 2 mg/kg rituximab hIgG1 or isotype control (Irr) and then harvested on Day 3 to assess depletion of target cells. B) The Target:Not-Target (T:NT) ratio of depletion in the blood, spleen and bone marrow. The result of 2 - 3 independent experiments (6 - 9 mice per group). Line = mean ±SD. Statistical analyses conducted using a one-way ANOVA with Sidak's multiple comparison test. Significance was compared between isotype/rituximab monotherapy and other treatment groups C) Representative expression profile of mFcγRIV on NoTIM splenic macrophages from each treatment group. D) The plotted MFI of each activatory mFcγR from key immune cells within the spleen. Bar = mean ±SD. Statistical analyses conducted using a one-way ANOVA with Tukey's multiple comparison test. * = $P \leq 0.05$, ** = ≤ 0.01, *** = $P \leq 0.001$, **** = $P \leq 0.0001$.

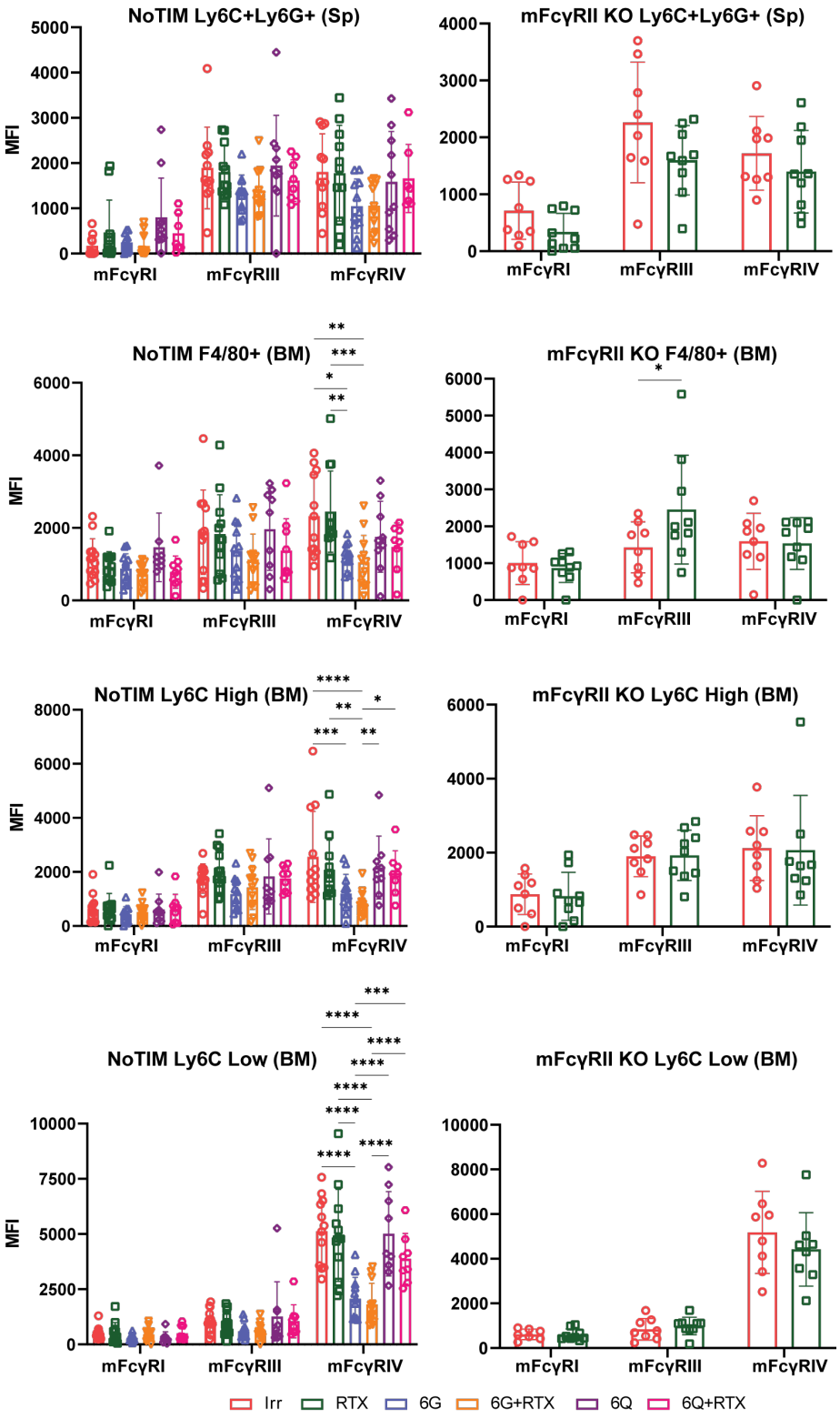

Figure 4.13: Activatory mFcγR profile on key immune cells within the spleen (sp) and bone marrow (BM) following adoptive transfer of mFcγRII KO B cells and mFcγRII KO/hCD20 B cells into mFcγRII KO and NoTIM recipients

A) mFcγRII KO B cells (non-targets) and mFcγRII KO/hCD20 B cells (targets) labelled with low and high CFSE respectively were adoptively transferred into mFcγRII KO and NoTIM recipients on Day 0. On Day 1 and Day 2 am, mice were treated with either 20 mg/kg of hFcγRIIB blocking mAb hIgG1 (6G), N297Q mutation (6Q), or isotype. 6 hours later, mice were treated with 2 mg/kg rituximab hIgG1 or isotype control (Irr) and then harvested on Day 3 to assess depletion of target cells. The detection of activatory mFcγR on key immune cells was then analysed in the spleen and bone marrow in mice to assess changes. Sp = spleen, BM = bone marrow. The result of 2 - 3 independent experiments (6 - 9 mice per group). Bar = mean ±SD. Statistical analyses conducted using a one-way ANOVA with Tukey's multiple comparison test. * = $P \leq 0.05$, ** = ≤ 0.01, *** = $P \leq 0.001$, **** = $P \leq 0.0001$.

4.4 Importance of hFcγRIIB on the depletion of other peripheral immune cells

To understand if these observations were unique to anti-CD20 mAb mediated depletion of B cells, a series of dose escalation experiments were designed to deplete other target cells with relevant mAbs. The depletion of CD19+, NK1.1+,CD8+ and CD25+ cells were assessed in mFcγRII KO, hFcγRIIB Tg and NoTIM mice.

4.4.1 CD19+ cell depletion

The depletion of CD19+ B cells was achieved by using the mAb clone 1D3 [329]. CD19 is a transmembrane glycoprotein found on B cells that positively regulates BCR signalling and is highly expressed on some lymphomas making it an attractive target for cancer mAb therapy [365]. It was hypothesised that depletion of CD19+ B cells would follow a similar pattern to CD20+ depletion. To identify B cells, mice were pre-bled and stained for CD20+/B220+, this was then established as the baseline percentage of B cells (100%).

In the pilot experiment, mFcγRII KO and NoTIM mice were treated intravenously with increasing doses of 1D3 mIgG1 (Figure 4.14 A). Two days after treatment with 50 μg 1D3 mIgG1 (D2), both NoTIM and mFcγRII KO mice showed little B cell depletion (2 - 8%). On Day 5, mice were subsequently treated with 100 μg and maximal depletion of 30% was seen in mFcγRII KO mice. A second dose of 100 μg mIgG1 given on Day 10 failed to increase depletion further. In an attempt to elicit more impressive depletion, two further doses of 50 μg and 200 μg of the mIgG2a subclass of 1D3 was given on Day 17 and Day 21. Having failed to see robust depletion, mice were treated with 250 μg of 18B12 mIgG2a on Day 27 to see if there was general resistance to B cell depletion. In most mice, there was near complete depletion of B cells. These data suggest that 1D3 is a poor depleting mAb and requires far larger doses to give significant target cell depletion.

To confirm this, the experiment was repeated using a bolus of 250 μg 1D3 mIgG2a given I.V. on Day 0 in mFcγRII KO, hFcγRIIB Tg and NoTIM mice (Figure 4.14 B). Over a period of a week, depletion was again poor with little differences between groups. To understand what was happening, seven days following treatment with mAb, blood was stained using a labelled mAb specific for mIgG (Figure 4.14 C). A second sample of blood from the same

mice was then stained with unlabelled 1D3 mIgG2a and subsequently with a labelled mAb specific for mIgG. This was to ascertain how much 1D3 mIgG2a was already pre-bound to cells in the blood and the total amount of CD19 on the cell surface that could be detected with 1D3. Mice treated with 1D3 showed little CD19 present on the cell surface. A treatment naïve mouse (UT) showed 3 fold higher level of cell surface expression of CD19 compared to those treated with 1D3. These data suggest that 1D3 mAb therapy results in the rapid internalisation of CD19, making 1D3 mAb therapy ineffective.

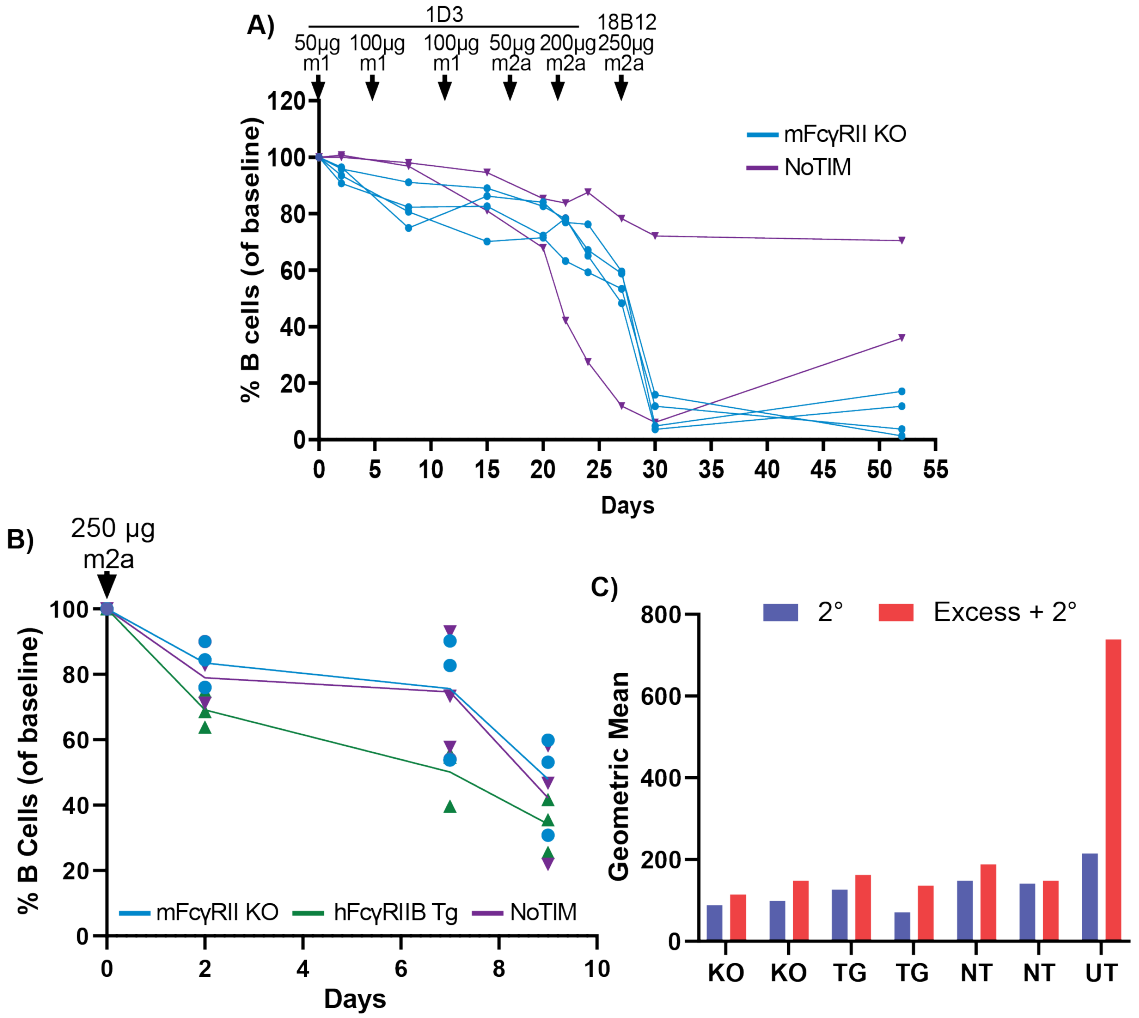

Figure 4.14: Depletion of CD19+ B cells in mFcγRII KO and NoTIM mice using 1D3 mIgG1 and mIgG2a
A) mFcγRII KO and NoTIM mice were pre-bled to establish the B cells (CD20+B220+) as a percentage of lymphocytes (100%) and then subsequently treated with increasing doses of 1D3 mIgG1 and mIgG2a via intravenous injection. Mice were bled in-between doses to ascertain the percentage of B cell depletion. B) mFcγRII KO, hFcγRIIB Tg and NoTIM mice were pre-bled to establish the B cells (CD20+B220+) as a percentage of lymphocytes (100%) and then subsequently treated with a bolus of 250 µg 1D3 mIgG2a via intravenous injection. Mice were bled to ascertain the percentage of B cell depletion. The result of one independent experiment (2 - 3 mice per group). Line = mean. C) Blood from mice treated with a bolus of 250 µg 1D3 mIgG2a was taken on Day 7 and stained using a labelled secondary mAb specific for mIgG. Blood was also incubated with excess 1D3 mIgG2a and then stained with the secondary mAb. Treated mice (KO, TG, NT) were then compared to an untreated mouse (UT).

4.4.2 NK1.1+ cell depletion

The mAb clone PK136 was next used to deplete NK1.1+ cells within the periphery, an antigen expressed on NK cells of C57BL/6J mice [331]. NK1.1 is thought to be involved in the regulation of NK cell function and is considered a good target for NK cell depletion [366]. Mice were pre-bled to establish the baseline NK cell percentages by identifying CD3-NKp46+ cells. Mice were then treated intravenously with 2 μg and then 10 μg of PK136 mIgG2a, with regular bleeding to ascertain NK cell depletion (Figure 4.15 A).

Two days after 2 μg of PK136, all mouse groups had a substantial decrease in NK cells, with mFcγRII KO mice displaying the biggest decrease (Figure 4.15 B). Over a two week period, NK cells slowly recovered, with hFcγRIIB Tg and NoTIM mice recovering at a faster rate than mFcγRII KO mice. After 10 μg of PK136 mIgG2a, all mice had a decrease in NK cells, with mFcγRII KO mice having the biggest drop. hFcγRIIB Tg and NoTIM mice had similar levels of NK cell depletion. At harvest on Day 21, NoTIM mice had the highest proportion of NK cells as a percentage of CD3-NKp46+ cells within the blood and iLN compared to other mouse models (Figure 4.15 C). However, NoTIM mice still showed significant depletion within the blood compared to untreated mice. In the spleen hFcγRIIB Tg mice had minimal depletion of NK cells compared to untreated mice, whilst NoTIM mice showed some depletion. In mFcγRII KO mice, NK cells were consistently depleted across all organs.

In summary, PK136 mIgG2a was shown to efficiently deplete NK cells at low doses, with mFcγRII KO being most susceptible to depletion with hFcγRIIB Tg and NoTIM having similar levels of inhibition, although the extent of this inhibition varied between tissues. These data suggest that hFcγRIIB mediated inhibitory signalling is not required for resistance to mAb mediated NK cell depletion.

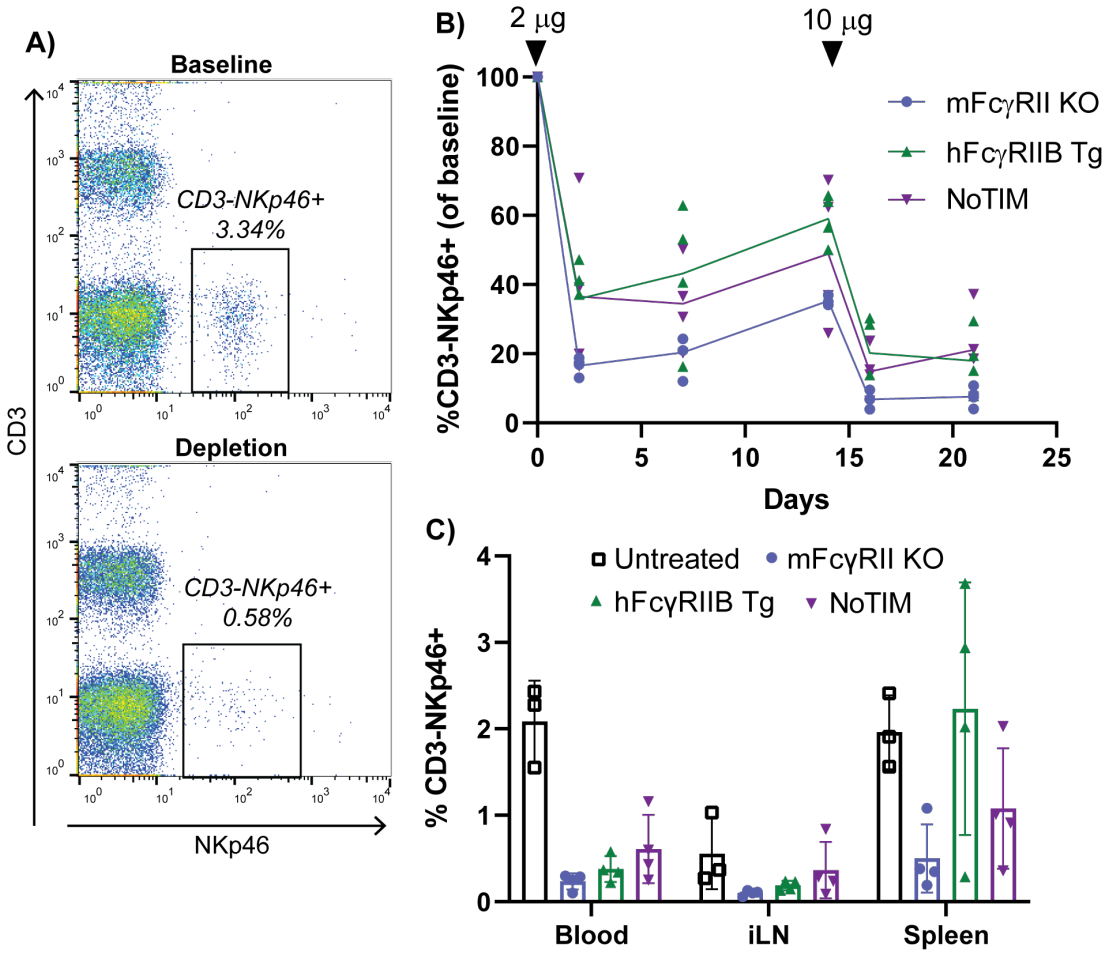

Figure 4.15: Depletion of NK1.1+ cells in mFcγRII KO, hFcγRIIB Tg and NoTIM mice using PK136 mIgG2a A) mFcγRII KO, hFcγRIIB Tg and NoTIM mice were pre-bled to establish baseline NK cells (CD3-NKp46+) as a percentage of lymphocytes (100%) and then subsequently treated with increasing doses of PK136 mIgG2a via intravenous injection. Mice were bled in-between doses to ascertain the percentage of NK cell depletion. B) The kinetics of depletion following treatment with 2 μg and 10 μg PK136 mIgG2a. The result of one independent experiment (4 mice per group). Line = mean. C) Mice were harvested on Day 21 and depletion was ascertained in the blood. inguinal lymph nodes (iLN) and spleen by comparing to untreated mice. Bar = mean ±SD.

4.4.3 CD8+ cell depletion

Next, depletion of CD8+ cells was evaluated. These cells were depleted using the mAb clone YTS169.4 [330]. CD8 acts as a co-receptor for the TCR on CTLs but can also be found on NK cells [367]. Mice were pre-bled to establish the baseline percentage of CD8+ cells by identifying CD3+CD4- negative cells (Figure 4.16 A). Mice were then treated intravenously with YTS169.4 mIgG1 or mIgG2a and were bled regularly to ascertain the kinetics of depletion.

In a pilot experiment, mFcγRII KO and NoTIM mice were treated with a 50 μg bolus of YTS169.4 mIgG1 (Figure 4.16 B). Surprisingly, strong depletion was observed in both

mouse models and nearly 60 days after treatment with mAb, CD8+ cells within the periphery had only recovered to a mean 40% of baseline. At the time it was hypothesised that the mIgG1 subclass may have driven an agonistic effect when bound to CD8, activating the cell and driving it out of the periphery and/or into activation-induced cell death. It was decided to repeat the experiment using the mIgG2a subclass and at much lower doses (Figure 4.16 C). mFcγRII KO, hFcγRIIB Tg and NoTIM mice were treated with 2 μg of mAb and bled two days later. Depletion was robust in all mouse models, with slightly more depletion on average in mFcγRII KO mice than the other groups. Mice were further treated with 10 μg of mAb on Day 14 and all groups experienced further strong depletion with little difference between strains. The experiment was repeated with FcR-γ-chain KO mice. These mice are deficient for the common γ-chain, critically required for the expression of activatory FcγRs. mAb therapy in these mice was ineffective, showing an absolute requirement for activatory FcγRs to elicit mAb mediated depletion of CD8 cells. These observations reduce the likelihood that the observed loss of CD8 cells was a result of a signalling phenomenon rather than effector cell depletion.

Mice were subsequently culled on Day 24 to examine depletion across blood, iLN and the spleen (Figure 4.16 D). Depletion was equal across the blood and spleen of each strain. NoTIM mice had slightly more CD8+ cells within the iLN than mFcγRII KO mice but this was non-significant (mean 12% vs 9%, respectively). γ-chain KO and untreated mice had high levels of CD8+ cells, showing that the other mouse models had robust depletion of CD8+ cells. Overall, it was concluded that YTS169.4 was a very effective depletor of CD8+ cells and made it difficult to see differences between mouse models whether they expressed an ITIM signalling functional or non-functional hFcγRIIB. Nevertheless in both hFcγRIIB Tg and NoTIM mice, peripheral deletion appeared equivalent and less effective than in the mFcγRII KO mouse at the 2 μg dose, supporting the observation that an hFcγRIIB without an ITIM is sufficient to impair target cell deletion.

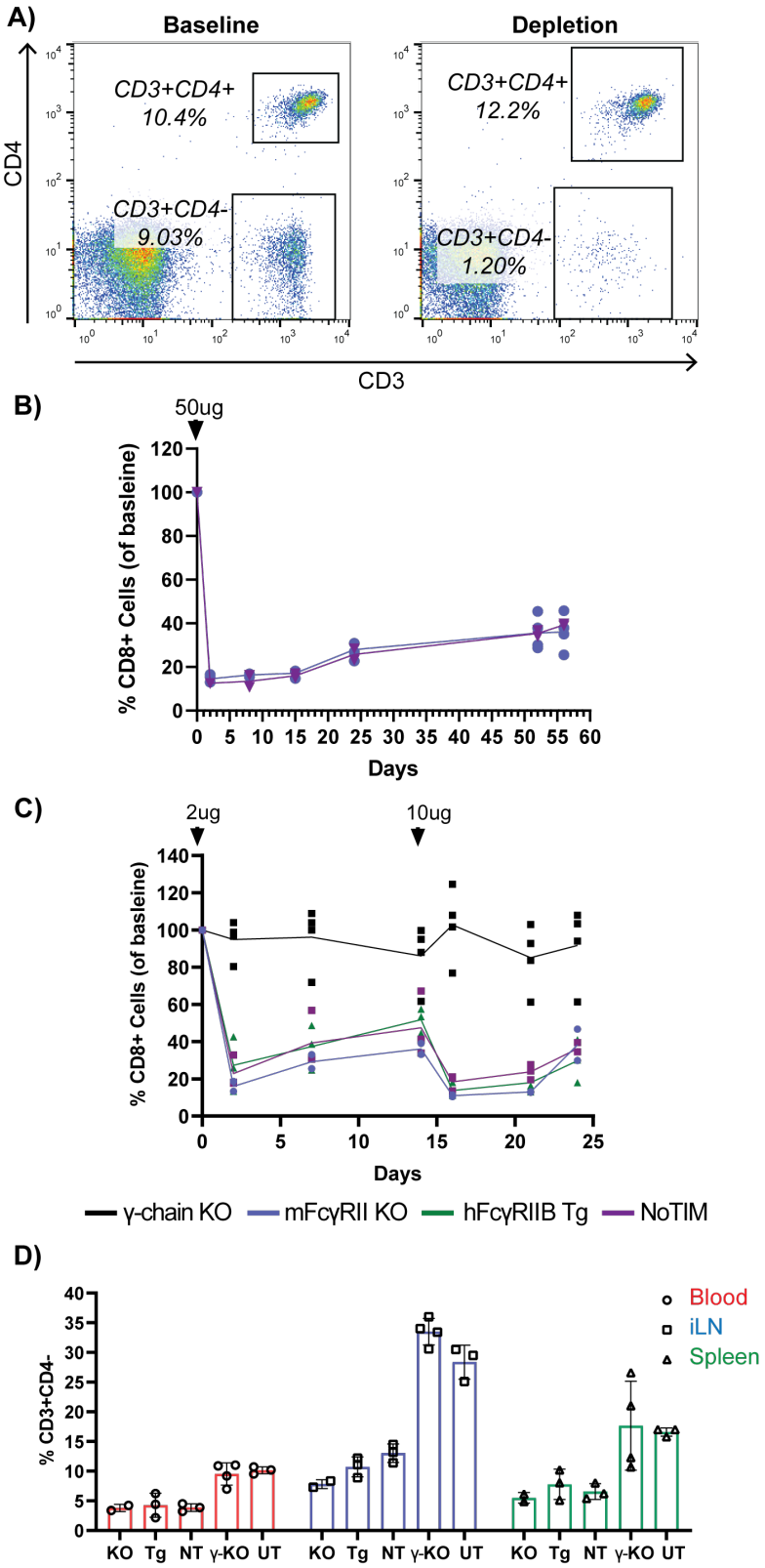

Figure 4.16: Depletion of CD8+ cells in mice using YTS169.4 mIgG1 and mIgG2a
A) γ-chain KO (γ-KO), mFcγRII KO (KO), hFcγRIIB Tg (Tg) and NoTIM (NT) mice were pre-bled to establish baseline CD8+ cells (CD3+CD4-) as a percentage of lymphocytes (100%) and then subsequently treated with YTS169.4 mIgG1 or mIgG2a via intravenous injection. Mice were bled doses to ascertain the percentage of CD3+CD4- cell depletion. B) The kinetics of depletion following treatment with 50 μg YTS169.4 mIgG1. The result of one independent experiment (2 - 3 mice per group). Lime = mean. C) The kinetics of depletion following treatment with 2 μg and 10 μg YTS169.4 mIgG2a. The result of one independent experiment (2 - 4 mice per group). Line = mean. D) Mice treated with YTS169.4 mIgG2a were harvested on Day 24 and depletion was ascertained in the blood, inguinal lymph nodes (iLN) and spleen by comparing to untreated mice (UT). Bar = mean ±SD.

4.4.4 CD25+ cell depletion

Next, depletion of T_{reg} cells was considered. The mAb PC61 binds to CD25, also known as the IL-2 receptor α-chain, a target that is found constitutively expressed on T_{reg} cells [332]. The depletion of T_{reg} cells is an active area of research and FcγRs have been shown to be critical for mAb-mediated depletion [368] [369]. Mice were treated with a bolus of 250 μg of rat (r)IgG1 PC61 or isotype control via intraperitoneal injection. The kinetics of T_{reg} depletion were then monitored over a week with a harvest conducted on Day 7 to look at depletion within the iLN and spleen (Figure 4.17 A). To identify T_{reg} cells, peripheral blood was stained for CD4+, CD8+ and the intracellular transcription factor FOXP3 (Figure 4.17 B).

mFcγRII KO, hFcγRIIB Tg and NoTIM mice experienced significant depletion of T_{reg} cells on Day 2, compared to isotype control (Figure 4.17 C). However between treatment groups, NoTIMs had significantly more peripheral T_{reg} cells remaining than hFcγRIIB Tg and mFcγRII KO mice. By Day 4, all treatment groups had a significant decrease in peripheral T_{reg} cells compared to isotype control whilst NoTIM mice still had significantly more T_{reg} cells than treated mFcγRII KO and hFcγRIIB Tg mice.

On Day 7, a harvest was conducted (Figure 4.17 C). Within the blood and spleen, all treatment groups were significantly depleted compared to isotype, whilst NoTIM mice had significantly more T_{reg} cells than mFcγRII KO mice. Within the iLN, all treatment groups had significant depletion of T_{reg} cells compared to isotype treated mice, with no significant difference between treatment groups. These experiments indicate that the non-signalling hFcγRIIB is able to inhibit direct targeting CD25 mAb depletion more effectively than the signalling competent hFcγRIIB.

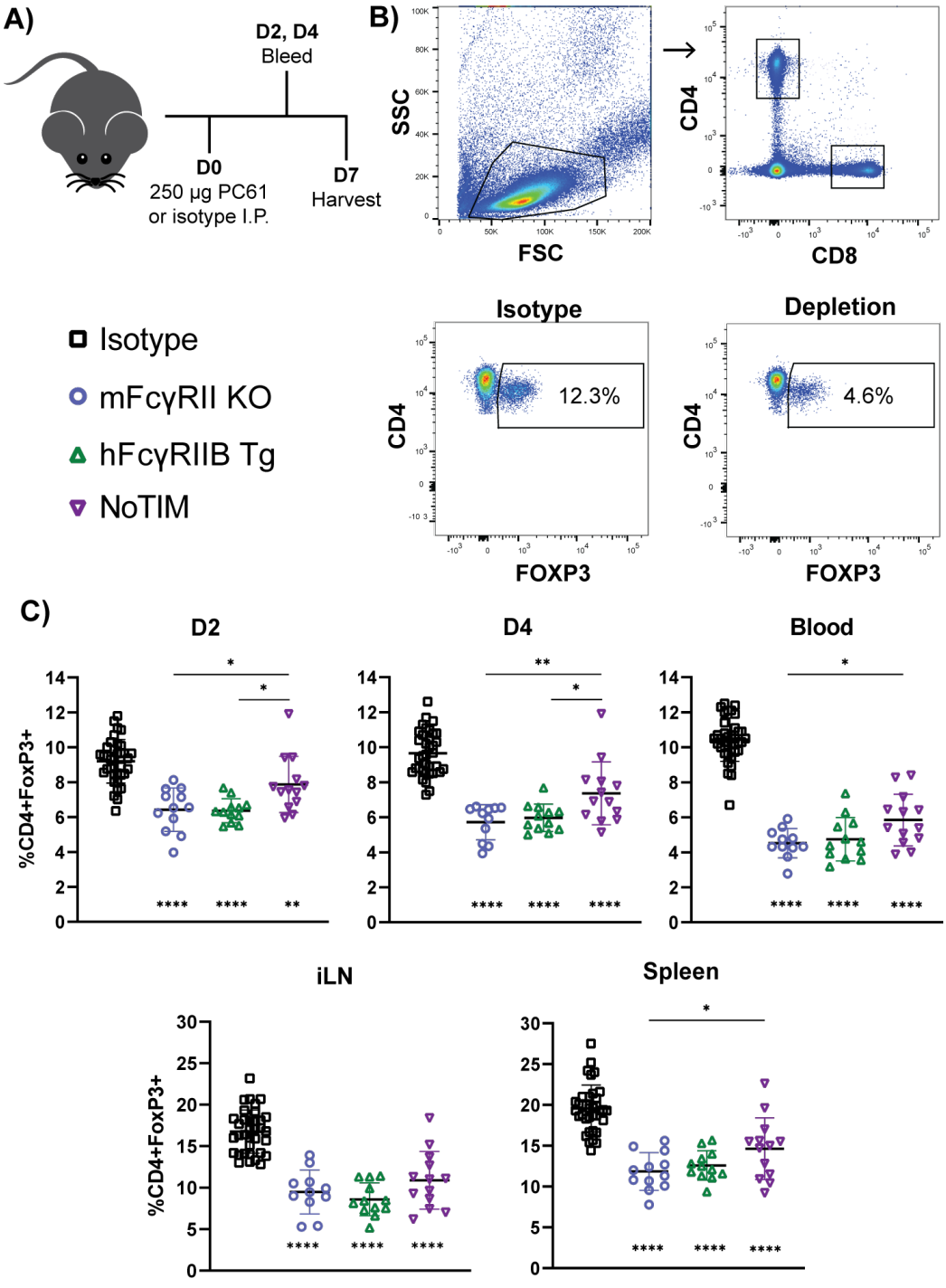

Figure 4.17: Depletion of CD25+ T regulatory cells in mice using PC61 rIgG1
A) mFcγRII KO, hFcγRIIB Tg and NoTIM mice were treated with an intraperitoneal bolus of 250 µg PC61 rIgG1 or isotype control (AT 107-2) and were bled over a week to monitor depletion of T_{reg} cells. B) T_{reg} cells were identified using flow cytometry based on CD4+ and FOXP3+ expression. C) The depletion kinetics of T_{reg} cells within the peripheral on Day 2 and Day 4, and at harvest on Day 7 within the blood, iLN and spleen. The result of three independent experiments (12 - 36 mice per group). Line = mean ±SD. Statistical analyses conducted using a one-way ANOVA with Tukey's multiple comparison test. * beneath mFcγRII KO, hFcγRIIB Tg and NoTIM mice denote significance between treatment groups and isotype treated mice. * above treatment groups denote significance between treated mouse models. * = $P \leq 0.05$, ** = ≤ 0.01, **** = $P \leq 0.0001$.

4.5 hFcγRIIB mediated mAb agonism of CD40+ cells

In the previous experiments documented in this chapter, it was demonstrated how hFcγRIIB elicits inhibition of direct targeting mAb therapy to various cell types and through different cell surface receptors. hFcγRIIB has also been shown to be critical for the agonistic activity of mAbs directed towards immunostimulatory targets such as those in the TNFR super family [308] [309] [145] [144]. These targets normally require receptor clustering to elicit signalling, a role typically reserved for the receptor's trimeric ligand. hFcγRIIB has been demonstrated to aid receptor clustering of mAbs directed against TNFR family members, by binding the Fc on the mAb to serve as a scaffold to mimic receptor clustering mediated by the ligand.

To investigate how the non-signalling hFcγRIIB expressed in the NoTIM mouse would perform this function, the OT-I adoptive transfer and OVA immunisation model was utilised in conjunction with the mAb clone 3/23, directed against mCD40 [370]. The OT-I transgenic mouse contains a transgenic TCR (Tcra-V2 and Tcrb-V5) found on CD8+ cells designed to recognise OVA residues 257-264 presented via MHC-I ($H2K^b$). Residues 257-264 form the well characterised SIINFEKL peptide. Splenocytes can be adoptively transferred from OT-I transgenic mice into C57BL/6J recipients in order to study the CD8+ T cell response to the model antigen OVA [336]. The OT-I model has commonly been used to study TNFR agonism as responses to OVA alone in the OT-I model are poor and require co-stimulation. Previous studies have demonstrated that CD40 agonism in the OT-I model via the mAb 3/23 was most effective as the mIgG1 subclass due to optimal interactions with mFcγRII, with little efficacy as a mIgG2a [308]. Therefore, 3/23 mIgG1 was utilised in this experiment for optimal target agonism.

In this experiment mFcγRII KO, hFcγRIIB Tg and NoTIM mice were adoptively transferred with OT-I cells. The following day they were administered 500 μg OVA with 100 μg 3/23 mIgG1 (or isotype control) and bled over a period of month to look for activation markers (CD62L low and CD44 high on endogenous CD8+ cells, CD23 expression on endogenous B cells) and OT-I expansion (Figure 4.18). OT-I specific cells can be identified using the SIINFEKL tetramer stain. The tetramer is a fluorescently labelled multimerised SIINFEKL-MHC complex designed to detect the TCR of OT-I cells [371]. Mice were then re-challenged with 50 μg OVA a month after the initial challenge to assess the secondary immune response.

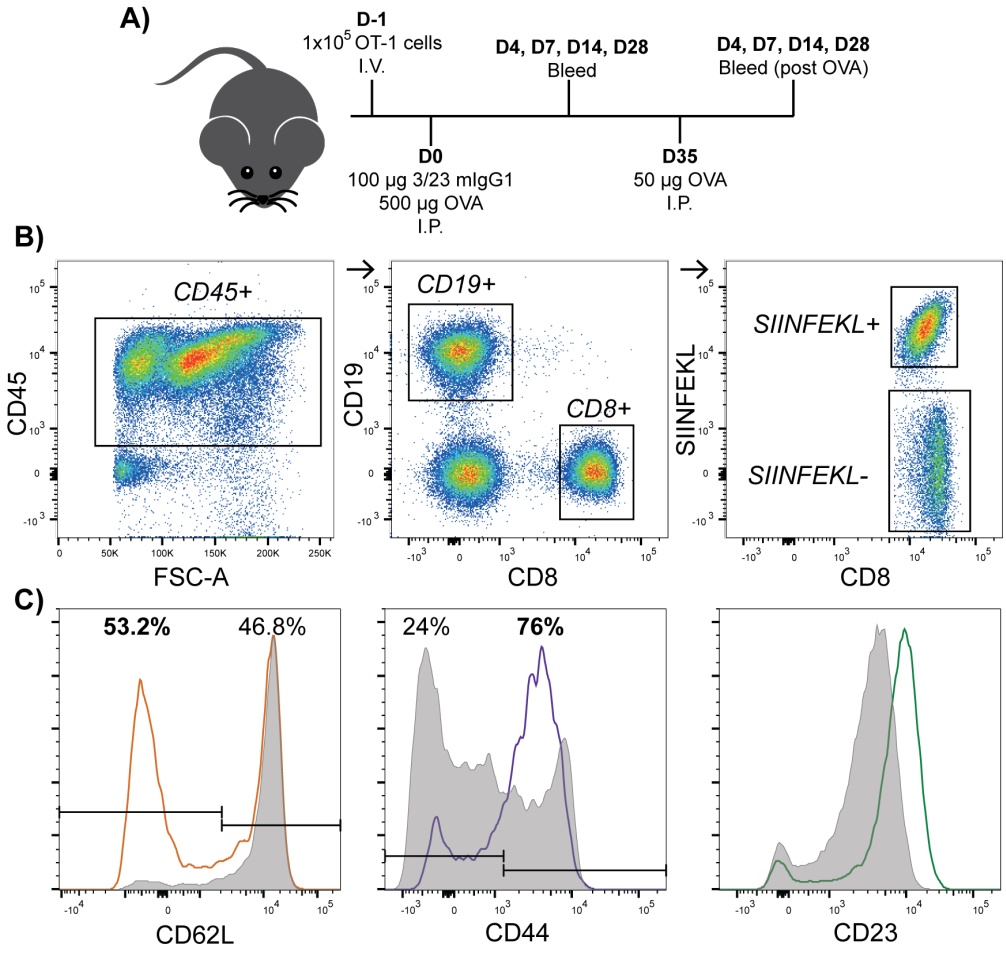

Figure 4.18: Experimental setup of the OT-I adoptive transfer with mCD40 agonism in mFcγRII KO, hFcγRIIB Tg and NoTIM mice

A) mFcγRII KO, hFcγRIIB Tg and NoTIM mice were adoptively transferred 1x10^5 OT-I cells via intravenous injection on Day -1. The following day (Day 0), mice were administered 100 µg 3/23 mIgG1 with 500 µg ovalbumin (OVA) via intraperitoneal injection and then bled over the space of a month to monitor OT-I responses. Approximately a month later (Day 35), mice were re-challenged with 50 µg OVA via intraperitoneal injection and bled over the course of the next month. B) Gating strategy used to identify B cells (CD45+/CD19+), endogenous CD8 cells (CD45+/CD8+/SIINFEKL-) and OT-I CD8 cells (CD45+/CD8+/SIINFEKL+). C) Example activation markers analysed on endogenous CD8 cells (CD62L low, CD44 high) and on B cells (expression of CD23) on Day 7. Grey = isotype treated NoTIM mouse, coloured line = NoTIM 3/23 treated mouse.

4.5.1 Kinetics of OT-I cell expansion

After the initial challenge with 500 µg OVA with 100 µg 3/23 mIgG1, hFcγRIIB Tg and NoTIM mice showed expansion of OT-I cells whilst mFcγRII KO showed little change in the OT-I population (Figure 4.19). During the primary response peak expansion was observed at Day 4 in mice treated with 3/23, with an average of 43% of OT-I cells (SIINFEKL+) as a percentage of CD8 cells in NoTIM mice. In hFcγRIIB Tg mice expansion was more limited at an average of 21.5% whilst mFcγRII KO had similar percentage OT-I as isotype control treated mice (average 1.9%). By Day 7, OT-I expansion began to drop, 3/23 treated NoTIM mice had an average 28% OT-I cells, whilst hFcγRIIB Tg had 8% with further

reductions by Day 14. However 3/23 treated NoTIM mice continued to have significantly higher percentage of OT-I cells compared to mFcγRII KO and hFcγRIIB Tg mice. These changes were also reflected in the absolute number of SIINFEKL cells (Figure 4.19 B).

Following secondary re-challenge with 50 μg OVA, 3/23 treated mice showed an expanded population of OT-I cells that was not as acute as during the primary challenge (Figure 4.19). On Day 4, 3/23 treated NoTIM mice displayed an average of 10% OT-I cells as a percentage of CD8s whilst hFcγRIIB Tg mice had 2.5%. 3/23 treated mFcγRII KO mice continued to show no change compared to isotype control (average 0.4%). By Day 7, both hFcγRIIB Tg and NoTIM mice treated with 3/23 peaked in their percentage of OT-I cells with an average of 5.4% and 12.3%, respectively. By Day 28, 3/23 treated NoTIM mice continued to maintain a significant percentage of OT-I cells compared to hFcγRIIB Tg and mFcγRII KO treated mice with an average 5.8% compared to 1.4% and 0.5%, respectively. These changes were also reflected in absolute cell number of SIINFEKL cells (Figure 4.19 B).

These data demonstrate that 3/23 mIgG1 driven agonism leading to OT-I expansion was strongest in NoTIM mice, intermediate in hFcγRIIB Tg mice and absent in mFcγRII KO mice. Together, these data supports that the expression of hFcγRIIB alone is required for a response, with ITIM signalling redundant.

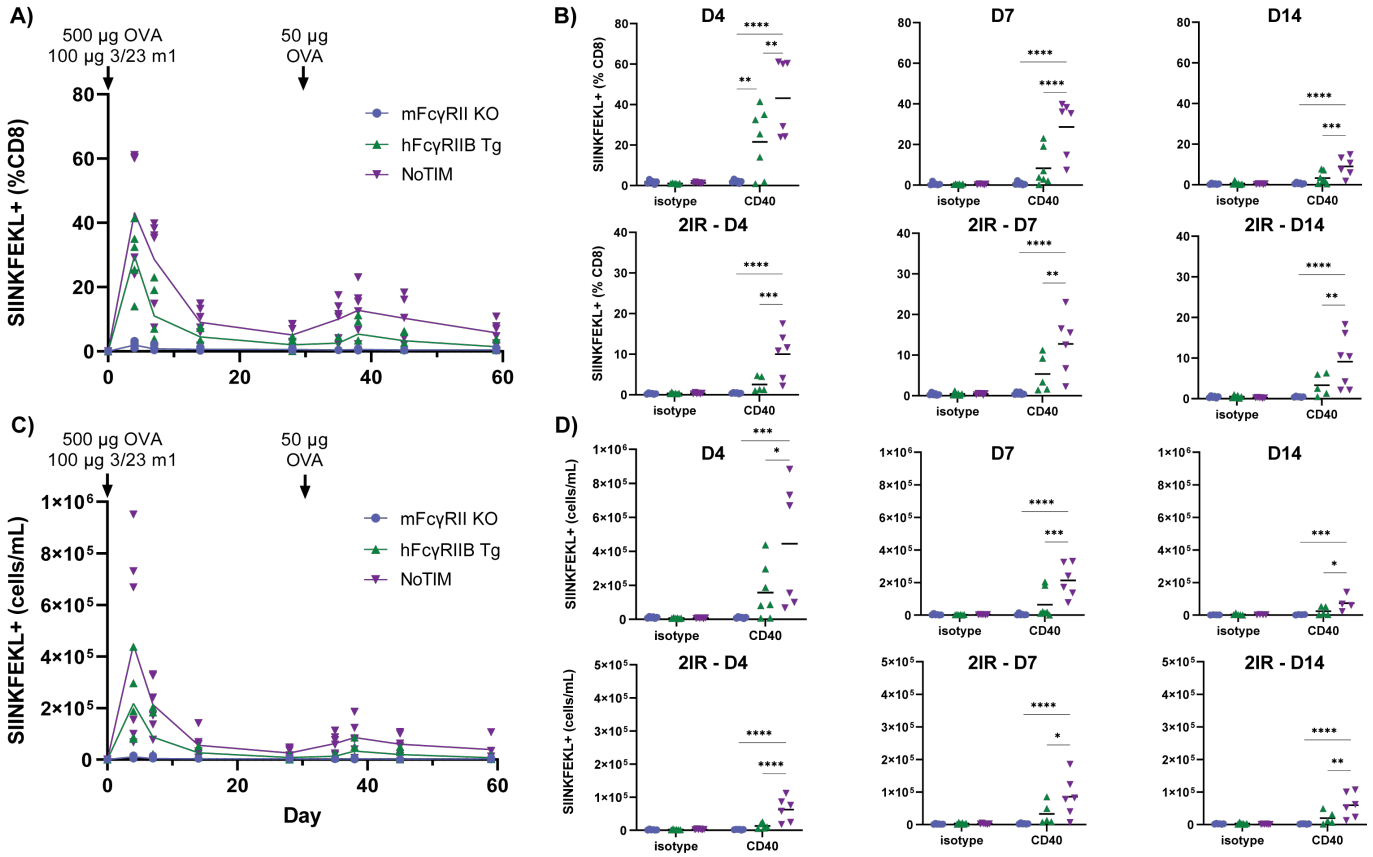

Figure 4.19: The kinetics of OT-I cell expansion in mFcγRII KO, hFcγRIIB Tg and NoTIM mice treated with 3/23 mIgG1 or isotype control

A) mFcγRII KO, hFcγRIIB Tg and NoTIM mice were adoptively transferred 1x10^5 OT-I cells via intravenous injection on Day -1. The following day (Day 0), mice were administered 100 µg 3/23 mIgG1 (or isotype control) with 500 µg ovalbumin (OVA) via intraperitoneal injection and then bled over the space of a month to monitor OT-I responses. On Day 35, mice were re-challenged with 50 µg OVA via intraperitoneal injection and bled over the course of the next month. B) The kinetics of OT-I (CD8+SIINFEKL+) expansion as a percentage of CD8 cells in the blood as determined by flow cytometry during the primary immune response (D4, D7, D14) and secondary immune response (2IR - D4, 2IR - D7, 2IR - D14). C) The kinetics of OT-I expansion as absolute number of CD8+SIINFEKL+ cells during the primary immune response and secondary immune response (2IR). D) The kinetics of OT-I expansion as absolute number of CD8+SIINFEKL+ cells during the primary immune response and secondary immune response. The result of two independent experiments (5 - 7 mice per group). Line = mean. Statistical analyses conducted using a one-way ANOVA with Tukey's multiple comparison test. * = P $\leq$ 0.05, ** = $\leq$ 0.01, *** = P $\leq$ 0.001, **** = P $\leq$ 0.0001.

4.5.2 Activation markers on endogenous CD8+ cells and B cells

The adoptively transferred OT-I T cells might be considered an artificial way to measure immune agonism. Therefore to additionally assess how CD40 agonism was influenced in the different models, the percentage of CD44 high and CD62L low CD8+ cells and CD23+ B cells were analysed. Typically these markers are used to denote CD8+ cell activation and the formation of the CD44 high CD62L low population indicates the development of a central memory T cell compartment. CD23 is a marker upregulated on activated B cells and gives an indication of the formation of a B cell memory response.

The data indicates that these activation markers were upregulated on endogenous cells at Day 7, with no differences indicated on Day 4, Day 14 or any other day during the primary or secondary immune response (Figure 4.20). NoTIM mice treated with 3/23 showed a significantly higher percentage of CD62L low and CD44 high endogenous CD8+ cells compared to hFcγRIIB Tg and mFcγRII KO treated mice. The geometric mean of CD23 was also significantly higher on B cells in NoTIM mice compared to other 3/23 treated mice.

These data indicate that as seen with OT-I cell expansion, CD40 mediated cellular activation was most efficacious in NoTIM mice (activation markers were highest in these mice). This supports the finding that high levels of hFcγRIIB expression are required for optimal agonism of CD40 mAbs and ITIM signalling is not required.

4.5.3 IgG response to ovalbumin challenge with CD40 agonism

Following the assessment of increased activation of CD8+ and B cells, it was decided to analyse the functional B cell response through assessment of anti-OVA IgG in the different strains. The IgG response was relatively low during the primary immune response however was stronger following secondary re-challenge (Figure 4.21). During the primary response, anti-OVA IgG was detected at a maximum of 8.5 μg/mL in 3/23 treated hFcγRIIB Tg mice on Day 14. On average, hFcγRIIB Tg had significantly more anti-OVA IgG than mFcγRII KO and NoTIM treated mice, however these levels remained low. Following re-challenge with OVA, the anti-OVA IgG response showed no change on Day 4 but peaked at Day 7 in mice treated with 3/23. NoTIM mice had the biggest average IgG response with a mean of 50 μg/mL, this was significantly more than mFcγRII KO mice and

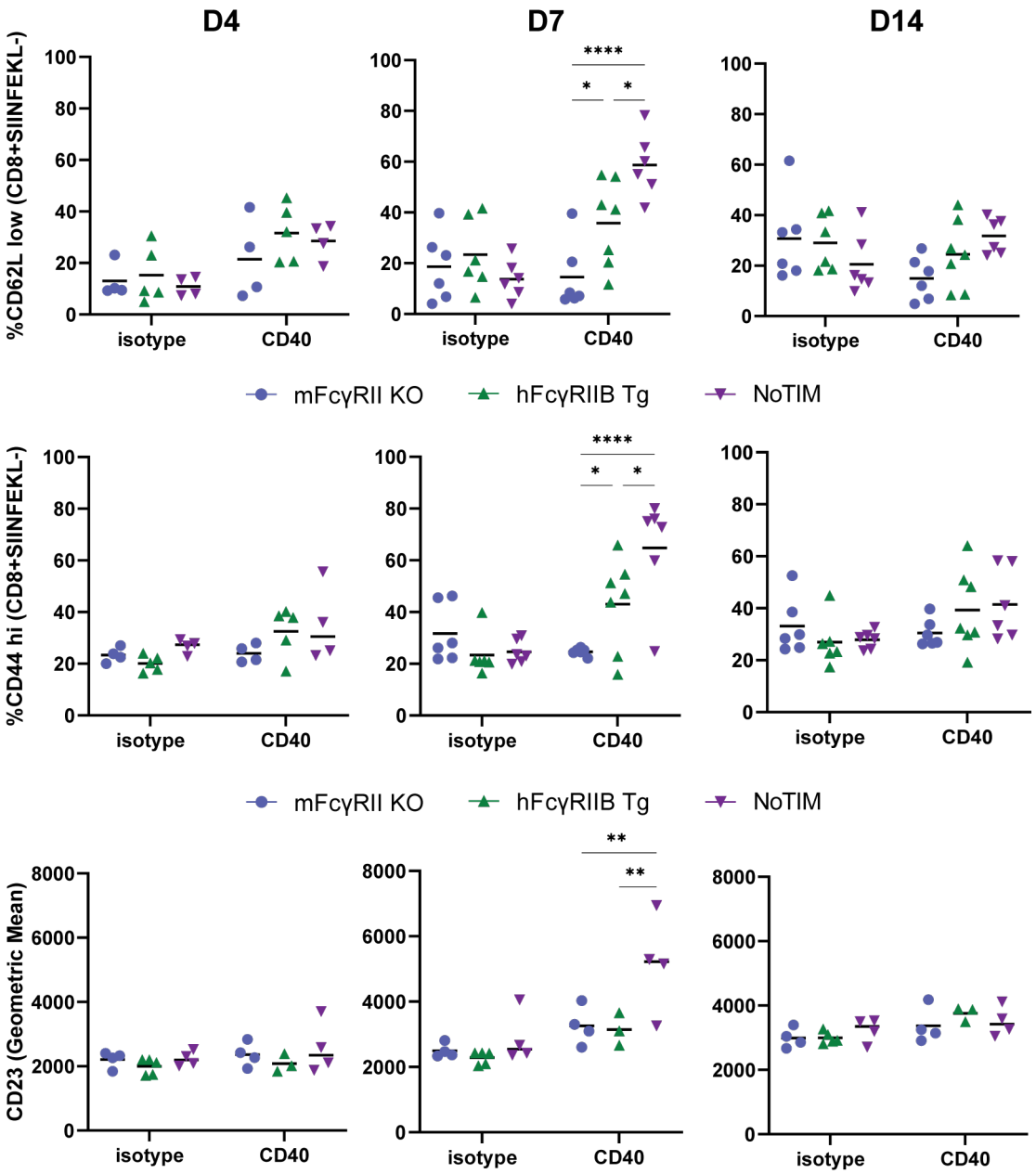

Figure 4.20: The change in activation markers on endogenous CD8+ cells and B cells in mFcγRII KO, hFcγRIIB Tg and NoTIM in mice treated with 3/23 mIgG1 during the primary immune response

mFcγRII KO, hFcγRIIB Tg and NoTIM mice were adoptively transferred 1x10^5 OT-I cells via intravenous injection on Day -1. The following day (Day 0), mice were administered 100 μg 3/23 mIgG1 with 500 μg ovalbumin (OVA) via intraperitoneal injection and then bled over the space of a month to monitor OT-I responses. On Day 35, mice were re-challenged with 50 μg OVA via intraperitoneal injection and bled over the course of the next month. The percentage of CD62L low and CD44 high endogenous CD8+ T cells and the geometric mean of CD23 on B cells were assessed during the primary immune response (D4, D7, D14). The result of one - two independent experiments (3 - 7 mice per group). Line = mean. Statistical analyses conducted using a one-way ANOVA with Tukey's multiple comparison test. * = $P \leq 0.05$, ** = ≤ 0.01, *** = $P \leq 0.001$, **** = $P \leq 0.0001$.

a modest increase over hFcγRIIB Tg mice. NoTIM mice continued to show an increased concentration of anti-OVA IgG on Day 14, although statistical significance was lost. This data suggests that more potent CD40 agonism seen in NoTIM mice correlates with an enhanced anti-OVA IgG response following secondary re-challenge.

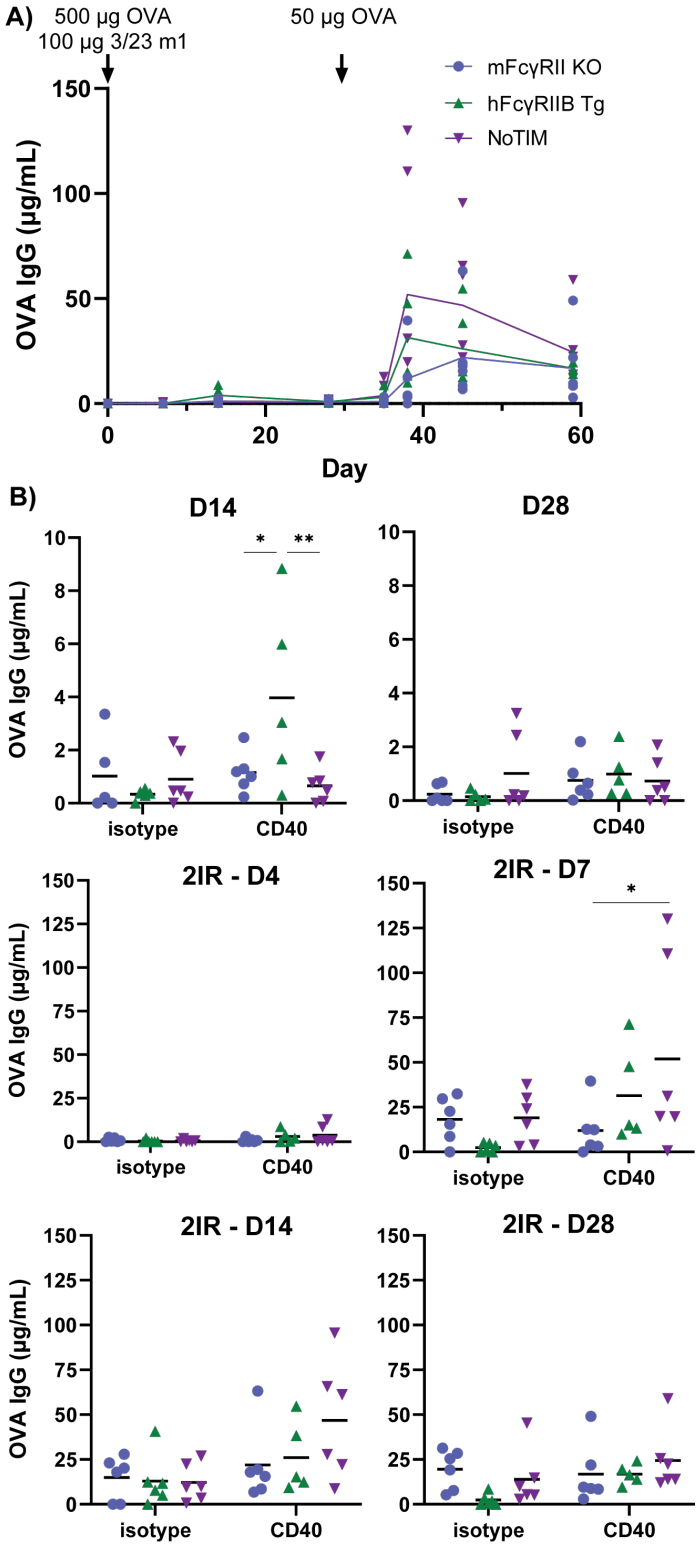

Figure 4.21: The kinetics of anti-OVA IgG production in mFcγRII KO, hFcγRIIB Tg and NoTIM mice treated with 3/23 mIgG1

mFcγRII KO, hFcγRIIB Tg and NoTIM mice were adoptively transferred 1x10^5 OT-I cells via intravenous injection on Day -1. The following day (Day 0), mice were administered 100 µg 3/23 mIgG1 with 500 µg ovalbumin (OVA) via intraperitoneal injection and then bled over the space of a month to monitor OT-I responses. On Day 35, mice were re-challenged with 50 µg OVA via intraperitoneal injection and bled over the course of the next month. A) The kinetics of the anti-OVA IgG response in mice treated with 3/23 mIgG1. B) The anti-OVA IgG response in mice treated with isotype control or 3/23 mIgG1 in the primary immune response (D14, D28) and the secondary immune response (2IR - D4, 2IR - D7, 2IR - D14, 2IR - D28). The result of two independent experiments (5 - 7 mice per group). Line = mean. Statistical analyses conducted using a one-way ANOVA with Tukey's multiple comparison test. * = P $\leq$ 0.05, ** = $\leq$ 0.01, *** = P $\leq$ 0.001, **** = P $\leq$ 0.0001.

4.6 Discussion

Characterisation of cells and tissues from the NoTIM mouse in the previous chapter showed that the loss of hFcγRIIB mediated ITIM signalling resulted in enhanced activatory functions such as BCR signalling and ADCP. Therefore it was assumed that *in vivo*, the NoTIM model would show increased mAb-mediated effector functions that are typically impaired by ITIM signalling. Surprisingly, the data in this chapter has shown that the NoTIM hFcγRIIB in fact elicits more inhibition of direct targeting mAb activity than the signalling competent hFcγRIIB. This effect was most pronounced when looking at the depletion of CD20+ B cells using both the mIgG1 and mIgG2a subclass. Further experiments suggested that differences in depletion seen within the mice models was not due to differences in internalisation of the mAb 18B12, nor due to differences in the pharmacokinetics *in vivo*. Instead, the data suggests that inhibition is driven by the level of hFcγRIIB expression; the higher the expression level the more inhibition was seen when depleting using 18B12. To ascertain if inhibition was driven by expression of hFcγRIIB on the target cells or on the immune effector cells, a series of adoptive B cell transfer experiments were performed that indicated that inhibition is driven through expression on the effector cell population.

On these cells, an Fc-inert but not Fc-competent anti-hFcγRIIB mAb was able to reverse the inhibition, indicating that Fc-engagement of target mAb by hFcγRIIB but not hFcγRIIB ITIM signalling is important for suppression of target cell deletion. As such, inhibition is believed to be driven through competition with activatory mFcγRs for the mAb Fc, rather than ITIM mediated signalling. To determine if this observation was applicable to targets beyond CD20 and B cells, the depletion of other cell targets was assessed. Depletion of peripheral immune cells was in general very effective (NK cells and CD8 T cells) making it difficult to observe differences between strains. However, even in these models both the hFcγRIIB Tg and NoTIM models showed signs of inhibition of depletion compared to mice lacking the mFcγRII, at low doses of depleting mAb, despite differences in ITIM status, supporting the hypothesis. Moreover, depletion of CD25+ T_{reg} cells was found to be least effective in NoTIM mice showing that inhibition of direct targeting mAb therapy is independent of ITIM signalling for multiple cell types and receptor targets. Finally, the signalling independent effect of mAb-target agonism was assessed in NoTIM mice using the anti-CD40 mAb, 3/23. These experiments showed that the high expression of the

non-signalling hFcγRIIB in NoTIM mice elicited potent target cell agonism and robust OT-I expansion (at higher levels than the signalling competent hFcγRIIB Tg mouse).

The 18B12 dose escalation experiments were designed to assess subtleties in the inhibition of direct targeting mAb therapy. B cells form the biggest lymphocyte population within the periphery and so incremental doses could be administered that would not deplete all cells [372]. From the administration of 10 μg 18B12 mIgG1, it was clear the depletion of B cells in NoTIM mice were significantly inhibited compared to mFcγRII KO mice (Figure 4.2). This observation held throughout the experiments with increasing antibody doses. As expected, depletion in mFcγRII KO was the most effective - several papers have indicated that direct targeting mAbs are more efficacious in this mouse model [233] [185] [248]. C57BL/6J mice showed resistance to B cell depletion due to the presence of mFcγRII, however 50 μg of 18B12 mIgG1 overcame this inhibition. hFcγRIIB Tg mice on average had depletion similar to C57BL/6J mice. However, when evaluating individual mice there was a consistent split in the data. Some mice had a depletion profile akin to NoTIM mice and some had a depletion profile akin to mFcγRII KO mice. Further analysis found a correlation between expression levels and 18B12 mediated depletion, the higher the hFcγRIIB transgene expression and/or the intensity of expression the more resistant B cells were to mAb mediated depletion (Figure 4.9).

These findings bear resemblance to how the signalling neutral hFcγRIIIB is thought to inhibit direct targeting mAb therapy. Treffers et al. showed that neutrophil mediated ADCC of anti-HER2 or anti-EGFR mAbs was impaired by hFcγRIIIB expression. The authors found that inhibition was elicited through competition with the activatory hFcγRIIA, and that increasing the copy number of hFcγRIIIB increased the level of inhibition [234]. Competition is a common theme observed in IgG:FcγR biology, for example immune complexes can compete with monomeric IgG to decrease FcγR mediated effector functions [373]. IgG subclasses and molecules also compete with each other for binding to FcRn, for example the poor half life of hIgG3 has been attributed to being out-competed (due to the higher affinity of hIgG1) [374]. Both of these observations act to regulate the immune response, serving to increase the threshold required for activation. Therefore, competition is an important inhibitory mechanism of FcγR activation. Taken together, it can be inferred that the major mechanism of hFcγRIIB mediated inhibition of direct targeting mAbs is driven by the expression level and subsequent competition with activatory FcγRs.

The dose escalation experiments were repeated using 18B12 mIgG2a to assess if the

increased affinity for activatory mFcγRs could overcome hFcγRIIB mediated inhibition (Figure 4.4). Depletion following each mAb dose was rapid, with a notable reduction in B cells across each mouse model. However, NoTIM mice showed less depletion and a faster recovery consistently across the experiments. This is most likely due to the high expression of hFcγRIIB in NoTIM mice. As with mIgG1, the receptor is likely to out-compete activatory mFcγRs for Fc binding, overcoming the increased affinity of the mIgG2a subclass for activatory mFcγRs and suppressing activatory effector functions. C57BL/6J mice were more susceptible to depletion using mIgG2a, from 10 μg mAb doses onward, the depletion kinetics were very similar to those in mFcγRII KO. A pilot receptor quantification experiment (data not shown) suggested mFcγRII in C57BL/6J mice is expressed to a lower extent than hFcγRIIB in NoTIM mice on splenic B cells and macrophages. Kerntke et al. has quantified FcγR expression on key cell types in mice and humans, finding that expression of hFcγRIIB on human B cells is nearly 3 fold higher than mFcγRII on murine B cells [192]. In-direct findings from the depletion experiments suggest that the increased resistance to mAb mediated depletion is due to expression, and it can be inferred that lower expression of mFcγRII (compared to hFcγRIIB in transgenic mice) and the high affinity of the mIgG2a subclass for activatory mFcγRs results in less mFcγRII mediated inhibition. hFcγRIIB Tg mice treated with 18B12 mIgG2a also had mice who responded well to mAb depletion and those who did not respond. However the differences between 'responders' and 'non-responders' were much smaller than observed in the mIgG1 experiment (Figure 4.9). Similarly to C57BL/6J mice, it can be inferred that the lowered expression level of hFcγRIIB in hFcγRIIB Tg mice is out-competed by mIgG2a binding to activatory mFcγRs, resulting in less profound inhibition of depletion.

The depletion of B cells within the spleen and iLN was similar across the mIgG1 and mIgG2a experiments. In both cases, NoTIM mice had most resistance to B cell depletion whilst mFcγRII KO mice were most susceptible. Unexpectedly, C57BL/6J mice had strong depletion in the spleen and iLN when treated with mIgG1 but not mIgG2a. The reason for this is unaccounted for, but perhaps reflects biological variation in this experiment. It is of note that C57BL/6J mice treated with 18B12 mIgG1 were treated at a separate time to mFcγRII KO, hFcγRIIB Tg and NoTIM mice - a difference in immune activation could result in this observation. It was also observed that there was little difference in B cell depletion between experiments in both the spleens and iLN of mIgG1 and mIgG2a treated mice. The reasons for this could be due to the presence of a CD20- population in both iLN and the spleen that would not be depleted by 18B12 [375]. To investigate further,

the un-depleted B cell population could be phenotyped to look for CD20 expression, and a harvest could be taken at an earlier time point to account for recovery.

Whilst the data indicates inhibition is driven by competition, it was important to rule out other potential factors. Type-I hCD20 mAbs have been shown to undergo hFcγRIIB enhanced internalisation (antibody bipolar bridging) and this has been shown to decrease mAb efficacy [299] [301] [300]. Therefore, internalisation of 18B12 was an important route of investigation. The data showed that 18B12 underwent internalisation over a 24 hour time period, however the percentage of internalisation was relatively low and not significantly different between the mouse models. The data showed the presence of either mFcγRII or hFcγRIIB does increased internalisation compared to mFcγRII KO B cells, however this appeared independent of expression level as indicated by the lack of variation within groups from different mice. Studies using rituximab (type-I) mAb over a 6 hour time period on CLL cells showed an internalisation percentage of 60%, whilst tositumomab (type-II) only internalised 20% [299]. Based on these observations, 18B12 seems to have the internalisation kinetics more akin to a type-II CD20 mAb. Type-I mAbs have been linked to worsened survival outcomes in lymphoma patients; those with high expression of hFcγRIIB had lowered survival outcomes when treated with rituximab potentially driven by hFcγRIIB mediated internalisation. In contrast, treatment with obinutuzumab (type-II mAb) there was no correlation with survival [302]. Therefore, 18B12 being closer to a type-II mAb and the lack of differences in internalisation between mouse models suggests that it is most likely not responsible for the impaired depletion in NoTIM mice.

hFcγRIIB has also been shown to have the potential to have an impact on mAb pharmacokinetics *in vivo* [364] [272]. Therefore the kinetics of B cell depletion and pharmacokinetic properties of 18B12 mIgG1 was investigated (Figure 4.7, Figure 4.8). As seen in the dose escalation experiments, NoTIM mice were most resistant to B cell depletion and mFcγRII KO most susceptible. Interestingly at the 1 hour time point, depletion was dynamic in each mouse model with differences only becoming evident at 6 hours. This suggests in the first hour that 18B12 binds to the available targets in the periphery and its Fc interactions with activatory FcγRs are not limited, allowing efficient depletion across all mice. By 6 hours, there was a decrease in 18B12 concentration, potentially resulting in more limited 18B12 Fc availability increasing competition between hFcγRIIB and activatory mFcγRs, limiting depletion.

These observations fit with the expected pharmacokinetic profile of mAb elimination. The

rapid distribution phase shows a substantial drop in mAb serum concentration that is attributed to the rapid distribution of mAb to tissues and interstitial fluid. The second phase is known as the slow elimination phase. Figure 4.7 demonstrates a linear elimination phase suggesting that the targets are saturated with mAb throughout the experiment (a non-linear phase is attributed to sub-optimal target saturation) [376]. Murine B cells *ex vivo* were found to saturate binding sites for 18B12 at 2.5 μg/mL and serum mAb concentration did not drop below this level for the whole experiment, further supporting these findings (Figure 4.7, Figure 4.8). Furthermore, the V_z was also equal between mouse models suggesting that target cells across mice were likely to be equally opsonised (Figure 4.8). This suggests that mAb-target availability is most likely not responsible for differences in depletion between mouse models. Other assessed parameters showed little differences between mouse models. The $t_{1/2}$ suggested that mFcγRII KO mice had a modest increase in this parameter compared to other mouse models, however the differences were small and unlikely to impact efficacy. The $AUC_{0\text{-}t}$ and CL parameters also suggested a slower rate of clearance within mFcγRII KO but this was deemed to not be of significance, with a > two fold difference suggested to impact mAb efficacy and this is not the case (personal communications with pharmacokinetics analysts at GSK).

Across the experiment, C57BL/6J, hFcγRIIB Tg and NoTIM mice consistently had less 18B12 in the serum than mFcγRII KO mice. As seen in the B cell internalisation experiments, it seems the presence of any inhibitory FcγR reduces peripheral 18B12 mIgG1. This agrees with published data - An experiment looking at the contribution of murine FcγRs to mAb half-life found that knocking out mFcγRII had a minor effect on mAb elimination but was not thought to be a major mechanism [377]. Despite the differences in the sensitivity of depletion, C57BL/6J and NoTIM mice have a similar concentration of 18B12 throughout the experiment, supporting that mAb consumption was not the reason for decreased B cell depletion. When 18B12 concentration was correlated with depletion at key time points, it was clear there was no obvious relationship (Figure 4.8). Because the inhibitory FcγR results in decreased serum concentration of 18B12 mIgG1, it was hypothesised that LSECs may be responsible. LSECs have been implicated in the regulation of SICs such as small antigens (e.g. OVA) and opsonised viral particles (e.g. HIV) [242] [272]. However, given the size of opsonised B cells, LSECs are unlikely to interact with target cells. The major mechanism of mAb clearance is linked to non-specific processes such as endocytosis and proteolysis. It is thought the specific FcγR-mediated elimination pathway does not impact mAb pharmacokinetics in isolation [378].

The half-life was also assessed for correlation with the geometric mean of hFcγRIIB (Figure 4.8). These data suggests the relationship is weak and unlikely to contribute to the efficacy of 18B12 mediated B cell depletion. To further interrogate the differences in pharmacokinetic parameters, a longer sampling schedule with more data points and mice would provide further confidence in the measured parameters. Further n numbers would allow for individual mouse variability and tightly controlling weight, sex and age of mice would reduce noise within the data. Unfortunately due to Home Office license bleeding restrictions, it would not be possible to increase the number of blood sampling time points per mouse; rather larger cohorts of mice spread across the time-points would be required.

To understand if inhibition of B cell depletion was directed by hFcγRIIB expression on target B cells or immune effector cells, an adoptive transfer system was utilised (Figure 4.10). The first set of experiments showed that hFcγRIIB on the target cells was not responsible for inhibition (Figure 4.11). Targeting hCD20/NoTIM B cells was highly efficient using rituximab as a monotherapy with even greater depletion seen using an Fc functional direct targeting mAb against hFcγRIIB (6G). The increased efficacy with 6G was most likely due to the higher level of target expression.

Antigen density has been shown previously to be an important factor in determining mAb activity. Studies looking at neutralising mAbs against gp120 on HIV found that those with lower affinity showed better binding kinetics when antigen density was increased [379]. Further to this, Bar et al. specifically looked at CD20 density and rituximab on a molecular scale, and found a moderate density of 46 pmol.cm^{-2} displayed the strongest mAb avidity and slowest dissociation rate. If CD20 concentration was lowered (2.8 pmol.cm^{-2}), or increased (85 pmol.cm^{-2}), avidity was decreased due to the loss of efficient bivalent F(ab')$_2$ binding [380]. These data indicate increases in target antigen density can improve mAb avidity but that there are limits. However, currently most biological evidence *in vitro* and *ex vivo* suggests that increasing CD20 molecule density correlates with enhanced CDC activity using hCD20 mAbs [381] [382]. An increase in antigen density has also been found to correlate with other targets; Temming et al. found that increasing the antigen density of opsonised RBCs resulted increased NK cell mediated ADCC [383].

Roghanian et al. utilised a similar adoptive B cell transfer model, and found that 6G alone could deplete hFcγRIIB expressing B cells as a monotherapy in the hFcγRIIB Tg mouse [323]. In those studies, depletion of hFcγRIIB Tg B cells was found to be as effective as rituximab, whereas here depletion of NoTIM expressing B cells found 6G to be more

effective than rituximab. It is likely that depletion of NoTIM/hCD20 B cells was more effective due to the higher expression of the NoTIM transgene compared to the hFcγRIIB Tg transgene. Taken together, these data highlight how antigen density influences target depletion. 6Q, the Fc null hFcγRIIB specific mAb did not elicit depletion of the NoTIM expressing B cells or augment rituximab therapy in the adoptive B cell transfer model. This suggests that in this short-term experiment, hFcγRIIB mediated internalisation of rituximab was not sufficient to reduce the efficacy of the mAb (also supporting the type II nature of 18B12).

In the reverse experiment, where the NoTIM was expressed only on the effectors and not target cells, hFcγRIIB expression on immune effector cells demonstrated inhibition of target cell depletion (Figure 4.12). In contrast to the previous model, the addition of the hIgG1 direct targeting mAb against hFcγRIIB (6G) did not improve rituximab efficacy, whereas the Fc null variant 6Q did. In a similar experimental setup Roghanian et al., showed that both 6G and 6Q were effective in depleting endogenous murine B cells that express hCD20 and hFcγRIIB Tg. In that model both the target and effector cell populations express the signalling competent hFcγRIIB, so 6G and 6Q are able to elicit dual mechanisms of action (depletion and target blockade) to achieve therapy [323]. In the experiments in this thesis, the non-signalling NoTIM receptor equally elicits inhibition of target cell depletion, and this is only over come through receptor blockade. Taken together, these data suggests that hFcγRIIB inhibition of mAb-mediated cell depletion is independent of ITIM signalling.

Analysis of FcγR occupancy helped provide an alternative mechanism. Although 6G could effectively block hFcγRIIB, the detection of activatory mFcγRs on several key immune effector cells was also significantly reduced (Figure 4.13). This suggests that 6G binds to both hFcγRIIB and activatory FcγRs through its Fc (Figure 4.22). This is reminiscent of a biological phenomenon known as the Kurlander effect [236] [235]. Kurlander et al. showed that an intact IgG can interact with both the target (through the F(ab')$_2$) and other FcγRs (through the Fc) if co-expressed on the same cell. Furthermore, it is possible that this monomeric interaction with activatory FcγRs may induce ITAMi signalling, further decreasing activatory mAb effector functions [227] [237]. Key immune effector cells such as macrophages express both activatory mFcγRs and hFcγRIIB, making them a prime candidate for the Kurlander effect when 6G is administered. 6Q is able to rescue hFcγRIIB mediated inhibition because it effectively blocks hFcγRIIB without interacting with additional FcγRs due to the Fc null mutation (N297Q). This allows rituximab to efficiently in-

teract with activatory mFcγRs. Again, this has similarity with the mechanism proposed by Treffers et al., where the addition of the FcγRIIIB blocking mAb (in a F(ab')$_2$ format) effectively blocked FcγRIIIB, enhancing activatory hFcγRIIA interactions with cetuximab [234].

The site of B cell depletion is largely thought to be in the liver, and specifically carried out by Kupffer cells. Studies by both Gül et al. and Grandjean et al. demonstrated the requirement of Kupffer cells to mediate the elimination of CD20 targets and it was found that depletion was dependent on interactions with mFcγRI and mFcγRIV [346] [304]. The data from the adoptive B cell transfer model also suggests that mFcγRIV is significantly blocked by 6G on a number of different immune cells (Figure 4.13). Due to the requirement of mFcγRIV for depletion, these studies may explain why 6G does not improve target cell depletion. To further investigate, it would be important to repeat the experiment and analyse FcγRIV occupation on Kupffer cells.

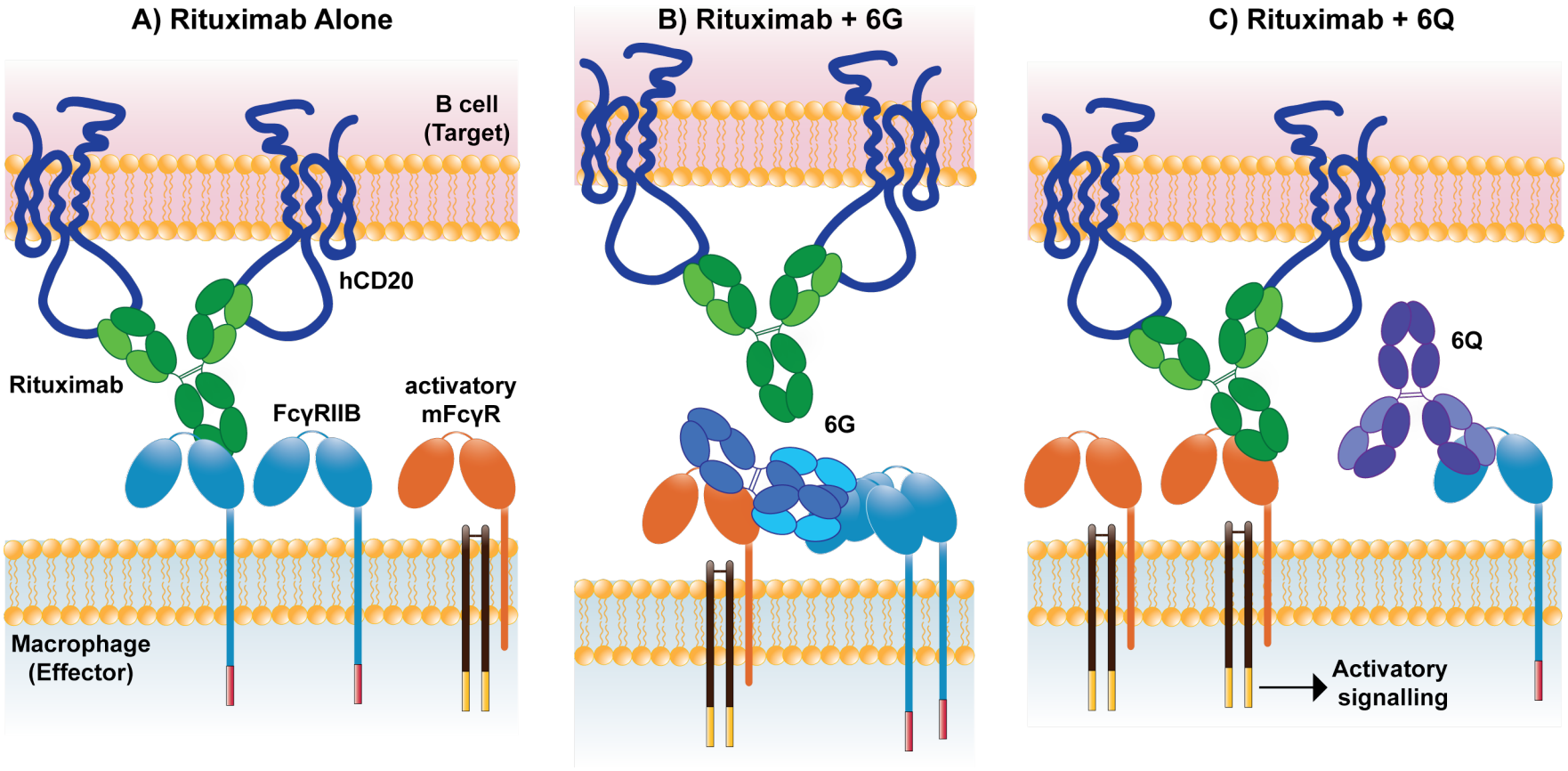

Figure 4.22: The proposed mechanism of inhibition by hFcγRIIB in the adoptive transfer B cell experiments
A) When NoTIM mice were treated with rituximab alone, the high expression of FcγRIIB out-competes activatory mFcγRs and elicits inhibition in a decoy receptor like fashion. This is independent of ITIM mediated inhibitory signalling. B) When 6G (hIgG1) is given with rituximab, it blocks hFcγRIIB but also binds to activatory mFcγRs on the same cell in a trans fashion. This stops rituximab from interacting with mFcγRIIB, also inhibiting target cell depletion. This is known as the Kurlander effect. C) When 6Q is administered with rituximab, hFcγRIIB is effectively blocked and 6Q does not interact with activatory mFcγRs as it is considered Fc null (hIgG1 with the N297Q mutation). Rituximab can now efficiently deplete hCD20+ target cells.

To understand if this biological mechanism was specific to CD20+ mAbs or more widely applicable, a series of other cellular targets were analysed. The targeting of CD19+ B cells for depletion was shown to be ineffective, with increasing doses of 1D3 mIgG1 and even 250 μg mIgG2a failing to effectively deplete B cells even in mFcγRII KO mice (Figure 4.14). This ineffective depletion appeared to be related to the internalisation of CD19, an observation that had also been noted in the literature. CD19 was found to be internalised within minutes following ligation with mAb in two different studies [384] [385]. An *in vivo* study of CD20 and CD19 mAbs concluded that the cytotoxic activity of CD20 mAbs were far superior to those directed to CD19 [386]. Therefore, CD19 mAbs were not suited for further investigation of the hypothesis.

NK cell depletion was achieved using the anti-NK1.1 mAb PK136 mIgG2a (Figure 4.15). Across the experimental groups, NoTIM and hFcγRIIB Tg mice were more resistant to NK cell depletion than mFcγRII KO mice, however the mAb was highly effective and unsuitable at the doses used to ascertain any differences between the transgenic mice. The efficacy of PK136 was recently reported in the literature. Gordan et al. found that 1 μg PK136 mIgG2a was as effective as 100 μg in depleting peripheral and splenic NK cells with depletion reliant on interactions with all activatory mFcγRs [366]. Nevertheless, the data showed that at the very least, the NoTIM receptor could elicit inhibition of depletion to a similar extent to the signalling competent hFcγRIIB receptor.

The mAb YTS169.4 mIgG1 and mIgG2a was used to assess depletion of CD8+ T cells (Figure 4.16). A pilot experiment using 50 μg of mIgG1 in mFcγRII KO and NoTIM mice resulted in long and sustained depletion in both mouse models. The experiment was therefore repeated using smaller doses of mIgG2a, and again across mFcγRII KO, hFcγRIIB Tg and NoTIM mice, depletion was robust. To understand if this was dependent on activatory mFcγRs, the experiment was repeated in FcR γ-chain KO mice. The mAb therapy was ineffective suggesting that depletion within the periphery was indeed dependent on the anticipated mAb mediated effector functions. This is in agreement with previous studies, showing the absolute requirement for functional activatory FcγR expression to elicit mAb mediated depletion [387] [388] [185] [186]. To ascertain if CD8+ T cells had migrated to other lymphoid organs, a harvest was carried out and revealed that depletion was systemic. It has been reported that mAbs directed against CD8+ can trigger CD8+ T cell activation in the absence of TCR stimulation [389]. There is a possibility that YTS169.4 elicited agonism of CD8 cells could under-pin the robust depletion and absence of recovery seen in mice treated with mIgG1 and depletion of precursor thymocytes could also

inhibit their recovery. However, the reason for their absence within the periphery is unknown. To further investigate, the mIgG1 experiments could be repeated with a harvest at earlier time points to see if CD8+ T cells had migrated to other lymphoid organs and thymocytes could be assessed for signs of significant depletion. Nevertheless, at 2 μg both hFcγRIIB Tg and NoTIM mice had more resistance to CD8+ cell depletion than mFcγRII KO mice suggesting the signalling or non-signalling hFcγRIIB can inhibit depletion.

The targeting of CD25+ T_{reg} cells using rIgG1 mAb showed clearly that depletion was inhibited to a greater extent in NoTIM mice as compared to hFcγRIIB Tg and mFcγRII KO mice (Figure 4.17). The kinetics of depletion of T_{reg} cells was comparatively slow compared to other cells within the periphery as detailed above. On day 2, NoTIM mice had significantly more T_{reg} cells than hFcγRIIB Tg and mFcγRII KO mice. However, this effect was lost by day 7. It is of note that the rIgG1 subclass has similar binding affinities to mFcγRs as mIgG1 ([369], Dr. Ian Mockridge, in-house data, unpublished). Setiady et al. showed that T_{reg} depletion using the parental PC61 relied on interactions with mFcγRIII found on murine macrophages, similar to mIgG1 dependence on mFcγRIII for activatory functions. The authors also found that 30% of T_{reg} cells could not be depleted due to an absence of CD25 expression [368], these findings largely agree with the experiment reported in this thesis. Interestingly, Setiady et al. did not show a depletion benefit of T_{reg} cells in mFcγRII KO mice compared to C57BL/6J mice [368]. However, within their experimental system the authors dosed mice three times with mAb before looking at T_{reg} cell depletion 8 days later, allowing sufficient time to deplete T_{reg} cells and overcome mFcγRII inhibition. In a separate study, mFcγRII was highlighted as a potential factor for the lack of PC61 efficacy in murine tumour models. Vargas et al. used rIgG1 PC61 in various murine tumour models and found that T_{reg} cell depletion was ineffective within the tumour microenvironment most likely due to high mFcγRII expression on immune effector cells [369]. To overcome this inhibition, the authors switched PC61 from a rIgG1 to a mIgG2a and found there was superior depletion of T_{reg} cells and improved survival of tumour bearing mice [369]. These data agree that the inhibitory receptor negatively impacts T_{reg} cell depletion and experiments in NoTIM mice show that this effect is independent of ITIM signalling.

Finally, the mFcγRII KO, hFcγRIIB and NoTIM models were utilised in an OT-I adoptive transfer model exploring CD40 agonism to see if the loss of hFcγRIIB mediated ITIM signalling in NoTIM mice impacted the activity of the 3/23 mIgG1 mAb. Throughout the experiment, mFcγRII KO mice treated with 3/23 showed no agonistic activity. This is

expected, with the lack of an inhibitory receptor unable to sufficiently cross-link or stabilise mAb-CD40 interactions and elicit CD40 signalling. hFcγRIIB Tg mice showed some CD40 agonism whilst NoTIM mice had statistically significant increases in OT-I populations and activation markers on endogenous cells. The observations made here agree with those within the literature. White et al. and Li et al. found the activity of 3/23 *in vivo* was reliant on cross linking by mFcγRII [308] [309]. Further research using SHIP deficient mice found OT-I expansion was similar to their WT counterparts, supporting that signalling downstream of mFcγRII was not important. [310]. Li et al. also examined CD40 agonism in the presence of hFcγRIIB expressing EL4 tumour cells; the authors found that the absence or presence of the hFcγRIIB cytoplasmic tail, FcγRIIB resulted in increased survival compared to isotype [310]. These data infer that the ITIM is not required for CD40 agonism facilitated by hFcγRIIB. However the authors do not address the contribution of the ITIM alone, nor the systemic expression within a physiological system - instead they used transfected cells. The study within this thesis confirms specifically the contribution of ITIM signalling to CD40 agonism and shows high hFcγRIIB expression confers 3/23 agonistic activity.

Published studies by Li et al. also looked at the level of mFcγRII expression required for agonism using homozgous, heterozygous and knockout mFcγRII mice. The authors demonstrated that high expression of mFcγRII was required for mAb agonism, with heterozygous mice showing a loss of CD40 agonism [310]. The hFcγRIIB Tg and NoTIM mice allowed for a closer examination of the level of hFcγRIIB expression required for agonism (not withstanding other differences between mouse strains). It was found in hFcγRIIB Tg mice that there was no relationship between transgene expression and OT-I cell expansion whilst the relationship between geometric mean and OT-I cell expansion was weak (data not shown). However, taken together the higher expression of hFcγRIIB in NoTIM mice is most likely responsible for increased OT-I expansion over hFcγRIIB Tg mice. The contradiction between the correlation data and OT-I expansion suggests that other factors influence CD40 agonism that are beyond the limits of this experiment. However, it cannot be ruled out that hFcγRIIB signalling may negatively impact agonistic responses when comparing hFcγRIIB Tg and NoTIM mice. Furthermore, hFcγRIIB dependent agonism is likely to be influenced by the expression, and the frequency of cell types expressing it. Ideally, cell selective or tissue selective knockout of hFcγRIIB could be utilised to ascertain the cell type and/or tissue responsible for eliciting agonism.

As CD40 mAb induced agonism does not act directly on OT-I cells [390], it was important

to look at the agonistic effect on endogenous cells. Activation markers were upregulated on endogenous CD8+ T cells and B cells 7 days after treatment with 3/23 and OVA. This effect was most likely driven by CD40 agonism on DCs and B cells, resulting in licensing that increases interactions with T cells and provided an immunostimulatory environment [391]. The lack of anti-OVA IgG in the primary immune response was a surprise. CD23 expression had shown that B cells were activated on day 7, however over the initial 28 day period the maximal anti-OVA concentration yielded was 10 μg/mL. Following re-challenge with OVA and the secondary immune response, anti-OVA IgG concentrations improved, with 3/23 treated mice showing higher titres. The reason for the lack of a primary response is unknown. Within the literature, groups focus on OT-I expansion and T cell responses, with few papers examining the coincident production of anti-OVA IgG. It can be hypothesised that the immune response is artificially dominated by the high number of OT-I cells during the primary response, negating the need for/impairing the production of IgG. Re-challenge when OT-I numbers had sufficiently reduced may have allowed the B cells to have been more appropriately stimulated to upregulate IgG production in tandem with OT-I activation. An interesting observation was also made in isotype treated mFcγRII KO and NoTIM mice. Following re-challenge, these mice had increased IgG production over their hFcγRIIB Tg counterparts. This could be a result of the lack of inhibitory signalling on B cells in these models driving an increased IgG response, a similar observation was previously made in aged mFcγRII KO mice that had increased circulating autoantibodies and IgG producing B cells [392].

To conclude, it has been shown that hFcγRIIB can elicit inhibition of antibody-mediated target cell depletion independently of ITIM signalling. Inhibition apparently is driven by hFcγRIIB expression and competition with activatory mFcγRs for the binding of the direct targeting mAb Fc. In addition, hFcγRIIB mediated cross-linking of CD40-CD40 mAb was also shown to be independent of ITIM signalling. Agonism was found to be higher in NoTIM mice compared to hFcγRIIB mice which could be associated with the higher level of transgene expression in these mice. These findings were then applied to the treatment of murine tumour models using direct targeting mAbs to understand if hFcγRIIB mediated inhibition was independent of ITIM signalling in the context of tumour.

Chapter 5

Role of the hFcγRIIB ITIM in the inhibition of direct targeting antibody therapy in cancer models

5.1 Chapter Introduction

In chapter 4 it was demonstrated using the NoTIM transgenic mouse model that inhibition of direct targeting mAb mediated depletion of circulating lymphocytes by hFcγRIIB is independent of ITIM signalling. It has been deduced that inhibition is elicited by FcγRIIB competing with (and sometimes out-competing) activatory FcγRs for mAb engagement on the surface of immune effector cells. It was then desired to assess if this effect impairs the anti-tumour activity of direct targeting mAb therapy used to deplete malignant cells.

Rituximab has significantly improved survival outcomes in patients diagnosed with CD20+ B cell malignancies [393]. Despite this success, several mechanisms of inhibition have since been identified that can reduce the clinical efficacy of rituximab and some of these are mediated through FcγRIIB. Patients with MCL, DLBCL and FL cells that express high level of FcγRIIB were found to have reduced responses to rituximab therapy and worsened survival outcomes [299] [302] [301].

Since the discovery of FcγRIIB mediated inhibition in murine cancer models and human lymphoma patients, the receptor has been suggested to contribute to the progression of

other cancers. A recent study of clear cell renal cell carcinoma patients found that FcγRIIB mRNA levels were significantly upregulated within the tumour cells themselves compared to healthy tissues, with expression levels negatively correlating with survival rates [394]. In two separate studies, increased mRNA expression of FcγRIIB within high risk glioblastoma samples has also been identified as part of an immune related signature that correlates with worsened survival outcomes [395] [396]. Interestingly, a study of FcγR polymorphisms comparing HER2+ breast cancer patients treated with chemotherapy alone or in combination with trastuzumab found that patients carrying the FcγRIIB loss-of-function allele (232T homozygous) (Section 1.4.4.1) derived less benefit from trastuzumab therapy than FcγRIIB 232I carriers [397]. The biological rationale is not fully understood but nevertheless highlights another human cancer where FcγRIIB is associated with disease outcomes.

FcγRIIB may be implicated in further cancer types due to its upregulation in the tumour microenvironment. Dahal et al. found using the murine BCL_1 tumour model, that the tumour created a microenvironment that co-opted TAMs to upregulate mFcγRII, creating an immunosuppressive microenvironment. The upregulation of mFcγRII was linked to worsened survival outcomes of BCL_1 tumour bearing mice when treated with direct targeting mAb therapy [359]. Despite these findings, the link between tumour microenvironment, FcγRIIB mediated inhibitory signalling and antibody therapy has yet to be investigated.

This chapter aims to understand the contribution of ITIM signalling to two different cancer models: the *in vivo* depletion of mCD20+ malignant murine Eμ-TCL1 B cells [398] and the depletion of OX40+ T_{reg} cells within the tumour microenvironment of the E.G7 murine thymoma [339]. It was proposed that FcγRIIB would elicit inhibition of mAb therapy independently of ITIM signalling and instead instead be driven by competition with other FcγRs.

5.2 Depleting mCD20+ murine Eμ-TCL1 B cells

The Eμ-TCL1 murine tumour model was developed as a tool to investigate the human B cell malignancy CLL. CLL is an aggressive disease that is characterised by sustained antigen-dependent stimulation of the BCR in secondary lymphoid organs, driving amplification of CLL cells [399]. TCL1 is found overexpressed in nearly all CLL patients, with high protein levels correlating with a more aggressive phenotype [400]. Functionally, TCL1 expression results in the activation of the PI3K pathway and enhances the AKT signalling pathway leading to increased cell proliferation and survival [399].

In Eμ-TCL1 trangenic mice, the human TCL1 gene is expressed under the control of the V_H-promoter-Ig_H-Eμ enhancer, and found to drive a CLL like disease *in vivo* [338]. The Eμ-TCL1 tumour spontaneously develops over a period of a year within the Eμ-TCL1 transgenic mouse. Leukaemic cells begin accumulating within the peritoneal cavity from 2 months of age, are first detected within the blood at 4 months of age with terminal disease observed between 300 - 450 days [338]. Eμ-TCL1 tumour cells can then be adoptively transferred from transgenic mice into a syngeneic C57BL/6 or immunodeficient mouse to study direct targeting mAb therapy.

Flow cytometry can be used to distinguish Eμ-TCL1 cells from endogenous murine B cells and follow the progression of the disease through regular blood sampling (Figure 5.1). Endogenous B cells are characterised as CD19+/CD5-/B220hi, whilst Eμ-TCL1 cells are CD19+/CD5+/B220lo. Importantly, both cell populations express murine CD20 and can therefore be depleted using the mAb clone 18B12. To ascertain how the NoTIM receptor impacted 18B12 mAb therapy, an experimental setup was designed where mFcγRII KO, hFcγRIIB Tg and NoTIM mice were adoptively transferred with 5-10 x10^6 Eμ-TCL1 cells via intraperitoneal injection. Tumour load was monitored weekly until the tumour reached 10-20% of murine lymphocytes in the periphery. Mice were then treated with 100 μg of 18B12 mIgG2a via intraperitoneal injection and then tumour depletion and recovery were assessed until terminal endpoints were met. These were defined as meeting 2 out of 3 criteria: Eμ-TCL1 cells as a percentage of lymphocytes exceeding 80%, a white blood cell count of >5x10^7 cells/mL or a splenomegaly score of 3 or above (approximately 3 cm long).

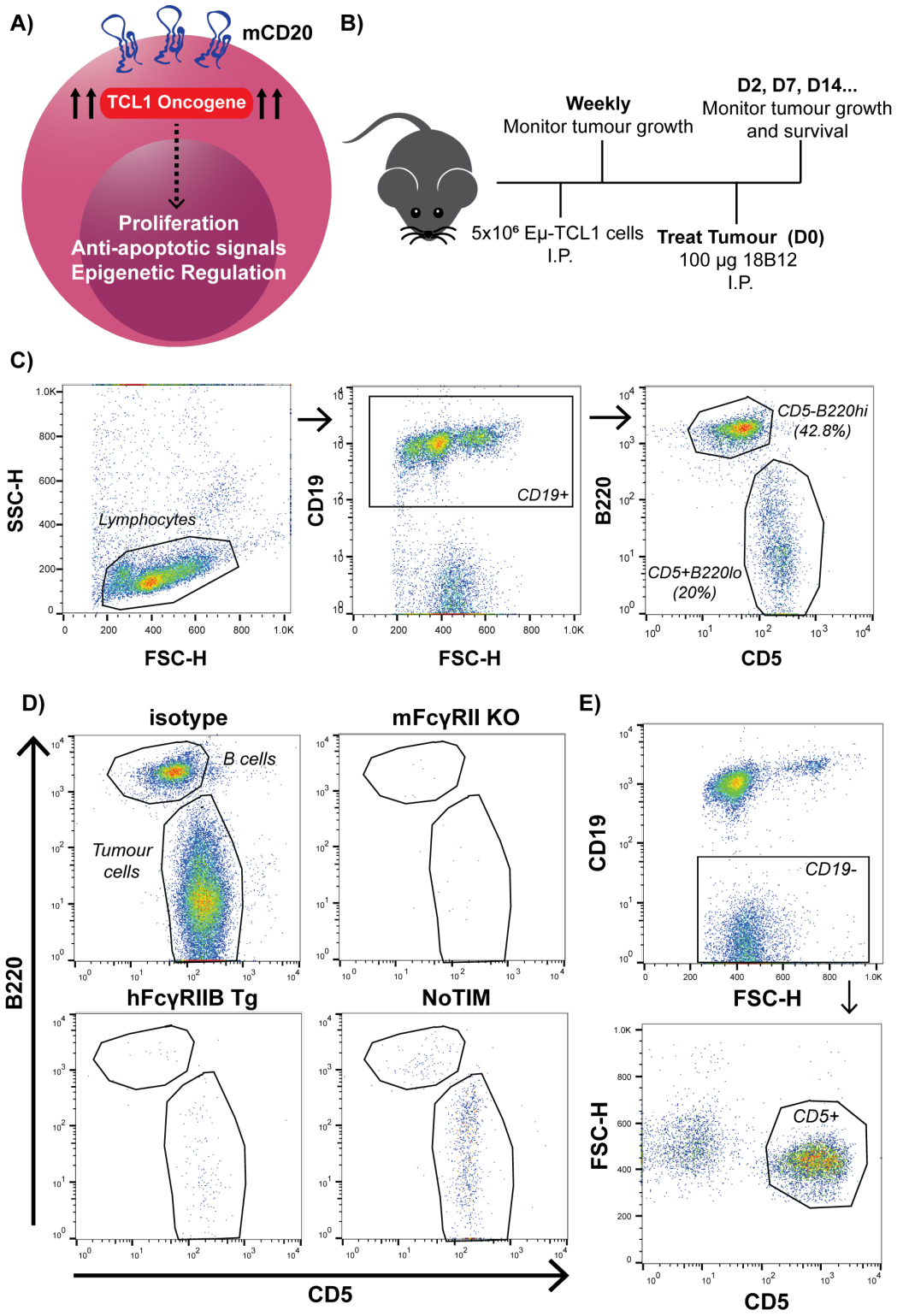

Figure 5.1: Eμ-TCL1 experimental setup and gating strategy

A) mFcγRII KO, hFcγRIIB Tg and NoTIM mice were adoptively transferred with 5-10 x10^6 Eμ-TCL1 cells via intraperitoneal injection. When tumour load made up reached 10-20% of murine lymphocytes in the periphery, mice were treated with 100 μg of 18B12 mIgG2a via intraperitoneal injection. Schematic depicting the key features of malignant murine Eμ-TCL1 B cells. The expression of mCD20 and mFcγRII is shown in histograms (isotype control is depicted in grey). B) The experimental setup for the therapeutic depletion of Eμ-TCL1 cells. C) The gating strategy used to assess Eμ-TCL1 cell (CD19+CD5+B220lo) and endogenous B cell (CD19+CD5-B220hi) depletion. D) Flow cytometry plots depicting depletion of endogenous B cells and Eμ-TCL1 tumour cells with 100 μg of isotype or 18B12 mIgG2a in each mouse model. E) Flow cytometry was also used to calculate the proportion of CD19-CD5+ T cells remaining; the gating strategy used to determine this was used to ascertain the T cell:TCL-1 ratio.

5.2.1 Depleting Eμ-TCL1 B cells using 18B12 mIgG2a

Following treatment with 18B12 mIgG2a, there was rapid and robust clearance of both cell types in all mouse models (Figure 5.1 D). Two days following treatment, there was near complete loss of both tumour cells and B cells in the periphery of mFcγRII KO mice with mean tumour cells/mL depleted to 1.6% of baseline and B cells/mL depleted to 1.5% of baseline. However, there were traces of both tumour and B cell populations in hFcγRIIB Tg and NoTIM mice, suggesting incomplete clearance in the periphery. hFcγRIIB Tg mice had a mean 3.4% tumour cells/mL and 2.8% B cells/mL of baseline, whilst NoTIM mice had even higher levels of retained cells; 23.4% tumour cells/mL and 8.9% B cells/mL of baseline (Figure 5.2).

To understand if the depletion of tumour cells and endogenous B cells was equal between groups, the fold decrease in tumour cells and B cells was quantified two days after treatment. The data shows that both tumour cells and endogenous B cells were depleted to a similar extent in each mouse model, with no significant differences between the groups. mFcγRII KO tumour cells were depleted by an average of 436 fold whilst B cells were depleted by 286 fold. hFcγRIIB Tg mice had an average 115 fold decrease in tumour cells and a 158 fold decrease in endogenous B cells. Finally, tumour cells within NoTIM mice were depleted by an average of 46 fold whilst endogenous B cells were depleted by 77 fold (Figure 5.3 B).

Mice were then assessed once a week following treatment until terminal endpoint was reached. On Day 7, peripheral tumour cells and B cells remained suppressed in mFcγRII KO mice (mean 6.4% and 0.9% of baseline, respectively), hFcγRIIB Tg mice showed a modest recovery of tumour cells with little change in B cells (mean 13.6% and 2.8%) whilst tumour cells within NoTIM mice expanded above baseline levels, with a modest increase in B cells recovery from Day 2 (mean 241% and 13.9%). Two weeks following treatment, tumour cells within mFcγRII KO mice began to recover whilst B cells continued to remain suppressed (mean 55.5% and 3.4%, respectively). hFcγRIIB Tg tumour cells surpassed baseline whilst B cells remained depressed (mean 162% and 5.9%) and tumour cells within NoTIM mice were now equivalent to isotype control treated NoTIM mice (18B12 treated NoTIM mice 1478%, isotype treated NoTIM mice 1305%) peripheral B cells making a steady recovery (mean 36% of baseline) (Figure 5.2).

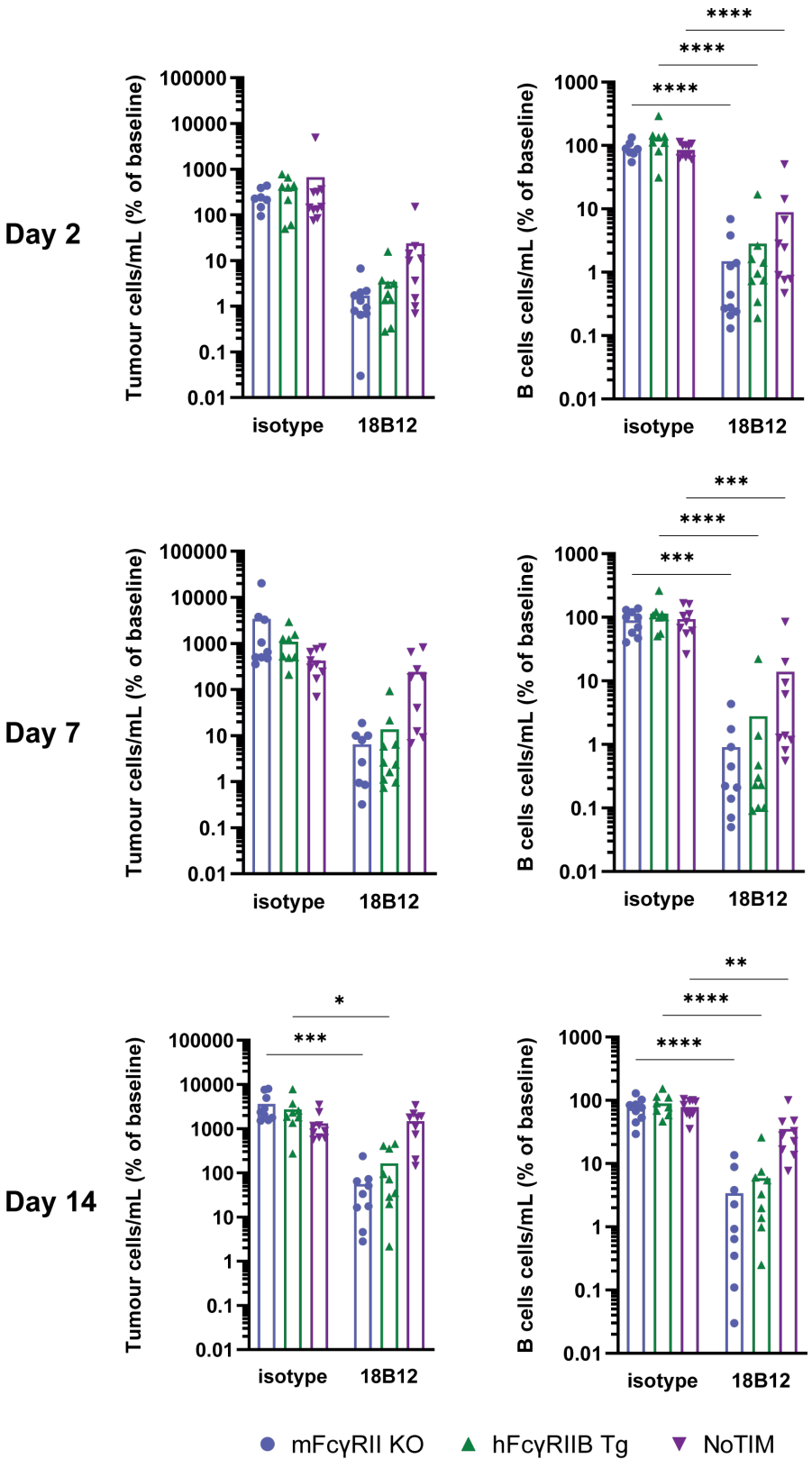

Figure 5.2: Recovery of Eμ-TCL1 cells and endogenous B cells following depletion using 18B12 mIgG2a mFcγRII KO, hFcγRIIB Tg and NoTIM mice were adoptively transferred with 5-10 x10^6 Eμ-TCL1 cells via intraperitoneal injection. When tumour load made up reached 10-20% of murine lymphocytes in the periphery, mice were treated with 100 μg of 18B12 mIgG2a or isotype control via intraperitoneal injection. Kinetics of Eμ-TCL1 tumour cells and endogenous B cell following treatment with 100 μg of isotype or 18B12 mIgG2a in each mouse model on Day 2, 7 and 14. The result of three independent experiments (8 - 9 mice per group). Bar = mean. Statistical analyses conducted using a one-way ANOVA with Tukey's multiple comparison test. * = $P \leq 0.05$, ** = ≤ 0.01, *** = $P \leq 0.001$, **** = $P \leq 0.0001$.

To ascertain how depletion of tumour cells compared to a population of cells that was not depleted, CD19-/CD5+ T cells were quantified by flow cytometry and compared to the tumour population by calculating the TCL1:T cell ratio (Figure 5.1 E). Before treatment, all three mouse models showed a ratio of approximately 0.8 - 1.7. Two days after treatment, mFcγRII KO experienced the biggest decrease in the ratio to a mean of 0.037. This did not recover to baseline until Day 14 (mean ratio of 1.4). hFcγRIIB Tg mice reached a mean ratio of 0.17 on Day 2 and surpassed baseline by Day 14 (mean ratio of 3.18). NoTIM mice had a mean ratio of 0.18 on Day 2 but recovered to baseline by Day 7 (mean ratio of 1.14). By Day 21, the TCL:T cell ratio was significantly higher in the NoTIM mice (mean ratio of 14.8) compared to hFcγRIIB Tg (mean ratio of 8.9) and mFcγRII KO mice (mean ratio of 4.4) (Figure 5.3 A).

Differences in circulating 18B12 mIgG2a may result in differences in target cell depletion. Therefore, to assess circulating 18B12 mIgG2a serum samples were collected two days following treatment. It was found that mFcγRII KO mice had an average of 23.2 μg/mL, hFcγRIIB Tg had 17.9 μg/mL and NoTIM mice had 15.5 μg/mL 18B12 mIgG2a in serum, with mFcγRII KO mice having significantly more than in NoTIM mice. This suggests that NoTIM mice have significantly less circulating 18B12, however when correlated against depletion of tumour cells on Day 2, there is no relationship between these two factors (Figure 5.3 C). These observations reflect those made in the pharmacokinetics study in Chapter 4.

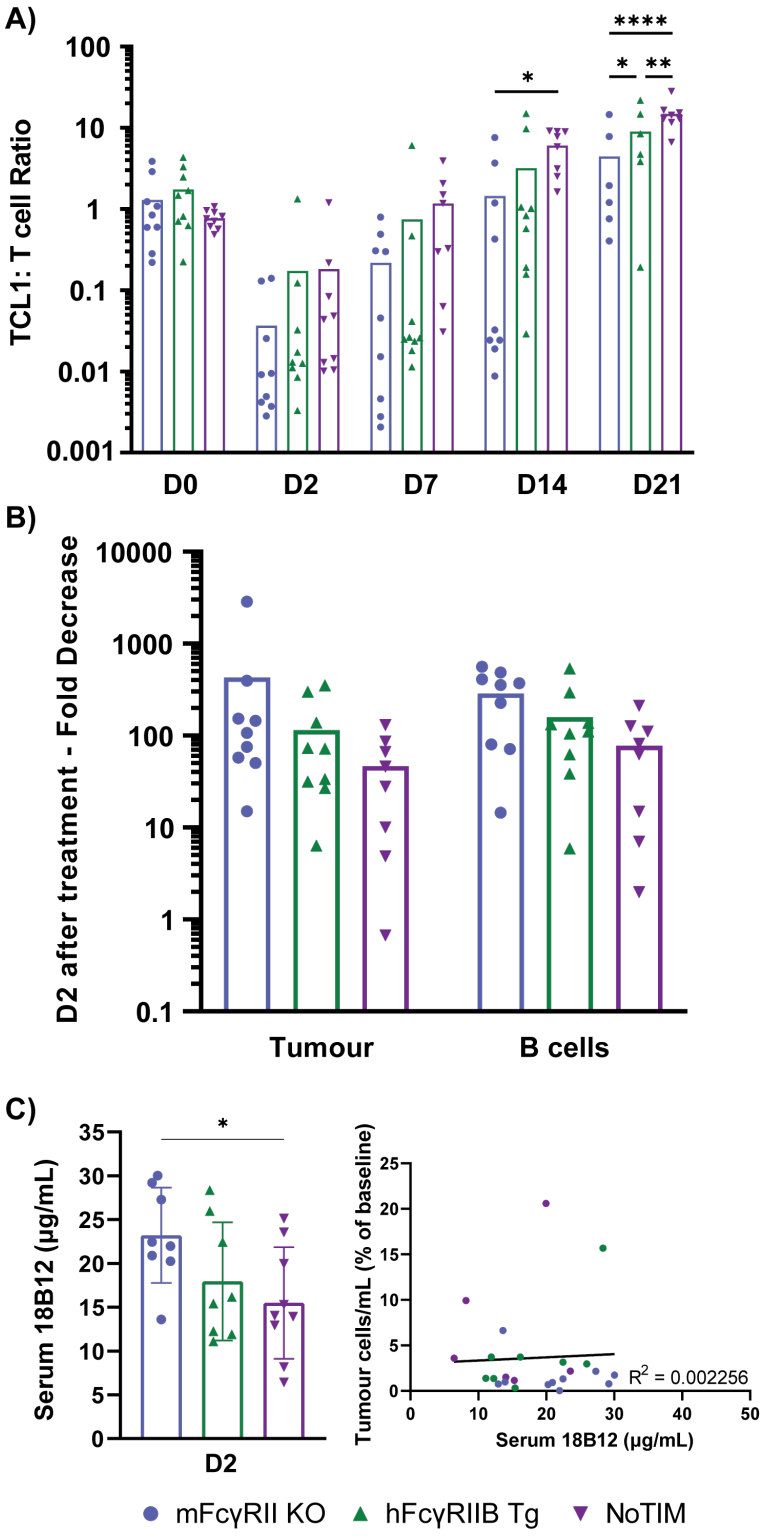

Figure 5.3: The TCL1:T cell ratio, fold decrease in tumour cells and B cells and serum available 18B12 following treatment with 18B12 mIgG2a

A) mFcγRII KO, hFcγRIIB Tg and NoTIM mice were adoptively transferred with 5-10 x10^6 Eμ-TCL1 cells via intraperitoneal injection. When tumour load made up reached 10-20% of murine lymphocytes in the periphery, mice were treated with 100 μg of 18B12 mIgG2a or isotype control via intraperitoneal injection. The TCL1:T cell ratio following treatment with 100μg 18B12 mIgG2a. B) The fold decrease in tumour cells and endogenous B cells on Day 2 after treatment with 100μg 18B12 mIgG2a C) Available 18B12 mIgG2a in the serum 2 days after treatment as determined using the π-BCL_1 cell binding assay. This was then correlated against tumour cell depletion on Day 2. The result of three independent experiments (8 - 9 mice per group). Bar = mean $\pm$ SD. Statistical analyses conducted using a one-way ANOVA (TCL1:T cell and serum comparison) or one-way ANOVA (fold decrease) with Tukey's multiple comparison test. * = P $\leq$ 0.05, ** = $\leq$ 0.01, *** = P $\leq$ 0.001, **** = P $\leq$ 0.0001.

To better understand how tumour cells were depleted and then recovered in mice treated with 18B12 compared to those with isotype, the number of tumour cells/mL in treatment mice were measured and normalised to numbers in isotype treated mice, with 100% in the isotype group equating to the mean tumour cells/mL in each mouse model at terminal endpoint (Figure 5.4 A). Whilst the majority of isotype treated mice reached terminal endpoint around Day 21, 18B12 treatment had a benefit in increasing survival across all mouse models. By Day 21, NoTIM mice had tumour cells that were approximately 50% of the number in isotype treated mice, whilst hFcγRIIB Tg mice had 20% and mFcγRII KO mice 10% tumour cells/mL compared with isotype. By Day 28, hFcγRIIB Tg and NoTIM mice were rapidly approaching 100% whilst mFcγRII KO were only 17%. These data indicate that tumour cell recovery is slower in mFcγRII KO mice than the other groups.

When assessing long term survival following 18B12 mIgG2a treatment, mFcγRII KO mice had the longest median survival of 42 days. hFcγRIIB Tg had a median survival of 35 days whilst NoTIM mice had the shortest median survival of 28 days. mFcγRII KO and hFcγRIIB Tg mice treated with 18B12 mIgG2a had significantly improved survival over their isotype treated counterparts (Mantel-Cox test P value of <0.0001 and <0.0009) whilst 18B12 treatment in NoTIM mice did not give a significant survival benefit (P = 0.0506). Treated mFcγRII KO mice also had a significant survival benefit over hFcγRIIB Tg mice (P = 0.0272) and NoTIM mice (P = 0.0016) but there was no statistical significance in survival between hFcγRIIB Tg and NoTIM mice (P = 0.1108) (Figure 5.3 B).

In summary, 18B12 mIgG2a treatment was significantly less effective in controlling Eμ-TCL1 tumour growth in mice containing the hFcγRIIB receptor and this effect was irrespective of the receptor's ability to initiate ITIM signalling. Whilst mFcγRII KO responded to mAb therapy and displayed long term tumour control (approximately 3 - 4 weeks), both hFcγRIIB Tg and NoTIM mice had ineffective tumour control and shortened survival outcomes. Next, it was assessed if the depletion of T_{reg} cells within the tumour microenvironment were negatively impacted by the NoTIM receptor.

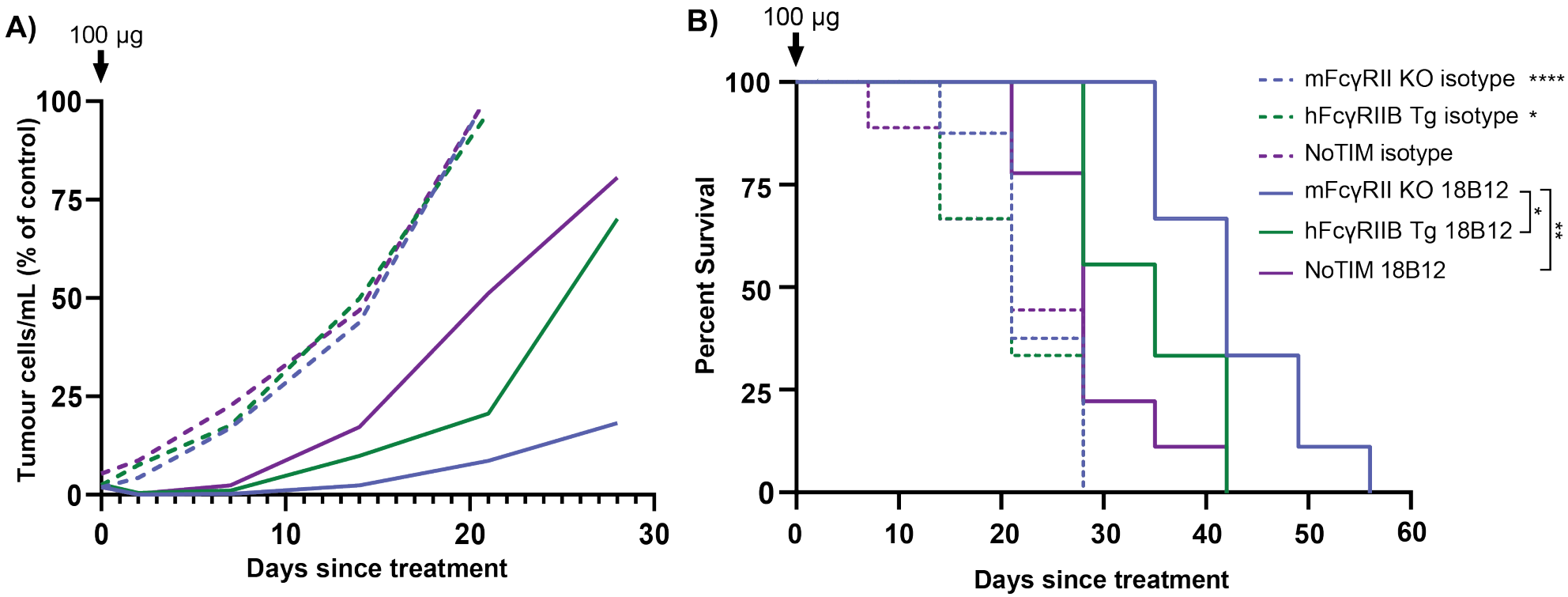

Figure 5.4: Eμ-TCL1 tumour cell growth and overall survival in mFcγRII KO, hFcγRIIB Tg and NoTIM mice

A) mFcγRII KO, hFcγRIIB Tg and NoTIM mice were adoptively transferred with 5-10 x10^6 Eμ-TCL1 cells via intraperitoneal injection. When tumour load made up reached 10-20% of murine lymphocytes in the periphery, mice were treated with 100 μg of 18B12 mIgG2a or isotype control via intraperitoneal injection. Tumour cell recovery in 18B12 treated mice was normalised to isotype treated mice within each group, with 100% set as the mean tumour cells/mL at terminal endpoint. B) A Kaplan Meier curve comparing survival between each different mouse group and treatment. The result of three independent experiments (8 - 9 mice per group). Statistical analyses conducted using the Mantel-Cox test. Statistical analyses next to isotype denotes significance between isotype treated and 18B12 treated mice (e.g. NoTIM isotype and NoTIM treated). Significance between 18B12 treated mice is denoted by the lines between the groups. * = P $\leq$ 0.05, ** = $\leq$ 0.01, **** = $\leq$ 0.0001.

5.3 Depleting OX40 murine T regulatory cells as therapy in the E.G7 thymoma tumour model

In Chapter 4, it was shown that the depletion of T_{reg} cells with an anti-CD25 mAb was also inhibited by hFcγRIIB independently of ITIM signalling. To investigate these findings in the context of a tumour model, the depletion of OX40+ T_{reg} cells within the tumour microenviroment of the syngeneic E.G7 thymoma model was assessed.

The depletion of T_{reg} cells has been an intensive area of research due to their associations with a poor prognosis in cancers such as ovarian cancer, hepatocellular carcinoma and breast cancer [401] [402] [403]. T_{reg} cells drive immune suppression and support tumour formation through mechanisms such as immunosuppressive cytokine production, promoting T_{reg} cell conversion and suppression of CTL cells [404]. Certain mAbs appear to achieve their effects through the depletion of tumour associated T_{reg} cells. For example, anti-CTLA-4 mAbs were developed to block CTLA-4 interactions with CD28, but subsequent research indicated that their success may also be driven by their ability to deplete CTLA-4+ T_{reg} cells [405] [148]. It has been suggested that the high expression of mFcγRII observed in the tumour microenvironment in mouse models limits T_{reg} cell depletion and is an avenue of interest in improving T_{reg} depletion [148].

E.G7 cells are derived from the parental cancerous EL4 T lymphoblast cell line. EL4 cells were initially established in a C57Bl/6N mouse by inducing spontaneous tumour formation through exposure to 9,10-dimethyl-1,2-benzanthracene [406]. EL4 cells were then transfected with a complete copy of the chicken OVA, resulting in EL4 cells that express and secrete OVA (now known as E.G7) [339]. The OVA produced by E.G7 cells has been found to be presented via the MHC-I antigen presentation pathway and has the ability to prime CTLs to destroy the E.G7 tumours cell, making the E.G7 tumour susceptible to regression and rejection [407]. Therefore, the E.G7 tumour is a model used to study the immune response to tumour neoantigens. In order to grow, tumours are known to induce an immunosuppresive environment. In the context of the CTL response, tumour associated T_{reg} cells can suppress CTL function and therefore mitigate tumour regression and enhance tumour escape and progression. In these set of experiments it was hypothesised that the efficient depletion of tumour associated T_{reg} cells would result in enhanced tumour regression. OX40 was chosen as the target antigen, due to its constitutively high expression on murine T_{reg} cells and transient expression on effector T cell compartments

[408]. mAb therapy has been directed against OX40 in pre-clinical models and has been successfully used to deplete T_{reg} cells as a cancer therapy [150].

To assess if the signalling independent NoTIM receptor was able to inhibit the depletion of T_{reg} cells in the tumour microenvironment, mFcγRII KO, hFcγRIIB Tg and NoTIM mice were given $5x10^5$ E.G7 cells via subcutaneous injection (s.c.). When the tumour had become palpable (approximately 30 - 75 mm^2) mice were treated with a dose of either OX86 (anti-mouse OX40) [333] mIgG2a or an isotype control, with an additional dose given two days later (Day 0 and Day 2). Mice were bled two days after the first dose, two days after the second dose and one week after the last dose to ascertain depletion of T_{reg} cells (bled on Day 2, Day 4 and Day 9). T_{reg} cells were identified using flow cytometry (CD4+FOXP3+ cells) and depletion was assessed by analysing the percentage CD4+FOXP3+ cells remaining as the proportion of CD4+ cells and absolute cell number (Figure 5.5).

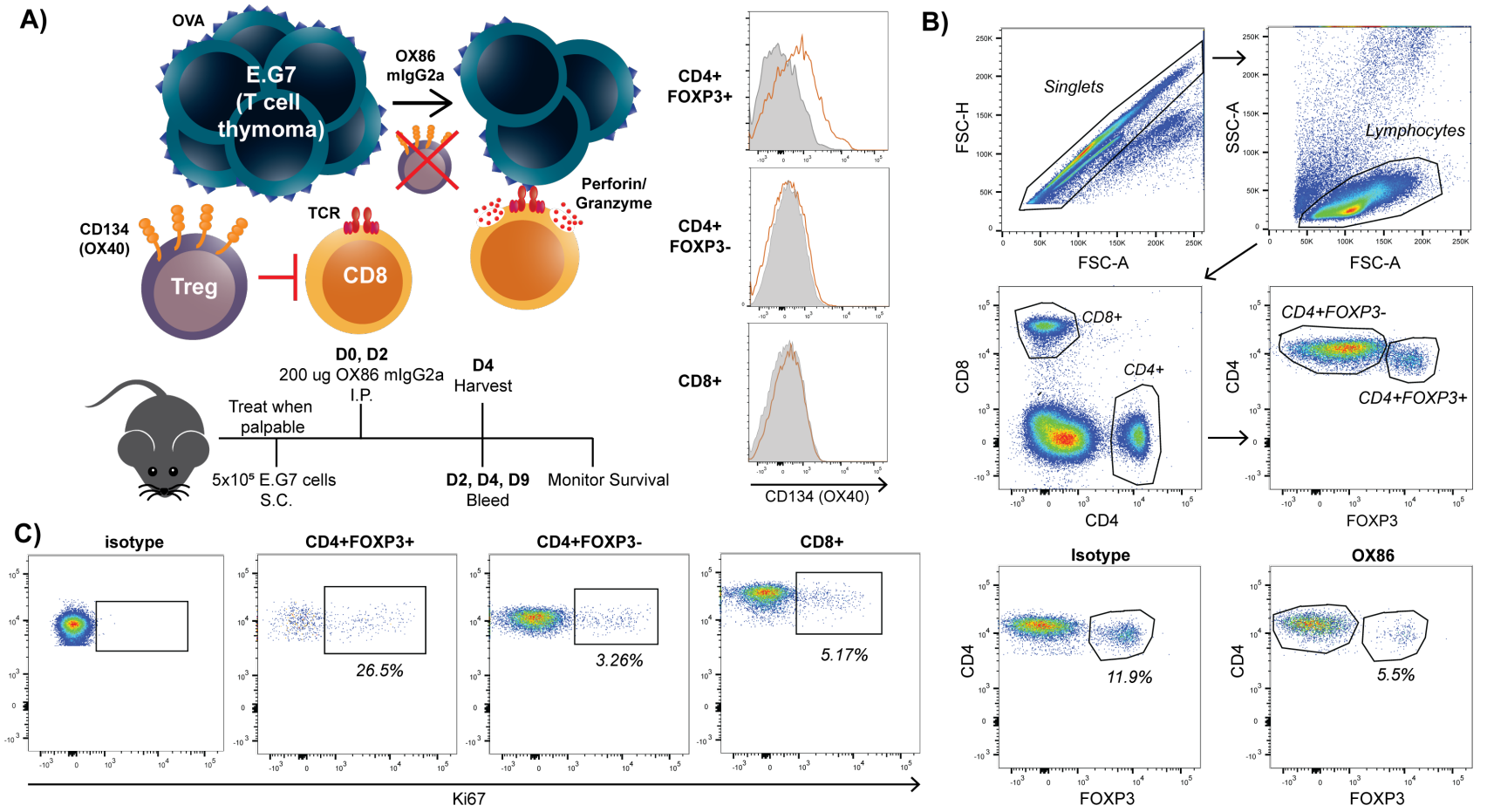

Figure 5.5: Schematic of the T_{reg} cells within the E.G7 tumour model, experimental setup, OX40 expression within the T cell compartment and gating strategy to identify depletion and T cell proliferation

A) Cartoon depicting the hypothesis of the E.G7 experiment and experimental setup. Histograms represent OX40 expression on CD4+FOXP3+, CD4+FOXP3- and CD8+ populations. Grey = isotype, yellow = OX40. B) The gating strategy used to identify T_{reg}, CD4 and CD8 cells and how depletion was ascertained. C) Examples of Ki67+ populations using an Ki67+ isotype mAb on T_{reg} cells, and Ki67+ mAb on T_{reg}, CD4 and CD8 cells

5.3.1 Depletion of peripheral T regulatory cells

To ascertain the depletive capacity of OX86 mIgG2a, mice were bled on Day 2, 4 and 9 to analyse T_{reg} cell depletion kinetics (Figure 5.6). Two days after the first dose of 200 μg dose of mAb, mFcγRII KO mice showed significant depletion in the periphery in both percent of CD4+FOXP3+ cells (mean 4.7%) and actual cell number when compared to isotype treated mice. This depletion was sustained on Day 4, but by Day 9 the percent of CD4+FOXP3+ cells recovered to broadly the same level as isotype treated mice. hFcγRIIB Tg mice showed a similar pattern of depletion but to a lesser extent. On Day 2, the percentage CD4+FOXP3+ cells was below isotype (mean 6.2%) with Day 4 showing a sustained decrease (mean 6.4%) and by Day 9 the percentage had recovered above isotype. These changes were also reflected in cell number but the differences were not as great.

NoTIM mice were most resistant to peripheral T_{reg} cell depletion with a small mean decrease in CD4+FOXP3+ percentage (mean 7.1%), which had recovered to above isotype by Day 4 and by Day 9 this had significantly increased to a mean of 16.4%. Again, these changes were also reflected in the actual number of T_{reg} cells/mL. Both mFcγRII KO and hFcγRIIB Tg OX86 treated mice showed a significant sustained decrease in percentage CD4+FOXP3+ cells on Day 2 and Day 4 when compared to isotype. In contrast, OX86 treated NoTIM mice showed initial depletion, followed by a sustained increase on Day 4 and Day 9 compared to isotype. mFcγRII KO and NoTIM mice treated with OX86 had a significantly different percentage and number of T_{reg} cells across the experiment (Figure 5.6).

The effect of OX86 induced depletion of T_{reg} cells on peripheral CD8+ T cells seemed to be minimal which was expected given their low expression of OX40. The number of circulating CD8+ cells broadly stayed consistent across the experiment, with a small but non-significant decrease in CD8+ cell number in OX86 treated mice compared to isotype in all groups (Figure 5.7). For example, the mean number of CD8 T cells for mFcγRII KO OX86 treated mice was $5.2x10^5$ cells/mL on Day 2, $4.01x10^5$ cells/mL on Day 4 and $3.7x10^5$ cells/mL on Day 9. hFcγRIIB Tg and NoTIM mice treated with OX86 showed a similar trend.

The CD8:T_{reg} cell ratio can be used as a readout of the effectiveness of treatments targeting T cells, a higher ratio can correlate with more favourable clinical outcomes due to the

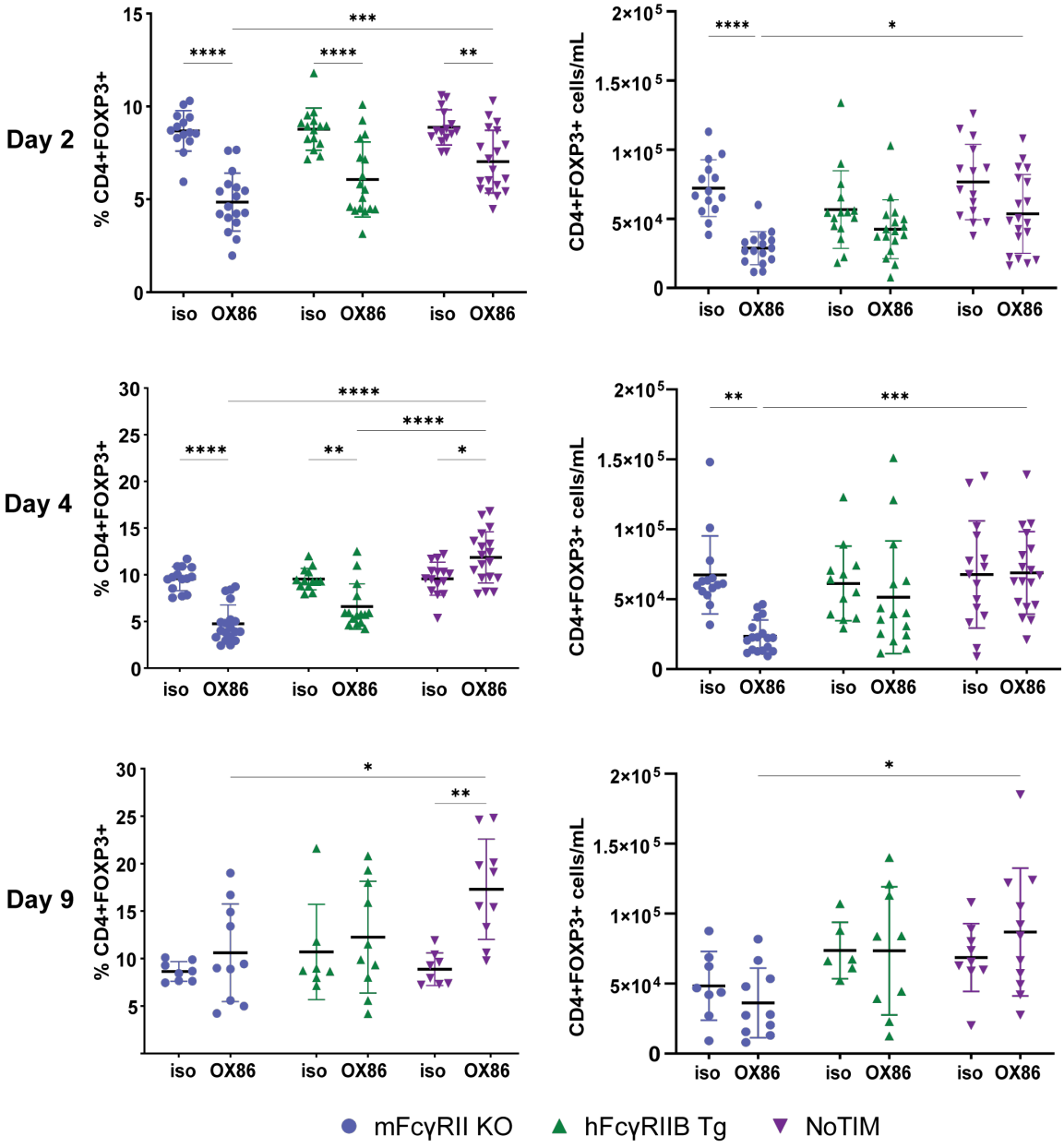

Figure 5.6: Depletion of peripheral T regulatory cells in E.G7 tumour bearing mFcγRII KO, hFcγRIIB Tg and NoTIM mice treated with OX86 mIgG2a or isotype control

MmFcγRII KO, hFcγRIIB Tg and NoTIM mice were given 5x10^5 E.G7 cells via subcutaneous injection. When the tumour had become palpable (approximately 30 - 75 mm^2) mice were treated with a dose of either OX86 (anti-mouse OX40) mIgG2a or an isotype control, with an additional dose given two days later (Day 0 and Day 2). The first column shows the percentage of CD4+FOXP3+ cells in isotype and OX86 treated mice across each time point. The second column shows the enumerated number of peripheral CD4+FOXP3+ cells across each time point. The result of two - three independent experiments (6 - 12 mice per group). Line = mean ± SD. Statistical analyses conducted using a two-way ANOVA with Tukey's multiple comparison test. * = $P \leq 0.05$, ** = ≤ 0.01, *** = $P \leq 0.001$, **** = $P \leq 0.0001$.

proposed loss of suppression by T_{reg} cells [409] [410]. On Day 2, OX86 treated mFcγRII KO mice had a significant increase to a mean ratio of 18.62. In comparison hFcγRIIB Tg mice had a moderate increase to a mean ratio of 15.2 whilst NoTIM mice had a smaller increase to a mean ratio of 11.62 (Figure 5.7). By Day 4, OX86 treated mFcγRII KO mice sustained an increased ratio whilst both hFcγRIIB Tg and NoTIM mice showed a decrease in the CD8:T_{reg} ratio, with NoTIM mice having the strongest decrease. By Day 9, mFcγRII KO mice showed CD8:T_{reg} ratios normalised towards the isotype control, whilst hFcγRIIB Tg decreased further and NoTIM mice sustained a lower CD8:T_{reg} ratio. At each time point, OX86 treated mFcγRII KO mice had a significant difference in their CD8:T_{reg} ratio compared to OX86 NoTIM treated mice (Figure 5.7). These data indicate T_{reg} cells are efficiently depleted in mFcγRII KO mice, allowing the relative increase in proportion of CD8 T cells, whilst hFcγRIIB Tg and NoTIM mice showed resistance to depletion and even provided evidence for T_{reg} cell expansion.

5.3.2 Proliferative capacity of peripheral T regulatory cells, CD4+ T cells and CD8+ T cells

Due to the dual nature of OX40 being a target for cell depletion but also a co-stimulatory receptor, the effects of OX86 mAb treatment on the proliferative capacity of CD4+FOXP3+, CD4+FOXP3- and CD8+ cells were analysed by measuring the expression of the nuclear protein Ki67. Ki67 is expressed during cellular proliferation, upregulated during all active phases of the cell cycle and absent from non-cycling quiescent cells [411].

T_{reg} cells initially showed little proliferation in response to treatment. On Day 2, mFcγRII KO T_{reg} cells were similar to isotype, whilst hFcγRIIB Tg and NoTIM T_{reg} cells had small increases above isotype (Figure 5.8). By Day 4, mFcγRII KO had a small increase in proliferating T_{reg} cells (mean 33.1%) whilst both hFcγRIIB Tg and NoTIM T_{reg} cells had significant increases compared to isotype control (mean 47.4% and 69.9%, respectively). The increase in Ki67+ T_{reg} cells in NoTIM mice were significantly more than seen in both mFcγRII KO and hFcγRIIB Tg mice. By Day 9, Ki67+ T_{reg} cells in OX86 treated mice were significantly increased compared to isotype but showed no differences between mouse models (mFcγRII KO mean 73.1%, hFcγRIIB Tg mean 72.4% and NoTIM mean 73%).

Effector CD4 cells had a delayed proliferative response to OX86 treatment. On Day 2, OX86 treated mice showed similar percentage of Ki67+ cells to isotype treated mice

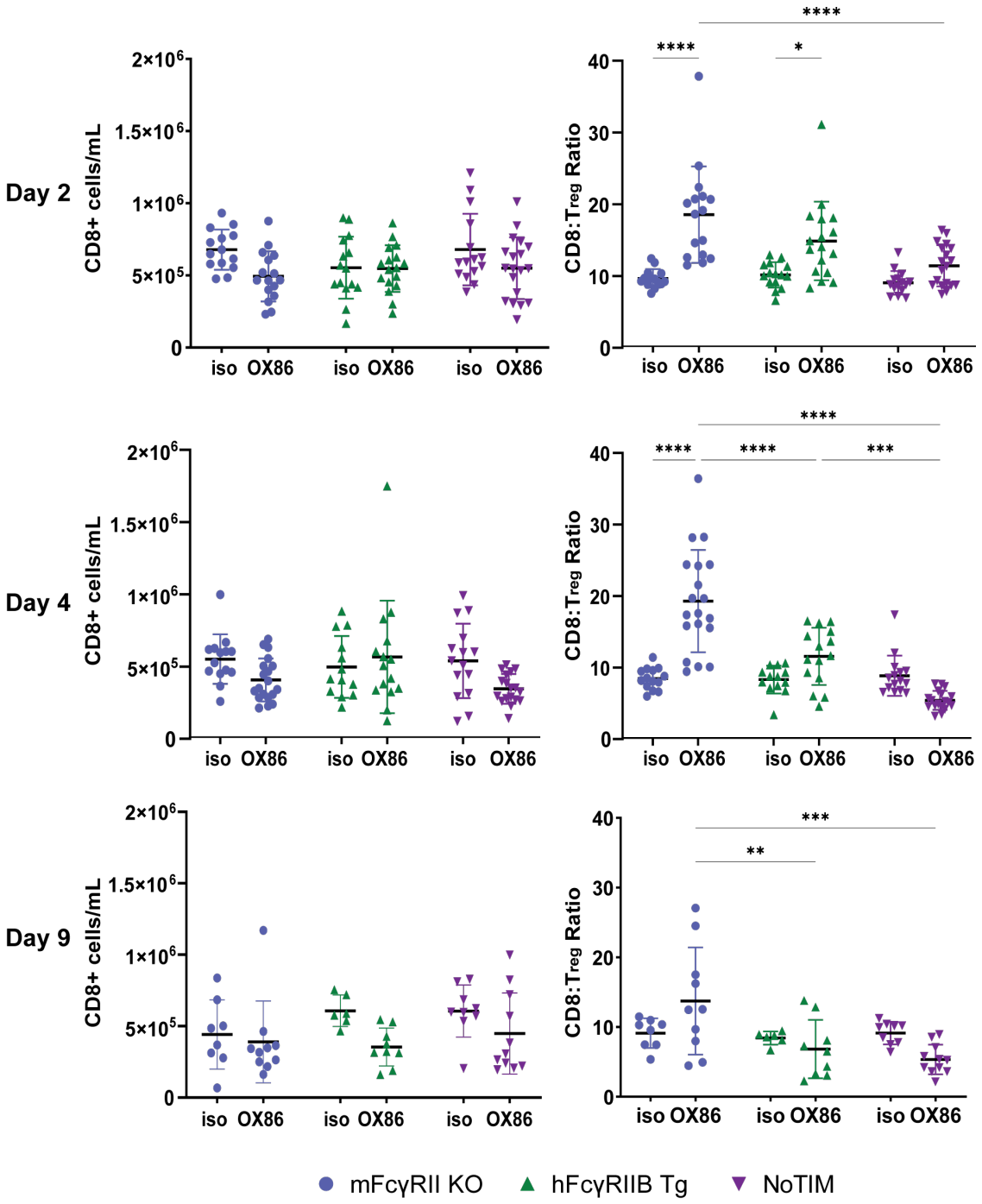

Figure 5.7: The change in CD8+ T cell number and CD8:T_{reg} ratio in E.G7 tumour bearing mFcγRII KO, hFcγRIIB Tg and NoTIM mice treated with OX86 mIgG2a or isotype control

mFcγRII KO, hFcγRIIB Tg and NoTIM mice were given 5x10^5 E.G7 cells via subcutaneous injection. When the tumour had become palpable (approximately 30 - 75 mm^2) mice were treated with a dose of either OX86 (anti-mouse OX40) mIgG2a or an isotype control, with an additional dose given two days later (Day 0 and Day 2). The first column shows the enumerated number of CD8+ cells in the periphery across each time point as determined by flow cytometry. The second column shows the calculated CD8:T_{reg} ratio from the enumerated number of circulating CD8+ and CD4+FOXP3+ cells across each time point. The result of two - three independent experiments (6 - 12 mice per group). Line = mean ± SD. Statistical analyses conducted using a two-way ANOVA with Tukey's multiple comparison test. * = $P \leq 0.05$, ** = ≤ 0.01, *** = $P \leq 0.001$, **** = $P \leq 0.0001$.

(Figure 5.8). By Day 4, mFcγRII KO CD4 cells showed no increase over isotype whilst hFcγRIIB Tg CD4 cells showed a modest increase above isotype. NoTIM CD4 cells had a significant increase in Ki67+ CD4 T cells (mean 14.9%) compared to isotype treated NoTIM mice as well as OX86 treated mFcγRII KO and hFcγRIIB Tg mice. By Day 9, mFcγRII KO mice had a significant increase in proliferating CD4+ T cells (mean 24%), whilst hFcγRIIB and NoTIM mice had a modest increase in Ki67+ CD4 cells compared to Day 4 (mean 17.2% and 18.6%, respectively).

Effector CD8 cells also had a delayed proliferative response to OX86 treatment. On Day 2, all OX86 treated mice showed no changes in Ki67+CD8+ cells across each treatment group (Figure 5.8). By Day 4, there was a small increase in proliferating CD8+ T cells in mFcγRII KO and hFcγRIIB Tg mice (8.49% and 6.49%, respectively) with a significant increase in NoTIM mice (mean 10.9%). By Day 9, mFcγRII KO mice demonstrated a significant increase in Ki67+ CD8 T cells (mean 32.8%) whilst hFcγRIIB Tg and NoTIM mice also showed an increase in Ki67+ however this was not significant compared to isotype treated mice (mean 19.4% and 26.9%, respectively).

Taken together, analysis of Ki67+ cells showed that T_{reg} cells, CD4+ and CD8+ cells proliferated from Day 4 in hFcγRIIB Tg and NoTIM mice suggesting that hFcγRIIB may be cross-linking OX86-OX40 to drive agonism. Proliferation of T cell compartments only becomes apparent on Day 9 in mFcγRII KO mice suggesting proliferation in these mice is driven by a homeostatic response to repopulate T_{reg} cells after their depletion.

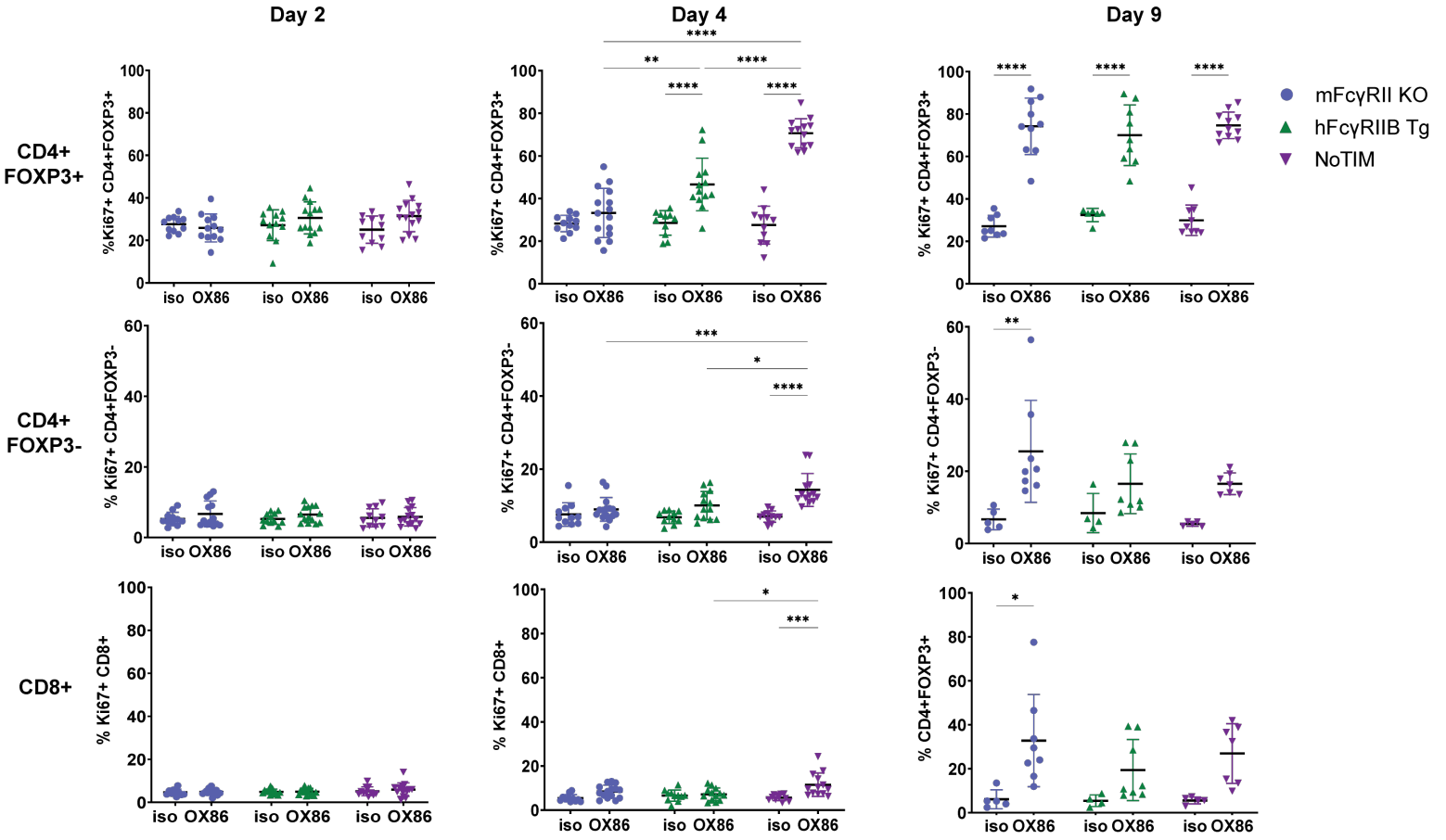

Figure 5.8: Ki67+ peripheral T cells in E.G7 tumour bearing mFcγRII KO, hFcγRIIB Tg and NoTIM mice treated with OX86 mIgG2a or isotype control

mFcγRII KO, hFcγRIIB Tg and NoTIM mice were given 5x10^5 E.G7 cells via subcutaneous injection. When the tumour had become palpable (approximately 30 - 75 mm^2) mice were treated with a dose of either OX86 (anti-mouse OX40) mIgG2a or an isotype control, with an additional dose given two days later (Day 0 and Day 2). The first row shows percentage CD4+FOXP3+Ki67+ cells, the second row shows percentage CD4+FOXP3-Ki67+ and the third row shows percentage CD8+Ki67+ cells. The result of two - three independent experiments (6 - 12 mice per group). Line = mean $\pm$ SD.. Statistical analyses conducted using a two-way ANOVA with Tukey's multiple comparison test. * = P $\leq$ 0.05, ** = $\leq$ 0.01, *** = P $\leq$ 0.001, **** = P $\leq$ 0.0001.

5.3.3 Systemic depletion of T regulatory cells and proliferation of T regulatory cells, CD4+ T cells and CD8+ T cells

To better appreciate how OX86 mIgG2a modulated T cells within the tissues as opposed to the periphery, mice harbouring tumours were culled on Day 4 (after receiving 400 μg of mAb) and tissues were processed into single cell suspensions. These samples were assessed by flow cytometry as above to ascertain depletion and T cell proliferation within the spleen and the tumour. Splenic T_{reg} cells and associated T cell populations were identified as they were in the periphery (Figure 5.5). Because the E.G7 thymoma is CD4+ derived, the previous gating strategy was re-assessed using *in vitro* cultured E.G7 cells and comparing them to the *in vivo* tumour to identify if the *in vivo* populations being observed were of tumour origin or were infiltrating lymphocytes. The lack of CD8+ expression on the cell line meant that infiltrating CD8+ cells could be readily identified. The E.G7 cell line was negative for FOXP3+ staining meaning the T_{reg} cell population could be identified with confidence. Because the endogenous CD4+FOXP3- population could not be separated from the CD4+FOXP3- E.G7 cell line, they were not analysed (Figure 5.9).

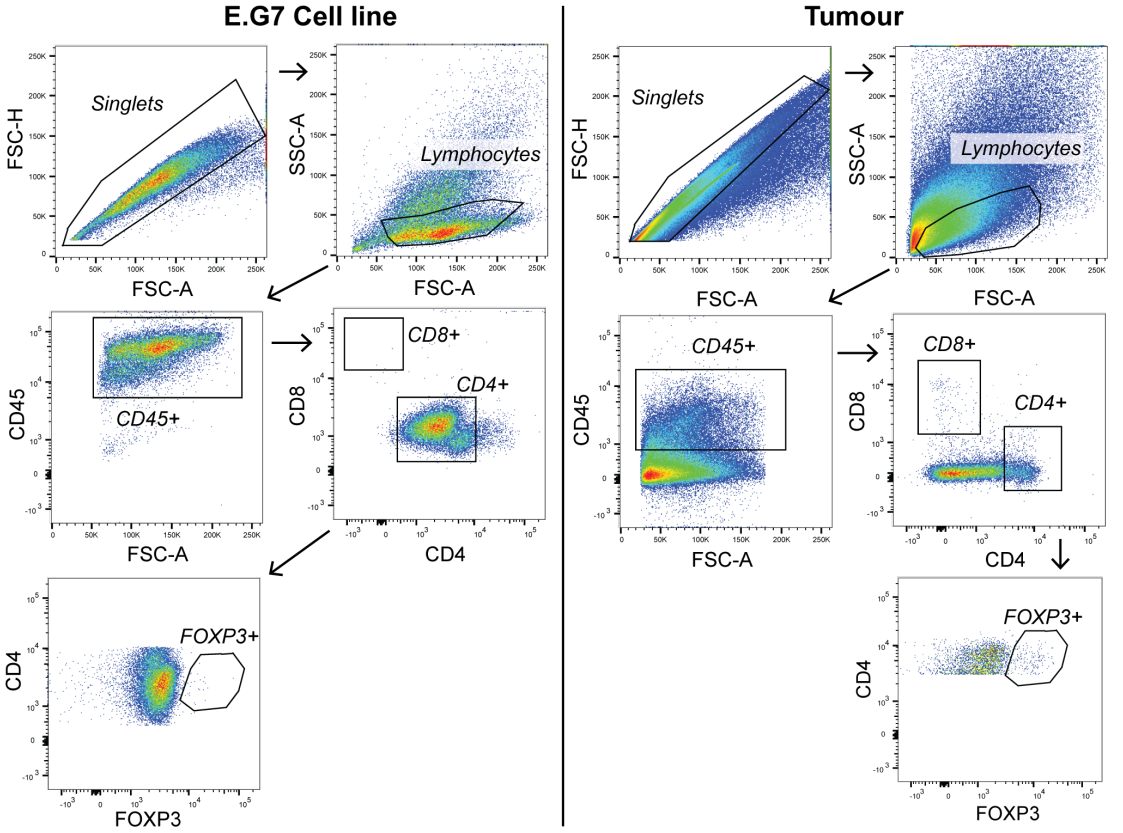

Figure 5.9: Flow cytometry gating strategy used to identify T regulatory and CD8 cells within E.G7 tumour bearing mFcγRII KO, hFcγRIIB Tg and NoTIM mice treated with OX86 mIgG2a or isotype control
The left hand figure indicates the gating strategy used on the E.G7 cell line. The same gating strategy was then used on tumour samples to ascertain endogenous CD8+ and T_{reg} cells from the E.G7 thymoma cells.

5.3.3.1 Modulation of T cell compartments within the spleen

The first organ to be assessed was the spleen. To ascertain cell numbers, spleens were harvested and weighed from each mouse. There was no significant difference in weight from the spleen taken from OX86 or isotype treated mice (data not shown). The number of T_{reg} cells per gram of spleen were quantified and the percentage of CD4+FOXP3+ cells were assessed. mFcγRII KO mice demonstrated a decreased number of T_{reg} cells and a significant decrease in the percentage of CD4+FOXP3+ cells after OX86 treatment (mean $5.97x10^7$ cells per gram of spleen and 9.29%, respectively) (Figure 5.10 A). hFcγRIIB Tg mice also showed a decrease in both cell number and percentage but this was not statistically significant whilst NoTIM mice demonstrated an increase in the number of cells and a significant increase in percentage (mean $1.25x10^8$ cells per gram of tissue and 17.7%, respectively).

The number of CD8+ cells was also quantified per gram of spleen and a CD8:T_{reg} ratio was generated (Figure 5.10 B). The data showed no change in the total number of CD8 cells in mFcγRII KO mice and a small, albeit non-significant decrease in total CD8s in hFcγRIIB Tg and NoTIM mice. The CD8:T_{reg} ratio demonstrated a significant increase in mFcγRII KO mice (mean 5.75), whilst hFcγRIIB Tg mice showed a small increase (mean 4.28) and NoTIM mice showed a significant decrease (mean 2.6). The difference in the ratio between mFcγRII KO and NoTIM mice as well as hFcγRIIB Tg and mFcγRII KO and NoTIM mice was significantly different.

Proliferation was assessed as above (Figure 5.5). The percentage of Ki67+ T_{reg} cells and CD8+ T cells in the spleen was quantified in each mouse model (Figure 5.10 C). mFcγRII KO mice showed no change in the proliferation of T_{reg} cells but significant proliferation of splenic CD8+ cells compared to isotype control (mean 17.2% and 10.24%, respectively). hFcγRIIB Tg mice showed a modest increase in both proliferating T_{reg} cells and CD8+ cells (mean 27.37% and 8.15%, respectively) whilst NoTIM mice had a significant increase in both proliferating T_{reg} cells and CD8+ cells (mean 50% and 12.33%, respectively).

The expansion of T_{reg} cells and the decrease in the CD8:T_{reg} ratio suggests NoTIM mice have a more immunosuppressive environment within the spleen than mFcγRII KO mice and this expansion is likely driven by hFcγRIIB cross linking of OX86-OX40 interactions.

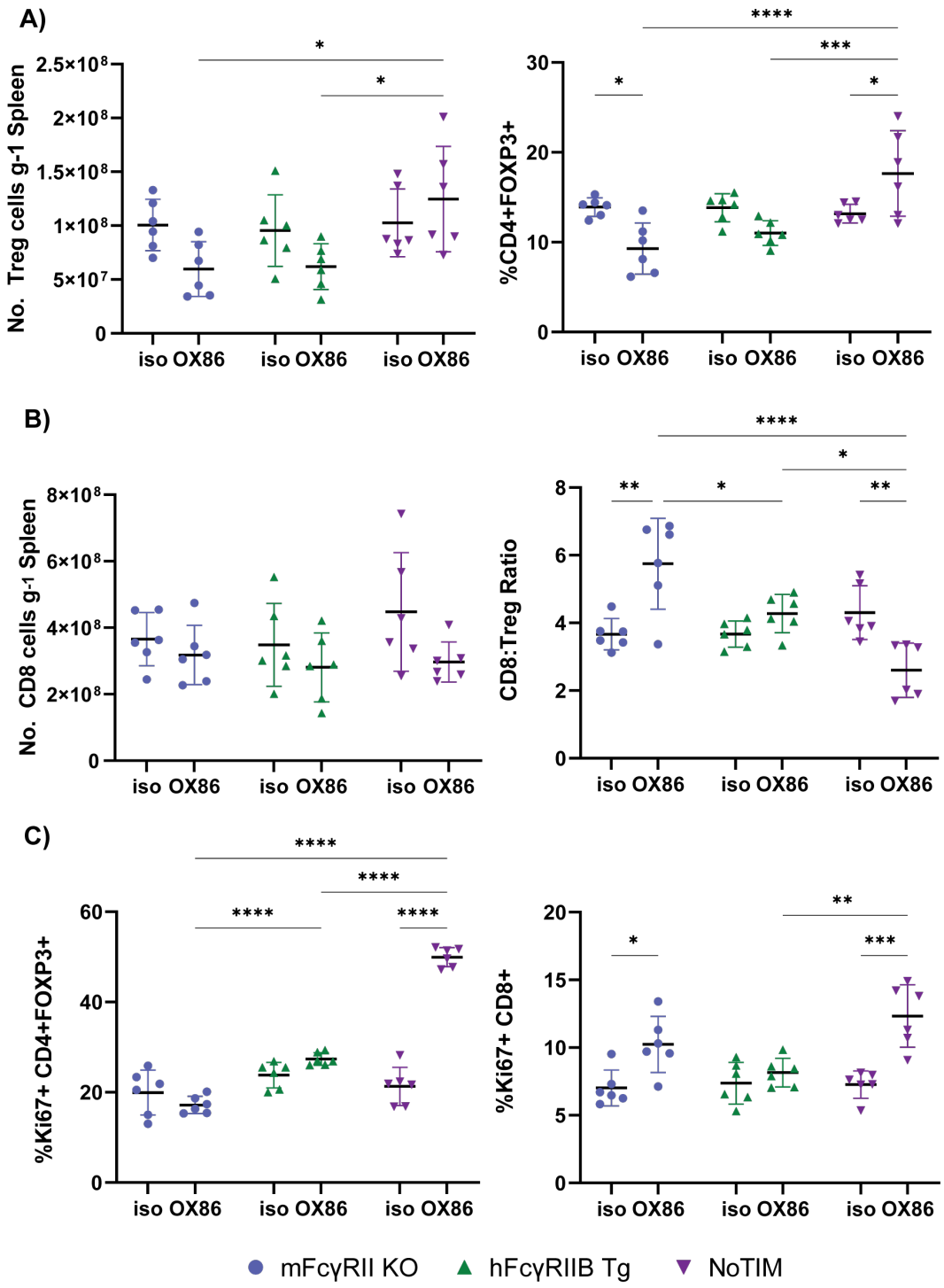

Figure 5.10: Dynamics of T regulatory cell depletion, changes in CD8+ cell populations and the proliferation of both T regulatory cells and CD8 cells within the spleen of E.G7 tumour bearing mFcγRII KO, hFcγRIIB Tg and NoTIM mice treated with OX86 mIgG2a or isotype control

mFcγRII KO, hFcγRIIB Tg and NoTIM mice were given $5x10^5$ E.G7 cells via subcutaneous injection. When the tumour had become palpable (approximately 30 - 75 mm^2) mice were treated with a dose of either OX86 (anti-mouse OX40) mIgG2a or an isotype control, with an additional dose given two days later (Day 0 and Day 2) and then harvested on Day 4. A) the number of T regulatory cells per gram of spleen and percentage of CD4+FOXP3+ cells. B) The number of CD8+ cells per gram of spleen and CD8:T_{reg} ratio. C) The percentage of Ki67+CD4+FOXP3+ and Ki67+CD8+ cells in the spleen. The result of two independent experiments (6 mice per group). Line = mean ± SD. Statistical analyses conducted using a two-way ANOVA with Tukey's multiple comparison test. * = $P \leq 0.05$, ** = ≤ 0.01, *** = $P \leq 0.001$, **** = $P \leq 0.0001$.

5.3.3.2 Modulation of T cell compartments within the tumour

OX86 treated mFcγRII KO mice showed a decrease in total T_{reg} cell number and a significant decrease in percentage CD4+FOXP3+ ($1.81x10^5$ cells per gram of tumour and 1.7%, respectively) after OX86 treatment (Figure 5.11 A). hFcγRIIB Tg showed a modest and non-significant decrease in both cell number and percentage ($2.22x10^5$ cells per gram of tumour and 2.6%, respectively) whilst NoTIM mice demonstrated no change in total cell number and a very small decrease in percentage when compared to the isotype control ($3.61x10^5$ cells per gram of tumour and 3%, respectively).

Quantification of CD8+ cells per gram of tumour showed little difference between isotype and OX86 treated mice (Figure 5.11 B). mFcγRII KO mice had an enhanced but non-significant increase in the CD8:T_{reg} ratio after OX86 treatment compared to other OX86 treated mice. T cell proliferation was assessed by determining Ki67+ expression as before. OX86 treated mFcγRII KO mice showed a decrease in Ki67+ T_{reg} cells in comparison to isotype treated mice (20.16% and 38.25 %, respectively) accompanied by an increase in CD8+Ki67+ cells (29.68% and 18.5%, respectively) (Figure 5.11 C). In contrast, hFcγRIIB Tg mice showed a modest increase in Ki67+ T_{reg} cells and no change in Ki67+ CD8+ cells in comparison to isotype treated (36.57% and 15.99%, respectively) whilst NoTIM mice demonstrated a substantial increase in both Ki67+ T_{reg} cells and CD8+ cells (43.78% and 24.58%, respectively).

These data suggest OX86 efficiently depletes tumour associated T_{reg} cells in mFcγRII KO mice but to a much lesser extent in both hFcγRIIB Tg and NoTIM mice. NoTIM mice are more prone to target cell agonism and proliferation whilst mFcγRII KO demonstrate sustained systemic depletion of suppressive T_{reg} cells.

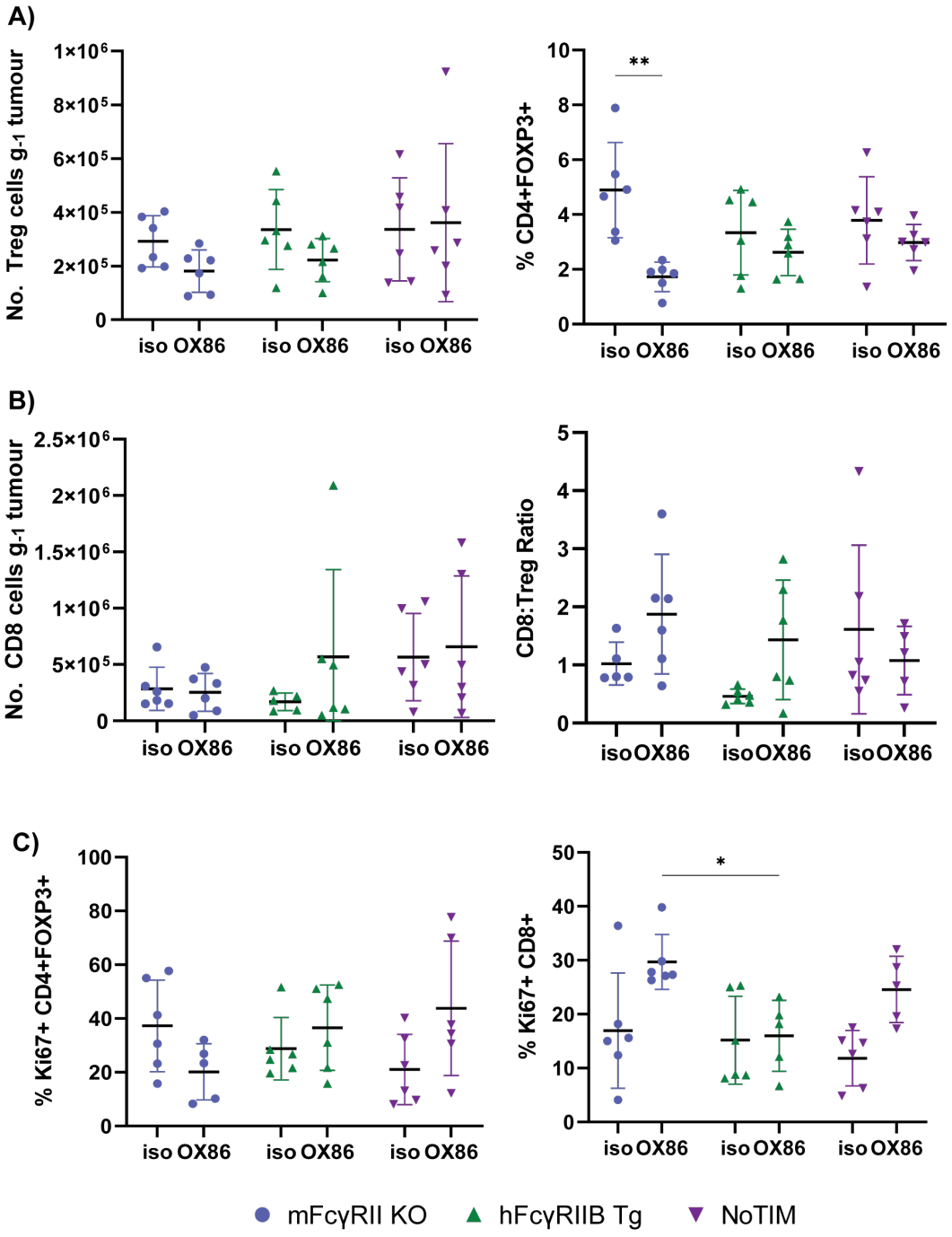

Figure 5.11: Dynamics of T regulatory cell depletion, changes in CD8+ cell populations and the proliferation of both T regulatory cells and CD8 cells within the tumour of E.G7 tumour bearing mFcγRII KO, hFcγRIIB Tg and NoTIM mice treated with OX86 mIgG2a or isotype control

mFcγRII KO, hFcγRIIB Tg and NoTIM mice were given 5x10^5 E.G7 cells via subcutaneous injection. When the tumour had become palpable (approximately 30 - 75 mm^2) mice were treated with a dose of either OX86 (anti-mouse OX40) mIgG2a or an isotype control, with an additional dose given two days later (Day 0 and Day 2) and then harvested on Day 4. A) the number of T regulatory cells per gram of tumour and percentage of CD4+FOXP3+ cells. B) The number of CD8+ cells per gram of tumour and CD8:T_{reg} ratio. C) The percentage of Ki67+ CD4+FOXP3+ and Ki67+CD8+ cells in the tumour. The result of two independent experiments (6 mice per group). Line = mean ± SD. Statistical analyses conducted using a two-way ANOVA with Tukey's multiple comparison test. * = P ≤ 0.05, ** = ≤ 0.01, *** = P ≤ 0.001, **** = P ≤ 0.0001.

5.3.4 Analysis of the myeloid compartment in the spleen and tumour following treatment with OX86 mIgG2a

Due to the nature of direct targeting antibodies requiring engagement of activatory FcγRs on myeloid cells to elicit target cell depletion, the myeloid compartment was interrogated in both the spleen and tumour. Due to tumours usually containing a high proportion of dying cells a live/dead indicator was used to isolate viable cells. PI was used for this purpose, it intercalates into the DNA of dying cells and critically is not permeable to live cells. This then allowed the identification of viable CD45+/CD11B+/Ly6C/+Ly6G cells (neutrophils), CD45+/CD11B+/Ly6C+ cells (Ly6C high monocytes) and CD45+/F4/80+/CD11Blo cells (F4/80+ macrophages) (Figure 5.12).

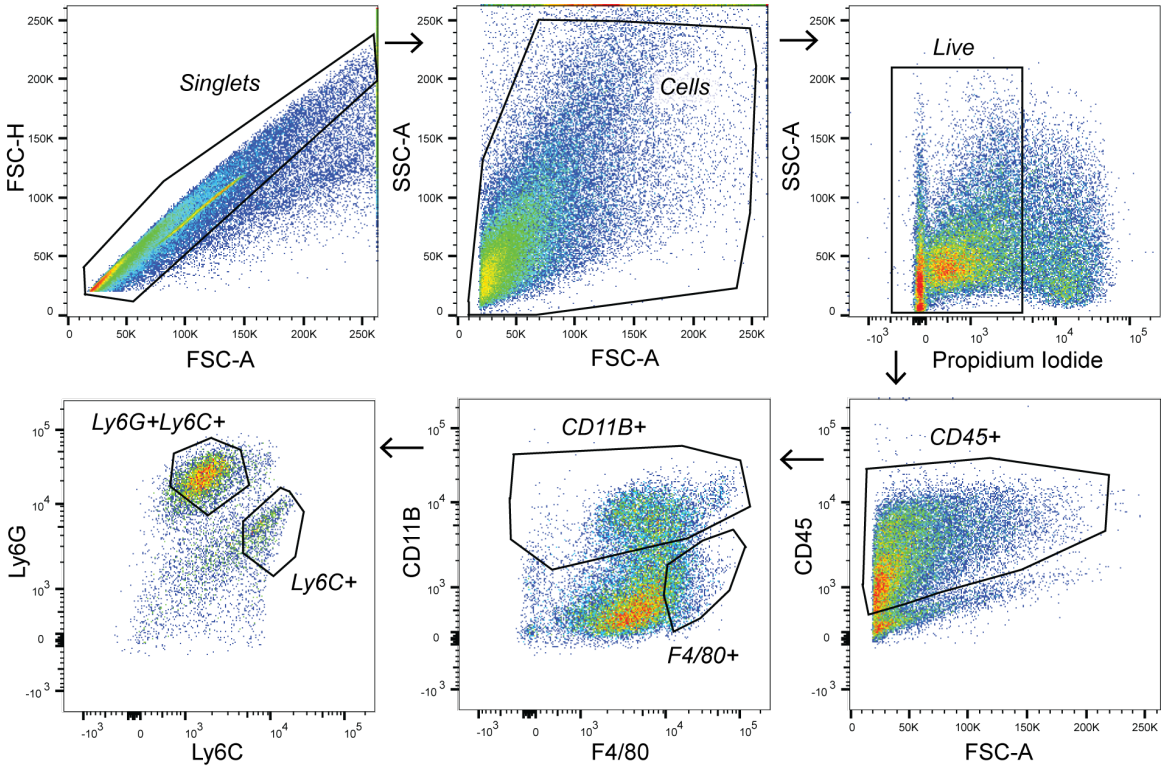

Figure 5.12: Gating strategy used to identify myeloid cells within the tumour microenvironment of E.G7 tumours
Cells negative for propidium iodide were analysed based on CD45+CD11B+Ly6C+Ly6G (neutrophils), CD45+CD11B+Ly6C+ (Ly6C high monocytes) and CD45+F4/80+CD11Blo (F4/80+ macrophages).

5.3.4.1 The myeloid compartment within the spleen following OX86 mIgG2a treatment in tumour bearing mice

The myeloid compartment within the spleen largely remained unchanged between mice treated with isotype or with OX86 (Figure 5.13). When quantifying the number of CD11B cells per gram of spleen and looking at the percentage of CD11B cells of CD45+ leukocytes, there was no differences observed between treatment group or mouse model. Due to the large variation in actual cell number it was difficult to draw any conclusions on the general myeloid population between treatment groups (Figure 5.13 A). Specific cell types showed some minor changes in proportions but these were not statistically significant again due to the large amount variation in individual mice (Figure 5.13 B). The proportion of macrophage cells in both hFcγRIIB Tg and mFcγRII KO mice showed a small decrease in comparison with isotype, whilst NoTIM mice had a slight increase. Ly6C high monocytes showed a similar trend. Changes in the neutrophils populations were minor.

5.3.4.2 The myeloid compartment within the tumour following OX86 mIgG2a treatment

Within the tumour, the myeloid populations showed some modest differences between those mice treated with isotype and OX86 (Figure 5.14). mFcγRII KO mice showed a small decrease in both cell number and percentage suggesting a reduction in myeloid infiltrate. hFcγRIIB Tg mice also showed a small decrease in cell number and no change in percentage compared to isotype treated mice whilst NoTIM mice showed an increase in the number of CD11B cells but a decrease as a percentage of CD45+ cells (Figure 5.14 A). This could indicate that NoTIM mice have a small increase in myeloid infiltrate as measured by cell number. The decrease in percentage could be due to the expanding T cell compartments.

Looking at individual cell populations, there were small but non-statistically significant changes when comparing isotype to OX86 treated mice (Figure 5.14 B). mFcγRII KO mice showed no change from isotype, whilst hFcγRIIB Tg mice had a small decrease and NoTIM mice had an increase in number of cells compared to isotype. Ly6C high monocyte infiltration was low across all mice with OX86 treated mice showing a modest decrease in the number of cells per tumour. Finally, neutrophil infiltration seemed to decrease in mFcγRII KO and hFcγRIIB Tg mice but showed no change in NoTIM mice.

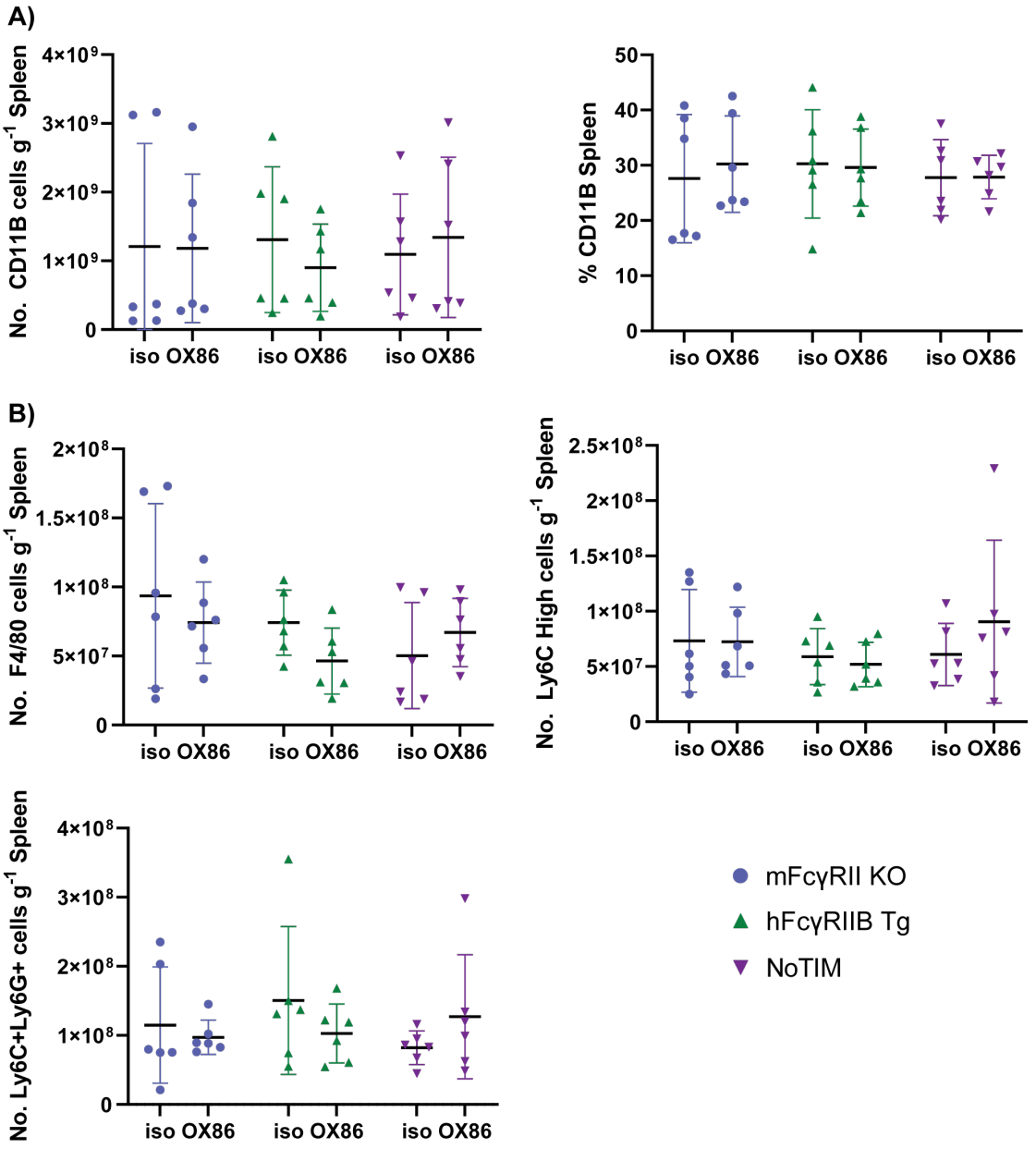

Figure 5.13: Myeloid compartment within the within the spleen of E.G7 tumour bearing mFcγRII KO, hFcγRIIB Tg and NoTIM mice treated with OX86 mIgG2a or isotype control

mFcγRII KO, hFcγRIIB Tg and NoTIM mice were given 5x10^5 E.G7 cells via subcutaneous injection. When the tumour had become palpable (approximately 30 - 75 mm^2) mice were treated with a dose of either OX86 (anti-mouse OX40) mIgG2a or an isotype control, with an additional dose given two days later (Day 0 and Day 2) and then harvested on Day 4. A) Enumerated CD11B cells per gram of spleen and percentage of CD11B+ cells of total CD45+ cells. B) The number of CD45+F4/80+CD11Blo (F4/80+ macrophages), CD45+CD11B+Ly6C+ (Ly6C high monocytes and CD45+CD11B+Ly6C+Ly6G (neutrophils). The result of two independent experiments (6 mice per group). Line = mean $\pm$ SD. Statistical analyses conducted using a two-way ANOVA with Tukey's multiple comparison test.

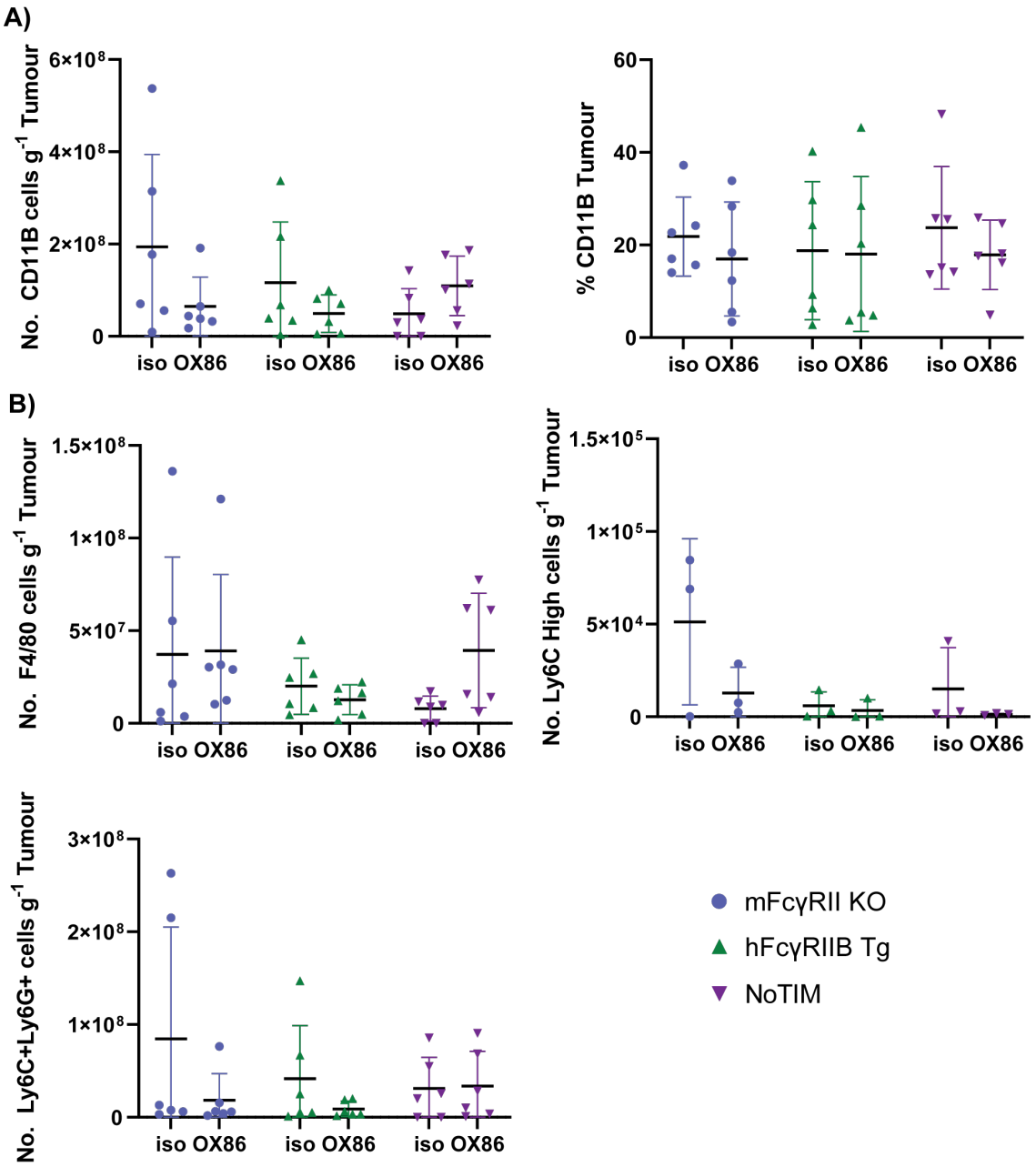

Figure 5.14: Myeloid compartment within the tumour of E.G7 tumour bearing mFcγRII KO, hFcγRIIB Tg and NoTIM mice treated with OX86 mIgG2a or isotype control

mFcγRII KO, hFcγRIIB Tg and NoTIM mice were given 5x10^5 E.G7 cells via subcutaneous injection. When the tumour had become palpable (approximately 30 - 75 mm^2) mice were treated with a dose of either OX86 (anti-mouse OX40) mIgG2a or an isotype control, with an additional dose given two days later (Day 0 and Day 2) and then harvested on Day 4. A) Enumerated CD11B cells per gram of spleen and percentage of CD11B+ cells of total CD45+ cells. B) The number of CD45+F4/80+CD11Blo (F4/80+ macrophages), CD45+CD11B+Ly6C+ (Ly6C high monocytes and CD45+CD11B+Ly6C+Ly6G (neutrophils). The result of two independent experiments (6 mice per group). Line = mean ± SD. Statistical analyses conducted using a two-way ANOVA with Tukey's multiple comparison test.

5.3.4.3 Impact of myeloid infiltrate on tumour progression

To understand if there was a link between myeloid infiltrate and tumour growth and/or tumour viability, a number of factors were analysed using linear regression. It was found that the more viable the tumour, the less CD11B+ cells within the tumour microenvrionment, however the relationship was weak (R^2 = 0.2019, P value = 0.0808) indicating other factors may be involved. The number of CD11B+ cells and the tumour size also showed a positive relationship, the larger the tumour the more CD11B+ cells within the tumour. This relationship was also weak with a R^2 value of 0.2311 and a P-value of 0.0434. Finally, the size of the tumour was correlated with tumour cell viability. This relationship had a negative correlation (R^2 value of 0.4521) and was deemed significant (P = 0.0022).

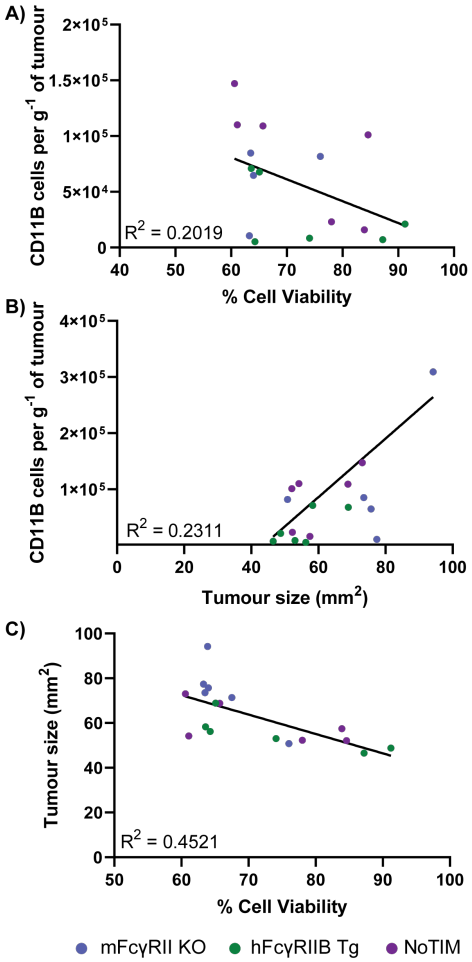

Figure 5.15: Simple linear regression of CD11B+ cell infiltrate, tumour size and cell viability within the tumour of E.G7 tumour bearing mFcγRII KO, hFcγRIIB Tg and NoTIM mice treated with OX86 mIgG2a or isotype control

mFcγRII KO, hFcγRIIB Tg and NoTIM mice were given 5x10^5 E.G7 cells via subcutaneous injection. When the tumour had become palpable (approximately 30 - 75 mm^2) mice were treated with a dose of either OX86 (anti-mouse OX40) mIgG2a or an isotype control, with an additional dose given two days later (Day 0 and Day 2) and then harvested on Day 4. A) Simple linear regression of CD11B+ cells per gram of tumour vs percentage cell viability. B) Simple linear regression of CD11B+ cells per gram of tumour vs tumour size. C) Simple linear regression of tumour size vs percentage cell viability. The result of two independent experiments (6 mice per group). The result of two independent experiments (6 mice per group).

5.3.4.4 hFcγRIIB expression within the spleen and tumour of E.G7 tumour bearing mice

To understand further how hFcγRIIB was modulating OX86 treatment in the E.G7 tumour model, the cellular expression of the receptor was analysed on key immune effector cells within the spleen (B cells, macrophages) and the tumour (TAMs) (Figure 5.16). The MFI of hFcγRIIB+ expression in NoTIM mice was found to be significantly higher than in hFcγRIIB Tg mice on both splenic B cells and macrophages. B cells had a MFI of 3969 in NoTIM mice, and a mean MFI of 2865 in hFcγRIIB Tg mice. Splenic macrophages were also assessed and had the highest MFI out of all assessed spleen populations (NoTIM mean MFI 4781, hFcγRIIB Tg mean MFI 1756). Within the tumour microenvironment, no B cells were detected (data not shown) and the only cell type present in sufficient quantities to assess receptor expression were TAMs. Interestingly, TAMs in the E.G7 model expressed hFcγRIIB at considerably lower levels than splenic macrophage populations. Nevertheless, NoTIM TAMs had a higher mean MFI (mean MFI 846) than that observed on hFcγRIIB Tg TAMs (mean MFI 599), however this was not statistically significant.

5.3.5 Survival of E.G7 tumour bearing mice treated with OX86 mIgG2a

Parallel cohorts of mice not used for tissue assessment were monitored for tumour growth and long term survival (Figure 5.18 and Figure 5.19). Those mice treated with the isotype control had a median survival of 8-11 days across each mouse model. All hFcγRIIB Tg mice treated with isotype mAb reached terminal endpoint (tumours of 225 mm^2), whilst 2/9 mFcγRII KO and 1/10 NoTIM mice had tumours that spontaneously regressed despite only receiving isotype control mAb. Tumour kinetics showed that the tumours grew exponentially once over 100 mm^2 in size with comparable growth rates in each mouse group.

Tumour kinetics in OX86 treated mice showed different patterns of growth and regression dependent on the mouse model (Figure 5.19). Broadly, mFcγRII KO mice were the most responsive to treatment, with most tumours reaching a size of 120 - 180 mm^2, before quickly regressing. mFcγRII KO 'non-responders' tended to grow to 50-75 mm^2, regressed in size after treatment and then began to grow in size after treatment was stopped albeit at a slower rate than observed in the isotype controls.

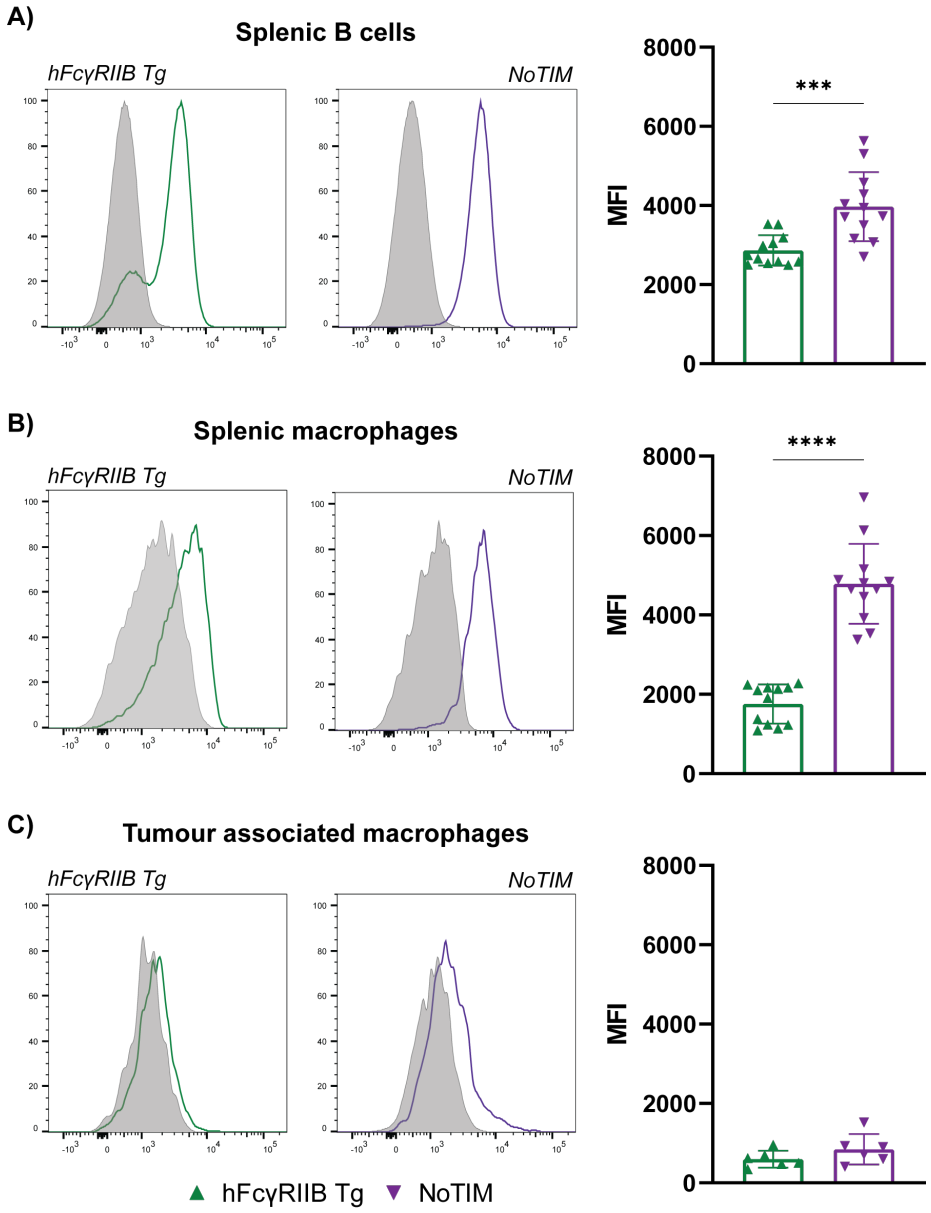

Figure 5.16: hFcγRIIB expression on splenic and tumour populations of E.G7 tumour bearing hFcγRIIB Tg and NoTIM mice treated with OX86 mIgG2a or isotype control

hFcγRIIB Tg and NoTIM mice were given 5x10^5 E.G7 cells via subcutaneous injection. When the tumour had become palpable (approximately 30 - 75 mm^2) mice were treated with a dose of either OX86 (anti-mouse OX40) mIgG2a or an isotype control, with an additional dose given two days later (Day 0 and Day 2) and then harvested on Day 4. A) Splenic B cell hFcγRIIB expression and MFI within hFcγRIIB Tg and NoTIM mice. B) Splenic macrophage hFcγRIIB expression and MFI within hFcγRIIB Tg and NoTIM mice. C) Tumour associated macrophage hFcγRIIB expression and MFI within hFcγRIIB Tg and NoTIM mice. Grey histogram = isotype control, coloured histogram = hFcγRIIB.The result of two independent experiments (6 mice per group). Line = mean ± SD. Statistical analyses conducted using a two-tailed unpaired t-test. *** = $P \leq 0.001$, **** = $P \leq 0.0001$.

Responding OX86 treated hFcγRIIB Tg mice had a mixture of kinetics. The majority of tumours grew to between 50 - 125 mm^2 before regressing whilst 'non-responders' typically grew unchecked. However, two 'non-responders' showed an initial response to treatment with some regression and then grew rapidly to experimental endpoint.

The majority of NoTIM mice which responded to OX86 treatment had tumours that grew

to 75 - 100 mm^2 before completely regressing. Like in hFcγRIIB Tg mice, some 'non-responders' either did not regress in response to treatment or grew to substantial size, showed some regression, before progressing to terminal endpoint.

When comparing response to therapy between mouse strains, there were 8/10 'responders' in the mFcγRII KO group, 6/12 'responders' in the hFcγRIIB Tg group and 7/12 'responders' in the NoTIM group (Figure 5.18). OX86 treatment provided a significant survival benefit compared to isotype treated mice for mFcγRII KO (P = 0.0030), hFcγRIIB Tg (P = 0.0011) and NoTIM mice (P = 0.0024). The Mantel-Cox statistical test found no significant difference between survival of OX86 treated mice (mFcγRII KO vs. hFcγRIIB Tg P = 0.1070, mFcγRII KO vs. NoTIM P = 0.2288). The median survival of hFcγRIIB Tg mice was 41 days, it is not possible to determine for mFcγRII KO and NoTIM mice due to the high number of surviving mice. Overall, OX86 provided a clear survival benefit in mice compared to those treated with isotype control, which was similar between each different mouse model. Although not statistically significant, mFcγRII KO mice appear to be more sensitive to OX86 treatment than mice carrying the hFcγRIIB transgene. in the E.G7 tumour model.

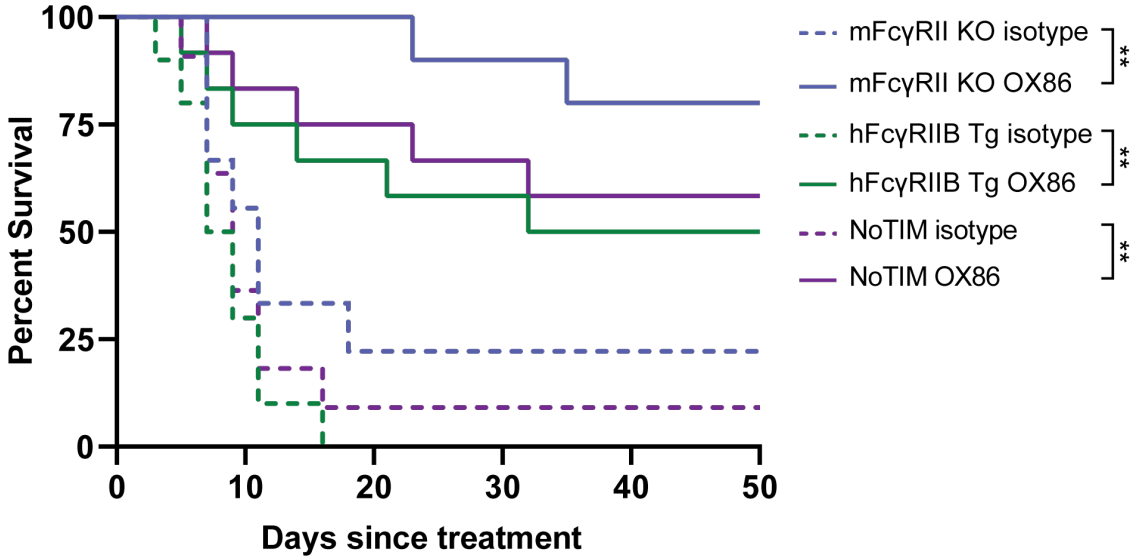

Figure 5.17: Kaplan-Meier survival in E.G7 tumour bearing mFcγRII KO, hFcγRIIB Tg and NoTIM mice treated with OX86 mIgG2a or isotype control

mFcγRII KO, hFcγRIIB Tg and NoTIM mice were given 5x10^5 E.G7 cells via subcutaneous injection. When the tumour had become palpable (approximately 30 - 75 mm^2) mice were treated with a dose of either OX86 (anti-mouse OX40) mIgG2a or an isotype control, with an additional dose given two days later (Day 0 and Day 2). Mice were then monitored until terminal endpoint (tumour measurement of 15x15 mm^2). A Kaplan Meier curve of E.G7 tumour bearing mice comparing survival between each different mouse group and treatment. The result of three independent experiments (10 - 12 mice per group). Statistical analyses conducted using the Mantel-Cox test. ** = $\leq$ 0.01.

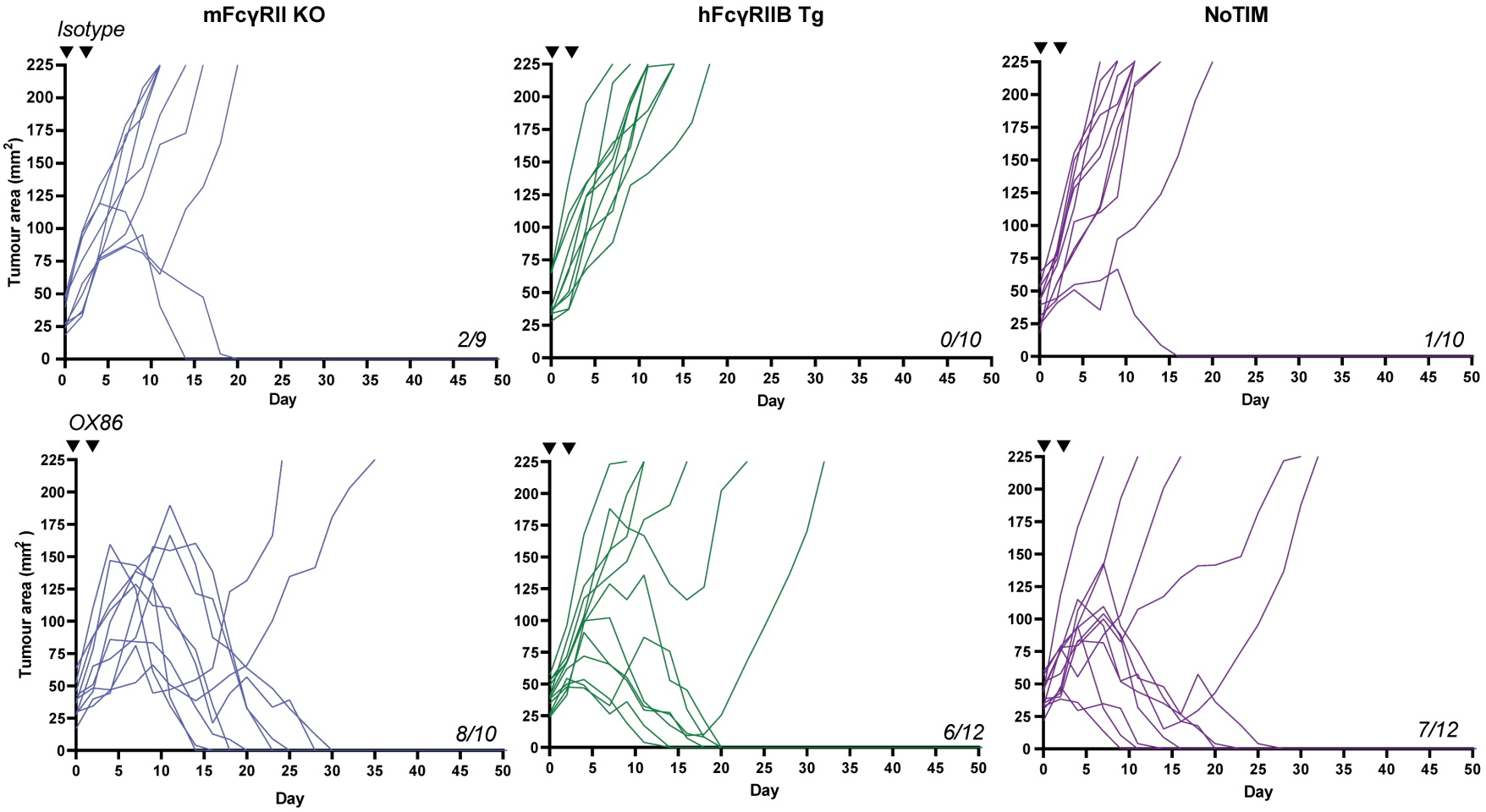

Figure 5.18: Kinetics of E.G7 tumour growth in mFcγRII KO, hFcγRIIB Tg and NoTIM mice treated with OX86 or isotype control

mFcγRII KO, hFcγRIIB Tg and NoTIM mice were given 5x10^5 E.G7 cells via subcutaneous injection. When the tumour had become palpable (approximately 30 - 75 mm^2) mice were treated with a dose of either OX86 (anti-mouse OX40) mIgG2a or an isotype control (indicated by the black arrow), with an additional dose given two days later (Day 0 and Day 2). Mice were then monitored until terminal endpoint (tumour measurement of 15x15 mm^2). The first row shows tumour kinetics in isotype treated mice whilst the second row shows tumour kinetics in OX86 treated mice. The result of three independent experiments (10 - 12 mice per group).

5.4 Discussion

In the previous chapter, evidence generated using the hFcγRIIB Tg and NoTIM mouse models suggested that FcγRIIB elicits inhibition of direct targeting antibody mediated cell depletion independently of the ITIM signalling motif. That chapter focused on the depletion of non-malignant normal cells; the aim of this chapter was to understand if the same principals applied to direct targeting antibody therapy in the context of murine tumour models. To investigate this, the syngeneic murine Eμ-TCL1 and E.G7 tumour models were utilised. The depletion of Eμ-TCL1 tumour cells was assessed using the anti-mCD20 mAb 18B12 mIgG2a, whilst E.G7 tumour therapy was examined through the depletion of T_{reg} cells using the anti-OX40 mAb OX86 mIgG2a. As expected, the depletion of both cell types was effective in mFcγRII KO mice, whilst hFcγRIIB Tg and NoTIM mice showed resistance. In the Eμ-TCL1 tumour model, mFcγRII KO mice had a significant improvement in survival over hFcγRIIB Tg and NoTIM mice, whilst in the E.G7 model mFcγRII KO mice had improved survival but this was not significant compared to other mice. The less marked improvement in the E.G7 tumour model is most likely down to the complex nature of OX40 biology and how high expression of FcγRIIB out-competes activatory mFcγRs to elicit crosslinking of OX86-OX40 and agonism, instead of depletion.

The Eμ-TCL1 tumour model was a natural progression from the previous chapter due to using the same anti-mCD20 mAb 18B12 as a depleting antibody. Like wild-type murine B cells, the malignant B cells express both mCD20 and mFcγRII but contain the human Eμ-TCL1 oncogene, driving uncontrolled proliferation (Figure 5.1). The expression of mFcγRII on the malignant B cells was considered to have minimal impact on target cell depletion. Previously it has been shown that 18B12 undergoes minimal internalisation in the presence of mFcγRII and inhibition by hFcγRIIB is driven through expression on immune effector cells (Chapter 4). Experiments were conducted using the mIgG2a subclass of 18B12 due to the aggressive nature of the Eμ-TCL1 tumour and it was found that mFcγRII KO mice showed strong and sustained depletion of both malignant cells and endogenous B cells for up to three weeks following treatment with 18B12 mIgG2a (Figure 5.2). In contrast, NoTIM mice had blunted depletion of malignant and endogenous B cells, with tumour cells recovering above baseline by Day 7. In every mouse model, 18B12 mAb therapy was shown to equally deplete malignant cells and endogenous B cells (Figure 5.3 B). Following mAb treatment, mFcγRII KO mice had the biggest fold decrease in target cell populations, NoTIM mice had the smallest fold decrease. Importantly, the differences

between malignant cells and endogenous B cells was not statistically different within each mouse model. This shows that there was not an innate difference in the modulation of direct targeting mAb therapy between each model; 18B12 was able to equally interact with CD20 on malignant cells and healthy cells. This means that any differences in depletion can be attributed to hFcγRIIB and not a tumour specific effect.

The TCL1:T cell ratio is another way to assess malignant cell recovery (Figure 5.1 E). By Day 7, all NoTIM mice had recovered above baseline (ratio of approximately 1) whilst mFcγRII KO and hFcγRIIB Tg took until Day 14 to surpass baseline. Individual hFcγRIIB Tg mice showed a broad differences in depletion, mirroring both mFcγRII KO and NoTIM depletion profiles. Together, these data show that the presence of the non-signalling hFcγRIIB results in less target cell depletion than seen in mFcγRII KO mice. Target cell recovery was substantially faster in mice containing a signalling or non-signalling variant of hFcγRIIB, suggesting that the presence of the receptor confers worsening outcomes for direct targeting mAb therapy. The tumour cells recovered at a particularly fast rate in NoTIM and hFcγRIIB Tg mice probably due to the lack of depletion in physiological niches were tumour cells reside. Human lymphomas have been shown to accumulate in regions that include the spleen, liver, gastrointestinal tracts and the peritoneal cavity [412]. In niches such as the spleen, the local environment can be considered to be immunosuppressive, with a dense network of immune cells modulating the adaptive and immune response [413]. In the previous chapter (Chapter 4) and analysing hFcγRIIB expression on splenic populations (Figure 5.16) it was shown with sub optimal doses of mAb, CD20+ cell clearance in the spleen was poor. This is most likely driven by the high expression of hFcγRIIB, allowing tumour cells to reside and repopulate. These tumour cells also reside in other immune suppressed environments such as the peritoneum [399]. mCD20 therapy was found to poorly deplete CD20+ resident peritoneum cells due to a lack of activatory myeloid cells [414]. Eμ-TCL1 cells are of B1 cell origin, and the peritoneum is a favoured niche of B1 B cells [399]. The peritoneum is also where cells are first injected into recipient mice. An increased reservoir of tumour cells in these locations due to poor depletion in NoTIM and hFcγRIIB Tg mice is likely to explain why peripheral cells recover at a faster rate than seen in mFcγRII KO mice. To investigate further, the hFcγRIIB expression profile could be screened within the peritoneum and enumeration of Eμ-TCL1 cells residing within the peritoneum could be compared between mouse models.

The depletion profile seen in hFcγRIIB Tg mice was varied. Some mice could be termed 'responders' with a depletion profile akin to mFcγRII KO mice whilst others were 'non-

responders' with a depletion profile akin to NoTIM mice. This is most likely the result of lower transgene expression (in comparison to NoTIM mice) and the mosaic expression pattern observed on some immune effector cells. Therefore, immune effector cells expressing little to no hFcγRIIB are able to optimally deplete target cells, whilst those cells with moderate expression are impaired in a similar manner to NoTIM effector cells. The net result is a depletion and recovery profile that sits between both mFcγRII KO and NoTIM mice. Following 18B12 mAb treatment, it is difficult to correlate transgene expression and MFI with depletion as a high level of depletion is initially observed irrespective of FcγRIIB expression level. Nevertheless, the pattern of depletion seen in hFcγRIIB Tg mice is reflective of the dose escalation experiments (Chapter 4). These data suggests the hFcγRIIB receptor elicits inhibition of mAb mediated target cell depletion of malignant cells also through competition with activatory mFcγRs. Published research has previously shown that Kupffer cells are responsible for mediating depletion of CD20+ tumour cells [346] and prior characterisation of the NoTIM model has shown high expression of hFcγRIIB on Kupffer cells (Chapter 3). Taken together, it can be hypothesised that competition between activatory mFcγRs and hFcγRIIB on liver resident Kupffer cells results in poor depletion of tumour cells in the transgenic models.

Previous work had looked at the link between target cell depletion and mAb concentration in the serum in normal mice (Chapter 4). To rule out a link between depletion and concentration in tumour bearing mice, 18B12 mIgG2a serum concentration was assessed. Although not directly comparable, it was important to formally investigate if the high expression of hFcγRIIB in NoTIM mice differentially modulated mAb half life in the presence of the Eμ-TCL1 tumour. Serum available 18B12 was analysed two days after mAb administration and as seen in the pharmacokinetics study (Chapter 4), NoTIM and hFcγRIIB Tg mice had less serum mAb than mFcγRII KO mice (Figure 5.3 C). This data suggests that the expression of hFcγRIIB is responsible for enhanced clearance of the mAb, and the higher expression observed in NoTIM mice may account for the significance between mFcγRII KO and NoTIM mice. However, once tumour cell depletion and mAb concentration were correlated, there was no relationship. It has been previously shown that 18B12 saturates mCD20 binding sites on splenic B cells at 2.5 μg/mL, and based on previous data we can assume that at least during the first 5 days all cells are equally saturated with mAb. In terms of mAb pharmacokinetics, it is accepted that the FcγR mediated eliminated pathway of mAbs cannot be saturated and therefore is not expected to substantially effect mAb pharmacokinetics (and therefore depletion) [378]. From this data we can be confident that differences in mAb concentration are not influencing target cell depletion.

Overall, mFcγRII KO mice treated with 18B12 mIgG2a had a significant improvement in survival compared to hFcγRIIB Tg and NoTIM mice (Figure 5.4 B). This is most likely due to the enhanced target cell depletion observed in mFcγRII KO mice, whilst target cell depletion was poor in both transgenic mouse models. The survival of NoTIM mice treated with 18B12 was particularly poor and was not able to provide a significant survival benefit over isotype, despite the fact the NoTIM receptor cannot initiate ITIM mediated signalling. These findings mirror the depletion of normal B cells (Chapter 4), where higher transgene expression in NoTIM mice compared to hFcγRIIB Tg mice was linked to poor depletion and faster recovery of target cells. To summarise, 18B12 mIgG2a mediated depletion of Eμ-TCL1 tumour cells was negatively impacted by the expression level of hFcγRIIB rather than the ability of the receptor to elicit ITIM mediated signalling. The higher the expression of hFcγRIIB, the less tumour cell depletion was observed and the quicker the tumour cells recovered, resulting in worsened survival outcomes.

To assess these conclusions more widely, the depletion of OX40+ T_{reg} cells using OX86 mIgG2a was examined in the subcutaneous E.G7 thymoma model. However, analysis of depletion in the three mouse models did not reveal straightforward impacts on outcome as seen in the Eμ-TCL1 tumour model. Nevertheless, the impact on T_{reg} cell depletion followed the expected pattern, with peripheral T_{reg} cell depletion strongest in mFcγRII KO mice with significantly less depletion observed in NoTIM mice on Day 2 (Figure 5.6). This resulted in an increase in the CD8:T_{reg} ratio of mFcγRII KO mice, with no change in NoTIM mice (Figure 5.7). The proliferative capacity of T_{reg}, CD4+FOXP3- and CD8 cells (as determined by Ki67+ staining) remained unchanged indicating that OX86 had the expected effect as a mIgG2a depleting antibody, in agreement with with previous observations (Chapter 4).

mFcγRII KO mice continued to demonstrate strong and sustained T_{reg} cell depletion and increased CD8:T_{reg} ratio, until a week after the last dose of mAb, when T_{reg} cells showed a recovery in terms of percentage and number (Figure 5.7). This observation was potentially expected as the depleting mAb would be consumed and reduced in the circulation. Anecdotally, within the laboratory and also briefly commented on in the literature [415], it has been seen that upon cessation of mAb treatment, T_{reg} cells can rapidly return to the periphery, even overshooting normal levels. In a non mAb T_{reg} cell depletion setting, using diphtheria toxin receptor-FOXP3 (DEREG) transgenic mice, it has been shown that following T_{reg} cell depletion, T_{reg} cells rebound and proliferate strongly to replace those that have been lost as an immune-homeostasis mechanism [416]. This same effect ap-

pears to be reflected in the Ki67+ data, where depleted T_{reg} cells on Day 2 and 4 show little change in proliferation whilst on Day 9 the T_{reg} cells proliferate strongly as they most likely attempt to repopulate T_{reg} cell niches. Further data generated using DEREG mice also suggested that extensively proliferating T_{reg} cells can become non-functional, having implications for the observations in all three mouse models [416]. However, it should be noted that these former experiments were conducted using systemic conditional depletion rather than mAb induced depletion which could result in different outcomes.

From Day 4, hFcγRIIB Tg and NoTIM mice deviated from the T_{reg} cell depletion profile (Figure 5.6) seen with anti-CD25 mAb depletion in Chapter 4. Instead, OX86 mIgG2a seemed to agonise OX40. In NoTIM mice, the percentage of T_{reg} cells had increased above isotype controls by Day 4, and by Day 9 there was a sustained statistically significant increase above isotype. hFcγRIIB Tg mice had an intermediate response, with some mice reflecting depletion as seen in mFcγRII KO mice and others expansion of T_{reg} cells as seen in the NoTIM mice. Despite the increase in T_{reg} cells, the CD8:T_{reg} ratio remained unchanged in NoTIM mice between Day 4 and Day 9 (Figure 5.7). This is most likely explained by the increase in proliferation of CD8+ cells observed from Day 4 and present at Day 9, itself likely as a result of the removal of T_{reg} suppression.

The data from the periphery suggests that in mFcγRII KO mice, where only activatory mFcγRs are present, there is a sustained depletion of OX40+ T_{reg} cells compared to isotype treated mice. On Day 9, T_{reg} cells showed strong proliferation as they began to repopulate alongside CD4+FOXP3- and CD8+ cells (Figure 5.8). In contrast, NoTIM mice initially show a blunted response to depletion of OX40+ T_{reg} cells. On Day 4, T_{reg} cells were highly proliferating with some indications of proliferation in the CD4+FOXP3- and CD8+ compartment. By Day 9, there is a strong increase in T_{reg} cells numbers but also in the proliferative capacity of CD4+FOXP3- and CD8+ cells, that are conceivably driven by direct OX40 agonism in these cell types. OX40 mAb agonism *in vivo* has been demonstrated using both murine OX40 and human OX40, where mAb isotypes that favour engagement with the inhibitory mFcγRII were shown to drive target agonism [417] [150]. Further studies have shown that mAb induced agonism of OX40 along with TCR stimulation induced expansion, differentiation and survival of CD4 and CD8 cells. Furthermore, If either the CD4 or CD8 compartment were depleted, OX40 agonism was no longer able to induce tumour regression [418] [419] [420]. These data indicate that OX40 agonism can drive better tumour control in murine models.

The mIgG2a subclass is usually utilised in murine models to induce potent target cell depletion. When targeting antigens with potentially dual functions on different cell types (e.g. OX40 and 4-1BB), successful strategies have utilised both the mIgG2a subclass to initially deplete T_{reg} cells and the mIgG1 subclass (which optimally engages the inhibitory mFcγRII) to agonise the receptor on effector T cell subsets to elicit proliferation and activation [145] [150]. In the context of the NoTIM mouse, it appears that the high expression of hFcγRIIB out-competes the high affinity interactions between mIgG2a and mFcγRI/mFcγRIV to crosslink OX86-OX40 interactions rather than deplete the target. This would explain why NoTIM mice show minimal depletion and strong proliferation of all T cell compartments from an early stage.

The direct effect of OX40 agonism on T_{reg} cells is disputed. Some published research suggests that direct agonism of OX40 on T_{reg} cells drives their suppressive function. One published paper suggests that OX40 agonism, using OX86 rIgG1, directly suppresses T_{reg} cells *in vitro* and *in vivo* and is not able to directly induce T_{reg} cell proliferation [421]. The authors go on to suggest that rested T_{reg} cells *in vitro* are susceptible to OX40 mediated suppression, however when activated with IL-2 and CD3 micro beads this suppression is no longer functional. However, OX86 mAb mediated selective suppression of naïve T_{regs} was only investigated *in vitro* and has not been shown *in vivo* [421]. In contrast, a later paper suggested that OX40 agonism of T_{reg} cells can drive expansion in the context of the right cytokines. It was found that naïve mice treated with OX86 rIgG1 had a significant increase in splenic T_{reg} cells. These expanded T_{reg} cells were also found to suppress CD8 effector cells as efficiently as isotype treated T_{reg} cells giving conflicting evidence for the change in phenotype/function after OX40 stimulation [422]. The authors went on to show in an autoimmune setting, that if OX86 rIgG1 was administered at the priming stage of the disease (i.e. before symptoms arise), treatment results in T_{reg} cell expansion and lessened disease severity. If administered during disease onset (i.e. after symptoms arise), it resulted in worsened disease severity, with enhanced production of IL-2, IL-6 and IFN-γ, attributed to a loss of T_{reg} cell suppression.

In the context of the syngeneic CT26 tumour, another group found that OX86 rIgG1 treatment resulted in better tumour control than isotype treated mice with no changes in number of T_{reg} cells within the tumour. They deduced that therapy was elicited through OX40 mediated inhibition of T_{reg} cells, the suppression of effector T cell conversion to T_{reg} cells and was dependent on CD8 cells being present within the tumour [423]. In contrast, another study highlighted that OX86 required activatory FcγRs to deplete T_{reg} cells within

the tumour microenvironment. Firstly, the authors found that OX86 rIgG1 depleted T_{reg} cells within the tumour of CT26 treated mice. This finding was found to be dependent on activatory FcγRs and knocking out mFcγRII enhanced therapy (as seen with OX86 mIgG2a therapy in E.G7 bearing mFcγRII KO mice [Figure 5.11]). Treatment was further enhanced when OX86 was switched to the mIgG2a subclass, adding weight to the requirement of activatory FcγRs for efficacy [424].

Taken together, the conflicting evidence across multiple studies suggests that OX40 mAbs are driving a combination of activatory FcγR mediated depletion, alongside mFcγRII mediated agonism leading to effector T cell activation and potentially T_{reg} cell suppression. Each individual mechanism may depend on differential FcγR expression levels, OX40 expression levels and relative cell proportions coupled to the complex cytokine milieu present in anatomical niches such as the tumour. As such, the prevailing mechanism of anti-OX40 mAb therapy is not understood and the use of different mouse models, antibody therapies, tumour models and dosing makes it difficult to ascertain the exact mechanism of OX40 agonism on T_{reg} cells *in vivo*. Here, when assessing the impact of T_{reg} cell depletion versus expansion on overall survival within each mouse model, it can be hypothesised that depletion of OX40+ T_{reg} cells provides therapy in the E.G7 tumour model, as shown by Bulliard et al. [424]. However, the strong expansion of T_{reg} cells in NoTIM mice also results in 7/12 mice surviving the experiment, suggesting OX40 agonism also provides a survival benefit. Taken together, these data suggests that perhaps the expanded T_{reg} cells seen in NoTIM mice could be non-functional or inhibited by OX40 agonism as shown by Piconese et al. and in the context of a growing tumour by Ruby et al. [423] [422]. Alternatively, or even concurrently, the CD8 T cells may be further agonized to deliver tumour control (albeit with a trend towards being less effective than mFcγRII KO mice). When a tumour is first established it is generally accepted that it invokes a pro-inflammatory microenvironment as the immune system responds to the malignant cells. As E.G7 cells produce a neoantigen in the form of OVA, this is likely to be the case for this tumour model too. Therefore, it can be inferred that when OX86 is given to mice after the tumour has been established, the milieu of pro-inflammatory cytokines within the tumour microenvironment may drive dysfunction and/or inhibition of T_{reg} cells alongside more potent CD8 stimulation when OX40 is agonised, allowing optimal CTL control of the tumour.

Analysis of T_{reg} cells within the spleen on Day 4 accentuated the data generated in the periphery (Figure 5.10). mFcγRII KO mice demonstrated a decrease in T_{reg} cells, with a substantial increase in CD8:T_{reg} cell ratio. Interestingly, the percentage of Ki67+ cells

in mFcγRII KO was significantly more after OX86 treatment than isotype control within the spleen. This was not observed in the periphery and could be a result of changing the balance of activatory:inhibitory cells within the spleen, having an impact upon CD8+ cells. The spleen is a dense network of immune cells with many cell:cell contacts. T_{reg} cells can exert inhibition of effector T cells through direct contact [425] and so by depleting the T_{reg} cells in mFcγRII KO mice and removing the cell:cell contact mediated inhibition, this could result in enhanced activation of effector T cells. In contrast, NoTIM mice showed an expansion of T_{reg} cells, a decrease in the CD8:T_{reg} cell ratio and strong proliferation of splenic T_{reg} cells and CD8+ cells. The strong expansion and proliferation of T cell populations within the spleen is probably driven by the high expression of hFcγRIIB delivering OX40 agonism as discussed above. It has been shown that NoTIM splenic B cell and macrophage populations express significantly higher hFcγRIIB than observed in hFcγRIIB Tg mice (Figure 5.16), therefore we would expect to see a higher degree of OX40-OX86 cross-linking in the NoTIM mice. This observation is supported by the stronger OT-I expansion seen in mCD40 mAb treated NoTIM mice in Chapter 4. Therefore it can be deduced that the Fc of OX86 is more likely to interact with hFcγRIIB if the receptor is highly expressed, leading to cross-linking and agonism of OX40 rather than target depletion.

Within the tumour, it was clear that mFcγRII KO mice experienced systemic T_{reg} cell depletion (Figure 5.11). This was statistically significant in terms of the percentage of CD4+FOXP3+ cells, whilst hFcγRIIB Tg and NoTIM mice showed a modest decrease in T_{reg} cells. An increase in Ki67+ T_{reg} cells suggested a mild agonistic effect in hFcγRIIB Tg and NoTIM mice as compared to the periphery and spleen, with no change in Ki67+ T_{reg} cells in mFcγRII KO mice. Proliferating CD8+ cells were present in larger numbers in mFcγRII KO mice than NoTIM mice suggesting that T_{reg} cell depletion had a stronger effect on CD8+ activation than OX40 agonism in this model. A noteworthy observation was the lack of T_{reg} cell expansion within the tumour microenvironment in NoTIM mice despite clear expansion in the spleen. Analysis of hFcγRIIB expression showed that the only hFcγRIIB+ cells present in substantial quantities were tumour associated macrophages (CD45+/F4/80+/CD11Blo), and the expression seen in hFcγRIIB Tg and NoTIM mice was significantly lower than observed on B cells or macrophages from the spleen (Figure 5.16). The lower expression of hFcγRIIB observed in the tumour could explain the lack of agonism in this niche, with not enough receptor to cross link OX40-OX86-hFcγRIIB. Therefore, the lower expression of hFcγRIIB results in inhibition of depletion rather than receptor agonism.

In a recently published paper, OX86 rIgG1 treatment in the MCA-205 tumour model showed that mAb treatment resulted in an expansion of splenic T_{reg} cells but a reduction in tumour associated T_{reg} cells, showing similar findings to those reported here in the E.G7 model [426]. The authors also found that OX86 treatment resulted in an increase in proliferation of all T cell compartments when mFcγRII was present, suggesting the mouse inhibitory receptor is driving agonism. This would be expected of the rIgG1 isotype as it behaves similarly to the mIgG1 isotype with respect to FcγR binding profile ([369], in-house data Dr Ian Mockridge). Critically, analysis of OX86 treated T_{reg} cells within the tumour showed no change in inhibitory function. *ex vivo* OX86 treated T_{reg} cells could still suppress effector T cell populations suggesting OX40 agonism does not inhibit T_{reg} cells. Instead, the authors suggested that effector CD4 cells enhance IL-2 production upon OX40 stimulation, supporting both T_{reg} and CD4+ effector cell proliferation. OX40 agonism of T_{reg} cells was also shown to result in the secretion of effector CD4 cytokines such as IFN-γ and TNF-α. These data from Polesso et al., share common features with the observations made in hFcγRIIB Tg and NoTIM mice suggesting that OX40 agonism may drive T_{reg} cells towards an effector cell phenotype when sufficient FcγR-mediated cross linking can take place.

Within the literature, analysis of the myeloid compartment within CT26 tumours treated with OX86 rIgG1 showed a decrease in the infiltration of myeloid derived suppressor cells and macrophages. The authors inferred OX40 agonism increased CD8 cell infiltration, decreasing the suppressive nature of the tumour microenvrionment and found an inverse correlation of response to treatment and myeloid infiltrate [418]. The myeloid compartments within the E.G7 model were also investigated and were found to be unaffected by OX86 mIgG2a treatment (Figure 5.13, Figure 5.14). Within the spleen, there are no notable changes between mouse groups or models (Figure 5.13) and within the tumour microenvironment, there is no immediate differences within the myeloid compartment (Figure 5.14). OX86 treatment may again increase F/80+ infiltrate in NoTIM mice but the effect is insignificant when compared to the infiltrate present in mFcγRII KO mice. The number of Ly6C+Ly6G+ cells seems to be decreased in OX86 treated mFcγRII KO and hFcγRIIB Tg whilst remaining unchanged in NoTIM mice. But again, the significance of these changes is not clear and is most likely due to biological variation within the tumour. Comparisons to the published data from Redmond et al. may differ because of different tumour models, genetic background of the mice, mAb isotype and the treatment regimen [418]. For example, the CT26 tumour is known to contain a particularly high T_{reg} cell infiltrate and

therefore may be more sensitive to OX40 mAb therapy than the E.G7 model [427]. The myeloid infiltrate is likely to differ between the two models as well.

When assessing overall survival of E.G7 bearing mice treated with OX86, the different mechanisms of action between the mouse models paints a complex picture (Figure 5.17). Isotype treated mice succumb to tumour endpoint broadly between Day 9 - 18. Tumour growth of OX86 treated mice showed significant variation, but with generalisable patterns. mFcγRII KO tumours grew to an advanced stage (125 - 175mm^2) before fully regressing, whilst 'non-responders' had tumours that regressed at a smaller size (75 - 125mm^2) before relapsing to reach terminal endpoint. hFcγRIIB Tg and NoTIM mice treated with OX86 had similar growth patterns. Responding mice had tumours that grew to a 50 - 125mm^2 before fully regressing, whilst 'non-responders' generally had no difference in tumour kinetics compared to isotype treated mice. Long term survival showed OX86 treatment provided a survival benefit, with better overall (but statistically non-significant) survival in mFcγRII KO than hFcγRIIB Tg or NoTIM mice (Figure 5.18). OX86 treatment was sufficient to arrest tumour growth in all mouse models, presumably through different mechanisms of action as discussed above. This data supports the dual mechanisms of action observed in the literature for the targeting of agonistic receptors on T_{reg}, CD4+FOXP3- and CD8+ T cells [424] [422] [150] [426].

The proposed mechanism of action based on the data and observations from the literature is as follows. The high expression of OX40 on T_{reg} cells facilitates target cell depletion in mFcγRII KO mice (Figure 5.19). The removal of T_{reg} cell suppression removes the homeostasis mechanisms that would otherwise keep CD4+FOXP3- and CD8+ activation in check and allows optimal proliferation and activation of these effector T cells. The activated effector T cell compartment then destroys the OVA-expressing tumours as 'non-self' (Figure 5.20). These data are supported by the observation that sufficient depletion of tumour associated T_{reg} cells (as seen in mFcγRII KO mice) provides anti-tumour immunity [424] [426]. The E.G7 treated mice whom reach terminal endpoint despite OX86 treatment could be a result of tumour escape through downregulation of OVA presentation, upregulation of inhibitory receptor ligands (such as PD-L1) or such a sharp rebound in T_{reg} cell numbers after treatment has ceased, re-instating the CD8+ T cell suppression.

In contrast, it is proposed that OX86 treatment in NoTIM mice initially results in modest depletion of T_{reg} cells (impaired by the NoTIM hFcγRIIB). The high expression of hFcγRIIB within these mice outcompete activatory FcγRs and further agonise OX40 sig-

nalling through crosslinking OX40-OX86 interactions (Figure 5.19). Crosslinking of OX40 is known to result in upregulation of cell proliferation, survival and activation of T effector cells, however the effects of OX40 agonism on T_{reg} cells is contested as discussed earlier. What is clear is that the high expression of hFcγRIIB drives OX40 agonism, resulting in a highly proliferative T_{reg} cell compartment and an expanded effector cell compartment. This could be achieved through direct OX40 agonism on the T_{reg} cell compartment during the priming phase [422] or agonism of CD4 effector cells providing IL-2 to enhance T_{reg} cell proliferation [426]. Direct OX40 agonism may also impart suppression on T_{reg} cells as discussed [421]. The overriding mechanism cannot be deduced from current data.

To identify the prevailing mechanism, it would be useful to isolate NoTIM tumour associated and splenic T_{reg} cells to conduct suppression assays and compare their activity. Single cell sequencing could be utilised on these T_{reg} cell subsets and compared to cells from isotype treated mice to establish if OX40 agonism changes the phenotype/transcriptional profile of the T_{reg} cells. The therapy experiment could be also repeated with mice either pre-treated with a CD25 blocking mAb or IL-2 neutralising mAb to ascertain if IL-2 release from effector T cells drives T_{reg} cell proliferation.

When looking at all T cell compartments, the expansion of T_{reg} cells seems to be the dominant effect in NoTIM mice and when translating into longer term survival this may result in the lower, but non-significant, decrease in survival compared to mFcγRII KO mice (Figure 5.20). The expansion of the effector T cell compartment results in tumour control and regression in some mice. But approximately 50% of tumours do not respond to treatment, suggesting that the expansion of the T_{reg} compartment is able to outweigh the effector cell expansion in these mice. Ultimately, the combination of both T_{reg} cell depletion and effector T cell expansion results in effective tumour control.

To conclude, in this chapter two different tumour models were used to ascertain if hFcγRIIB could elicit inhibition of direct targeting mAb therapy independently of ITIM signalling. In both models, it was clear that the deficiency of an inhibitory receptor (mFcγRII KO mice) resulted in robust target cell clearance and enhanced tumour control. Both the signalling (hFcγRIIB Tg) and non-signalling hFcγRIIB (NoTIM) transgenic mice displayed resistance to mAb mediated target cell depletion. These findings confirm that in the context of murine tumour models, hFcγRIIB mediated inhibition of mAb mediated depletion is independent of ITIM inhibitory signalling.

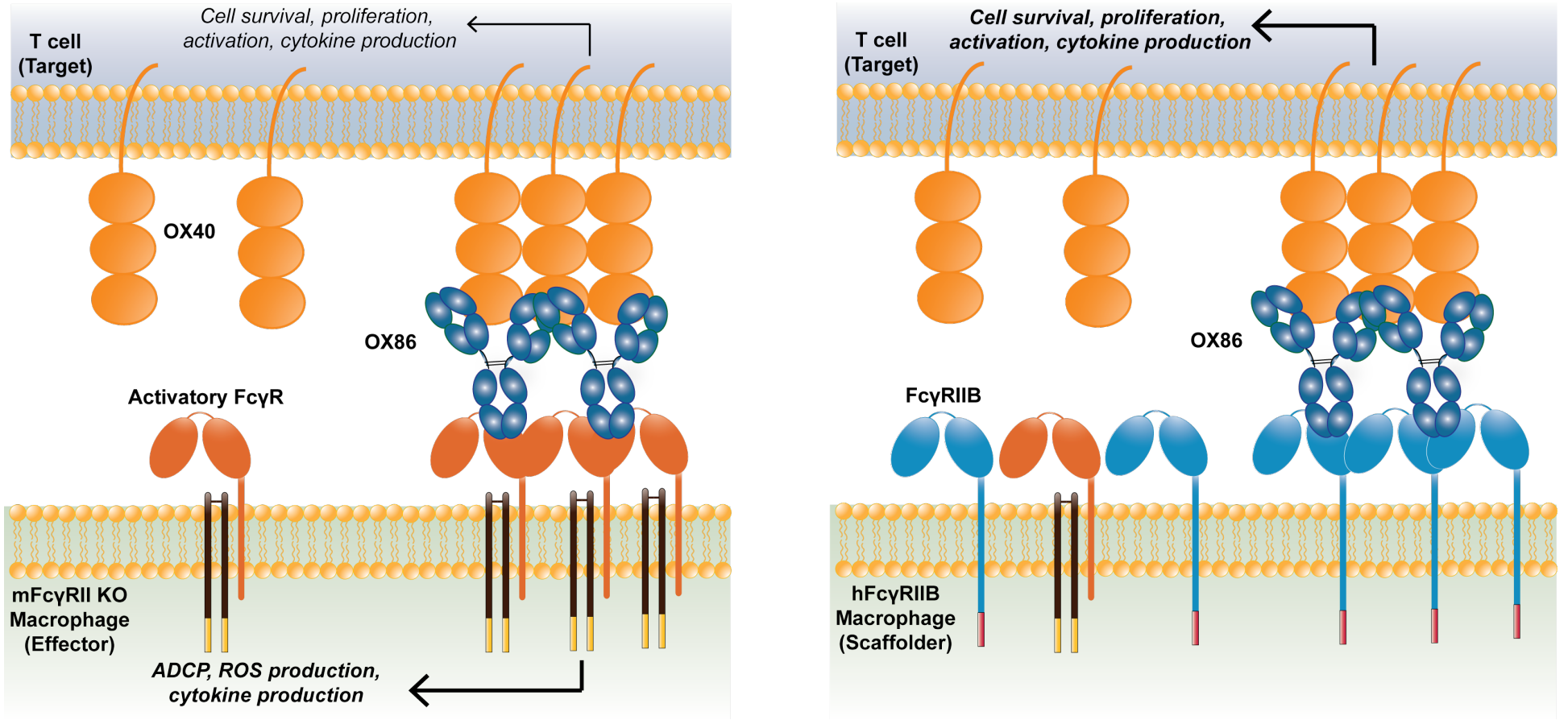

Figure 5.19: Proposed Molecular mechanism of OX40-OX86 interactions
The left hand side depicts OX86-OX40 interactions within mFcγRII KO mice. Depletion driven by activatory FcγR interactions on immune effector cells is likely to drive target depletion. The right hand side depicts interactions in hFcγRIIB TG/NoTIM mice. hFcγRIIB is likely to outcompete activatory FcγRs, cross-linking OX40 and driving activatory signalling on the target cell.

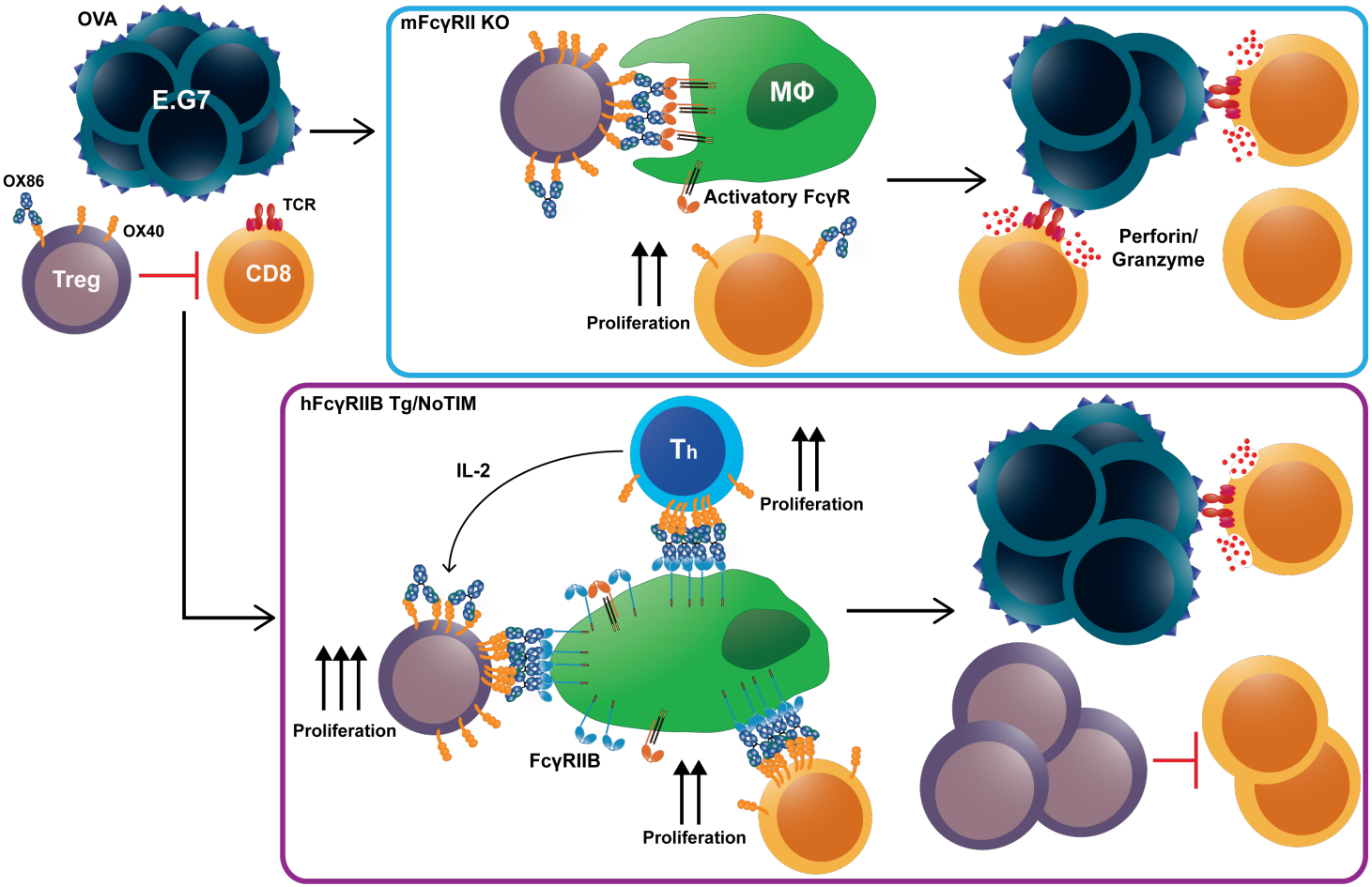

Figure 5.20: Proposed cellular mechanism of action of OX86 treatment
The top part shows the proposed mechanism of action in mFcγRII KO mice (blue box). Efficient interactions of OX86 with activatory mFcγRs drives depletion of T_{reg} cells resulting in activation and proliferation of effector T cells, resulting in tumour control. In hFcγRIIB Tg/NoTIM mice (purple box), hFcγRIIB may outcompete activatory mFcγRs to drive OX40 agonism expanding T_{reg} cells and effector T cells. This expansion can also result in tumour control. T_h = effector CD4 T cell, Mϕ = macrophage.

Chapter 6

General discussion

Since the discovery of the human FcγRIIB transcript [320], a large body of research has been dedicated to understanding how the single inhibitory FcγR regulates the immune system in health and disease. The ITIM signalling motif was discovered through crosslinking FcγRIIB on the surface of B cells, where it was found to inhibit ITAM signalling elicited by the BCR [428] [240]. FcγRIIB mediated inhibition of IgG effector functions was first characterised through manipulation of the murine homologue mFcγRII, and identified that mice deficient in the inhibitory receptor had enhanced inflammation in response to immune complexes and increased IgG dependent macrophage effector functions [233]. Further to this, Clynes et al. found murine tumour models were more responsive to direct targeting mAb therapy if treatment was conducted in an FcγRII deficient mouse [185]. These seminal findings led to the currently accepted dogma that the inhibitory FcγR elicits inhibition of direct targeting mAb therapy through ITIM signalling.

However, more recently, it has been found that FcγRIIB can regulate the formation of the BCR immunological synapse [253] [254], internalise type-I CD20 mAbs [300] and modulate the activity of immunomodulatory mAbs [308] [310] independently of FcγRIIB mediated ITIM signalling. As these signalling independent mechanisms have been identified, it has led to the re-evaluation of how critical ITIM mediated signalling is to the inhibition of mAb target cell depletion *in vivo*.

This question – what is the contribution of ITIM signalling to hFcγRIIB mediated inhibition of direct targeting mAb target cell depletion - was evaluated in this thesis using two parallel mouse models. One contained the wild-type hFcγRIIB that was able to elicit ITIM

signalling (hFcγRIIB Tg mice), the other a signalling-defective hFcγRIIB incorporating two mutations - Y254F and Y273F in the intracellular tail (NoTIM mice) (Figure 3.1).

Murine and human FcγRs share similarities in terms of structure and function, however there are limitations to the extrapolation of findings in mice to humans. Critical differences include cellular expression patterns (for example, human platelets express hFcγRIIA, whilst murine platelets express no FcγRs [192]), human receptor polymorphisms, the A:I ratio dictating the thresholds of activation (governed by differences in expression pattern, IgG subclasses and affinity [341]), and the key mediators of direct targeting mAb therapy (hFcγRIIIA on NK cells is highly expressed and thought to be important for mAb therapy in humans, mFcγRIII on murine NK cells is weakly expressed has been shown to be dispensable [429] [430] [431]). Therefore, efforts have been made to generate transgenic mouse models containing only human FcγRs and these have improved our understanding of human mAb biology [432] [342] [341]. However, the genetic deletion of murine mFcγRs and insertion of the human hFcγR, even at the same genetic locus have resulted in models that do not fully recapitulate human FcγR expression, meaning an element of caution is required when interpreting results even using these mouse models. Whilst the function of FcγRs are well conserved between mouse and human, the expression pattern of activatory FcγRs vary quite significantly between species [433]. The inhibitory FcγR shows greater similarities between mouse and human, with fewer differences in expression observed, Therefore, the hFcγRIIB transgenic mouse models provide a relatively simple *in vivo* model to study how this human receptor regulates activatory FcγRs.

The expression of FcγRs in hFcγRIIB expressing transgenic mice was extensively characterised against a further mouse model lacking mFcγRII, containing only activatory mouse FcγRs (mFcγRII KO) and the wild-type C57BL/6J mouse containing all endogenous murine FcγRs (Figure 3.11). The results showed that activatory mFcγR expression was broadly similar across mice alongside appropriate expression (or lack) of mFcγRII and hFcγRIIB. The expression pattern of hFcγRIIB in NoTIM mice had a closer expression profile to that seen in humans and reported in the literature compared to mFcγRII expression [56] [192]. The splenic architecture was preserved with appropriate expression of hFcγRIIB on B cells, whilst in the liver, hFcγRIIB had a differing expression pattern compared to mFcγRII (Figure 3.4, Figure 3.15, Figure 3.17, Figure 3.18). hFcγRIIB Tg mice were noted to have a mosaic expression pattern of the hFcγRIIB on some cell types and was an important observation that would inform findings from *in vivo* experiments

(Figure 3.13). The NoTIM mice by contrast had consistent expression on all hFcγRIIB+ cell types.

Once the cellular and tissue expression pattern of the NoTIM mouse was assessed, the consequences of the NoTIM mutations were probed, initially *in vitro*. Agonism of the NoTIM receptor showed that it was unable to be phosphorylated on the ITIM domain, nor result in phosphorylation of the inhibitory signalling mediator SHIP-1. This was in contrast to agonism of the WT hFcγRIIB, which showed both phosphorylation of the ITIM and SHIP-1 (Figure 3.19). Inhibition of BCR induced calcium flux by hFcγRIIB agonism was successfully demonstrated in hFcγRIIB Tg B cells, evident as a reduced and delayed increase in intracellular calcium. When repeated on NoTIM B cells, agonistic anti-hFcγRIIB mAb did not influence calcium flux, suggesting the ITIM signalling domain was non-functional (Figure 3.20). The internalisation of ahIgG (a surrogate for immune complex) was also investigated and showed that signalling competent hFcγRIIB Tg B cells resulted in faster internalisation compared to signalling mutant NoTIM B cells during the first 30 minutes of the experiment (Figure 3.21). In contrast, the internalisation of the anti-CD20 mAb 18B12 mIgG1 was similar between hFcγRIIB Tg and NoTIM B cells (Figure 4.6). These findings indicate the NoTIM mutations most likely affect the clathrin dependent ahIgG internalisation mechanism [434] [239]. In contrast, lacking a functional ITIM did not alter the impact of hFcγRIIB on internalisation of CD20 mAbs, which is known to be independent of the FcγRIIB cytoplasmic domain [300]. Finally, the influence of the NoTIM receptor on phagocytosis of opsonised cells by BMDMs was investigated. Here, ITIM signalling was indicated to negatively regulate target cell ADCP with BMDMs from NoTIM mice more active than those from hFcγRIIB Tg mice (Figure 3.24, Figure 3.25). Clynes et al. previously demonstrated that murine peritoneal macrophages deficient in mFcγRII had enhanced phagocytic potential [233]. The evidence generated using NoTIM mice goes further and directly implicates the ITIM signalling motif, demonstrating the non-signalling NoTIM receptor conveys better ADCP than the signalling competent hFcγRIIB Tg receptor. Importantly, ADCP could be partially rescued in hFcγRIIB Tg BMDMs by pre-blocking the receptor with a specific Fc null mAb, whilst blocking the NoTIM receptor did not improve ADCP.

ADCP is an important immune effector function that is responsible for removing pathogens but also malignant cells. As previously mentioned, the depletion of circulating tumour cells *in vivo* using direct targeting mAbs in mice has been shown to be reliant on ADCP by Kupffer cells [346]. Therefore, various strategies are being researched and deployed to

improve ADCP in cancer patients treated with direct targeting mAbs [435]. The use of the antagonistic hIgG1 hFcγRIIB blocking mAb is currently being investigated as a strategy to improve rituximab mediated depletion of lymphoma cells [326]. The Fc null variant of hIgG1 hFcγRIIB blocking mAb is also going through pre-clinical testing as a combination therapy with the dual function (checkpoint blockade and T_{reg} cell depletion) anti-CTLA-4 mAb [325]. The evidence generated suggested ITIM signalling negatively regulates IgG effector functions and validated the concept of therapeutically blocking hFcγRIIB mediated signalling in cancer models.

These data described in Chapter 3 led to the hypothesis that direct targeting mAb depletion would be enhanced in NoTIM mice compared to hFcγRIIB Tg mice *in vivo*. To test this, mice were treated with mAbs designed to deplete peripheral lymphocytes and the kinetics of depletion were examined. Different mAb isotypes were utilised based on their availability and known FcγR affinities to identify any subtleties in depletion between different mouse models. The anti-mCD20 mAb 18B12 was first used and showed superior B cell depletion in mFcγRII KO mice with moderate levels of inhibition observed in hFcγRIIB Tg and C57BL/6J mice (Figure 4.2, Figure 4.4). NoTIM mice consistently showed the most inhibition of the depletion of CD20+ B cells, irrespective of mAb subclass. This observation was not mCD20 or B cell specific, since depletion of both NK cells and T_{reg} cells using anti-NK1.1 or anti-CD25/anti-OX40 targeting mAb respectively, was less effective in NoTIM mice (Figure 4.15, Figure 4.17), Figure 5.6).

The strong inhibition observed in NoTIM mice was unexpected. To investigate how inhibition was elicited, further studies were conducted. Neither internalisation of 18B12 by B cells nor the modulation of mAb by hFcγRIIB were thought to be the main determinant of differences in target cell depletion between each mouse model. Experimental evidence did show that the presence of the mouse or human inhibitory receptor did increase B cell mediated antibody internalisation in-vitro and result in a decrease in 18B12 mAb persistence *in vivo* (Figure 4.6) (Figure 4.7) (Figure 5.3). However, these findings were not significantly different and so did not explain the observed target cell depletion profile.

Once these factors had been excluded, the data from the 18B12 dose escalation experiments were re-evaluated (Figure 4.2, Figure 4.4). hFcγRIIB Tg mice treated with mIgG1 split into two groupings, 'responders' (with a mFcγRII KO like depletion profile) and 'non-responders' (with a NoTIM like depletion profile) (Figure 4.9). The mosaic expression of the hFcγRIIB transgene was analysed in these mice (Figure 3.13), and it was found that

mice who displayed a higher expression (percentage positive transgenic cells and geometric mean of positive population) were more resistant to B cell depletion. Based on these data the working hypothesis changed to state hFcγRIIB inhibition is elicited through expression, not ITIM signalling.

To understand if inhibition was mediated through expression on target cells or effector cells, a series of adoptive transfer experiments with target B cells were devised (Figure 4.10). These experiments found that target cell expression of the NoTIM receptor did not inhibit target cell depletion, but that instead it could act as an effective second cell surface target, meaning mAbs directed against the receptor (6G) could synergise with rituximab to enhance target cell depletion (Figure 4.11). Other published studies have also used hFcγRIIB as a target to elicit lymphoma cell depletion, validating these findings [323] [133]. However, when the NoTIM receptor was only expressed on effector cells, there was inhibition of target cell depletion in the NoTIM mice as compared to mFcγRII KO mice (Figure 4.11). Inhibition could only be overcome by using an Fc-null mAb (6Q) to block hFcγRIIB. The hIgG1 blocking mAb (6G) did not improve depletion despite binding to the same epitope as 6Q. It was postulated that 6G was ineffective because it bound to both hFcγRIIB (Fab interaction) and activatory mFcγRs (Fc interaction) on the surface of immune effector cells, also known as the Kurlander effect [236] (Figure 4.12). This would block the direct targeting mAb rituximab from interacting with activatory FcγRs, therefore inhibiting depletion of target cells. Taken together, these data suggest that the major mechanism of inhibition of hFcγRIIB, in these mouse models at least, is through competition between activatory FcγRs and the inhibitory hFcγRIIB for the Fc of the direct targeting mAb (Figure 4.22).

mFcγRII KO mice demonstrate that in the absence of an inhibitory receptor, mAb mediated target cell depletion is robust. In comparison, NoTIM mice showed clear resistance to mAb target cell depletion, similar to the wild-type hFcγRIIB Tg mice, despite the lack of ITIM signalling. These findings were surprising. The in-vitro ADCP assay (Figure 3.25) indicated that inhibitory signalling negatively regulated mAb effector functions, whilst *in vivo* ITIM signalling appears to be redundant for hFcγRIIB to elicit inhibition. The reason for this discrepancy could be due to the saturating concentrations of mAb used in-vitro compared to *in vivo*. In most experiments *in vivo*, sub-optimal doses of mAb were used which most likely resulted in target opsonisation but allowed competition between FcγRs. *In Vitro*, the high concentrations of mAb used would negate competition as a mechanism of inhibition, potentially emphasising the impact of ITIM mediated signalling on ADCP. It

is also difficult to assess the relative contribution of ITIM signalling to inhibition of *in vivo* target cell depletion in hFcγRIIB Tg mice due to differing levels of transgene expression and mosaic expression pattern. To address this question more effectively, both hFcγRIIB Tg and NoTIM mice would be required to demonstrate the same levels of receptor expression and equivalent gene penetrance. Current technologies could utilise CRISPR-Cas9 genetic manipulation to re-engineer in the functional tyrosine phosphorylation sites back into NoTIM mice. However, costs remain a barrier and these data suggest that the major mechanism of inhibition is elicited through competition, and that blocking the receptor with an Fc null mAb is enough to restore target cell depletion to a level similarly seen in mFcγRII KO mice.

It was subsequently assessed if these principles were also applicable in a tumour setting. The depletion of mCD20+ Eμ-TCL1 cells was investigated using 18B12 as before, allowing for a direct comparison with findings made with respect to normal B cell depletion in Chapter 4. The experiment utilised the mIgG2a subclass, and as seen previously Eμ-TCL1 cell depletion was significantly less effective in NoTIM mice compared to mFcγRII KO and hFcγRIIB Tg mice (Figure 5.2). Both endogenous B cells and Eμ-TCL1 cells were equally depleted across all models, however the Eμ-TCL1 cells recovered substantially faster than the B cells, as expected for a malignant, rapidly proliferating, cell. The fast pace of tumour cell recovery (especially in NoTIM mice) could be due to the physiological niche occupied by the Eμ-TCL1 tumour cells. The peritoneal cavity (where cells are injected and the proposed cellular origin of Eμ-TCL1 cells) is considered to be immunosuppressive [399] and therefore it could potentially have higher expression of the inhibitory FcγR on the resident macrophage population. Higher hFcγRIIB expression in NoTIM mice would inhibit target cell depletion and allow faster re-population of tumour cells than seen in hFcγRIIB Tg and mFcγRII KO mice.

Long term survival in tumour bearing mice showed a significant survival benefit in 18B12 treated mFcγRII KO mice compared to isotype treated as well as hFcγRIIB Tg and NoTIM 18B12 treated mice (Figure 5.4). In comparison, NoTIM mice had no significant survival benefit with 18B12 treatment compared to isotype treated NoTIM mice which can be explained by the systemically high hFcγRIIB expression inhibiting tumour cell depletion. These findings agree with other published observations. For example, the high expression of the inhibitory mFcγRII in the tumour microenvironment was linked to the ineffective depletion of T_{reg} cells with anti-CD25 mAb in the MCA-205 tumour model [369]. It was also found in the BCL_1 tumour model that the tumour co-opts the microenvironment to up-

regulating the expression of mFcγRII, reducing the ability of anti-CD20 mAb to deplete B cells and the tumour cells themselves [359]. These examples show how up-regulated expression of the inhibitory receptor results in decreased target cell depletion and worsened survival outcomes. To see if inhibition in the Eμ-TCL1 tumour model could be overcome, mice could be co-administered 18B12 with 6Q (hFcγRIIB Fc null blocking mAb). Nevertheless, these data indicate that hFcγRIIB elicits signalling independent inhibition of direct targeting mAb therapy in the context of the Eμ-TCL1 tumour.

To validate these findings in another murine tumour model, the depletion of OX40+ T_{reg} cells was assessed in the E.G7 thymoma model. mFcγRII KO mice treated with OX86 mIgG2a were most susceptible to T_{reg} cell depletion within the periphery, spleen and tumour (Figure 5.6, Figure 5.10, Figure 5.11), consistent with their susceptibility to depletion of CD25+ T_{reg} cells (Figure 4.17). hFcγRIIB Tg and NoTIM mice had also shown some resistance to T_{reg} cell depletion in the CD25+ depletion model, however the targeting of OX40 using OX86 mIgG2a was more complex to interpret due to the potential for these mAb to elicit both agonism as well as depletion of multiple cell populations [423] [422] [426] [150]. Across the experiment, depletion of T_{reg} cells was less effective in both hFcγRIIB Tg and NoTIM mice within the periphery and tumour microenvironment compared to mFcγRII KO mice. However, the lack of depletion and potential contribution of OX40 agonism resulted in greater proliferation of multiple T cell compartments, likely impacting tumour growth rates and overall survival (Figure 5.6, Figure 5.8, Figure 5.10, Figure 5.11).

The agonistic function of the OX40 mAb seen in hFcγRIIB Tg and NoTIM mice was most likely elicited by hFcγRIIB ability to cross-link mAb-OX40 interactions, resulting in OX40 signalling on target cells. hFcγRIIB elicited agonism has been well characterised in the literature for the TNFR superfamily, with a particular focus on mAbs targeted to CD40, 4-1BB and OX40 [308] [309] [143] [144] [145] [150].

The ability of both hFcγRIIB transgenic mouse models (WT and NoTIM) to elicit CD40 agonism was formally investigated using the OT-I adoptive transfer model after OVA immunisation. It was found that NoTIM mice treated with anti-CD40 mIgG1 had a significantly greater expansion of the OT-I cell population than hFcγRIIB Tg mice, whilst mAb treatment in mFcγRII KO mice were completely inert (Figure 4.19). These data fully supports previous studies showing that the high expression of the inhibitory FcγR drives strong CD40

agonism and this effect is independent of the cytoplasmic domain of the receptor [308] [309] [310].

Together, these results demonstrate that hFcγRIIB can inhibit direct targeting mAb independently of ITIM signalling. These results were surprising as, a substantial body of work on mFcγRII and hFcγRIIB as well as a plethora of other ITIM containing receptors have suggested ITIM signalling is the predominant inhibitory mechanism [436]. ITIM mediated signalling is clearly important to some physiological processes, for example B cell clonal selection and depletion - mice deficient in mFcγRII have been found to have more circulating B cells and a lower quality IgG response [392]. However in B cells, FcγRIIB mediated ITIM signalling only negatively regulates BCR ITAM signalling. In contrast, immune effector cells, such as macrophages, express a number of different activatory FcγRs. The single inhibitory FcγRIIB may have a diverse expression pattern however, studies have shown that activatory FcγRs considerably outnumber the inhibitory receptor on effector cells [56] [192]. Second to this, FcγRIIB contains only one ITIM domain compared to two ITAM domains for several activatory FcγRs. It is therefore possible that FcγRIIB would be unable to elicit efficient inhibition of activatory FcγRs if the only mechanism of action depended on ITIM signalling. The initial intracellular signalling mechanisms also provide evidence in favour of this hypothesis. For effective SHIP-1 recruitment to the ITIM motif (the major phosphatase of ITIM signalling), not only is phosphorylation of the ITIM required but also a further downstream non-ITIM phosphorylated tyrosine to aid binding - increasing the requirements to elicit ITIM mediated inhibitory signalling [437] [438]. Surprisingly, binding was also found to be reliant on the presence of Syk, the key kinase that elicits ITAM downstream signalling [438]. In comparison, Syk itself was found to be a highly efficient kinase and only required the present of the double phosphorylated ITAM to induce strong binding/signalling [439]. The 'simpler' mechanics of Syk mediated signalling seem to be favoured over SHIP-1 signalling and suggests Syk could mediate signalling more easily than SHIP-1.

A single inhibitory receptor with one ITIM domain regulating a family of activatory receptors is unusual in immune regulation. Most inhibitory receptors contain two or more ITIMs in their intracellular tails, such as the LILRB family (ranging from 2 - 4 ITIM domains) [440], SIRPα (3 ITIM domains) [441], and LAIR1 (2 ITIM domains) [442]. Receptors containing one ITIM tend to be coupled with an immunoreceptor tyrosine-based switch motif (ITSM - a receptor that can convey either activatory or inhibitory signalling depending on the context), such as PD-1 where the ITSM and ITIM are both critical to eliciting

inhibitory signalling [443]. Alternatively, there are multiple inhibitory receptors to regulate multiple activatory receptors such as within the KIR receptor system [440]. Finally, ITIM containing inhibitory receptors bind to ligands without competition (e.g. SIRPα and CD47) or groupings of activatory and inhibitory receptors have very different ligands (KIR and LILR families) allowing the effective transduction of inhibitory restrictions to occur. FcγRIIB does not have any of the additional advantages of other inhibitory receptors that allow potent signalling to take place. Taken together, it seems unlikely that FcγRIIB ITIM mediated signalling would be able to singularly regulate the diverse activities of multiple ITAM-containing activatory FcγRs.

However, modulation of activatory IgG responses is still critical to maintaining immune homeostasis. mFcγRII knockout mouse models have demonstrated that there is a risk of increased mortality following repeated immunisations with pathogens compared to WT mice (although it should be noted this was observed at very high doses) [247]. Data generated from autoimmune patients has also shown that those carrying the inhibition defective 232T hFcγRIIB polymorphism and/or display a downregulation of hFcγRIIB compared to healthy patients are more susceptible to the development of SLE [282], rheumatoid arthritis [283] and anti-glomerular basement membrane disease [284]. These examples demonstrate the importance of the inhibitory FcγR to temper activatory receptors. Therefore, the data generated in this thesis suggests that an important additional mechanism of FcγRIIB mediated inhibition of activatory FcγRs is elicited through competition for the Fc of the IgG molecule, independent of ITIM signalling. As the common ligand for all of these receptors is immune complexed IgG, hFcγRIIB does not have to rely on ITIM signalling to reduce activatory FcγR mediated ITAM signalling, it simply needs to out-compete these other receptors for binding to the Fc. As described in Chapter 4, this mechanism of inhibition resembles that employed by the signalling neutral hFcγRIIIB. Treffers et al. found hFcγRIIIB restricts neutrophil effector functions by competing with hFcγRIIA for the Fc of the direct targeting mAb, acting as a decoy receptor [234]. These lines of evidence suggest that both FcγRIIB and FcγRIIIB operate similarly as negative regulators of direct targeting mAbs, by acting as decoy receptors.

The inhibitory FcγRIIB has been well conserved across evolution in mammalian species, suggesting the receptor is well equipped to modulate activatory FcγRs [433]. In contrast since diverging from rodents, primates have evolved to contain more activatory FcγRs [433]. These findings may be the result of the importance of FcγRs in eliciting adaptive immune functions through innate immune cells. Potent activatory FcγR effector functions

are necessary to specifically eradicate pathogens, whereas limiting these functions is only important for the reduction of collateral tissue damage and/or subsequent autoimmunity [247]. Therefore, inhibition largely elicited through competition may be advantageous to minimally inhibit FcγR activatory signalling. Instead of utilising strong ITIM signalling to counteract ITAM signalling, competition perhaps allows a robust IgG effector response to be mounted under potentially rapidly changing IgG, immune complex and/or cellular stimulation conditions. This may also explain why FcγRIIB has a broad expression pattern whilst activatory FcγRs are restricted. To further explore this hypothesis, a genetically engineered hFcγRIIB expressing two or more ITIM domains could be generated. This could be then compared to the NoTIM receptor and the functional (single ITIM) hFcγRIIB receptor, all with similar expression levels. This would provide some insight to the contribution of ITIM signalling to the inhibition of direct targeting mAb therapy.

The observations in this thesis show that competition is a major mechanism of action. However it is difficult to extrapolate these findings directly to humans because there is limited information on FcγR expression in different human tissues and therefore it is difficult to definitively say if the high transgene expression recapitulates human expression. Experiments using transgenic mice show if the low affinity hFcγRIIB is expressed highly enough, then the receptor can outcompete the endogenous (often higher affinity) activatory mFcγRs. However, in a human physiological setting it is difficult to state if competition would be such a potent mechanism of inhibition. More investigation is required to establish this in humans, however observations showing the potential upregulation of the inhibitory FcγR in diseased states (e.g. the tumour microenvironment) in murine models suggests that competition may be a major mechanism of action in disease [369]. Alternate mechanisms of inhibition outside the ITIM domain and structural inhibition elicited by FcγRIIB also remain unanswered. Early studies by Fong et al. probed alternative signalling motifs of FcγRIIB B1 upon receptor activation and found evidence of phosphorylation outside the ITIM but no immediate downstream effect [258]. It cannot be ruled out that a alternative and/or un-categorised inhibitory signalling motif may elicit intracellular inhibitory signalling and is responsible for inhibition observed within NoTIM mice. These alternative hypotheses would require thorough investigation before they competition can be identified as the definitive mechanism of inhibition.

Direct targeting mAbs are critical therapeutic tools used in the treatment of diseases such as autoimmunity and cancer, relying on FcγRs to elicit their efficacy. Despite their evident success, treatment failures are common and further research is required to improve their

depletive potential. With a specific focus on cancer, it is clear that upregulation of the inhibitory FcγR within the tumour microenvironment and potentially on the tumour itself is detrimental to IgG effector functions [185] [369] [359] [302]. Strategies have been utilised to block hFcγRIIB with success in both pre-clinical testing and human clinical trials [323] [325] [327] [326]. The research within this thesis suggests that ITIM signalling is redundant for hFcγRIIB to elicit its inhibitory potential. Instead, competition for the antibody seems to be the major mechanism if inhibition. These data further validates the approach of targeting the receptor itself, instead of the inhibitory signalling pathway to improve direct targeting mAb therapy in humans. In regards to cancer, hFcγRIIB specific mAbs could have the potential to reverse the prognoses of relapsed refractory cancers using hFcγRIIB expression as a resistance mechanism to mAb therapy.

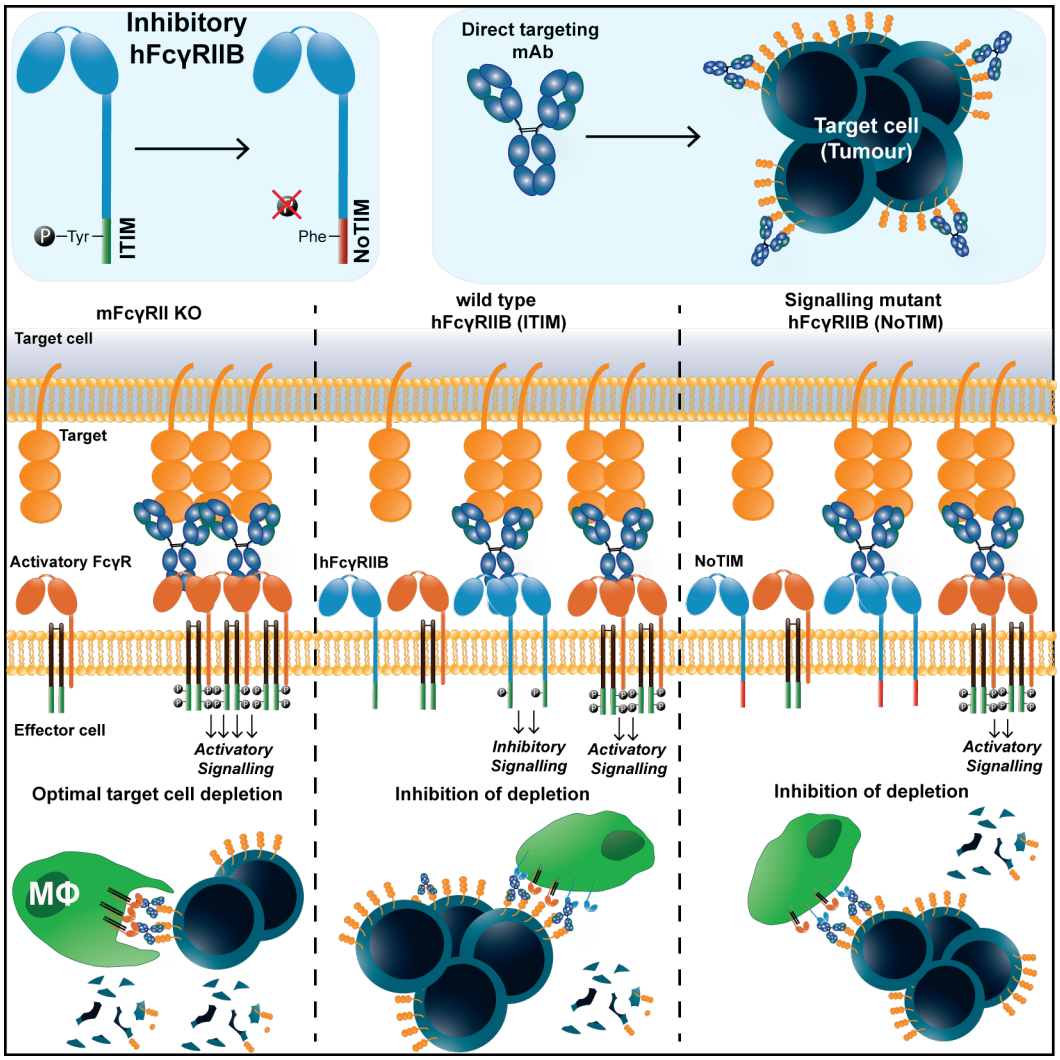

Figure 6.1: Summary of hFcγRIIB mediated inhibition of direct targeting mAb therapy
Graphical abstract of how hFcγRIIB mediates inhibition to direct targeting mAb therapy *in vivo*. Three mouse models were used consistently throughout this experiment - mFcγRII KO mice (expressing only activatory mFcγRs), hFcγRIIB Tg mice (expressing activatory mFcγRs and wild type (WT) hFcγRIIB) and NoTIM mice (expressing activatory mFcγRs and ITIM signalling mutant hFcγRIIB). A series of *in vivo* experiments were conducted using direct targeting mAbs to identify the contribution of ITIM mediated signalling by hFcγRIIB to the inhibition of target cell depletion. Depletion in mFcγRII KO mice was most efficient, due to the lack of an inhibitory receptor. Depletion in both WT hFcγRIIB and NoTIM mice was restricted in the presence of the receptor, independently of the ability of the receptor to initiate inhibitory signalling. Instead, in these mouse models the main mechanism of hFcγRIIB mediated inhibition was driven by competition with activatory mFcγRs for the Fc of the depleting mAb.

References

1. Ahmad, A. S., Ormiston-Smith, N. & Sasieni, P. D. Trends in the lifetime risk of developing cancer in Great Britain: Comparison of risk for those born from 1930 to 1960. *British Journal of Cancer* **112,** 943–947 (Mar. 2015).
2. McGranahan, N. & Swanton, C. *Clonal Heterogeneity and Tumor Evolution: Past, Present, and the Future* Feb. 2017.
3. Hanahan, D. & Weinberg, R. A. *The hallmarks of cancer* Jan. 2000.
4. Hanahan, D. & Weinberg, R. A. *Hallmarks of cancer: The next generation* Mar. 2011.
5. Khan, N., Afaq, F. & Mukhtar, H. *Lifestyle as risk factor for cancer: Evidence from human studies* 2010.
6. Roy, R., Chun, J. & Powell, S. N. *BRCA1 and BRCA2: Different roles in a common pathway of genome protection* Jan. 2012.
7. Doorbar, J. *et al. Human papillomavirus molecular biology and disease association* Mar. 2015.
8. Dunn, G. P. *et al. Cancer immunoediting: From immunosurveillance to tumor escape* 2002.
9. Gajewski, T. F., Schreiber, H. & Fu, Y. X. *Innate and adaptive immune cells in the tumor microenvironment* 2013.
10. Sambi, M., Bagheri, L. & Szewczuk, M. R. *Current challenges in cancer immunotherapy: Multimodal approaches to improve efficacy and patient response rates* 2019.
11. Kennedy, L. B. & Salama, A. K. S. A review of cancer immunotherapy toxicity. *CA: A Cancer Journal for Clinicians* **70,** 86–104 (Mar. 2020).
12. Akamatsu, Y. & Oettinger, M. A. Distinct Roles of RAG1 and RAG2 in Binding the V(D)J Recombination Signal Sequences. *Molecular and Cellular Biology* **18,** 4670–4678 (Aug. 1998).
13. Shankaran, V. *et al.* IFNγ, and lymphocytes prevent primary tumour development and shape tumour immunogenicity. *Nature* **410,** 1107–1111 (Apr. 2001).
14. Beral, V. & Newton, R. *Overview of the epidemiology of immunodeficiency-associated cancers.* Mar. 1998.
15. Frisch, M., Biggar, R. J., Engels, E. A. & Goedert, J. J. Association of cancer with AIDS-related immunosuppression in adults. *Journal of the American Medical Association* **285,** 1736–1745 (Apr. 2001).
16. Ljunggren, H. G. & Kärre, K. In search of the 'missing self': MHC molecules and NK cell recognition. *Immunology Today* **11,** 237–244 (1990).
17. Dunn, G. P., Koebel, C. M. & Schreiber, R. D. *Interferons, immunity and cancer immunoediting* Nov. 2006.
18. Chaplin, D. D. Overview of the immune response. *Journal of Allergy and Clinical Immunology* **125,** S3 (Feb. 2010).

19. Bennett, R., Phipps, R., Strange, A. & Grey, P. *Environmental and human health impacts of growing genetically modified herbicide-tolerant sugar beet: A life-cycle assessment* **4,** 273–278 (2004).
20. Amarante-Mendes, G. P. *et al. Pattern recognition receptors and the host cell death molecular machinery* Oct. 2018.
21. Turner, M. D., Nedjai, B., Hurst, T. & Pennington, D. J. Cytokines and chemokines: At the crossroads of cell signalling and inflammatory disease. *Biochimica et Biophysica Acta - Molecular Cell Research* **1843,** 2563–2582 (Nov. 2014).
22. Immunity, I. CHAPTER 14 Innate Immunity. *Immunology* **125,** 1–4 (2006).
23. Gasteiger, G. *et al. Cellular Innate Immunity: An Old Game with New Players* 2017.
24. Yang, J. *et al. Monocyte and macrophage differentiation: Circulation inflammatory monocyte as biomarker for inflammatory diseases* 2014.
25. Jakubzick, C. V., Randolph, G. J. & Henson, P. M. Monocyte differentiation and antigen-presenting functions. *Nature Reviews Immunology* **17,** 349–362 (Apr. 2017).
26. Stansfield, B. K. & Ingram, D. A. Clinical significance of monocyte heterogeneity. *Clinical and Translational Medicine* **4** (2015).
27. Boyette, L. B. *et al.* Phenotype, function, and differentiation potential of human monocyte subsets. *PLoS ONE* **12** (ed Zissel, G.) e0176460 (Apr. 2017).
28. Sprangers, S., Vries, T. J. & Everts, V. Monocyte Heterogeneity: Consequences for Monocyte-Derived Immune Cells. *Journal of Immunology Research* **2016,** 1–10 (July 2016).
29. Xue, J. *et al.* Transcriptome-Based Network Analysis Reveals a Spectrum Model of Human Macrophage Activation. *Immunity* **40,** 274–288 (2014).
30. Ponzoni, M. *et al.* Targeting macrophages as a potential therapeutic intervention: Impact on inflammatory diseases and cancer. *International Journal of Molecular Sciences* **19** (July 2018).
31. Wu, Y. & Hirschi, K. K. Tissue-Resident Macrophage Development and Function. *Frontiers in Cell and Developmental Biology* **8,** 1750 (Jan. 2021).
32. Bruggeman, C. W. *et al.* Tissue-specific expression of IgG receptors by human macrophages ex vivo. *PLOS ONE* **14,** e0223264 (Oct. 2019).
33. Vorsatz, C., Friedrich, N., Nimmerjahn, F. & Biburger, M. There Is Strength in Numbers: Quantitation of Fc Gamma Receptors on Murine Tissue-Resident Macrophages. *International Journal of Molecular Sciences 2021, Vol. 22, Page 12172* **22,** 12172 (Nov. 2021).
34. Piccolo, V. *et al.* Opposing macrophage polarization programs show extensive epigenomic and transcriptional cross-talk. *Nature Immunology* **18,** 530–540 (May 2017).
35. Bonilla, F. A. & Oettgen, H. C. Adaptive immunity. *Journal of Allergy and Clinical Immunology* **125,** S33–S40 (2010).
36. Blum, J. S., Wearsch, P. A. & Cresswell, P. *Pathways of antigen processing* 443–473 (2013).
37. Van Panhuys, N. TCR signal strength alters T-DC activation and interaction times and directs the outcome of differentiation. *Frontiers in Immunology* **7,** 6 (Jan. 2016).
38. Linsley, P. S., Clark, E. A. & Ledbetter, J. A. T-cell antigen CD28 mediates adhesion with B cells by interacting with activation antigen B7/BB-1. *Proceedings of the National Academy of Sciences of the United States of America* **87,** 5031–5035 (July 1990).

39. Hathcock, K. S. *et al.* Identification of an alternative CTLA-4 ligand costimulatory for T cell activation. *Science* **262,** 905–907 (Nov. 1993).

40. Chen, L. & Flies, D. B. Molecular mechanisms of T cell co-stimulation and co-inhibition. *Nature Reviews Immunology* **13,** 227–242 (Apr. 2013).

41. Callahan, M. K., Postow, M. A. & Wolchok, J. D. Targeting T Cell Co-receptors for Cancer Therapy. *Immunity* **44,** 1069–1078 (May 2016).

42. Lee, W. & Lee, G. R. Transcriptional regulation and development of regulatory T cells. *Experimental and Molecular Medicine* **50,** e456 (Mar. 2018).

43. Knutson, K. L. & Disis, M. L. *Tumor antigen-specific T helper cells in cancer immunity and immunotherapy* 2005.

44. Alberts, B., Johnson, A. & Lewis, J. *Helper T cells and Lymphocyte Activation* 1–8 (Garland Science, 2002).

45. Schrek, R. & Donnelly, W. J. *"Hairy" cells in blood in lymphoreticular neoplastic disease and "flagellated" cells of normal lymph nodes.* **2,** 199–211 (1966).

46. Trolle, T. *et al.* The Length Distribution of Class I–Restricted T Cell Epitopes Is Determined by Both Peptide Supply and MHC Allele–Specific Binding Preference. *The Journal of Immunology* **196,** 1480–1487 (Feb. 2016).

47. Maher, J. & Davies, E. T. *Targeting cytotoxic T lymphocytes for cancer immunotherapy* 2004.

48. Lauvau, G. & Soudja, S. M. Mechanisms of memory T Cell activation and effective immunity. *Advances in Experimental Medicine and Biology* **850,** 73–80 (2015).

49. Behrens, E. M. & Koretzky, G. A. *Review: Cytokine Storm Syndrome: Looking Toward the Precision Medicine Era* 2017.

50. Jonuleit, H. & Schmitt, E. The Regulatory T Cell Family: Distinct Subsets and their Interrelations. *The Journal of Immunology* **171,** 6323–6327 (2003).

51. Mougiakakos, D. *et al.* Regulatory T Cells in Cancer. *Advances in Cancer Research* **107,** 57–117 (2010).

52. Abe, B. T. & Macian, F. *Uncovering the mechanisms that regulate tumor-induced T-cell anergy* 2013.

53. Lebien, T. W. & Tedder, T. F. B lymphocytes: How they develop and function. *Blood* **112,** 1570–1580 (Sept. 2008).

54. Pieper, K., Grimbacher, B. & Eibel, H. B-cell biology and development. *Journal of Allergy and Clinical Immunology* **131,** 959–971 (Apr. 2013).

55. Nagasawa, T. Microenvironmental niches in the bone marrow required for B-cell development. *Nature Reviews Immunology* **6,** 107–116 (Feb. 2006).

56. Tutt, A. L. *et al.* Development and Characterization of Monoclonal Antibodies Specific for Mouse and Human Fc Receptors. *The Journal of Immunology* **195,** 5503–5516 (Dec. 2015).

57. Roth, D. B. V(D)J Recombination: Mechanism, Errors, and Fidelity. *Microbiology Spectrum* **2** (Dec. 2014).

58. Hoffman, W., Lakkis, F. G. & Chalasani, G. B cells, antibodies, and more. *Clinical Journal of the American Society of Nephrology* **11,** 137–154 (2016).

59. Woyach, J. A., Johnson, A. J. & Byrd, J. C. *The B-cell receptor signaling pathway as a therapeutic target in CLL* 2012.

60. Akkaya, M. *et al.* Second signals rescue B cells from activation-induced mitochondrial dysfunction and death. *Nature Immunology* **19,** 871–884 (Aug. 2018).

61. Jeurissen, A., Ceuppens, J. L. & Bossuyt, X. *T lymphocyte dependence of the antibody response to 'T lymphocyte independent type 2' antigens* 2004.

62. Rothstein, T. L. *et al.* Human B-1 cells take the stage. *Annals of the New York Academy of Sciences* **1285,** 97–114 (May 2013).

63. Maul, R. W. & Gearhart, P. J. in *Advances in Immunology* C, 159–191 (Academic Press Inc., 2010).

64. Kuppers, R., Zhao, M., Hansmann, M. L. & Rajewsky, K. Tracing B cell development in human germinal centres by molecular analysis of single cells picked from histological sections. *EMBO Journal* **12,** 4955–4967 (Dec. 1993).

65. Berek, C., Berger, A. & Apel, M. Maturation of the immune response in germinal centers. *Cell* **67,** 1121–1129 (Dec. 1991).

66. Stavnezer, J., Guikema, J. E. & Schrader, C. E. *Mechanism and regulation of class switch recombination* 2008.

67. Xu, Z. *et al. Immunoglobulin class-switch DNA recombination: Induction, targeting and beyond* July 2012.

68. Weisel, F. & Shlomchik, M. Memory B cells of mice and humans. *Annual Review of Immunology* **35,** 255–284 (Apr. 2017).

69. Khodadadi, L., Cheng, Q., Radbruch, A. & Hiepe, F. The Maintenance of Memory Plasma Cells. *Frontiers in Immunology* **10,** 721 (Apr. 2019).

70. Kurosaki, T., Kometani, K. & Ise, W. Memory B cells. *Nature Reviews Immunology* **15,** 149–159 (Mar. 2015).

71. Akkaya, M., Kwak, K. & Pierce, S. K. *B cell memory: building two walls of protection against pathogens* Apr. 2020.

72. Lipman, N. S., Jackson, L. R., Trudel, L. J. & Weis-Garcia, F. Monoclonal versus polyclonal antibodies: Distinguishing characteristics, applications, and information resources. *ILAR Journal* **46,** 258–267 (2005).

73. Gore, S. *et al.* Heparin surfaces: Impact of immobilization chemistry on hemocompatibility and protein adsorption. *Journal of Biomedical Materials Research - Part B Applied Biomaterials* **102,** 1817–1824 (2014).

74. Schroeder, H. W. & Cavacini, L. Structure and function of immunoglobulins. *Journal of Allergy and Clinical Immunology* **125,** S41 (Feb. 2010).

75. Sela-Culang, I., Kunik, V. & Ofran, Y. The structural basis of antibody-antigen recognition. *Frontiers in Immunology* **4** (2013).

76. Shade, K.-T. & Anthony, R. Antibody Glycosylation and Inflammation. *Antibodies* **2,** 392–414 (June 2013).

77. Stoop, J. W., Zegers, B. J., Sander, P. C. & Ballieux, R. E. Serum immunoglobulin levels in healthy children and adults. *Clinical and experimental immunology* **4,** 101–12 (Jan. 1969).

78. Woof, J. M. & Russell, M. W. *Structure and function relationships in IgA* Nov. 2011.

79. Kato-Nagaoka, N. *et al.* Enhanced differentiation of intraepithelial lymphocytes in the intestine of polymeric immunoglobulin receptor-deficient mice. *Immunology* **146,** 59–69 (Sept. 2015).

80. Liu, J. *et al.* Role of the IgM Fc receptor in immunity and tolerance. *Frontiers in Immunology* **10,** 529 (Mar. 2019).

81. Riesbeck, K. & Nordström, T. *Structure and immunological action of the human pathogen Moraxella catarrhalis IgD-binding protein* 2006.

82. Gould, H. J. *et al.* The biology of IgE and the basis of allergic disease. *Annual Review of Immunology* **21,** 579–628 (Apr. 2003).

83. Vidarsson, G., Dekkers, G. & Rispens, T. IgG subclasses and allotypes: From structure to effector functions. *Frontiers in Immunology* **5** (2014).

84. Barrett, D. J. & Ayoub, E. M. IgG2 subclass restriction of antibody to pneumococcal polysaccharides. *Clinical and experimental immunology* **63,** 127–34 (Jan. 1986).

85. Hammarström, L. & Smith, C. I. IgG2 deficiency in a healthy blood donor. Concomitant lack of IgG2, IgA and IgE immunoglobulins and specific anti-carbohydrate antibodies. *Clinical and experimental immunology* **51,** 600–4 (1983).

86. Chu, T. H., Patz, E. F. & Ackerman, M. E. *Coming together at the hinges: Therapeutic prospects of IgG3* 2021.

87. Rispens, T., Ooijevaar-De Heer, P., Bende, O. & Aalberse, R. C. Mechanism of immunoglobulin G4 Fab-arm exchange. *Journal of the American Chemical Society* **133,** 10302–10311 (2011).

88. Collins, A. M. *IgG subclass co-expression brings harmony to the quartet model of murine IgG function* 2016.

89. Nimmerjahn, F. & Ravetch, J. V. Immunology: Divergent immunoglobulin G subclass activity through selective Fc receptor binding. *Science* **310,** 1510–1512 (2005).

90. Martin, R. M., Brady, J. L. & Lew, A. M. The need for IgG2c specific antiserum when isotyping antibodies from C57BL/6 and NOD mice. *Journal of Immunological Methods* **212,** 187–192 (Mar. 1998).

91. Foss, S. *et al. TRIM21—From intracellular immunity to therapy* Aug. 2019.

92. Hanson, Q. M. & Barb, A. W. A perspective on the structure and receptor binding properties of immunoglobulin G Fc. *Biochemistry* **54,** 2931–2942 (May 2015).

93. Temming, A. R. *et al.* Human DC-SIGN and CD23 do not interact with human IgG. *Scientific Reports* **9** (Dec. 2019).

94. Ghetie, V., Ward, E. S. & Vitetta, E. S. in *Handbook of Anticancer Pharmacokinetics and Pharmacodynamics* 475–498 (Humana Press, 2004).

95. Vieira, P. & Rajewsky, K. The half-lives of serum immunoglobulins in adult mice. *European Journal of Immunology* **18,** 313–316 (Feb. 1988).

96. Klein-Schneegans, A. S., Kuntz, L., Fonteneau, P. & Loor, F. Serum concentrations of IgM, IgG1, IgG2b, IgG3 and IgA in C57BL 6 mice and their congenics at the lpr (lymphoproliferation) locus. *Journal of Autoimmunity* **2,** 869–875 (1989).

97. Michaelsen, T. E. *et al.* The four mouse IgG isotypes differ extensively in bactericidal and opsonophagocytic activity when reacting with the P1.16 epitope on the outer membrane PorA protein of Neisseria meningitidis. *Scandinavian Journal of Immunology* **59,** 34–39 (Jan. 2004).

98. Bruhns, P. Properties of mouse and human IgG receptors and their contribution to disease models. *Blood* **119,** 5640–5649 (June 2012).

99. Vonderheide, R. H. & Glennie, M. J. Agonistic CD40 antibodies and cancer therapy. *Clinical Cancer Research* **19,** 1035–1043 (2013).

100. Zheng, K. *et al.* Influence of glycosylation pattern on the molecular properties of monoclonal antibodies. *mAbs* **6,** 649–658 (2014).

101. Van de Bovenkamp, F. S., Hafkenscheid, L., Rispens, T. & Rombouts, Y. The Emerging Importance of IgG Fab Glycosylation in Immunity. *The Journal of Immunology* **196,** 1435–1441 (Feb. 2016).

102. Pučić, M. *et al.* High throughput isolation and glycosylation analysis of IgG-variability and heritability of the IgG glycome in three isolated human populations. *Molecular and Cellular Proteomics* **10,** M111.010090 (Oct. 2011).

103. Jennewein, M. F. & Alter, G. The Immunoregulatory Roles of Antibody Glycosylation. *Trends in Immunology* **38,** 358–372 (May 2017).

104. Krapp, S. *et al.* Structural analysis of human IgG-Fc glycoforms reveals a correlation between glycosylation and structural integrity. *Journal of Molecular Biology* **325,** 979–989 (Jan. 2003).

105. Subedi, G. P. & Barb, A. W. The Structural Role of Antibody N-Glycosylation in Receptor Interactions. *Structure* **23,** 1573–1583 (Sept. 2015).

106. Inman, B. A., Longo, T. A., Ramalingam, S. & Harrison, M. R. Atezolizumab: A PD-L1-blocking antibody for bladder cancer. *Clinical Cancer Research* **23,** 1886–1890 (Apr. 2017).

107. Li, M. *et al.* Next generation of anti-PD-L1 Atezolizumab with enhanced anti-tumor efficacy in vivo. *Scientific Reports* **11,** 5774 (Dec. 2021).

108. Shields, R. L. *et al.* Lack of fucose on human IgG1 N-linked oligosaccharide improves binding to human FcγRIII and antibody-dependent cellular toxicity. *Journal of Biological Chemistry* **277,** 26733–26740 (July 2002).

109. Bruggeman, C. W. *et al.* Enhanced Effector Functions Due to Antibody Defucosylation Depend on the Effector Cell Fcγ Receptor Profile. *The Journal of Immunology* **199,** 204–211 (July 2017).

110. Pereira, N. A., Chan, K. F., Lin, P. C. & Song, Z. *The "less-is-more" in therapeutic antibodies: Afucosylated anti-cancer antibodies with enhanced antibody-dependent cellular cytotoxicity* July 2018.

111. Wang, Z., Zhu, J. & Lu, H. *Antibody glycosylation: impact on antibody drug characteristics and quality control* Mar. 2020.

112. Tobinai, K., Klein, C., Oya, N. & Fingerle-Rowson, G. *A Review of Obinutuzumab (GA101), a Novel Type II Anti-CD20 Monoclonal Antibody, for the Treatment of Patients with B-Cell Malignancies* Feb. 2017.

113. Anthony, R. M. & Ravetch, J. V. A novel role for the IgG Fc glycan: The anti-inflammatory activity of sialylated IgG Fcs. *Journal of Clinical Immunology* **30,** 9–14 (May 2010).

114. Markina, Y. V. *et al. Sialylated immunoglobulins for the treatment of immuno-inflammatory diseases* Aug. 2020.

115. Luo, C. *et al.* Glycoengineering of pertuzumab and its impact on the pharmacokinetic/pharmacodynamic properties. *Scientific Reports* **7** (Apr. 2017).

116. Chakraborty, S. *et al.* Proinflammatory IgG Fc structures in patients with severe COVID-19. *Nature Immunology* **22,** 67–73 (Jan. 2021).

117. Hoepel, W. *et al.* High titers and low fucosylation of early human anti-SARS-CoV-2 IgG promote inflammation by alveolar macrophages. *Science Translational Medicine* **13** (June 2021).

118. Bye, A. P. *et al.* Aberrant glycosylation of anti-SARS-CoV-2 spike IgG is a prothrombotic stimulus for platelets. *Blood* (July 2021).

119. Larsen, M. D. *et al.* Afucosylated IgG characterizes enveloped viral responses and correlates with COVID-19 severity. *Science* **371** (Feb. 2021).

120. Wang, J. R. *et al.* Glycomic signatures on serum IgGs for prediction of postvaccination response. *Scientific Reports* **5,** 1–11 (Jan. 2015).

121. Köhler, G. & Milstein, C. Continuous cultures of fused cells secreting antibody of predefined specificity. *Nature* **256,** 495–497 (Aug. 1975).

122. Zitvogel, L. *et al.* Mouse models in oncoimmunology. *Nature Reviews Cancer* **16,** 759–773 (Dec. 2016).

123. Lu, R. M. *et al. Development of therapeutic antibodies for the treatment of diseases* Jan. 2020.

124. Mullard, A. *FDA approves 100th monoclonal antibody product* May 2021.

125. Mayes, J. T. *et al.* Reexposure to OKT3 in renal allograft recipients. *Transplantation* **45,** 349–353 (Feb. 1988).

126. Li, F. *et al.* Cell culture processes for monoclonal antibody production. *mAbs* **2,** 466–479 (2010).

127. Chames, P., Van Regenmortel, M., Weiss, E. & Baty, D. Therapeutic antibodies: Successes, limitations and hopes for the future. *British Journal of Pharmacology* **157,** 220–233 (May 2009).

128. Schirrmann, T. *et al.* Phage display for the generation of antibodies for proteome research, diagnostics and therapy. *Molecules* **16,** 412–426 (Jan. 2011).

129. Rami, A. *et al. An overview on application of phage display technique in immunological studies* July 2017.

130. Kunert, R. & Reinhart, D. *Advances in recombinant antibody manufacturing* Apr. 2016.

131. Butler, M. & Spearman, M. *The choice of mammalian cell host and possibilities for glycosylation engineering* 2014.

132. Yamane-Ohnuki, N. *et al.* Establishment of FUT8 knockout Chinese hamster ovary cells: An ideal host cell line for producing completely defucosylated antibodies with enhanced antibody-dependent cellular cytotoxicity. *Biotechnology and Bioengineering* **87,** 614–622 (Sept. 2004).

133. Lu, H. *et al.* Development of anti-CD32b antibodies with enhanced Fc function for the treatment of B and plasma cell malignancies. *Molecular Cancer Therapeutics* **19,** 2089–2104 (Oct. 2020).

134. Kaplon, H., Muralidharan, M., Schneider, Z. & Reichert, J. M. Antibodies to watch in 2020. *mAbs* **12,** 1703531 (Jan. 2020).

135. Adler, M. J. & Dimitrov, D. S. *Therapeutic Antibodies Against Cancer* June 2012.

136. Dempke, W. C., Fenchel, K., Uciechowski, P. & Dale, S. P. *Second- and third-generation drugs for immuno-oncology treatment—The more the better?* Mar. 2017.

137. Gajria, D. & Chandarlapaty, S. HER2-amplified breast cancer: Mechanisms of trastuzumab resistance and novel targeted therapies. *Expert Review of Anticancer Therapy* **11,** 263–275 (Feb. 2011).

138. Vu, T. & Claret, F. X. Trastuzumab: Updated mechanisms of action and resistance in breast cancer. *Frontiers in Oncology* **2 JUN,** 62 (2012).

139. Takeda, K. *et al. Targeting death-inducing receptors in cancer therapy* May 2007.

140. Alsaab, H. O. *et al.* PD-1 and PD-L1 checkpoint signaling inhibition for cancer immunotherapy: mechanism, combinations, and clinical outcome. *Frontiers in Pharmacology* **8,** 561 (2017).

141. Sun, Z. *et al.* IL10 and PD-1 cooperate to limit the activity of tumor-specific CD8+ T cells. *Cancer Research* **75,** 1635–1644 (Apr. 2015).

142. Davies, A. M. & Sutton, B. J. Human IgG4: A structural perspective. *Immunological Reviews* **268,** 139–159 (Nov. 2015).

143. White, A. L. *et al.* Fcγ Receptor Dependency of Agonistic CD40 Antibody in Lymphoma Therapy Can Be Overcome through Antibody Multimerization. *The Journal of Immunology* **193,** 1828–1835 (Aug. 2014).

144. Zhang, D., Goldberg, M. V. & Chiu, M. L. Fc engineering approaches to enhance the agonism and effector functions of an Anti-OX40 antibody. *Journal of Biological Chemistry* **291,** 27134–27146 (2016).

145. Buchan, S. L. *et al.* Antibodies to Costimulatory Receptor 4-1BB Enhance Antitumor Immunity via T Regulatory Cell Depletion and Promotion of CD8 T Cell Effector Function. *Immunity* **49,** 958–970 (Nov. 2018).

146. Yu, X. *et al.* Isotype Switching Converts Anti-CD40 Antagonism to Agonism to Elicit Potent Antitumor Activity. *Cancer Cell* **37,** 850–866 (June 2020).

147. Peggs, K. S. *et al.* Blockade of CTLA-4 on both effector and regulatory T cell compartments contributes to the antitumor activity of anti-CTLA-4 antibodies. *Journal of Experimental Medicine* **206,** 1717–1725 (Aug. 2009).

148. Vargas, F. A. *et al.* Fc Effector Function Contributes to the Activity of Human Anti-CTLA-4 Antibodies. *Cancer Cell* **33,** 649–663 (Apr. 2018).

149. Romano, E. *et al.* Ipilimumab-dependent cell-mediated cytotoxicity of regulatory T cells ex vivo by nonclassical monocytes in melanoma patients. *Proceedings of the National Academy of Sciences of the United States of America* **112,** 6140–6145 (May 2015).

150. Griffiths, J. *et al.* Domain binding and isotype dictate the activity of anti-human OX40 antibodies. *Journal for ImmunoTherapy of Cancer* **8,** 1557 (Dec. 2020).

151. Garber, K. *Immune agonist antibodies face critical test* Jan. 2020.

152. Bournazos, S. *et al.* Human IgG Fc domain engineering enhances antitoxin neutralizing antibody activity. *Journal of Clinical Investigation* **124,** 725–729 (2014).

153. Bournazos, S. *et al.* Broadly neutralizing anti-HIV-1 antibodies require Fc effector functions for in vivo activity. *Cell* **158,** 1243–1253 (2014).

154. Iwasaki, A. & Yang, Y. *The potential danger of suboptimal antibody responses in COVID-19* Apr. 2020.

155. Willey, S. *et al.* Extensive complement-dependent enhancement of HIV-1 by autologous non-neutralising antibodies at early stages of infection. *Retrovirology* **8** (Mar. 2011).

156. Seshacharyulu, P. *et al.* Targeting the EGFR signaling pathway in cancer therapy. *Expert Opinion on Therapeutic Targets* **16,** 15–31 (Jan. 2012).

157. Honeychurch, J. *et al.* Antibody-induced nonapoptotic cell death in human lymphoma and leukemia cells is mediated through a novel reactive oxygen species-dependent pathway. *Blood* **119,** 3523–3533 (Apr. 2012).

158. Lefebvre, M. L., Krause, S. W., Salcedo, M. & Nardin, A. Ex vivo-activated human macrophages kill chronic lymphocytic leukemia cells in the presence of rituximab: Mechanism of antibody-dependent cellular cytotoxicity and impact of human serum. *Journal of Immunotherapy* **29,** 388–397 (July 2006).

159. Van der Kolk, L. E. *et al. Analysis of CD20-dependent cellular cytotoxicity by G-CSF-stimulated neutrophils* Apr. 2002.

160. Jefferis, R. Isotype and glycoform selection for antibody therapeutics. *Archives of Biochemistry and Biophysics* **526,** 159–166 (Oct. 2012).

161. Desjardins, M., Huber, L. A., Parton, R. G. & Griffiths, G. Biogenesis of phagolysosomes proceeds through a sequential series of interactions with the endocytic apparatus. *Journal of Cell Biology* **124,** 677–688 (1994).

162. Lam, G. Y., Huang, J. & Brumell, J. H. *The many roles of NOX2 NADPH oxidase-derived ROS in immunity* 2010.

163. Lu, L. L., Suscovich, T. J., Fortune, S. M. & Alter, G. Beyond binding: Antibody effector functions in infectious diseases. *Nature Reviews Immunology* **18,** 46–61 (Oct. 2018).

164. Valgardsdottir, R. *et al.* Human neutrophils mediate trogocytosis rather than phagocytosis of CLL B cells opsonized with anti-CD20 antibodies. *Blood* **129,** 2636–2644 (May 2017).

165. Velmurugan, R. *et al.* Macrophage-mediated trogocytosis leads to death of antibody-opsonized tumor cells. *Molecular Cancer Therapeutics* **15,** 1879–1889 (Aug. 2016).

166. Beum, P. V. *et al.* Loss of CD20 and Bound CD20 Antibody from Opsonized B Cells Occurs More Rapidly Because of Trogocytosis Mediated by Fc Receptor-Expressing Effector Cells Than Direct Internalization by the B Cells. *The Journal of Immunology* **187,** 3438–3447 (Sept. 2011).

167. Zhou, X., Hu, W. & Qin, X. The Role of Complement in the Mechanism of Action of Rituximab for B-Cell Lymphoma: Implications for Therapy. *The Oncologist* **13,** 954–966 (Sept. 2008).

168. Overdijk, M. B., Verploegen, S., Bleeker, W. K. & Parren, P. W. Role of IgG Fc Receptors in Monoclonal Antibody Therapy of Cancer. *Antibody Fc: Linking Adaptive and Innate Immunity,* 239–255 (Jan. 2013).

169. Walshe, C. A. *et al.* Induction of cytosolic calcium flux by CD20 is dependent upon B cell antigen receptor signaling. *Journal of Biological Chemistry* **283,** 16971–16984 (June 2008).

170. Morsy, D. E. D. *et al.* Reduced T-Dependent Humoral Immunity in CD20-Deficient Mice. *The Journal of Immunology* **191,** 3112–3118 (Sept. 2013).

171. Cragg, M. S., Walshe, C. A., Ivanov, A. O. & Glennie, M. J. in *Current directions in autoimmunity* 140–174 (KARGER, Basel, 2005).

172. Marshall, M. J., Stopforth, R. J. & Cragg, M. S. *Therapeutic antibodies: What have we learnt from targeting CD20 and where are we going?* Oct. 2017.

173. Klein, C. *et al.* Epitope interactions of monoclonal antibodies targeting CD20 and their relationship to functional properties. *mAbs* **5,** 22–33 (Jan. 2013).

174. Oettgen, H. C. *et al.* Further biochemical studies of the human B-cell differentiation antigens B1 and B2. *Hybridoma* **2,** 17–28 (1983).

175. Cleary, K. L. S. *et al.* Antibody Distance from the Cell Membrane Regulates Antibody Effector Mechanisms. *The Journal of Immunology* **198,** 3999–4011 (May 2017).

176. Meyer, S. *et al.* New insights in Type I and II CD20 antibody mechanisms-of-action with a panel of novel CD20 antibodies. *British Journal of Haematology* **180,** 808–820 (Mar. 2018).

177. Cragg, M. S. *et al.* Complement-mediated lysis by anti-CD20 mAb correlates with segregation into lipid rafts. *Blood* **101,** 1045–1052 (Feb. 2003).

178. Niederfellner, G. *et al.* Epitope characterization and crystal structure of GA101 provide insights into the molecular basis for type I/II distinction of CD20 antibodies. *Blood* **118,** 358–367 (July 2011).

179. Beers, S. A. *et al.* Antigenic modulation limits the efficacy of anti-CD20 antibodies: Implications for antibody selection. *Blood* **115,** 5191–5201 (June 2010).

180. Beurskens, F. J. *et al. Complement activation impacts B-cell depletion by both type I and type II CD20 monoclonal antibodies* Nov. 2008.

181. Diebolder, C. A. *et al.* Complement is activated by IgG hexamers assembled at the cell surface. *Science* **343,** 1260–1263 (2014).

182. Boross, P. & Leusen, J. H. W. Mechanisms of action of CD20 antibodies. *American journal of cancer research* **2,** 676–90 (2012).

183. Goede, V., Klein, C. & Stilgenbauer, S. *Obinutuzumab (GA101) for the Treatment of Chronic Lymphocytic Leukemia and Other B-Cell Non-Hodgkin's Lymphomas: A Glycoengineered Type II CD20 Antibody* 2015.

184. Herter, S. *et al. GA101 P329GLALA, a variant of obinutuzumab with abolished ADCC, ADCP and CDC function but retained cell death induction, is as efficient as rituximab in B-cell depletion and antitumor activity* Jan. 2018.

185. Clynes, R. A., Towers, T. L., Presta, L. G. & Ravetch, J. V. Inhibitory Fc receptors modulate in vivo cytoxicity against tumor targets. *Nature Medicine* **6,** 443–446 (Apr. 2000).

186. De Haij, S. *et al.* In vivo cytotoxicity of type I CD20 antibodies critically depends on Fc receptor ITAM signaling. *Cancer Research* **70,** 3209–3217 (Apr. 2010).

187. DiLillo, D. J. & Ravetch, J. V. Differential Fc-receptor engagement drives an anti-tumor vaccinal effect. *Cell* **161,** 1035–1045 (May 2015).

188. Capel, P. J., van de Winkel, J. G., van den Herik-Oudijk, I. E. & Verbeekt, J. S. Heterogeneity of Human IgG Fc Receptors. *ImmunoMethods* **4,** 25–34 (Feb. 1994).

189. Sun, P. in *Antibody Fc: Linking Adaptive and Innate Immunity* 131–144 (Academic Press, Jan. 2013).

190. Bruhns, P. & Jönsson, F. Mouse and human FcR effector functions. *Immunological Reviews* **268,** 25–51 (Nov. 2015).

191. Li, X., Ptacek, T. S., Brown, E. E. & Edberg, J. C. Fcγ receptors: Structure, function and role as genetic risk factors in SLE. *Genes and Immunity* **10,** 380–389 (July 2009).

192. Kerntke, C., Nimmerjahn, F. & Biburger, M. There Is (Scientific) Strength in Numbers: A Comprehensive Quantitation of Fc Gamma Receptor Numbers on Human and Murine Peripheral Blood Leukocytes. *Frontiers in Immunology* **11** (Feb. 2020).

193. Guilliams, M. *et al. The function of Fcγ receptors in dendritic cells and macrophages* Feb. 2014.

194. Kiyoshi, M. *et al.* Structural basis for binding of human IgG1 to its high-affinity human receptor FcγRI. *Nature Communications* **6** (Apr. 2015).

195. Hoffmeyer, F., Witte, K. & Schmidt, R. E. The high-affinity FcγRI on PMN: Regulation of expression and signal transduction. *Immunology* **92,** 544–552 (Dec. 1997).

196. Mancardi, D. A. *et al.* The high-affinity human IgG receptor FcγRI (CD64) promotes IgG-mediated inflammation, anaphylaxis, and antitumor immunotherapy. *Blood* **121,** 1563–1573 (Feb. 2013).

197. Van der Poel, C. E., Spaapen, R. M., van de Winkel, J. G. J. & Leusen, J. H. W. Functional Characteristics of the High Affinity IgG Receptor, FcγRI. *The Journal of Immunology* **186,** 2699–2704 (Mar. 2011).

198. Powell, M. S. *et al.* Alteration of the FcγRIIa Dimer Interface Affects Receptor Signaling but Not Ligand Binding. *The Journal of Immunology* **176,** 7489–7494 (June 2006).

199. Nimmerjahn, F. & Ravetch, J. V. Fcγ receptors as regulators of immune responses. *Nature Reviews Immunology* **8,** 34–47 (Jan. 2008).

200. Shashidharamurthy, R. *et al.* Dynamics of the Interaction of Human IgG Subtype Immune Complexes with Cells Expressing R and H Allelic Forms of a Low-Affinity Fcγ Receptor CD32A. *The Journal of Immunology* **183,** 8216–8224 (Dec. 2009).

201. Clark, M. R. *et al.* A single amino acid distinguishes the high-responder from the low-responder form of Fc receptor II on human monocytes. *European Journal of Immunology* **21,** 1911–1916 (Aug. 1991).

202. Castro-Dopico, T. & Clatworthy, M. R. *IgG and Fcγ receptors in intestinal immunity and inflammation* 2019.

203. Smith, K. G. & Clatworthy, M. R. FcγRIIB in autoimmunity and infection: Evolutionary and therapeutic implications. *Nature Reviews Immunology* **10,** 328–343 (May 2010).

204. Breunis, W. B. *et al.* Copy number variation at the FCGR locus includes FCGR3A, FCGR2C and FCGR3B but not FCGR2A and FCGR2B. *Human Mutation* **30,** E640–E650 (May 2009).

205. Ernst, L. K., Metes, D., Herberman, R. B. & Morel, P. A. Allelic polymorphisms in the FcγRIIC gene can influence its function on normal human natural killer cells. *Journal of Molecular Medicine* **80,** 248–257 (Nov. 2002).

206. Pincetic, A. *et al. Type i and type II Fc receptors regulate innate and adaptive immunity* 2014.

207. Su, K. *et al.* Genomic organization of classical human low-affinity Fcγ receptor genes. *Genes and Immunity* **3,** S51–S56 (2002).

208. Park, J. G., Isaacs, R. E., Chien, P. & Schreiber, A. D. In the absence of other Fc receptors, FcγRIIIA transmits a phagocytic signal that requires the cytoplasmic domain of its γ subunit. *Journal of Clinical Investigation* **92,** 1967–1973 (1993).

209. Golay, J., Leidi, M., Palumbo, G. A. & Introna, M. Human Macrophages Phagocytose Rituximab Opsonised Leukemic Cells Via CD16, CD32 and CD64 but Do Not Mediate ADCC. *Blood* **108,** 2507–2507 (Nov. 2006).

210. Ravetch, J. V. & Perussia, B. Alternative membrane forms of FcγRIII(CD16) on human natural killer cells and neutrophils. Cell type-specific expression of two genes that differ in single nucleotide substitutions. *Journal of Experimental Medicine* **170,** 481–497 (1989).

211. Congy-Jolivet, N. *et al.* FcγRIIIa expression is not increased on natural killer cells expressing the FcγRIIIa-158V allotype. *Cancer Research* **68,** 976–980 (Feb. 2008).

212. Kaifu, T. & Nakamura, A. Polymorphisms of immunoglobulin receptors and the effects on clinical outcome in cancer immunotherapy and other immune diseases: A general review. *International Immunology* **29,** 319–325 (July 2017).

213. Cartron, G. *et al.* Therapeutic activity of humanized anti-CD20 monoclonal antibody and polymorphism in IgG Fc receptor FcγrIIIa gene. *Blood* **99,** 754–758 (Feb. 2002).

214. Cartron, G., Houot, R. & Kohrt, H. E. Scientific significance of clinically insignificant FcγRIIIa-V158F polymorphism. *Clinical Cancer Research* **22,** 787–789 (Feb. 2016).

215. Kenkre, V. P. *et al.* Fc gamma receptor 3A and 2A polymorphisms do not predict response to rituximab in follicular lymphoma. *Clinical Cancer Research* **22,** 821–826 (Feb. 2016).

216. Fernandes, M. J. *et al.* CD16b associates with high-density, detergent-resistant membranes in human neutrophils. *Biochemical Journal* **393,** 351–359 (Jan. 2006).

217. Fossati, G., Moots, R. J., Bucknall, R. C. & Edwards, S. W. Differential role of neutrophil Fcγ receptor IIIb (CD16) in phagocytosis, bacterial killing, and responses to immune complexes. *Arthritis and Rheumatism* **46,** 1351–1361 (May 2002).

218. Reusch, U. *et al.* A novel tetravalent bispecific TandAb (CD30/CD16A) efficiently recruits NK cells for the lysis of CD30+ tumor cells. *mAbs* **6,** 727–738 (2014).

219. Pyzik, M. *et al.* FcRn: The Architect Behind the Immune and Nonimmune Functions of IgG and Albumin. *The Journal of Immunology* **194,** 4595–4603 (May 2015).

220. Yamaguchi, H., Hirai, M., Kurosawa, Y. & Hashimoto, K. A highly conserved major histocompatibility complex class I-related gene in mammals. *Biochemical and Biophysical Research Communications* **238,** 697–702 (Sept. 1997).

221. Biburger, M. *et al.* Monocyte Subsets Responsible for Immunoglobulin G-Dependent Effector Functions In Vivo. *Immunity* **35,** 932–944 (Dec. 2011).

222. Nimmerjahn, F., Bruhns, P., Horiuchi, K. & Ravetch, J. V. FcγRIV: A novel FcR with distinct IgG subclass specificity. *Immunity* **23,** 41–51 (July 2005).

223. Mancardi, D. A. *et al.* Cutting Edge: The Murine High-Affinity IgG Receptor FcγRIV Is Sufficient for Autoantibody-Induced Arthritis. *The Journal of Immunology* **186,** 1899–1903 (Feb. 2011).

224. Jönsson, F. *et al.* Mouse and human neutrophils induce anaphylaxis. *Journal of Clinical Investigation* **121,** 1484–1496 (Apr. 2011).

225. Ober, R. J., Radu, C. G., Ghetie, V. & Ward, E. S. Differences in promiscuity for antibody-FcRn interactions across species: Implications for therapeutic antibodies. *International Immunology* **13,** 1551–1559 (Dec. 2001).

226. Underhill, D. M. & Goodridge, H. S. The many faces of ITAMs. *Trends in Immunology* **28,** 66–73 (Feb. 2007).

227. Getahun, A. & Cambier, J. C. *Of ITIMs, ITAMs, and ITAMis: Revisiting immunoglobulin Fc receptor signaling* Nov. 2015.

228. Bournazos, S., Wang, T. T. & Ravetch, J. V. The Role and Function of Fcγ Receptors on Myeloid Cells. *Microbiology Spectrum* **4** (Dec. 2016).

229. Flannagan, R. S., Jaumouillé, V. & Grinstein, S. *The cell biology of phagocytosis* Feb. 2012.

230. Scott, C. C. *et al.* Phosphatidylinositol-4, 5-bisphosphate hydrolysis directs actin remodeling during phagocytosis. *Journal of Cell Biology* **169,** 139–149 (Apr. 2005).

231. Dhodapkar, K. M. *et al.* Selective blockade of inhibitory Fcγ receptor enables human dendritic cell maturation with IL-12p70 production and immunity to antibody-coated tumor cells. *Proceedings of the National Academy of Sciences of the United States of America* **102,** 2910–2915 (Feb. 2005).

232. Ahmed, A. A., Keremane, S. R., Vielmetter, J. & Bjorkman, P. J. Structural characterization of GASDALIE Fc bound to the activating Fc receptor FcγRIIIa. *Journal of Structural Biology* **194,** 78–89 (Apr. 2016).

233. Clynes, R. *et al.* Modulation of immune complex-induced inflammation in vivo by the coordinate expression of activation and inhibitory Fc receptors. *Journal of Experimental Medicine* **189,** 179–185 (Jan. 1999).

234. Treffers, L. W. *et al.* FcγRIIIb restricts antibody-dependent destruction of cancer cells by human neutrophils. *Frontiers in Immunology* **10,** 3124 (Jan. 2019).

235. Kurlander, R. J. Blockade of Fc receptor-mediated binding to U-937 cells by murine monoclonal antibodies directed against a variety of surface antigens. *The Journal of Immunology* **131,** 140–147 (1983).

236. Kurlander, R. J. Reversible and irreversible loss of Fc receptor function of human monocytes as a consequence of interaction with immunoglobulin G. *Journal of Clinical Investigation* **66,** 773–781 (Oct. 1980).

237. Dunn-Siegrist, I. *et al.* Pivotal involvement of Fcγ receptor IIA in the neutralization of lipopolysaccharide signaling via a potent novel anti-TLR4 monoclonal antibody 15C1. *Journal of Biological Chemistry* **282,** 34817–34827 (Nov. 2007).

238. Stuart, S. G. *et al.* Human IgG Fc receptor (hFcRII; CD32) exists as multiple isoforms in macrophages, lymphocytes and IgG-transporting placental epithelium. *EMBO Journal* **8,** 3657–3666 (Dec. 1989).

239. Budde, P. *et al.* Tyrosine-containing sequence motifs of the human immunoglobulin G receptors FcRIIb1 and FcRIIb2 essential for endocytosis and regulation of calcium flux in B cells. *Journal of Biological Chemistry* **269,** 30636–30644 (Dec. 1994).

240. Muta, T. *et al.* A 13-amino-acid motif in the cytoplasmic domain of FcγRIIB modulates B-cell receptor signalling. *Nature* **368,** 70–73 (Mar. 1994).

241. Minskoff, S. A., Matter, K. & Mellman, I. *Fc gamma RII-B1 regulates the presentation of B cell receptor-bound antigens.* tech. rep. 5 (1998), 2079–20783.

242. Ganesan, L. P. *et al.* FcγRIIb on Liver Sinusoidal Endothelium Clears Small Immune Complexes. *The Journal of Immunology* **189,** 4981–4988 (Nov. 2012).

243. Esposito-Farese, M. E. *et al.* Membrane and soluble Fc gamma RII/III modulate the antigen-presenting capacity of murine dendritic epidermal Langerhans cells for IgG-complexed antigens. *Journal of immunology (Baltimore, Md. : 1950)* **155,** 1725–36 (Aug. 1995).

244. Barrow, A. D. & Trowsdale, J. You say ITAM and I say ITIM, let's call the whole thing off: The ambiguity of immunoreceptor signalling. *European Journal of Immunology* **36,** 1646–1653 (July 2006).

245. Masao, O. *et al.* Deletion of SHIP or SHP-1 reveals two distinct pathways for inhibitory signaling. *Cell* **90,** 293–301 (July 1997).

246. Ivashkiv, L. B. How ITAMs inhibit signaling. *Science Signaling* **4,** pe20 (Apr. 2011).

247. Clatworthy, M. R. & Smith, K. G. FcγRIIb Balances Efficient Pathogen Clearance and the Cytokine-mediated Consequences of Sepsis. *Journal of Experimental Medicine* **199,** 717–723 (Mar. 2004).

248. Kasahara, Y., Shirota, H., Umegaki, S. & Ishioka, C. Contribution of Fcγ receptor IIB to creating a suppressive tumor microenvironment in a mouse model. *Cancer Immunology, Immunotherapy* **68,** 1769–1778 (Nov. 2019).

249. Van Lent, P. *et al.* The Inhibitory Receptor FcγRII Reduces Joint Inflammation and Destruction in Experimental Immune Complex-Mediated Arthritides Not Only by Inhibition of FcγRI/III but Also by Efficient Clearance and Endocytosis of Immune Complexes. *American Journal of Pathology* **163,** 1839–1848 (Nov. 2003).

250. Heyman, B. Feedback regulation by IgG antibodies. *Immunology Letters* **88,** 157–161 (Aug. 2003).

251. Fong, D. C. *et al.* Mutational Analysis Reveals Multiple Distinct Sites Within Fcγ Receptor IIB That Function in Inhibitory Signaling. *The Journal of Immunology* **165,** 4453–4462 (2000).

252. Stopforth, R. J. *et al.* Detection of Experimental and Clinical Immune Complexes by Measuring SHIP-1 Recruitment to the Inhibitory FcγRIIB. *The Journal of Immunology* **200,** ji1700832 (Mar. 2018).

253. Liu, W. *et al.* Antigen-Induced Oligomerization of the B Cell Receptor Is an Early Target of FcγRIIB Inhibition. *The Journal of Immunology* **184,** 1977–1989 (Feb. 2010).

254. Xu, L. *et al.* Through an ITIM-Independent Mechanism the FcγRIIB Blocks B Cell Activation by Disrupting the Colocalized Microclustering of the B Cell Receptor and CD19. *The Journal of Immunology* **192,** 5179–5191 (June 2014).

255. Tzeng, S. J. *et al.* The B cell inhibitory Fc receptor triggers apoptosis by a novel c-Abl family kinase-dependent pathway. *Journal of Biological Chemistry* **280,** 35247–35254 (Oct. 2005).

256. Xu, Y. *et al.* No receptor stands alone: IgG B-cell receptor intrinsic and extrinsic mechanisms contribute to antibody memory. *Cell Research* **24,** 651–664 (June 2014).

257. Jonsson, S. *et al.* Identification of sequence variants influencing immunoglobulin levels. *Nature Genetics 2017 49:8* **49,** 1182–1191 (June 2017).

258. Fong, D. C. *et al.* Mutational Analysis Reveals Multiple Distinct Sites Within Fcγ Receptor IIB That Function in Inhibitory Signaling. *The Journal of Immunology* **165,** 4453–4462 (Oct. 2000).

259. Miettinen, H. M. *et al.* Fc receptor endocytosis is controlled by a cytoplasmic domain determinant that actively prevents coated pit localization. *Journal of Cell Biology* **116,** 875–888 (Feb. 1992).

260. Kalergis, A. M. & Ravetch, J. V. Inducing tumor immunity through the selective engagement of activating Fcγ receptors on dendritic cells. *Journal of Experimental Medicine* **195,** 1653–1659 (June 2002).

261. Bergtold, A., Desai, D. D., Gavhane, A. & Clynes, R. Cell surface recycling of internalized antigen permits dendritic cell priming of B cells. *Immunity* **23,** 503–514 (Nov. 2005).

262. Qin, D. *et al.* Fcγ Receptor IIB on Follicular Dendritic Cells Regulates the B Cell Recall Response. *The Journal of Immunology* **164,** 6268–6275 (June 2000).

263. Van der Poel, C. E. *et al.* Follicular Dendritic Cells Modulate Germinal Center B Cell Diversity through FcγRIIB. *Cell Reports* **29,** 2745–2755 (Nov. 2019).

264. Daëron, M. *et al.* Regulation of high-affinity IgE receptor-mediated mast cell activation by murine low-affinity IgG receptors. *Journal of Clinical Investigation* **95,** 577–585 (Feb. 1995).

265. Storni, F. *et al.* Vaccine against peanut allergy based on engineered virus-like particles displaying single major peanut allergens. *Journal of Allergy and Clinical Immunology* **145,** 1240–1253 (Apr. 2020).

266. Roghanian, A., Stopforth, R. J., Dahal, L. N. & Cragg, M. S. New revelations from an old receptor: Immunoregulatory functions of the inhibitory Fc gamma receptor, FcγRIIB (CD32B). *Journal of Leukocyte Biology* **103,** 1077–1088 (June 2018).

267. Poisson, J. *et al.* Liver sinusoidal endothelial cells: Physiology and role in liver diseases. *Journal of Hepatology* **66,** 212–227 (Jan. 2017).

268. Knolle, P. A. & Wohlleber, D. Immunological functions of liver sinusoidal endothelial cells. *Cellular and Molecular Immunology* **13,** 347–353 (2016).

269. Bilzer, M., Roggel, F. & Gerbes, A. L. Role of Kupffer cells in host defense and liver disease. *Liver International* **26,** 1175–1186 (Dec. 2006).

270. Fox, E. S., Thomas, P. & Broitman, S. A. Comparative studies of endotoxin uptake by isolated rat Kupffer and peritoneal cells. *Infection and Immunity* **55,** 2962–2966 (Dec. 1987).

271. Sørensen, K. K., Simon-Santamaria, J., McCuskey, R. S. & Smedsrød, B. in *Comprehensive Physiology* 4, 1751–1774 (John Wiley & Sons, Inc., Hoboken, NJ, USA, Sept. 2015).

272. Turman, J. M. *et al.* Accelerated Clearance and Degradation of Cell-Free HIV by Neutralizing Antibodies Occurs via FcγRIIb on Liver Sinusoidal Endothelial Cells by Endocytosis. *The Journal of Immunology* **206,** 1284–1296 (Feb. 2021).

273. Morris, A. B. *et al.* Signaling through the Inhibitory Fc Receptor FcγRIIB Induces CD8+ T Cell Apoptosis to Limit T Cell Immunity. *Immunity* **52,** 136–150 (Jan. 2020).

274. Clémenceau, B. *et al.* FcγRIIIa (CD16) induction on human T lymphocytes and CD16pos T-lymphocyte amplification. *Journal of immunotherapy (Hagerstown, Md. : 1997)* **34,** 542–549 (Sept. 2011).

275. Holgado, M. P. *et al.* CD32 ligation promotes the activation of CD4+T cells. *Frontiers in Immunology* **9,** 2814 (Nov. 2018).

276. Starbeck-Miller, G. R., Badovinac, V. P., Barber, D. L. & Harty, J. T. Cutting Edge: Expression of FcγRIIB Tempers Memory CD8 T Cell Function In Vivo. *The Journal of Immunology* **192,** 35–39 (Jan. 2014).

277. Liu, H. *et al.* The FGL2-FcγRIIB pathway: A novel mechanism leading to immunosuppression. *European Journal of Immunology* **38,** 3114–3126 (2008).

278. Farley, C. R. *et al.* FcγRIIB is a T cell checkpoint in antitumor immunity. *JCI Insight* **6** (Feb. 2021).

279. Fukuyama, H., Nimmerjahn, F. & Ravetch, J. V. The inhibitory Fcγ receptor modulates autoimmunity by limiting the accumulation of immunoglobulin G+ anti-DNA plasma cells. *Nature Immunology* **6,** 99–106 (Jan. 2005).

280. Carlucci, F. *et al.* Identification and Characterization of a Lupus Suppressor 129 Locus on Chromosome 3. *The Journal of Immunology* **184,** 6256–6265 (June 2010).

281. Boross, P. *et al.* The Inhibiting Fc Receptor for IgG, FcγRIIB, Is a Modifier of Autoimmune Susceptibility. *The Journal of Immunology* **187,** 1304–1313 (Aug. 2011).

282. Mackay, M. *et al.* Selective dysregulation of the FcγIIB receptor on memory B cells in SLE. *Journal of Experimental Medicine* **203,** 2157–2164 (Sept. 2006).

283. Radstake, T. R. *et al.* The functional variant of the inhibitory Fcγ receptor IIb (CD32B) is associated with the rate of radiologic joint damage and dendritic cell function in rheumatoid arthritis. *Arthritis and Rheumatism* **54,** 3828–3837 (Dec. 2006).

284. Zhou, X. j. *et al.* Copy number variation of FCGR3A rather than FCGR3B and FCGR2B is associated with susceptibility to anti-GBM disease. *International Immunology* **22,** 45–51 (Jan. 2009).

285. Iruretagoyena, M. I. *et al.* Activating and inhibitory Fcγ receptors can differentially module T cell-mediated autoimmunity. *European Journal of Immunology* **38,** 2241–2250 (Aug. 2008).

286. Bruin, M. *et al.* Platelet count, previous infection and FCGR2B genotype predict development of chronic disease in newly diagnosed idiopathic thrombocytopenia in childhood: Results of a prospective study. *British Journal of Haematology* **127,** 561–567 (Dec. 2004).

287. Floto, R. A. *et al.* Loss of function of a lupus-associated FcγRIIb polymorphism through exclusion from lipid rafts. *Nature Medicine* **11,** 1056–1058 (Oct. 2005).

288. Kono, H. *et al.* FcγRIIB Ile232Thr transmembrane polymorphism associated with human systemic lupus erythematosus decreases affinity to lipid rafts and attenuates inhibitory effects on B cell receptor signaling. *Human Molecular Genetics* **14,** 2881–2892 (Oct. 2005).

289. Hu, W. *et al.* FcγRIIB-I232T polymorphic change allosterically suppresses ligand binding. *eLife* **8** (July 2019).

290. Negi, V. S. *et al.* Intravenous immunoglobulin: An update on the clinical use and mechanisms of action. *Journal of Clinical Immunology* **27,** 233–245 (May 2007).

291. Tackenberg, B. *et al.* Impaired inhibitory Fcγ receptor IIB expression on B cells in chronic inflammatory demyelinating polyneuropathy. *Proceedings of the National Academy of Sciences of the United States of America* **106,** 4788–4792 (Mar. 2009).

292. Kaneko, Y., Nimmerjahn, F., Madaio, M. P. & Ravetch, J. V. Pathology and protection in nephrotoxic nephritis is determined by selective engagement of specific Fc receptors. *Journal of Experimental Medicine* **203,** 789–797 (Mar. 2006).

293. Fitzpatrick, E. A., Wang, J. & Strome, S. E. *Engineering of Fc Multimers as a Protein Therapy for Autoimmune Disease* Mar. 2020.

294. Kaneko, Y., Nimmerjahn, F. & Ravetch, J. V. Anti-inflammatory activity of immunoglobulin G resulting from Fc sialylation. *Science* **313,** 670–673 (Aug. 2006).

295. Schwab, I. & Nimmerjahn, F. *Intravenous immunoglobulin therapy: How does IgG modulate the immune system?* Mar. 2013.

296. Nagelkerke, S. Q. & Kuijpers, T. W. *Immunomodulation by IVIg and the role of Fc-gamma receptors: Classic mechanisms of action after all?* 2015.

297. Yu, X. *et al.* Dissecting the molecular mechanism of IVIg therapy: The interaction between serum IgG and DC-SIGN is independent of antibody glycoform or Fc domain. *Journal of Molecular Biology* **425,** 1253–1258 (Apr. 2013).

298. Zuercher, A. W. *et al. Next-generation Fc receptor–targeting biologics for autoimmune diseases* Oct. 2019.

299. Lim, S. H. *et al.* Fc gamma receptor IIb on target B cells promotes rituximab internalization and reduces clinical efficacy. *Blood* **118,** 2530–2540 (Sept. 2011).

300. Vaughan, A. T. *et al.* Activatory and inhibitory Fcγ receptors augment rituximab-mediated internalization of CD20 independent of signaling via the cytoplasmic domain. *Journal of Biological Chemistry* **290,** 5424–5437 (Feb. 2015).

301. Lee, C. S. *et al. Expression of the inhibitory Fc gamma receptor IIB (FCGR2B, CD32B) on follicular lymphoma cells lowers the response rate to rituximab monotherapy (SAKK 35/98)* Jan. 2015.

302. Nowicka, M. *et al.* Prognostic significance of FCGR2B expression for the response of DLBCL patients to rituximab or obinutuzumab treatment. *Blood Advances* **5,** 2945–2957 (2021).

303. Montalvao, F. *et al.* The mechanism of anti-CD20-mediated B cell depletion revealed by intravital imaging. *Journal of Clinical Investigation* **123,** 5098–5103 (Dec. 2013).

304. Grandjean, C. L. *et al.* Intravital imaging reveals improved Kupffer cell-mediated phagocytosis as a mode of action of glycoengineered anti-CD20 antibodies. *Scientific Reports* **6,** 34382 (2016).

305. Boross, P. & Leusen, J. H. W. Mechanisms of action of CD20 antibodies. *American journal of cancer research* **2,** 676–90 (2012).

306. Elgueta, R. *et al. Molecular mechanism and function of CD40/CD40L engagement in the immune system* May 2009.

307. Ara, A., Ahmed, K. A. & Xiang, J. Multiple effects of CD40–CD40L axis in immunity against infection and cancer. *ImmunoTargets and Therapy* **Volume 7,** 55–61 (June 2018).

308. White, A. L. *et al.* Interaction with FcγRIIB Is Critical for the Agonistic Activity of Anti-CD40 Monoclonal Antibody. *The Journal of Immunology* **187,** 1754–1763 (Aug. 2011).

309. Li, F. & Ravetch, J. V. Inhibitory Fcγ receptor engagement drives adjuvant and anti-tumor activities of agonistic CD40 antibodies. *Science* **333,** 1030–1034 (Aug. 2011).

310. Li, F. & Ravetch, J. V. Antitumor activities of agonistic anti-TNFR antibodies require differential FcγRIIB coengagement in vivo. *Proceedings of the National Academy of Sciences of the United States of America* **110,** 19501–19506 (Nov. 2013).

311. White, A. L. *et al.* Conformation of the human immunoglobulin G2 hinge imparts superagonistic properties to immunostimulatory anticancer antibodies. *Cancer Cell* **27,** 138–148 (Jan. 2015).

312. Mimoto, F. *et al.* Engineered antibody Fc variant with selectively enhanced FcγRIIb binding over both FcγRIIaR131 and FcγRIIaH131. *Protein Engineering, Design and Selection* **26,** 589–598 (Oct. 2013).

313. Dahan, R. *et al.* Therapeutic Activity of Agonistic, Human Anti-CD40 Monoclonal Antibodies Requires Selective FcγR Engagement. *Cancer Cell* **29,** 820–831 (June 2016).

314. Knorr, D. A., Dahan, R. & Ravetch, J. V. Toxicity of an Fc-engineered anti-CD40 antibody is abrogated by intratumoral injection and results in durable antitumor immunity. *Proceedings of the National Academy of Sciences of the United States of America* **115,** 11048–11053 (Oct. 2018).

315. Yu, X. *et al.* TNF receptor agonists induce distinct receptor clusters to mediate differential agonistic activity. *Communications Biology* **4,** 772 (Dec. 2021).

316. Richards, J. O. *et al.* Optimization of antibody binding to FcγRIIa enhances macrophage phagocytosis of tumor cells. *Molecular Cancer Therapeutics* **7,** 2517–2527 (2008).

317. Brinkhaus, M. *et al.* Glycine 236 in the Lower Hinge Region of Human IgG1 Differentiates FcγR from Complement Effector Function. *The Journal of Immunology* **205,** 3456–3467 (Dec. 2020).

318. Liu, R. *et al.* Fc-Engineering for Modulated Effector Functions—Improving Antibodies for Cancer Treatment. *Antibodies* **9,** 64 (Nov. 2020).

319. Salles, G. *et al.* Tafasitamab plus lenalidomide in relapsed or refractory diffuse large B-cell lymphoma (L-MIND): a multicentre, prospective, single-arm, phase 2 study. *The Lancet Oncology* **21,** 978–988 (July 2020).

320. Brooks, D. G., Qiu, W. Q., Luster, A. D. & Ravetch, J. V. Structure and expression of human IgG (FcRII(CD32). Functional heterogeneity is encoded by the alternatively spliced products of multiple genes. *Journal of Experimental Medicine* **170,** 1369–1385 (1989).

321. Williams, E. L. *et al.* Immunotherapy Targeting Inhibitory Fcγ Receptor IIB (CD32b) in the Mouse Is Limited by Monoclonal Antibody Consumption and Receptor Internalization. *The Journal of Immunology* **191,** 4130–4140 (Oct. 2013).

322. Veri, M. C. *et al.* Monoclonal antibodies capable of discriminating the human inhibitory Fcγ-receptor IIB (CD32B) from the activating Fcγ-receptor IIA (CD32A): Biochemical, biological and functional characterization. *Immunology* **121,** 392–404 (July 2007).

323. Roghanian, A. *et al.* Antagonistic Human FcγRIIB (CD32B) Antibodies have anti-tumor activity and overcome resistance to antibody therapy invivo. *Cancer Cell* **27,** 473–488 (Apr. 2015).

324. NIH U.S. National Library of Medicine. *A Study of BI-1206 in Combination With Rituximab in Subjects With Indolent B-Cell Non-Hodgkin Lymphoma - ClinicalTrials.gov* 2019.

325. Mårtensson, L. *et al. Abstract 1642: A novel FcγRIIB-blocking antibody to enhance FcγR-dependent antitumor immunity* in *Cancer Research* **81** (American Association for Cancer Research, July 2021), 1642–1642.

326. Jerkeman, M. *et al.* 17-BI-1206-02 Phase 1/2a Clinical Trial of BI-1206, a Monoclonal Antibody to Fcgriib, in Combination with Rituximab in Subjects with Indolent B-Cell Non-Hodgkin Lymphoma That Has Relapsed or Is Refractory to Rituximab. *Blood* **136,** 36–37 (Nov. 2020).

327. AB, B. I. *BioInvent Phase I/IIa data suggest BI-1206 restores activity of rituximab in relapsed non-Hodgkin's lymphoma patients*

328. Deckert, J., Tavares, D. J. & Park, P. U. Cd20 antibodies and uses thereof. *Patent* **849** (Dec. 2011).

329. Krop, I. *et al.* Self-renewal of B-1 lymphocytes is dependent on CD19. *European Journal of Immunology* **26,** 238–242 (Jan. 1996).

330. Cobbold, S. P. *et al.* Therapy with monoclonal antibodies by elimination of T-cell subsets in vivo. *Nature* **312,** 548–551 (1984).

331. Koo, G. C. *et al.* The NK-1.1(-) mouse: a model to study differentiation of murine NK cells. *Journal of immunology (Baltimore, Md. : 1950)* **137,** 3742–7 (1986).

332. Sakaguchi, S. *et al.* Immunologic self-tolerance maintained by activated T cells expressing IL-2 receptor alpha-chains (CD25). Breakdown of a single mechanism of self-tolerance causes various autoimmune diseases. *Journal of immunology (Baltimore, Md. : 1950)* **155,** 1151–64 (1995).

333. Al-Shanikhani, A. *et al.* OX40 is differentially expressed on activated rat and mouse T cells and is the sole receptor for the OX40 ligand. *European Journal of Immunology* **26,** 1695–1699 (Aug. 1996).

334. Shepard, H. M. *et al.* Monoclonal antibody therapy of human cancer: Taking the HER2 protooncogene to the clinic. *Journal of Clinical Immunology* **11,** 117–127 (May 1991).

335. Beers, S. A. *et al.* Type II (tositumomab) anti-CD20 monoclonal antibody out performs type I (rituximab-like) reagents in B-cell depletion regardless of complement activation. *Blood* **112,** 4170–4177 (Nov. 2008).

336. Hogquist, K. A. *et al.* T cell receptor antagonist peptides induce positive selection. *Cell* **76,** 17–27 (Jan. 1994).

337. Zhang, Y., Huo, M., Zhou, J. & Xie, S. PKSolver: An add-in program for pharmacokinetic and pharmacodynamic data analysis in Microsoft Excel. *Computer Methods and Programs in Biomedicine* **99,** 306–314 (Sept. 2010).

338. Bichi, R. *et al.* Human chronic lymphocytic leukemia modeled in mouse by targeted TCL1 expression. *Proceedings of the National Academy of Sciences of the United States of America* **99,** 6955–6960 (May 2002).

339. Moore, M. W., Carbone, F. R. & Bevan, M. J. Introduction of soluble protein into the class I pathway of antigen processing and presentation. *Cell* **54,** 777–785 (Sept. 1988).

340. Pundir, S., Martin, M. J. & O'Donovan, C. UniProt Tools. *Current Protocols in Bioinformatics* **53,** 1–1 (Mar. 2016).

341. Casey, E. *et al.* A new mouse expressing human Fcγ receptors to better predict therapeutic efficacy of human anti-cancer antibodies. *Leukemia* **32,** 547–549 (Feb. 2018).

342. Gillis, C. M. *et al.* Mechanisms of anaphylaxis in human low-affinity IgG receptor locus knock-in mice. *Journal of Allergy and Clinical Immunology* **139,** 1253–1265 (Apr. 2017).

343. Nishimura, T. *et al.* Characterization of the human FcγRIIB gene promoter: human zinc-finger proteins (ZNF140 and ZNF91) that bind to different regions function as transcription repressors. *International Immunology* **13,** 1075–1084 (Aug. 2001).

344. Greenman, J. *et al.* Characterization of a new monoclonal anti-Fcγ RII antibody, AT10, and its incorporation into a bispecific F(ab')2 derivative for recruitment of cytotoxic effectors. *Molecular Immunology* **28,** 1243–1254 (Nov. 1991).

345. Weiskopf, K. & Weissman, I. L. *Macrophages are critical effectors of antibody therapies for cancer* Mar. 2015.

346. Gül, N. *et al.* Macrophages eliminate circulating tumor cells after monoclonal antibody therapy. *Journal of Clinical Investigation* **124,** 812–823 (Feb. 2014).

347. Lynch, R. W. *et al.* An efficient method to isolate Kupffer cells eliminating endothelial cell contamination and selective bias. *Journal of Leukocyte Biology* **104,** 579–586 (Sept. 2018).

348. Mockridge, C. I. *et al.* Reversible anergy of sIgM-mediated signaling in the two subsets of CLL defined by VH-gene mutational status. *Blood* **109,** 4424–4431 (May 2007).

349. Zimmermann, H. W., Trautwein, C. & Tacke, F. Functional role of monocytes and macrophages for the inflammatory response in acute liver injury. *Frontiers in Physiology* **3 OCT,** 56 (2012).

350. Dal-Secco, D. *et al.* A dynamic spectrum of monocytes arising from the in situ reprogramming of CCR2+ monocytes at a site of sterile injury. *Journal of Experimental Medicine* **212,** 447–456 (Apr. 2015).

351. Robinett, R. A. *et al.* Dissecting FcγR Regulation through a Multivalent Binding Model. *Cell Systems* **7,** 41–48 (July 2018).

352. Marenkova, T. V., Loginova, D. B. & Deineko, E. V. *Mosaic patterns of transgene expression in plants* Mar. 2012.

353. Cho, A., Haruyama, N. & Kulkarni, A. B. Generation of Transgenic Mice. *Current Protocols in Cell Biology* **42,** Unit (Mar. 2009).

354. Farrar, M. A. & Schreiber, R. D. *The molecular cell biology of interferon-γ and its receptor* 1993.

355. Heidary, F. & Gharebaghi, R. *Ivermectin: a systematic review from antiviral effects to COVID-19 complementary regimen* June 2020.

356. Strauss, O. *et al.* Immunofluorescence identifies distinct subsets of endothelial cells in the human liver. *Scientific Reports* **7,** 1–13 (Mar. 2017).

357. Wu, X. *et al.* Human Liver Macrophage Subsets Defined by CD32. *Frontiers in Immunology* **11,** 2108 (Sept. 2020).

358. MacParland, S. A. *et al.* Single cell RNA sequencing of human liver reveals distinct intrahepatic macrophage populations. *Nature Communications* **9,** 1–21 (Oct. 2018).

359. Dahal, L. N. *et al.* STING activation reverses lymphoma-mediated resistance to antibody immunotherapy. *Cancer Research* **77,** 3619–3631 (July 2017).

360. Uhlén, M. *et al.* Tissue-based map of the human proteome. *Science* **347** (Jan. 2015).

361. Lesourne, R., Bruhns, P., Fridman, W. H. & Daëron, M. Insufficient Phosphorylation Prevents FcγRIIB from Recruiting the SH2 Domain-containing Protein-tyrosine Phosphatase SHP-1. *Journal of Biological Chemistry* **276,** 6327–6336 (Mar. 2001).

362. Mousavi, S. A. *et al.* Receptor-mediated endocytosis of immune complexes in rat liver sinusoidal endothelial cells is mediated by FcγRIIb2. *Hepatology* **46,** 871–884 (Sept. 2007).

363. Minard-Colin, V. *et al.* Lymphoma depletion during CD20 immunotherapy in mice is mediated by macrophage FcγRI, FcγRIII, and FcγRIV. *Blood* **112,** 1205–1213 (Aug. 2008).

364. Oldham, R. J. *et al.* FcγRII (CD32) modulates antibody clearance in NOD SCID mice leading to impaired antibody-mediated tumor cell deletion. *Journal for ImmunoTherapy of Cancer* **8,** e000619 (June 2020).

365. Wang, K., Wei, G. & Liu, D. CD19: a biomarker for B cell development, lymphoma diagnosis and therapy. *Experimental Hematology & Oncology* **1,** 36 (2012).

366. Gordan, S. *et al.* The Immunological Organ Environment Dictates the Molecular and Cellular Pathways of Cytotoxic Antibody Activity. *Cell Reports* **29,** 3033–3046 (Dec. 2019).

367. Campbell, J. P. *et al.* Total lymphocyte CD8 expression is not a reliable marker of cytotoxic T-cell populations in human peripheral blood following an acute bout of high-intensity exercise. *Brain, Behavior, and Immunity* **22,** 375–380 (Mar. 2008).

368. Setiady, Y. Y., Coccia, J. A. & Park, P. U. In vivo depletion of CD4+FOXP3+ Treg cells by the PC61 anti-CD25 monoclonal antibody is mediated by FcγRIII+ phagocytes. *European Journal of Immunology* **40,** 780–786 (Mar. 2010).

369. Arce Vargas, F. *et al.* Fc-Optimized Anti-CD25 Depletes Tumor-Infiltrating Regulatory T Cells and Synergizes with PD-1 Blockade to Eradicate Established Tumors. *Immunity* **46,** 577–586 (Apr. 2017).

370. Hasboldu, J. *et al.* Properties of mouse CD40: Cellular distribution of CD40 and B cell activation by monoclonal anti-mouse CD40 antibodies. *European Journal of Immunology* **24,** 1835–1842 (Aug. 1994).

371. Altman, J. D. *et al.* Pillars Article : Phenotypic Analysis of. *Journal of immunology (Baltimore, Md. : 1950)* **274,** 94–97 (1996).

372. Bio-Rad. *Cell Frequencies in Common Samples* 2021.

373. Kelton, J. *et al.* The concentration of IgG in the serum is a major determinant of Fc-dependent reticuloendothelial function. *Blood* **66,** 490–495 (Sept. 1985).

374. Stapleton, N. M. *et al.* Competition for FcRn-mediated transport gives rise to short half-life of human IgG3 and offers therapeutic potential. *Nature Communications* **2,** 599 (2011).

375. Häusler, D. *et al.* Functional characterization of reappearing B cells after anti-CD20 treatment of CNS autoimmune disease. *Proceedings of the National Academy of Sciences of the United States of America* **115,** 9773–9778 (Sept. 2018).

376. Kamath, A. V. *Translational pharmacokinetics and pharmacodynamics of monoclonal antibodies* Sept. 2016.

377. Abuqayyas, L. & Balthasar, J. P. Application of knockout mouse models to investigate the influence of FcγR on the tissue distribution and elimination of 8C2, a murine IgG1 monoclonal antibody. *International Journal of Pharmaceutics* **439,** 8–16 (Dec. 2012).

378. Ovacik, M. & Lin, K. Tutorial on Monoclonal Antibody Pharmacokinetics and Its Considerations in Early Development. *Clinical and Translational Science* **11,** 540–552 (Nov. 2018).

379. Hadzhieva, M. *et al.* Impact of Antigen Density on the Binding Mechanism of IgG Antibodies. *Scientific Reports* **7,** 1–11 (June 2017).

380. Bar, L. *et al.* Impact of Antigen Density on Recognition by Monoclonal Antibodies. *Analytical Chemistry* **92,** 5396–5403 (Apr. 2020).

381. Teeling, J. L. *et al.* The Biological Activity of Human CD20 Monoclonal Antibodies Is Linked to Unique Epitopes on CD20. *The Journal of Immunology* **177,** 362–371 (July 2006).

382. Golay, J. *et al.* CD20 levels determine the in vitro susceptibility to rituximab and complement of B-cell chronic lymphocytic leukemia: Further regulation by CD55 and CD59. *Blood* **98,** 3383–3389 (Dec. 2001).

383. Temming, A. R. *et al.* Functional Attributes of Antibodies, Effector Cells, and Target Cells Affecting NK Cell–Mediated Antibody-Dependent Cellular Cytotoxicity. *The Journal of Immunology* **203,** 3126–3135 (Dec. 2019).

384. Yan, J. *et al.* Targeting antigen to CD19 on B cells efficiently activates T cells. *International Immunology* **17,** 869–877 (July 2005).

385. Ingle, G. S. *et al.* High CD21 expression inhibits internalization of anti-CD19 antibodies and cytotoxicity of an anti-CD19-drug conjugate. *British Journal of Haematology* **140,** 46–58 (Jan. 2008).

386. Hooyberg, E. *et al.* Enhanced Antitumor Effects of CD20 over CD19 Monoclonal Antibodies in a Nude Mouse Xenograft Model. *Cancer Research* **55,** 840–846 (1995).

387. Takai, T. *et al.* FcR γ chain deletion results in pleiotrophic effector cell defects. *Cell* **76,** 519–529 (Feb. 1994).

388. Clynes, R. *et al.* Fc receptors are required in passive and active immunity to melanoma. *Proceedings of the National Academy of Sciences of the United States of America* **95,** 652–656 (Jan. 1998).

389. Clement, M. *et al.* Anti-CD8 Antibodies Can Trigger CD8 + T Cell Effector Function in the Absence of TCR Engagement and Improve Peptide–MHCI Tetramer Staining. *The Journal of Immunology* **187,** 654–663 (July 2011).

390. Lefrançois, L., Altman, J. D., Williams, K. & Olson, S. Soluble Antigen and CD40 Triggering Are Sufficient to Induce Primary and Memory Cytotoxic T Cells. *The Journal of Immunology* **164,** 725–732 (Jan. 2000).

391. Richards, D. M. *et al. Concepts for agonistic targeting of CD40 in immuno-oncology* Feb. 2020.

392. Bolland, S. & Ravetch, J. V. Spontaneous autoimmune disease in FcγRIIB-deficient mice results from strain-specific epistasis. *Immunity* **13,** 277–285 (Aug. 2000).

393. Dotan, E., Aggarwal, C. & Smith, M. R. *Impact of rituximab (Rituxan) on the treatment of B-cell non-Hodgkin's lymphoma* Mar. 2010.

394. Li, F. *et al.* Bioinformatics analysis and verification of gene targets for renal clear cell carcinoma. *Computational Biology and Chemistry* **92,** 107453 (June 2021).

395. Cheng, W. *et al.* Bioinformatic profiling identifies an immune-related risk signature for glioblastoma. *Neurology* **86,** 2226–2234 (June 2016).

396. Wang, S. & Xu, X. An Immune-Related Gene Pairs Signature for Predicting Survival in Glioblastoma. *Frontiers in Oncology* **11,** 564960 (Mar. 2021).

397. Norton, N. *et al.* Association studies of Fcγ receptor polymorphisms with outcome in HER2+ breast cancer patients treated with trastuzumab in NCCTG (Alliance) Trial N9831. *Cancer immunology research* **2,** 962–969 (Oct. 2014).

398. Johnson, A. J. *et al.* Characterization of the TCL-1 transgenic mouse as a preclinical drug development tool for human chronic lymphocytic leukemia. *Blood* **108,** 1334–1338 (Aug. 2006).

399. Bresin, A. *et al. TCL1 transgenic mouse model as a tool for the study of therapeutic targets and microenvironment in human B-cell chronic lymphocytic leukemia* 2016.

400. Pekarsky, Y. *et al.* Tcl1 expression in chronic lymphocytic leukemia is regulated by miR-29 and miR-181. *Cancer Research* **66,** 11590–11593 (Dec. 2006).

401. Wolf, D. *et al.* The expression of the regulatory T cell-specific forkhead box transcription factor FoxP3 is associated with poor prognosis in ovarian cancer. *Clinical Cancer Research* **11,** 8326–8331 (Dec. 2005).

402. Kobayashi, N. *et al.* FOXP3+ regulatory T cells affect the development and progression of hepatocarcinogenesis. *Clinical Cancer Research* **13,** 902–911 (Feb. 2007).

403. Bates, G. J. *et al.* Quantification of regulatory T cells enables the identification of high-risk breast cancer patients and those at risk of late relapse. *Journal of Clinical Oncology* **24,** 5373–5380 (Dec. 2006).

404. Wang, H., Franco, F. & Ho, P. C. Metabolic Regulation of Tregs in Cancer: Opportunities for Immunotherapy. *Trends in Cancer* **3,** 583–592 (Aug. 2017).

405. Simpson, T. R. *et al.* Fc-dependent depletion of tumor-infiltrating regulatory t cells co-defines the efficacy of anti-CTLA-4 therapy against melanoma. *Journal of Experimental Medicine* **210,** 1695–1710 (Aug. 2013).

406. Gorer, P. A. Studies in antibody response of mice to tumour inoculation. *British Journal of Cancer* **4,** 372–379 (1950).

407. Vasović, L. V. *et al.* Synergy between an antibody and CD8+ cells in eliminating an established tumor. *European Journal of Immunology* **27,** 374–382 (1997).

408. Kitamura, N. *et al.* OX40 costimulation can abrogate Foxp3+ regulatory T cell-mediated suppression of antitumor immunity. *International Journal of Cancer* **125,** 630–638 (Aug. 2009).

409. Baras, A. S. *et al.* The ratio of CD8 to Treg tumor-infiltrating lymphocytes is associated with response to cisplatin-based neoadjuvant chemotherapy in patients with muscle invasive urothelial carcinoma of the bladder. *OncoImmunology* **5** (May 2016).

410. Takada, K. *et al.* Use of the tumor-infiltrating CD8 to FOXP3 lymphocyte ratio in predicting treatment responses to combination therapy with pertuzumab, trastuzumab, and docetaxel for advanced HER2-positive breast cancer. *Journal of Translational Medicine* **16,** 1–11 (Apr. 2018).

411. Sun, X. & Kaufman, P. D. *Ki-67: more than a proliferation marker* June 2018.

412. Manzella, A., Borba-Filho, P., D'Ippolito, G. & Farias, M. Abdominal Manifestations of Lymphoma: Spectrum of Imaging Features. *ISRN Radiology* **2013,** 1–11 (Sept. 2013).

413. Bronte, V. & Pittet, M. J. *The spleen in local and systemic regulation of immunity* Nov. 2013.

414. Hamaguchi, Y. *et al.* The Peritoneal Cavity Provides a Protective Niche for B1 and Conventional B Lymphocytes during Anti-CD20 Immunotherapy in Mice. *The Journal of Immunology* **174,** 4389–4399 (Apr. 2005).

415. Quezada, S. A. & Peggs, K. S. *Lost in translation: Deciphering the mechanism of action of anti-human CTLA-4* Feb. 2019.

416. Lahl, K. & Sparwasser, T. In vivo depletion of FoxP3+ Tregs using the DEREG mouse model. *Methods in molecular biology (Clifton, N.J.)* **707,** 157–172 (2011).

417. Ruby, C. E., Redmond, W. L., Haley, D. & Weinberg, A. D. Anti-OX40 stimulation in vivo enhances CD8+ memory T cell survival and significantly increases recall responses. *European Journal of Immunology* **37,** 157–166 (Jan. 2007).

418. Redmond, W. L. *et al.* Defects in the Acquisition of CD8 T Cell Effector Function after Priming with Tumor or Soluble Antigen Can Be Overcome by the Addition of an OX40 Agonist. *The Journal of Immunology* **179,** 7244–7253 (Dec. 2007).

419. Gough, M. J. *et al.* OX40 agonist therapy enhances CD8 infiltration and decreases immune suppression in the tumor. *Cancer Research* **68,** 5206–5215 (July 2008).

420. Linch, S. N., McNamara, M. J. & Redmond, W. L. OX40 agonists and combination immunotherapy: Putting the pedal to the metal. *Frontiers in Oncology* **5** (2015).

421. Valzasina, B. *et al.* Triggering of OX40 (CD134) on CD4+CD25+ T cells blocks their inhibitory activity: A novel regulatory role for OX40 and its comparison with GITR. *Blood* **105,** 2845–2851 (Apr. 2005).

422. Ruby, C. E. *et al.* Cutting Edge: OX40 Agonists Can Drive Regulatory T Cell Expansion if the Cytokine Milieu Is Right. *The Journal of Immunology* **183,** 4853–4857 (Oct. 2009).

423. Piconese, S., Valzasina, B. & Colombo, M. P. OX40 triggering blocks suppression by regulatory T cells and facilitates tumor rejection. *Journal of Experimental Medicine* **205,** 825–839 (Apr. 2008).

424. Bulliard, Y. *et al.* OX40 engagement depletes intratumoral Tregs via activating FcγRs, leading to antitumor efficacy. *Immunology and Cell Biology* **92,** 475–480 (July 2014).

425. Ermann, J. *et al.* CD4 + CD25 + T Cells Facilitate the Induction of T Cell Anergy. *The Journal of Immunology* **167,** 4271–4275 (Oct. 2001).

426. Polesso, F. *et al.* OX40 Agonist Tumor Immunotherapy Does Not Impact Regulatory T Cell Suppressive Function. *The Journal of Immunology* **203,** 2011–2019 (Oct. 2019).

427. Yu, J. W. *et al.* Tumor-immune profiling of murine syngeneic tumor models as a framework to guide mechanistic studies and predict therapy response in distinct tumor microenvironments. *PLoS ONE* **13** (Nov. 2018).

428. Amigorena, S. *et al.* Cytoplasmic domain heterogeneity and functions of IgG Fc receptors in B lymphocytes. *Science* **256,** 1808–1812 (June 1992).

429. Seidel, U. J., Schlegel, P. & Lang, P. Natural killer cell mediated antibody-dependent cellular cytotoxicity in tumor immunotherapy with therapeutic antibodies. *Frontiers in Immunology* **4** (2013).

430. Cheung, J. C. *et al.* The mechanism of activation of NK-cell IFN-γ production by ligation of CD28. *Molecular Immunology* **36,** 361–372 (Apr. 1999).

431. Uchida, J. *et al.* The innate mononuclear phagocyte network depletes B lymphocytes through Fc receptor-dependent mechanisms during anti-CD20 antibody immunotherapy. *Journal of Experimental Medicine* **199,** 1659–1669 (June 2004).

432. Smith, P. *et al.* Mouse model recapitulating human Fcγ receptor structural and functional diversity. *Proceedings of the National Academy of Sciences of the United States of America* **109,** 6181–6186 (Apr. 2012).

433. Lejeune, J., Brachet, G. & Watier, H. Evolutionary story of the low/medium-affinity IgG Fc receptor gene cluster. *Frontiers in Immunology* **10,** 1297 (2019).

434. Ukkonen, P. *et al.* Transport of macrophage Fc receptors and fc receptor-bound ligands to lysosomes. *Journal of Experimental Medicine* **163,** 952–971 (Apr. 1986).

435. Feng, M. *et al. Phagocytosis checkpoints as new targets for cancer immunotherapy* Oct. 2019.

436. Zarrin, A. A. & Monteiro, R. C. Editorial: The Role of Inhibitory Receptors in Inflammation and Cancer. *Frontiers in Immunology* **11,** 3452 (Dec. 2020).

437. Isnardi, I. *et al.* Two distinct tyrosine-based motifs enable the inhibitory receptor FčRIIB to cooperatively recruit the inositol phosphatases SHIP1/2 and the adapters Grb2/Grap. *Journal of Biological Chemistry* **279,** 51931–51938 (Dec. 2004).

438. Pauls, S. D. & Marshall, A. J. Regulation of immune cell signaling by SHIP1: A phosphatase, scaffold protein, and potential therapeutic target. *European Journal of Immunology* **47,** 932–945 (June 2017).

439. Tsang, E. *et al.* Molecular mechanism of the Syk activation switch. *Journal of Biological Chemistry* **283,** 32650–32659 (Nov. 2008).

440. Zhang, C. in *Encyclopedia of Signaling Molecules* 2869–2878 (Springer, Cham, 2018).

441. Zen, K. *et al.* Inflammation-induced proteolytic processing of the SIRPα cytoplasmic ITIM in neutrophils propagates a proinflammatory state. *Nature Communications* **4,** 1–11 (Sept. 2013).

442. Kang, X. *et al.* The ITIM-containing receptor LAIR1 is essential for acute myeloid leukaemia development. *Nature Cell Biology* **17,** 665–677 (Apr. 2015).

443. Patsoukis, N., Wang, Q., Strauss, L. & Boussiotis, V. A. Revisiting the PD-1 pathway. *Science Advances* **6** (Sept. 2020).